LIGHTNING INDUCED VOLTAGES ON POWER LINES: THEORY AND EXPERIMENT

By

MANECK JAL MASTER

A DISSERTATION PRESENTED TO THE GRADUATE COUNCIL OF
THE UNIVERSITY OF FLORIDA
IN PARTIAL FULFILLMENT OF THE REQUIREMENTS FOR THE
DEGREE OF DOCTOR OF PHILOSOPHY

UNIVERSITY OF FLORIDA

1982

ACKNOWLEDGEMENTS

I wish to express my deep sense of gratitude to my guru, Dr. Martin A. Uman, for introducing me to the exciting world of lightning research. His astute advice and constant support have contributed significantly to the successful completion of this dissertation. I would also like to thank Dr. M. Darveniza of the University of Queensland, Australia, without whose labors this project would not have materialized. I am indebted to Dr. W. H. Beasley who has freely given me his time and help, especially during data extraction from tapes, and who was in charge of the initial data collection. I wish to add a big THANK YOU to Drs. A. D. Sutherland, R. L. Sullivan, T. E. Bullock, and G. R. Lebo, for their helpful comments and suggestions. I want to express my appreciation to Mr. J. Preta, Mr. V. de la Torre, and Mr. K. Whiteleather for their assistance with the data analysis.

The research reported in this thesis was funded in part by the Department of Energy and the National Science Foundation. The Tampa Electric Company constructed the test line and the Florida Power Corporation provided significant financial support towards constructing the TV network used in this thesis.

I am thankful for the congenial atmosphere at home created by my wife, Vrinda, and the constant support and encouragement from our families in India, which helped keep my mind focussed on this

project. I would also like to express my appreciation to Ms. Lynda Brown and Ms. Linda Grable for converting this dissertation into a presentable form.

TABLE OF CONTENTS

		Page
ACKNOWLEDGEMENTS		ii
LIST OF FIGURES		vi
LIST OF TABLES		xvii
ABSTRACT		xix
CHAPTER		
I	REVIEW	1
	1.1 Introduction	1
	1.2 Lightning	1
	1.2.1 The Thundercloud	1
	1.2.2 Ground Lightning	5
	1.2.3 Cloud Discharge	9
	1.3 Induced Overvoltages	10
II	EXPERIMENTAL RESULTS	19
	2.1 Introduction	19
	2.2 Experimental Environment	20
	2.3 Data Acquisition Systems	20
	2.3.1 Field Measurements	26
	2.3.2 Voltage Measurements	30
	2.3.3 Lightning Location	31
	2.3.4 Relative Timing	33
	2.4 The Data Base	34
	2.4.1 Flash Selection	34
	2.4.2 Field and Voltage Records	35
	2.4.3 Location and Calibration	35
	2.5 An Example	38
	2.5.1 Location	38
	2.5.2 Film Records	43
	2.5.3 Instrumentation Tape Records	43
	2.5.4 Conclusions	52
	2.6 Data Analysis	56
	2.6.1 Analysis of Vertical Electric Field Records	76
	2.6.2 Analysis of Voltage Records	113
	2.6.3 Correlation between Voltage and Field Records	122

III THEORETICAL ANALYSIS..... 139

3.1 Introduction..... 139
3.2 Electric and Magnetic Fields Illuminating the Test-Line..... 142
3.2.1 The Return Stroke Model..... 142
3.2.2 Electromagnetic Field Calculation..... 144
3.2.3 Wavetilt Formulation..... 148
3.3 Induced Line Voltage..... 169
3.3.1 Theoretical Model..... 169
3.3.2 Computer Solution..... 182

IV RESULTS..... 192

4.1 Introduction..... 192
4.2 Short Line..... 192
4.3 Long Line..... 223
4.4 Comparison of Measured Voltages with Theory..... 234

V CONCLUSIONS..... 252

APPENDICES

A ELECTRIC AND MAGNETIC FIELDS PRODUCED BY A VERTICAL DIPOLE ABOVE GROUND..... 257

B TEST LINE VOLTAGES INDUCED BY NEARBY STEPPED LEADERS..... 269

C COMPUTER PROGRAMS..... 279

C.1 Return Stroke Program..... 279
C.2 Parameters of Lossless Transmission Lines..... 294
C.3 Wavetilt Program..... 300
C.4 Coupling Program..... 304

D DISTRIBUTION OF PEAK VOLTAGES..... 314

REFERENCES..... 317

BIOGRAPHICAL SKETCH..... 324

LIST OF FIGURES

Figure		Page
1.1	Electrical configuration of a typical thundercloud; the bold dots represent the locations of the effective charge centers. (Adapted from Malan, 1963; and Uman, 1969).....	4
2.1	The TV network used for location of the ground strike point. The shaded cones indicate the field of view for each TV in degrees, 0° being North.....	22
2.2	Detailed sketch of the experimental test-line. Important parameters are listed in Table 2.1.....	24
2.3	Schematic diagram of the recording systems used inside the Mobile Lightning Laboratory to record the electric and magnetic fields due to lightning, the test-line voltage, and time and thunder signals....	28
2.4	Six-channel strip-chart record for the 190610 flash during run #79196TR27, showing four channels of electric field signals, one channel of thunder, and one of time-code.....	40
2.5	Location of the ground strike point for the 190610 flash during run #79196TR27 using the bearings from TV1E and TV2S.....	42
2.6(a)	Records of the vertical electric and horizontal magnetic fields and the test-line voltages obtained from the left oscilloscope film for the 190610 flash during run #79196TR27. The electric field is on a scale of 120 V/m per division and the voltage scale is 65 kV/division. All records are 200 μs full-scale. The relative displacement in time between the vertical electric field and the voltage records is due to different pre-trigger delay settings on the respective Biomation recorders.....	45

2.6(b) Records of the vertical electric and horizontal magnetic fields and the test-line voltages obtained from the right oscilloscope film for the 190610 flash during run #79196TR27. The electric field is on a 600 V/m per division scale, and the voltage scale is 165 kV/division All records are 200 μs full-scale. The relative displacement in time between the vertical electric field and the voltage records is due to different pre-trigger delay settings on the respective Biomation recorders..... 47

2.7 Vertical electric field record for the whole flash obtained from instrumentation tape for the 190610 flash during run #79196TR27. The FM channel sensitivity is 870 V/m per division and direct channel is 90 V/m per division. Both records are 200 ms full-scale..... 49

2.8 Vertical electric field and test-line voltages for all three return strokes of the flash obtained from the direct channels of the instrumentation tape recorder for the 190610 flash during run #79196TR27. The electric field and voltage scales are shown for each stroke. All records are 80 μs full-scale. The relative displacement in time between the electric field and the voltage records is due to the positioning of the record and reproduce heads of the Instrumentation Tape Recorder..... 51

2.9 Comparison between simultaneously recorded voltage signals on the direct and FM channels of the instrumentation tape recorder for a single stroke flash at 192238 UT during run #79199TR31..... 54

2.10 Number of strokes in the analyzed data plotted as a function of the angle from the Mobile Lightning Laboratory. The shaded data indicate subsequent strokes which have been classified as first strokes..... 78

2.11 Number of strokes in the analyzed data plotted as a function of the distance from the Mobile Lightning Laboratory. The shaded data indicate subsequent strokes which have been classified as first strokes..... 80

2.12(a) Histogram showing the number of strokes per flash for the data analyzed. The mean is 3.8 with a standard deviation of 3.0. The median is 3..... 82

2.12(b) Cumulative distribution function for the number of strokes per flash showing the correlation between data obtained in this thesis and other studies..... 84

2.13(a) Histogram of time intervals between successive return strokes in a flash..... 86

2.13(b) Cumulative distribution function for interstroke time intervals showing the correlation between data obtained in this thesis and other studies..... 88

2.14(a) Peak vertical electric field for first and subsequent strokes, plotted as a function of distance from the Mobile Lightning Laboratory. The dashed and solid lines represent the peak radiation field inverse distance relationship for first and subsequent strokes, respectively..... 93

2.14(b) Peak vertical electric field of the return stroke normalized to 100 km. For 112 first strokes the mean is 6.2 V/m with a standard deviation of 3.4 V/m; without the shaded data the mean for 90 first strokes is 6.5 V/m with a standard deviation of 3.5 V/m. For 237 subsequent strokes, the mean and standard deviation are 3.8 V/m and 2.2 V/m, respectively..... 95

2.15 Distribution of the zero-to-peak risetime of the vertical electric field. For 105 first strokes the mean and standard deviation are 4.4 μs and 1.8 μs, respectively; for 220 subsequent strokes, 2.8 μs and 1.5 μs, respectively. Without the shaded data the mean for 84 first strokes is 4.6 μs with a standard deviation of 1.8 μs 99

2.16 Distribution of the 10%-to-90% risetime of the vertical electric field. For 105 first strokes mean and standard deviation are 2.6 μs and 1.2 μs, respectively; for 220 subsequent strokes, 1.5 μs and 0.9 μs, respectively. Without the shaded data the mean is 2.7 μs with a standard deviation of 1.2 μs for 84 first strokes..... 102

2.17 Distribution of the 10%-to-90% risetime of the fast transition in the vertical electric field. For 102 first strokes the mean and standard deviation are 0.97 μs and 0.68 μs, respectively; for 217 subsequent strokes, 0.61 μs and 0.27 μs, respectively. Without the shaded data the mean is 1 μs with a standard deviation of 0.70 μs for 82 first strokes..... 105

2.18 Distribution of the duration of the slow initial front in the first stroke vertical electric field. For 105 first strokes the mean is 2.9 μs with a standard deviation of 1.3 μs; without the shaded data the mean and standard deviation are 3.0 μs and 1.3 μs, respectively, for 83 first strokes..... 108

2.19 Distribution of the first stroke slow initial front amplitude as a percentage of the peak vertical electric field. For 105 first strokes the mean is 28% with a standard deviation of 15%; without the shaded data, the mean is 27% with a 15% standard deviation for 83 first strokes..... 110

2.20 Peak induced voltage on the test-line for first and subsequent strokes as a function of the distance of the stroke from the Mobile Lightning Laboratory..... 115

2.21 Distribution of peak induced voltage on the test line. For 112 first strokes the mean and standard deviation are 22.6 kV and 22.4 kV, respectively; for 237 subsequent strokes, 10.8 kV and 9.0 kV, respectively..... 117

2.22 Distribution of the zero-to-peak risetime of the induced voltage on the test-line. For 105 first strokes the mean and standard deviation are 6.0 μs and 3.8 μs, respectively; for 218 subsequent strokes, 4.0 μs and 2.3 μs, respectively..... 121

2.23 Distribution of the 10%-to-90% risetime of the induced voltage on the test-line. For 105 first strokes the mean and standard deviation are 4.0 μs and 3.2 μs, respectively; for 218 subsequent strokes, 2.6 μs and 1.7 μs, respectively..... 124

2.24 Ratio of the 10%-to-90% risetime of the induced voltage to the 10%-to-90% risetime of the simultaneously recorded vertical electric field..... 126

2.25 Induced voltages on the test line and vertical electric field due to lightning for return strokes at three different locations..... 130

2.26 Ratio of initial peak induced voltage to initial peak vertical electric field for first strokes vs. angle of the lightning ground strike point from the Mobile Lightning Laboratory; the circled point represents the mean and the vertical bars represent the standard deviation for the indicated number of points in each 10° interval..... 133

2.27 Ratio of initial peak induced voltage to initial peak vertical electric field for subsequent strokes vs. angle of the lightning ground strike point from the Mobile Lightning Laboratory; the circled point represents the mean and the vertical bars represent the standard deviation for the indicated number of points in each 10° interval..... 135

3.1 Geometry for field computations based on the model of Master et al. (1981)..... 146

3.2 Typical subsequent return stroke current at ground. The three current components of the model are also indicated..... 150

3.3 Electric and magnetic fields produced by a typical subsequent return stroke at a distance of 3 km from the channel at an altitude of 10 m..... 152

3.4 Example of a piecewise linear vertical electric field due to a return stroke..... 156

3.5 Piecewise-linear version of the vertical electric field given in Figure 3.3 and the derived horizontal field for $\varepsilon_r = 10$ and $\sigma = 10^{-3}$ mhos/m..... 162

3.6 Piecewise-linear version of the vertical electric field calculated at 100 km and extrapolated to 3 km and the derived horizontal field for $\varepsilon_r = 10$ and $\sigma = 10^{-3}$ mhos/m..... 164

3.7 Piecewise-linear version of the magnetic field given in Figure 3.3 and the derived horizontal electric field for $\varepsilon_r = 10$ and $\sigma = 10^{-3}$ mhos/m..... 167

3.8 The two conductor test-line above a perfectly conducting earth..... 173

3.9 Solution scheme for the coupled set of first-order transmission-line equations..... 186

3.10 Circuit diagram for a single-conductor line above a ground plane. To solve the Telegrapher's Equations for the scattered voltage and current in the line the horizontal electric field is required at all points along the line and the vertical electric is needed only at the ends..... 191

4.1 Calculated voltage waveforms at the North end of the 500 m overhead line for lightning 200 m from the line for $\sigma = 10^{-2}$ mhos/m and $\varepsilon_r = 15$. The solid lines represent the calculated waveforms when the line is open-circuited at both ends. The dotted lines represent the calculated waveforms for the line terminated in 500 Ω at each end. The factor 'x a' on any waveform indicates that the waveform shown is 'a' times the actual waveform. The ground strike points are indicated by asterisks (*)..... 197

4.2 Calculated voltage waveforms at the North end of the 500 m overhead line for lightning 200 m from the line for $\sigma = 10^{-3}$ mhos/m and $\varepsilon_r = 8$. The solid lines represent the calculated waveforms when the line is open-circuited at both ends. The dotted lines represent the calculated waveforms for the line terminated in 500 Ω at each end. The factor 'x a' on any waveform indicates that the waveform shown is 'a' times the actual waveform. The ground strike points are indicated by asterisks (*)..... 199

4.3 Calculated voltage waveforms at the North end of the 500 m overhead line for lightning 200 m from the line for $\sigma = 10^{-4}$ mhos/m and $\varepsilon_r = 3$. The solid lines represent the calculated waveforms when the line is open-circuited at both ends. The dotted lines represent the calculated waveforms for the line terminated in 500 Ω at each end. The factor 'x a' on any waveform indicates that the waveform shown is 'a' times the actual waveform. The ground strike points are indicated by asterisks (*)..... 201

4.4 Calculated voltage waveforms at the North end of the 500 m overhead line for lightning 200 m from the line for $\sigma = 10^{-5}$ mhos/m and $\varepsilon_r = 3$. The solid lines represent the calculated waveforms when the line is open-circuited at both ends. The dotted lines represent the calculated waveforms for the line terminated in 500 Ω at each end. The factor 'x a' on any waveform indicates that the waveform shown is 'a' times the actual waveform. The ground strike points are indicated by asterisks (*)..... 203

4.5 Calculated voltage waveforms at the North end of the 500 m overhead line for lightning 1 km the line for $\sigma = 10^{-2}$ mhos/m and $\varepsilon_r = 15$. The solid lines represent the calculated waveforms when the line is open-circuited at both ends. The dotted lines represent the calculated waveforms for the line terminated in 500 Ω at each end. The factor 'x a' on any waveform indicates that the waveform shown is 'a' times the actual waveform. The ground strike points are indicated by asterisks (*)..... 205

4.6 Calculated voltage waveforms at the North end of the 500 m overhead line for lightning 1 km from the line for $\sigma = 10^{-3}$ mhos/m and $\varepsilon_r = 8$. The solid lines represent the calculated waveforms when the line is open-circuited at both ends. The dotted lines represent the calculated waveforms for the line terminated in 500 Ω at each end. The factor 'x a' on any waveform indicates that the waveform shown is 'a' times the actual waveform. The ground strike points are indicated by asterisks (*)..... 207

4.7 Calculated voltage waveforms at the North end of the 500 m overhead line for lightning 1 km from the line for $\sigma = 10^{-4}$ mhos/m and $\varepsilon_r = 3$. The solid lines represent the calculated waveforms when the line is open-circuited at both ends. The dotted lines represent the calculated waveforms for the line terminated in 500 Ω at each end. The factor 'x a' on any waveform indicates that the waveform shown is 'a' times the actual waveform. The ground strike points are indicated by asterisks (*)..... 209

4.8 Calculated voltage waveforms at the North end of the 500 m overhead line for lightning 1 km from the line for $\sigma = 10^{-5}$ mhos/m and $\varepsilon_r = 3$. The solid lines represent the calculated waveforms when the line is open-circuited at both ends. The dotted lines represent the calculated waveforms for the line terminated in 500 Ω at each end. The factor 'x a' on any waveform indicates that the waveform shown is 'a' times the actual waveform. The ground strike points are indicated by asterisks (*)..... 211

4.9 Calculated voltage waveforms at the North end of the 500 m overhead line for lightning 5 km from the line for $\sigma = 10^{-2}$ mhos/m and $\varepsilon_r = 15$. The solid lines represent the calculated waveforms when the line is open-circuited at both ends. The dotted lines represent the calculated waveforms for the line terminated in 500 Ω at each end. The factor 'x a' on any waveform indicates that the waveform shown is 'a' times the actual waveform. The ground strike points are indicated by asterisks (*)..... 213

4.10 Calculated voltage waveforms at the North end of the 500 m overhead line for lightning 5 km from the line for $\sigma = 10^{-3}$ mhos/m and $\varepsilon_r = 8$. The solid lines represent the calculated waveforms when the line is open-circuited at both ends. The dotted lines represent the calculated waveforms for the line terminated in 500 Ω at each end. The factor 'x a' on any waveform indicates that the waveform shown is 'a' times the actual waveform. The ground strike points are indicated by asterisks (*)..... 215

4.11 Calculated voltage waveforms at the North end of the 500 m overhead line for lightning 5 km from the line for $\sigma = 10^{-4}$ mhos/m and $\varepsilon_r = 3$. The solid lines represent the calculated waveforms when the line is open-circuited at both ends. The dotted lines represent the calculated waveforms for the line terminated in 500 Ω at each end. The factor 'x a' on any waveform indicates that the waveform shown is 'a' times the actual waveform. The ground strike points are indicated by asterisks (*)..... 217

4.12 Calculated voltage waveforms at the North end of the 500 m overhead line for lightning 5 km from the line for $\sigma = 10^{-5}$ mhos/m and $\varepsilon_r = 3$. The solid lines represent the calculated waveforms when the line is open-circuited at both ends. The dotted lines represent the calculated waveforms for the line terminated in 500 Ω at each end. The factor 'x a' on any waveform indicates that the waveform shown is 'a' times the actual waveform. The ground strike points are indicated by asterisks (*)..... 219

4.13 Calculated voltage waveforms for a 5 km line for lightning 200 m from the line for $\sigma = 10^{-2}$ mhos/m and $\varepsilon_r = 15$. The solid lines represent the voltage waveform calculated for point V_1; the dotted lines represent the voltage waveform calculated for point V_2. Waveforms marked 'x a' indicate that the waveform shown is 'a' times the actual waveform. The location of the ground strike points are indicated by asterisks (*)..... 225

4.14 Calculated voltage waveforms for a 5 km line for lightning 200 m from the line for $\sigma = 10^{-4}$ mhos/m and $\varepsilon_r = 3$. The solid lines represent the voltage waveform calculated for point V_1; the dotted lines represent the voltage waveform calculated for point V_2. Waveforms marked 'x a' indicate that the waveform shown is 'a' times the actual waveform. The location of the ground strike points are indicated by asterisks (*)..... 227

4.15 Calculated voltage waveforms for a 5 km line for lightning 1 km from the line for $\sigma = 10^{-2}$ mhos/m and $\varepsilon_r = 15$. The solid lines represent the voltage waveform calculated for point V_1; the dotted lines represent the voltage waveform calculated for point V_2. Waveforms marked 'x a' indicate that the waveform shown is 'a' times the actual waveform. The location of the ground strike points are indicated by asterisks (*)..... 229

4.16 Calculated voltage waveforms for a 5 km line for lightning 1 km from the line for $\sigma = 10^{-4}$ mhos/m and $\varepsilon_r = 13$. The solid lines represent the voltage waveform calculated for point V_1; the dotted lines represent the voltage waveform calculated for point V_2. Waveforms marked 'x a' indicate that the waveform shown is 'a' times the actual waveform. The location of the ground strike points are indicated by asterisks (*)..... 231

4.17 Comparisons between data and theory for the first stroke in the 170455 UT flash during run #79199TR31 located at a range of 10.7 km and bearing of 8° from the North end of the line at which the voltage is measured. The top two traces are the measured vertical electric field and the calculated horizontal electric field for $\sigma = 10^{-5}$ mhos/m and $\varepsilon_r = 3$. The remaining traces show the measured voltage waveform (V_{meas}) and the calculated voltages when the South end is open-circuited (V_{OC}), short circuited to the 60 Ohm ground rod (V_{SC}), and terminated in 500 Ohms (V_M)..... 238

4.18 Comparisons between data and theory for the first stroke in the 171407 UT flash during run #79199TR31 located at a range of 13.6 km and bearing of 53° from the North end of the line at which the voltage is measured. The top two traces are the measured vertical electric field and the calculated horizontal electric field for $\sigma = 10^{-5}$ mhos/m and $\varepsilon_r = 3$. The remaining traces show the measured voltage waveform (V_{meas}) and the calculated voltages when the South end is open-circuited (V_{OC}), short circuited to the 60 Ohm ground rod (V_{SC}), and terminated in 500 Ohms (V_M)..... 240

4.19 Comparisons between data and theory for the first stroke in the 184600 UT flash during run #79199TR31 located at a range of 1.2 km and bearing of 82° from the North end of the line at which the voltage is measured. The top two traces are the measured vertical electric field and the calculated horizontal electric field for $\sigma = 10^{-5}$ mhos/m and $\varepsilon_r = 3$. The remaining traces show the measured voltage waveform (V_{meas}) and the calculated voltages when the South end is open-circuited (V_{OC}), short circuited to the 60 Ohm ground rod (V_{SC}), and terminated in 500 Ohms (V_M)..... 242

4.20 Comparisons between data and theory for the second stroke in the 190004 UT flash during run #79196TR27 located at a range of 5.5 km and bearing of 92° from the North end of the line at which the voltage is measured. The top two traces are the measured vertical electric field and the calculated horizontal electric field for $\sigma = 10^{-5}$ mhos/m and $\varepsilon_r = 3$. The remaining traces show the measured voltage waveform (V_{meas}) and the calculated voltages when the South end is open-circuited (V_{OC}), short circuited to the 60 Ohm ground rod (V_{SC}), and terminated in 500 Ohms (V_M)..... 244

4.21 Comparisons between data and theory for the first stroke in the 185842 UT flash during run #79196TR27 located at a range of 5.8 km and bearing of 104° from the North end of the line at which the voltage is measured. The top two traces are the measured vertical electric field and the calculated horizontal electric field for $\sigma = 10^{-5}$ mhos/m and $\varepsilon_r = 3$. The remaining traces show the measured voltage waveform (V_{meas}) and the calculated voltages when the South end is open-circuited (V_{OC}), short circuited to the 60 Ohm ground rod (V_{SC}), and terminated in 500 Ohms (V_M)..... 246

4.22 Comparisons between data and theory for the second stroke in the 220319 UT flash during run #79208TR44 located at a range of 10.2 km and bearing of 175° from the North end of the line at which the voltage is measured. The top two traces are the measured vertical electric field and the calculated horizontal electric field for $\sigma = 10^{-5}$ mhos/m and $\varepsilon_r = 3$. The remaining traces show the measured voltage waveform (V_{meas}) and the calculated voltages when the South end is open-circuited (V_{OC}), short circuited to the 60 Ohm ground rod (V_{SC}), and terminated in 500 Ohms (V_M)..... 248

A.1 Definition of the geometrical factors used in the derivation of the electric and magnetic fields at any arbitrary point due to a current carrying dipole at the origin..... 262

B.1 Vertical electric field change associated with the 185337 flash during run #79196TR27. The FM channel record has a sensitivity of 1.1 kV/m per division and the direct channel 90 V/m per division. Both traces are 100 ms full-scale..... 271

B.2 Location of the ground strike point of the 185337 flash during run #79196TR27..... 273

B.3 Simultaneous records of the induced voltage on the test-line and the vertical electric field for the return stroke at 185337 during run #79196TR27. The voltage scale is 65 kV/division and the vertical electric field 440 V/m per division. Both records are 200 μs full-scale. The voltage record is obtained from the direct channel and hence produces an accurate response for only about 50 μs..... 275

B.4 Stepped leader induced voltages and simultaneously recorded vertical electric field for the 185337 flash during run #79196TR27. The top two traces are 8 μs/division, the bottom two traces 4 μs/division. The voltage scale is 6.5 kV per division, the vertical electric field 18/Vm per division..... 227

D.1 Distribution of first return stroke peak induced voltage on the test-line during run #79220TR57 for times between 184000 UT and 201000 UT..... 316

LIST OF TABLES

Table		Page
2.1	Parameters of interest for the unenergized test-line	25
2.2	Summary of the values of the vertical electric field initial radiation peak and peak test-line voltage obtained from oscillograms made via Biomation waveform recorders and replay of instrumentation tape records for the flash at 190610 UT during run #79196TR27	55
2.3(a)	List of flashes studied in this thesis from thunderstorms on July 15, 1979, run #79196TR27, and salient measurements made from the vertical electric field and induced voltage records. The location of the ground strike point from the Mobile Lightning Laboratory is given. The letter F or S given with each stroke number indicates whether the stroke has been classified as a first (F) or as a subsequent (S) stroke	57
2.3(b)	List of flashes studied in this thesis from thunderstorms on July 18, 1979, run #79199TR31, and salient measurements made from the vertical electric field and induced voltage records. The location of the ground strike point from the Mobile Lightning Laboratory is given. The letter F or S given with each stroke number indicates whether the stroke has been classified as a first (F) or as a subsequent (S) stroke	63
2.3(c)	List of flashes studied in this thesis from thunderstorms on July 27, 1979, run #79208TR44, and salient measurements made from the vertical electric field and induced voltage records. The location of the ground strike point from the Mobile Lightning Laboratory is given. The letter F or S given with each stroke number indicates whether the stroke has been classified as a first (F) or as a subsequent (S) stroke	66
2.4	Summary of flash statistics from selected studies	91

2.5 Summary of return stroke vertical electric field statistics from selected studies..... 111

2.6 Summary of induced voltage statistics..... 127

Abstract of Dissertation Presented to the Graduate Council of the University of Florida in Partial Fulfillment of the Requirements for the Degree of Doctor of Philosophy

LIGHTNING INDUCED VOLTAGES ON POWER LINES: THEORY AND EXPERIMENT

By

Maneck Jal Master

August 1982

Chairman: Martin A. Uman
Major Department: Electrical Engineering

In this thesis we present the first measurements of simultaneously recorded lightning return stroke vertical electric field and induced voltage on a power line. Data are given for about 100 first strokes and over 200 subsequent strokes with the lightning ground strike point located by a combination of a TV network, thunder ranging, and observer comments. Voltages were measured at one end of a 460 m distribution line which was specially constructed for the experiment. The voltage and vertical electric field time-domain signals are recorded on film from oscilloscope faces and on magnetic instrumentation tape with an effective frequency response from less than 1 Hz to over 1 MHz. The measured voltage waveforms do not resemble the "classical induced positive surge" described in the literature. Both the magnitude and polarity of the induced voltages

are found to be strong functions of the location of the lightning ground strike point.

Theory is presented which predicts induced surges of both polarities, as measured. First, the return stroke horizontal electric field associated with a finite ground conductivity is derived from the measured vertical electric field. Then, the Telegraphers' Equations are solved by computer using the vertical and horizontal electric fields as forcing functions to predict the line voltages. Calculated voltage waveforms are presented for a 500 m line and for a 5 km line for earth conductivities ranging from 10^{-2} mhos/m to 10^{-5} mhos/m, earth permittivities ranging from $\varepsilon_r = 15$ to $\varepsilon_r = 3$, and lightning ground strike points ranging from 0.2 km to 5.0 km from the line.

Direct comparisons are made between the measured voltages on the 460 m line and calculated voltage waveforms. Calculated waveshapes are in moderately good agreement with the measurements. However, there is a consistent discrepancy in the magnitudes: the calculated values are about a factor of 4 lower than those measured. Possible errors in both theory and measurement are discussed. Where possible, comparisons are made between voltage measurements reported by other investigators and our theory.

In addition to the lightning return stroke data, we present the first stepped leader induced voltages correlated with stepped leader vertical electric fields. The voltages induced by stepped leaders on the 460 m test line are an order of magnitude lower than the voltage induced by the following return stroke.

CHAPTER I

REVIEW

1.1 Introduction

In this chapter a brief discussion of the lightning discharge process will be presented and the terminology used in this thesis will be defined. Attention will be focussed on the cloud-to-ground lightning discharge because it is this discharge which is of relevance to power line problems. The second half of the chapter will be devoted to a critical discussion of the work which has been done to date regarding the understanding of lightning induced voltages on power lines.

1.2 Lightning

1.2.1 The Thundercloud

The present discussion of the lightning discharge process is not intended to be complete or exhaustive; it is included here for the sake of completeness. The discussion presented here is more or less the consensus view of the discharge process. For a more detailed discussion, the reader may refer to several standard monographs, e.g., Malan (1963), Chalmers (1967), Uman (1969), and Golde (1977a). Lightning has been defined by Uman (1969) as "a transient,

high-current electric discharge, whose path length is generally measured in kilometers." The most common source of lightning is the electrical charge separation in the cumulonimbus cloud. All lightning discharges can be roughly divided into cloud discharges and ground discharges. Lightning discharges which take place entirely within a cloud, between two clouds, or between a cloud and the surrounding air are called cloud discharges or cloud lightning. Lightning discharges which take place between the cloud and the ground are referred to as cloud-to-ground discharges or ground lightning. The ratio of cloud lightning to ground lightning has been reported by Pierce (1970) and Prentice and Mackerras (1977) to be a function of the geographical latitude. Livingston and Krider (1978) have found that for individual storms, the ratio is a function of storm stage.

The mechanisms for charge separation in a thundercloud are not fully understood. Generally, thunderclouds are formed in an atmosphere with layers of cold dense air at higher levels and warm moist air at lower levels, giving rise to an unstable condition. This instability results in the warm air rising in a strong updraft, which in the presence of a temperature gradient and the gravitational field, is responsible for the formation of the thundercloud. Recent reviews of the proposed cloud electrification processes have been presented by Magono (1980) and Latham (1981).

The electrical configuration of a typical thundercloud is shown in Figure 1.1. Typically, the upper portion of the thundercloud carries a net positive charge (the P region), whereas there is a preponderance of negative charge in the lower portion (the N

Figure 1.1. Electrical configuration of a typical thundercloud; the bold dots represent the locations of the effective charge centers. (Adapted from Malan, 1963; and Uman, 1969)

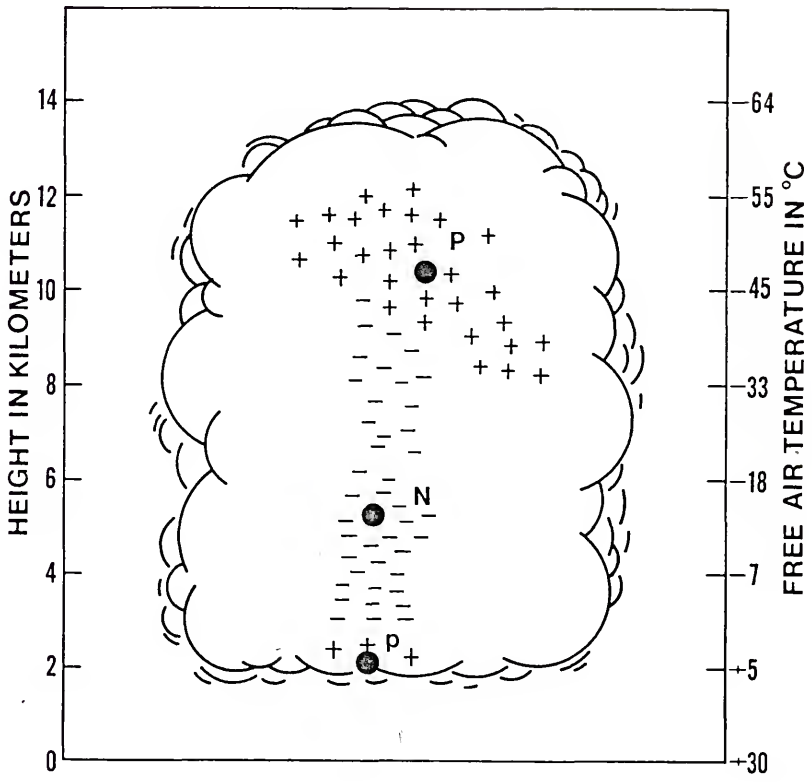
HEIGHT IN KILOMETERS
14
12
10
8
6
4
2
0
64
55
45
33
18
7
+5
+30
FREE AIR TEMPERATURE IN °C
P
N
p

region). In addition to these main charge centers, there is a small pocket of positive charge (the p region) at the base of the cloud. The basic electrical structure of the cloud was first determined from in-cloud measurements by Simpson and Scrase (1937). More recent studies reported by Huzita and Ogawa (1976) and by Winn et al. (1981) have confirmed the validity of this basic electrical structure, although it is now recognized that there may be large horizontal displacements, of the order of kilometers, between the P and N regions.

1.2.2 Ground Lightning

A typical cloud-to-ground discharge commences in the cloud, and eventually results in the neutralization of tens of coulombs of negative cloud charge. There is some disagreement on the exact nature and location of the process responsible for the origin of the ground discharge (e.g., Clarence and Malan, 1957; Rustan et al., 1980; Beasley et al., 1982). However, it is believed that the discharge is initiated by a preliminary breakdown within the cloud probably between either the N and p regions or the P and N regions shown in Figure 1.1. This preliminary breakdown sets the stage for electrons from the N region to be funneled away from the cloud and towards the ground in a series of faintly luminous steps. This phase of the discharge is the stepped leader. Photographic observations of stepped leaders give the typical duration as 1 μs for steps 40 to 80 m in length, with a pause time between steps of about 50 μsec. The total stepped leader process typically takes about 20 ms and results in the distribution of about 5 C of negative cloud charge along 5 km

of channel length from cloud-to-ground; the average downward velocity is about 2.5×10^5 m/sec. The stepped leader electric field records indicate a smooth transfer of charge from the cloud onto the channel, indicating that the stepping process itself is not associated with any appreciable lowering of charge.

When the leader gets within a few hundred to a few tens of meters of the ground, the electric field beneath it is high enough to cause the initiation of upward-moving discharges from objects on the ground, thereby commencing the attachment process. The attachment process is of considerable practical interest, especially to power engineers, since it determines the point at which the lightning strikes the transmission or distribution lines. The height of the leader above ground at the time when the attachment process begins is defined as the "striking distance" of the lightning, a parameter which has assumed importance in the study of direct lightning strikes to power lines. The concept of striking distance has been discussed in detail in Chapter 17 of Golde (1977b).

When one of the upward-moving discharges contacts the downward-moving leader, typically some tens of meters above ground, it initiates the return stroke phase. The first return stroke propagates up the previously ionized leader path, and is typically associated with a peak current of 30 kA at ground level. The return stroke wavefront travels up the channel at about one-third the speed of light, making the trip from the ground to the cloud in about 100 μs, neutralizing some or all of the charge stored on the stepped leader channel. The rapid release of the return stroke energy heats the channel to about 30,000°K, generating a high-

pressure channel which expands against the atmospheric pressure. This rapid expansion creates a shock wave which eventually becomes thunder.

After the return stroke current has ceased to flow, the flash may end. However, if any additional charge is made available at the top of the channel through J- or K-processes, a dart leader may propagate down the residual channel. A typical dart leader travels continuously down the channel at an average velocity of 3×10^6 m/sec, and lowers about 1 C of charge into the channel. The dart leader then initiates a subsequent return stroke, the leader return stroke combination occurring three or four times during a typical flash. Data reported by Weidman and Krider (1980) indicate that a typical subsequent stroke current has a smaller peak current, about 15 kA, faster zero-to-peak risetime, but similar maximum rate-of-change of current as a typical first return stroke.

A dart leader may not always be able to make its complete trip from cloud to ground down the defunct stepped leader channel. In fact, there is a significant percentage of leaders which begin as dart leaders, but become stepped leaders close to the ground. These leaders are known as dart-stepped leaders. The average return stroke initiated by a dart-stepped leader would be expected to have a peak current which lies between the 30 kA value for an average first stroke and the 15 kA value for an average subsequent stroke, as discussed above. It is therefore not very clear whether subsequent strokes initiated by dart-stepped leaders should be classified as first strokes or as subsequent strokes. Historically, the term "first stroke" has been used to denote only the very first stroke in

a flash, and statistical distributions for various parameters associated with return strokes have been investigated under this assumption. However, if the conversion of the dart leader to a stepped leader takes place sufficiently high in the cloud the location of the ground strike point due to the new channel may differ from that of the previous channel by distances of the order of kilometers. The TV pictures for data presented in this thesis for such cases show completely different channels below the Florida cloud base, typically about 1 km. It is generally believed that the initial portions of the vertical electric and horizontal magnetic fields produced by the return stroke are due to the bottom 1 km or less of the cloud to ground channel. Furthermore, a new channel to ground involves a new attachment process which is of prime importance in studies involving overhead power lines. For these reasons, in this thesis all "subsequent" strokes which exhibit completely different channels on the TV pictures are treated as first strokes. However, to facilitate comparisons with extant data, these "first strokes" will be clearly labeled when data are being presented.

The time interval between strokes is typically 40 ms. However, the interstroke interval may be tenths of a second if a continuing current flows in the channel after the stroke. Continuing currents represent direct charge transfer between cloud and ground and are of the order of 100 A. From a study of five storms, Livingston and Krider (1978) report that 29% to 46% of all ground flashes in Florida have a continuing current component.

We have discussed the cloud to ground discharge as being initiated by a downward-moving negatively charged leader. A ground

discharge of this type is called a negative ground flash. A typical negative ground flash lasts about 0.5 seconds and has three or four return strokes. However, cloud-to-ground lightning may also be initiated by a downward-moving positive discharge. Positive ground flashes are rare in Florida. Positive flashes have larger peak currents and charge transfers than negative flashes, and rarely have multiple strokes (Berger et al., 1975; Brook et al., 1982). In addition, cloud-to-ground discharges may be initiated by upward-going positively- or negatively-charged leaders. In this thesis the negative ground flash is the only type of cloud-to-ground discharge that we will consider. Hence the phrase "ground flash" will be used to mean a negative ground flash initiated by a downward moving leader.

1.2.3 Cloud Discharge

Cloud discharges occur between negative and positive charge centers in the same cloud, or between two clouds or between cloud and the surrounding air. A typical cloud flash lasts about 0.5 msec, has a path length between 5 and 10 km, and results in the neutralization of 10 to 30 coulombs of charge. The discharge is believed to be initiated by a continuously propagating leader which generates 5 to 6 weak return strokes known as recoil streamers or K-changes when the leader contacts pockets of charge opposite its own. Cloud discharges have not been as extensively studied as cloud to ground discharges. In the context of power line protection, cloud discharges have always been assumed to produce negligible effects. However, it is important to keep in mind that ground lightning has significant in-cloud

components and hence may share many common features with cloud lightning.

1.3 Induced Overvoltages

Lightning is responsible for a significant percentage of all disruptions in the electrical power transmission and distribution network. In fact, the details of the disruptive mechanism have been the subject of research for almost eighty years, as we shall discuss below.

Lightning overvoltages on power lines may be grouped into two categories: (1) voltages caused by the lightning current injection due to direct strikes to phase wires, ground wires, or towers; and (2) voltages due to the coupling of lightning generated electromagnetic fields emanating from nearby lightning which does not physically contact any part of the power system, often referred to as an indirect strike or induced effect. In the present thesis, we consider only the voltages induced on the line by nearby lightning.

Perhaps the earliest attempt at studying lightning induced voltages on overhead lines was due to K. W. Wagner (1908). According to him the electrical charge was induced by a thundercloud on an overhead line which was electrostatically held at ground potential due to leakage over insulator strings and grounding of transformer neutrals. When the cloud was discharged by lightning, the bound charge on the line was released, giving rise to traveling waves on the line.

Adendorff (1911) presented an excellent discussion on the various power line problems created by lightning. Using some very simple models, he calculated the potential difference between cloud and ground to be about 2.6×10^7 V for a cloud height of 5 miles. He also noted that overhead ground wires solidly earthed to ground at the poles would greatly reduce the effects due to a direct strike on the line, the effect being "entirely preventative and not curative." The following quotation on page 166 of Adendorff (1911) reflected the consensus view at that time vis-a-vis direct lightning strikes to lines: "If the discharge is very heavy, as usually is the case, the probabilities are that a portion of the section struck will completely disappear . . . ."

In the earlier years of research, it was believed that the power line should be protected from induced surges, the implication being that not much could be done in the case of direct strikes. However, as power transmission expanded, so did the disruption and damage due to direct lightning strokes. Thus, it is not surprising that during the late 1920s and 1930s various theoretical and experimental studies were undertaken to study the mechanism and effects of direct lightning surges on power transmission lines, e.g., Cox et al. (1927), Fortescue et al. (1929), Cox and Beck (1930), Lewis and Foust (1930), Bewley (1931), Peek (1931), Rendell and Gaff (1933), Perry (1941), and Perry et al. (1942).

As the understanding of direct strikes to lines increased, and lines were adequately protected against them, attention was again shifted to the consideration of induced voltages. The most significant of the early research on induced overvoltages is due to Wagner

and McCann (1942). They considered most of the essential features of the discharge process including the effects due to the return stroke channel. Using very simple models, they showed that induced effects due to cloud flashes were negligible, whereas induced voltages due to close ground lightning have an appreciable magnitude.

Szpor (1948) calculated the induced voltage on the line caused by a nearby lightning stroke. However, according to his own estimates, the quasi-static nature of his solution restricted the applicability of his results to points within about 100 m of the lightning discharge.

A comparison of the frequencies of occurrence of surges due to direct strikes and those due to induced effects was made by Golde (1954) for various types of overhead lines. He used more refined models for his processes: (a) channel charge was exponentially distributed by the leader; (b) charge neutralization by the return stroke did not take place instantaneously, but took some finite time due to the charge stored on the corona sheath; and (c) velocity of the return stroke was assumed to decrease exponentially with height. The detailed theory used in his calculations was presented in an earlier paper by Bruce and Golde (1941).

Lundholm (1957) developed explicit expressions for induced voltages based on the simple model described by Wagner and McCann (1942). He used the concept of retarded potentials, thereby avoiding the quasi-static solution due to Szpor (1948). He derived independent expressions for the scalar potential in terms of the charge on the channel and the vector potential in terms of the assumed channel current. However, his final results for these potentials fail to

satisfy the Lorentz Condition as dictated by his equations and are hence in error.

Rusck (1958) developed expressions for the induced voltage on multi-conductor lines. He found that the induced voltage on any one conductor was not influenced by the presence of other conductors--a surprising result. Further, his theoretical analysis followed that due to Lundholm (1957) and was therefore in error.

In Wagner and McCann (1942), the authors argue that the voltages induced on an overhead power line by all phases of ground lightning, except the return stroke, are insignificant, because only "during the progress of the return streamer, the rates of field change with time are sufficient to induce a voltage." Owa (1964) calculated the induced voltage on a power line due to a stepped leader. Using the stepped leader mechanism proposed by Griscom (1958) and Griscom et al. (1958), which gives the stepped leader current as 100 kA, and using a theoretical method of solution parallel to that given by Lundholm (1957) and Rusck (1958) , he found peak induced voltages of about 1 MV produced by the stepped leader for a line height of about 10 meters. However, currents derived from measured electric field waveforms by Krider and Radda (1975) and Krider et al. (1977) indicate that the peak stepped leader current is of the order of 1 kA. Further, measurements of induced voltages on power lines reported in the literature have never approached the order of magnitude calculated by Owa (1964), indicating that the theory of Griscom (1958) is in error. The first data on simultaneously recorded stepped leader vertical electric field and induced test-line

voltage are presented in Appendix B and do not support the theoretically deduced values of Owa (1964).

A mathematical determination of the induced voltage on a power line was the highlight of the Ph.D. dissertation of Chowdhuri (1966). Contrary to the findings of Rusck (1958), he reported that the induced voltage on a conductor of a multi-conductor line was influenced by the presence of other conductors. Chowdhuri and Gross (1969) reported that induced voltage was higher in the presence of other conductors and could be determined from a consideration of their mutual coupling. However, his derivation of the lightning fields followed that due to Lundholm (1957) and was therefore also incorrect.

Another theoretical treatise on induced voltages on overhead lines was presented by Singarajah (1971). He used the old model of Wagner and McCann (1942) but included the effect of the upward-going streamer on the return stroke. He plotted the induced voltage waveforms from his equations, using various parameters. He found that the voltage on any one conductor was not affected by the presence of other insulated conductors of a multi-conductor line. However, the presence of a grounded earth wire was found to reduce the induced voltage on the line by about 10% to 25%.

An experimental program initiated by the South African National Electrical Engineering Research Institute (NEERI) involves the measurement of lightning overvoltages on a specially constructed, unenergized, 9.9 km, 3-phase, 11 kV distribution line. However, no attempts have been made to simultaneously record the electric and magnetic fields due to lightning. A description of the test-line and

some of the preliminary results on measured overvoltages were presented by Eriksson and Meal (1980). They reported measurements of 100 oscillograms with a median value of 25 kV for voltages induced on the line due to nearby lightning. These measurements were obtained as triggered records with a threshold of 12 kV. In more recent reports, Eriksson et al. (1982) and Eriksson and Meal (1982) give a distribution of 300 overvoltages measured on their line. For 32 "good quality overvoltage recordings" the mean was 45 kV with a standard deviation of 35 kV. The maximum measured surge is 300 kV which is also the Basic Insulation Level (BIL) of the line. Typical measured overvoltages are shown and comparisons are made with theoretically calculated waveshapes based on the incorrect derivation due to Rusck (1958).

In 1973, a new facility to study artificially triggered lightning was built by various cooperating agencies in France. A description of their main facility at St. Privat d'Allier has been given by Fieux et al. (1978). As part of the program two overhead lines were built: one a telecommunications line, 2.1 km in length, and the other a 260 m medium voltage power line. Both lines were terminated at either end in resistances equal to their respective characteristic impedances. Hamelin et al. (1979) reported that for triggered lightning, an average peak voltage of about 1 kV was measured on the telecommunications line at one end, the lightning being 1.4 km from the other end. Recordings made at one end of the medium voltage line have an average peak of 74 kV, the distance to the lightning being 50 m from the other end. The analytical result derived for the electric and magnetic fields produced by a vertical

dipole is essentially correct. However, their theoretical analysis suffers because they use a very simplified return stroke model current with a double exponential waveshape. More recently, attempts have been made to incorporate the effects of an imperfectly conducting ground plane into the theory by Leteinturier et al. (1980) and Djebari et al. (1981). Though the theory presented appears to be correct, the lightning fields are computed from the same simple but incorrect model. Further, due to computation problems, the calculations are performed only for times greater than 2 μs, when the field variation is relatively slow. Thus, computed results for the first two microseconds are not available, although the fast changes occurring within this period may be of prime importance in power-line coupling.

Prior to 1980, all the theories put forth to explain power-line voltages induced by nearby lightning were based on the premise that the induced line voltage is dependent only on the vertical electric field due to lightning. Since the vertical electric field at the ground due to a negative return stroke is negative (see Appendix A), it follows that the induced line voltage would have a positive polarity. Thus, we have the classical assumption that induced surges on lines have a positive polarity. On the other hand, if a negative return stroke terminates directly on the line, it produces a negative current injection and hence a negative voltage surge. Based on this dichotomy alone, measured surges on single phase lines have often been classified into direct and induced surges.

However, results from a recent Japanese study presented by Koga et al. (1981) show measurements of induced surges of negative

polarity as well. Simultaneously measured waveforms for induced voltage on a 1 km line indicate a surge of negative polarity at one end and another of positive polarity at the other end. The theory presented by Koga et al. (1981) uses the incorrect model presented by Chowdhuri (1966). However, their theoretical derivation of the horizontal electric field due to a finite earth conductivity appears to be essentially correct and is similar to the formulation which will be adopted in this thesis. Further, lack of any simultaneous records of lightning fields and induced voltages correlated with the ground strike point prevented them from making any direct comparisons between their theory and data.

The experimental data recorded during the summer of 1979 and presented in this thesis show that the induced voltage on the 460-meter unenergized test-line may be of positive or of negative polarity depending on the location of the ground strike point. Further, it will be shown theoretically that the induced voltage on the line is not produced by the vertical electric field coupling alone: the horizontal electric field resulting from a finite ground conductivity must also be taken into account, since the voltage produced by it may dominate that due to the vertical electric field.

Coupling of incident electromagnetic fields to overhead conductors has been studied by various groups studying the effects of the Nuclear Electromagnetic Pulse (NEMP) on overhead conductors. Formulations of the transmission line equations involving a horizontal electric field have been discussed by Smith (1977) and Vance (1978) among others. A complete formulation of the general problem in the time domain has been presented by Agrawal et al. (1980). The

solution scheme outlined by Agrawal et al. (1980) will be used in this thesis. The complexity involved in applying this type of formulation to lightning will be indicated.

CHAPTER II

EXPERIMENTAL RESULTS

2.1 Introduction

In the first part of this chapter, a complete description of the experimental setup will be given. The systems used to record the vertical electric and the horizontal magnetic fields produced by lightning will be described. The specifications to which the unenergized test-line was built, the apparatus used to measure the voltage, and the various systems used to locate the ground strike point, or points, of a lightning ground flash will be discussed.

In the second half of this chapter, data on induced test-line voltages will be presented together with the simulaneously measured vertical electric field due to lightning return strokes. From the analysis of the vertical electric field records it will be established that the lightning return stroke sample being considered is not unusual and is similar to other observations of lightning, both in Florida and around the world. Finally, the new findings with regard to the measured line voltages will be presented. Data obtained from simultaneous records of line voltage and vertical electric field due to the lightning stepped leader, which precedes the first return stroke, will be discussed in Appendix B.

2.2 Experimental Environment

The Mobile Lightning Laboratory (MLL) was housed inside a 12 m long trailer which was located near Wimauma, in the Tampa Bay area of Florida and southeast of Tampa. The Unenergized Test Line (UTL) was located 160 m to the south of the MLL. A network of five remotely switchable TV cameras was located over an area of roughly 60 km^2 around the MLL. One of the five TV cameras, a still camera, and a dynamic thunder-sensing microphone were located at the MLL site. The geographical locations of the TV cameras and their fields of view, the MLL, and the UTL, are shown in Figure 2.1. For measurement accuracy and personal safety a "true" ground plane, 60 m in diameter, was built from a wire mesh and buried in the ground beneath the MLL. At various points, 3 m ground rods were sunk vertically into the ground, with a 15 m rod at the center of the mesh. The effective resistance of this ground plane was less than 1 Ohm. The MLL was bonded to this ground plane, as was the distribution transformer which supplied power to the MLL. A shallow trench was dug over the distance from the UTL to the MLL, and all measurement cables were buried in this trench. Figure 2.2 shows a sketch of the MLL and the UTL to scale, and Table 2.1 lists some of the important parameters of the line.

2.3 Data Acquisition Systems

The purpose of the research reported in this thesis was not to collect voluminous data on induced line voltages but rather to

Figure 2.1. The TV network used for location of the ground strike point. The shaded cones indicate the field of view for each TV in degrees, 0° being North.

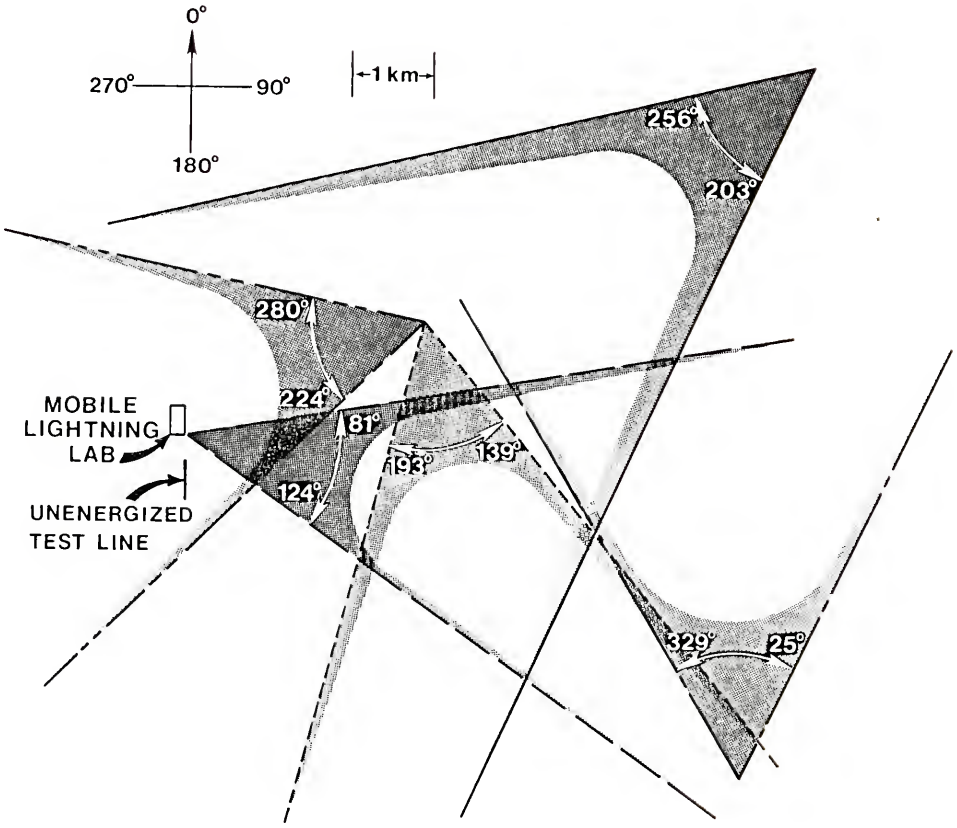
0°
270°
90°
180°
1 km
256°
203°
280°
224°
81°
93°
39°
124°
MOBILE
LIGHTNING
LAB
UNENERGIZED
TEST LINE
329°
25°

Figure 2.2. Detailed sketch of the experimental test-line. Important parameters are listed in Table 2.1.

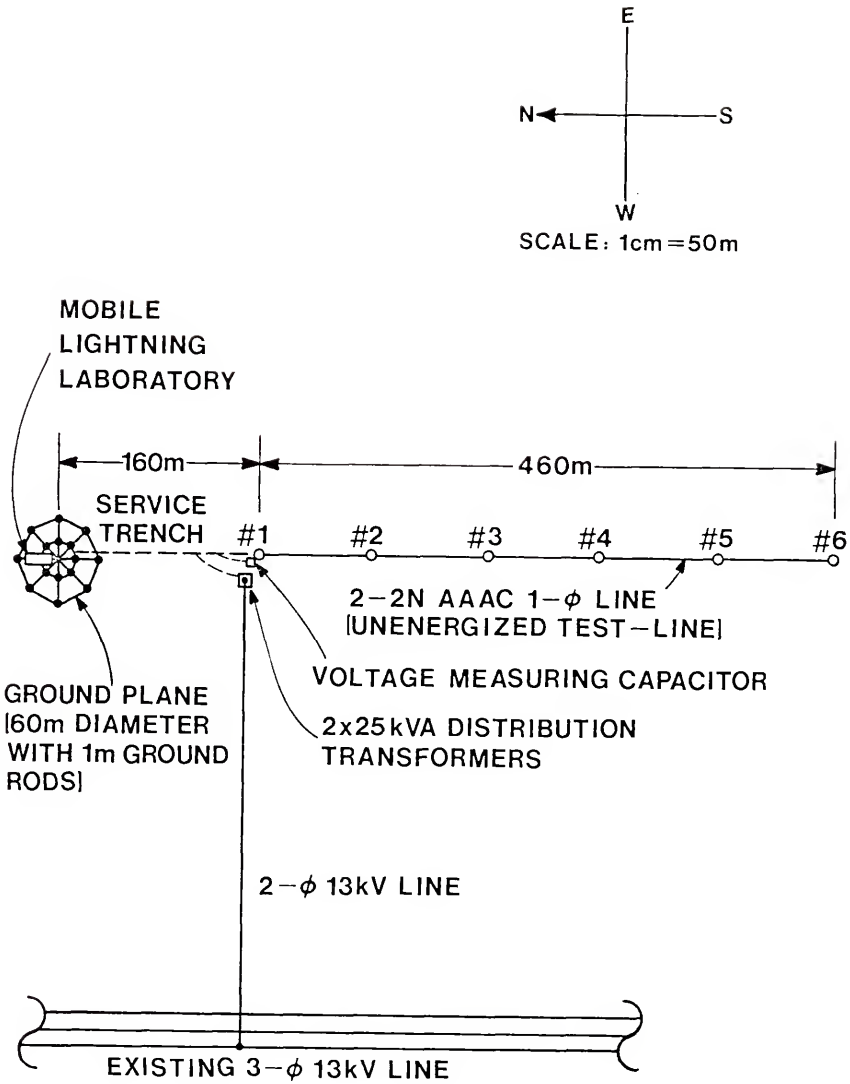
E
N
S
W
SCALE: 1cm=50m
MOBILE
LIGHTNING
LABORATORY
160m
460m
SERVICE
TRENCH
#1
#2
#3
#4
#5
#6
2−2N AAAC 1−φ LINE
(UNENERGIZED TEST−LINE)
VOLTAGE MEASURING CAPACITOR
2x25kVA DISTRIBUTION
TRANSFORMERS
GROUND PLANE
(60m DIAMETER
WITH 1m GROUND
RODS)
2−φ 13kV LINE
EXISTING 3−φ 13kV LINE

Table 2.1. Parameters of interest for the unenergized test-line.

(A) Unenergized Test Line (UTL) heights in meters. Poles are 12 meters high.

	POLE #1	MS+	POLE #2	MS+	POLE #3	MS+	POLE #4	MS+	POLE #5	MS+	POLE #6
PRIMARY	10.5	9.6	10.3	9.5	10.3	9.6	10.4	9.7	10.4	9.3	9.9
NEUTRAL	8.6	7.4	7.9	7.2	7.9	7.3	8.1	7.5	8.1	7.1	7.9

+Midspan

(B) Ground resistances:

Pole #1: 20 ohms
Pole #6: 60 ohms {12 mm diameter, 12 m long, vertical driven rods}

(C) Diameter of phase/neutral conductor = 8 mm.

correlate the voltage measurements with the electromagnetic field produced by the lightning together with the location of the ground strike point. Thus, there are three pieces of information which make up the complete data set: the fields produced by lightning, the induced line voltage, and the location of the ground strike point.

2.3.1 Field Measurements

Simultaneous measurements of the lightning fields and the induced line voltages were made on two separate systems: one continuous and one triggered. A schematic diagram of the complete recording system is shown in Figure 2.3.

The electric field sensing was done by three circular flat-plate antennas one having an area of 0.5 m^2 and two an area of 0.2 m^2 each. The antenna outputs, which give the derivative of the electric field, were electronically integrated and recorded either on 35 mm film or on an analog 7-channel Ampex FR-1900 Instrumentation Tape Recorder (ITR), at a speed of 120 ips. The 0.5 m^2 antenna and one of the 0.2 m^2 antennas were followed by integrators and amplifiers to provide four channels of electric field signals with a 3 db bandwidth from 0.03 Hz to 1 MHz and an 80 db dynamic range, covering electric field strengths from 4 V/m to 40,000 V/m. These signals were recorded in FM mode on channels 1 through 4 of the ITR, with a record/reproduce bandwidth from dc to 500 kHz (-6 db). The third antenna (area = 0.2 m^2) was also followed by an integrator and amplifier and provided two channels of electric field signals with a 3 db bandwidth from 160 Hz to 2 MHz and 40 db dynamic range. These two channels were normally recorded in direct mode on channels 5 and

Figure 2.3. Schematic diagram of the recording systems used inside the Mobile Lightning Laboratory to record the electric and magnetic fields due to lightning, the test-line voltage, and time and thunder signals.

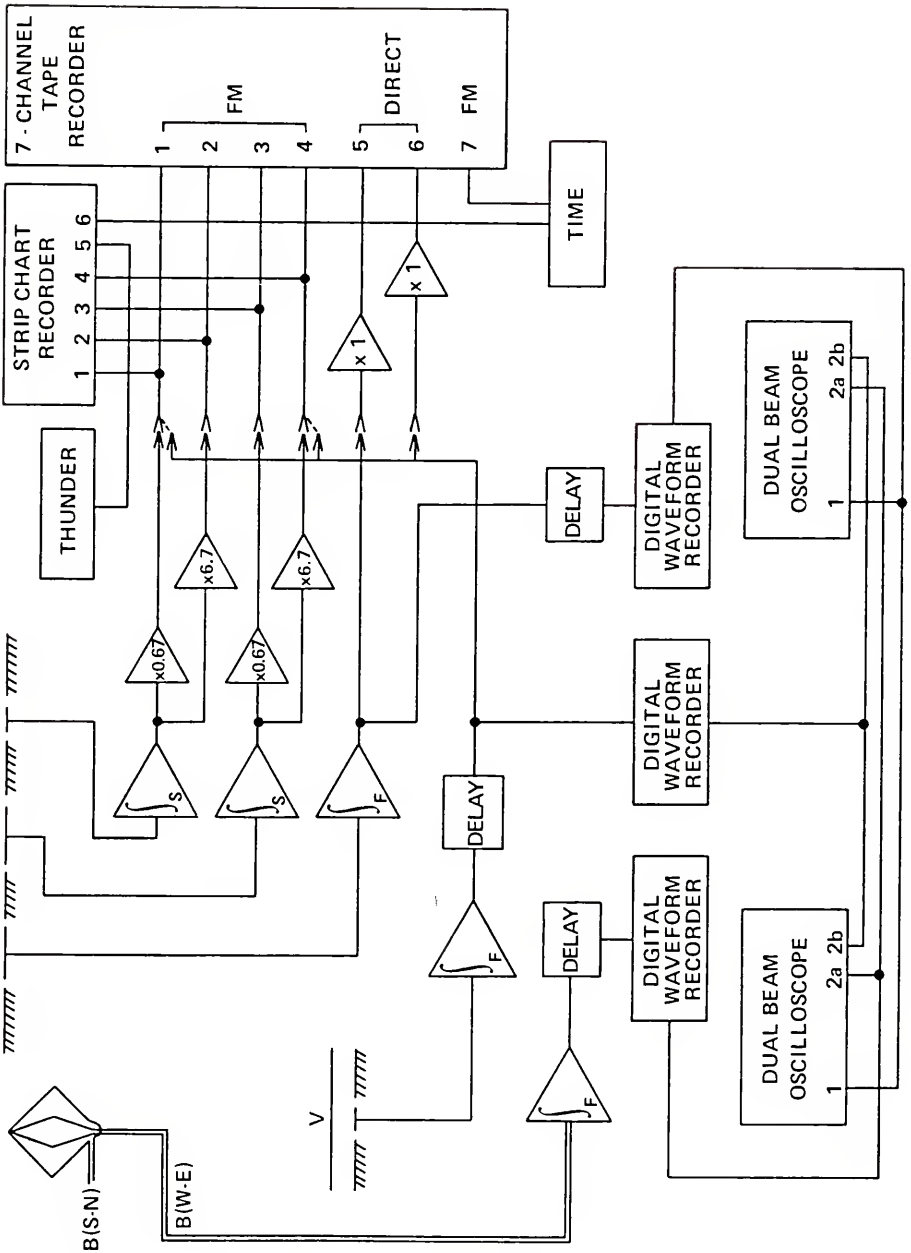
7 - CHANNEL TAPE RECORDER
1
2
FM
3
4
5
DIRECT
6
7 FM
STRIP CHART RECORDER
1 2 3 4 5 6
TIME
THUNDER
x 1
x 1
x6.7
x6.7
x0.67
x0.67
E1
E2
E3
B(S-N)
B(W-E)
V
DELAY
DELAY
DELAY
DIGITAL WAVEFORM RECORDER
DIGITAL WAVEFORM RECORDER
DIGITAL WAVEFORM RECORDER
DUAL BEAM OSCILLOSCOPE
1
2a 2b
DUAL BEAM OSCILLOSCOPE
1
2a 2b

6 of the ITR, with a 3 db bandwidth from 400 Hz to 1.5 MHz. However, for the purpose of this experiment the electric field signal was recorded only on channel 5. The input to direct channel 5 of the ITR was connected in parallel to the input of the Biomation 805 Digital Waveform Recorder (DWR). The DWR was triggered off the initial portion of the return stroke field and delayed by a pre-set amount in order to display the complete waveform on two different gain settings of the top traces of two Textronix 555 dual-beam oscilloscopes. The lower beams were chopped and used to display the W-E component of the magnetic field and the UTL voltage, as discussed later. The oscilloscopes were fitted with cameras loaded with film which was moved vertically past the screens at a linear speed of about 5 cm/s, perpendicular to the beam sweep direction, so that a permanent, spatially-separated record of the waveforms of each individual return stroke is obtained. The oscilloscope time base was generally set to 200 μs full-scale. The effective 3 db bandwidth of these records was from 160 Hz to 2 MHz.

Inputs to FM channels 1 through 4 of the ITR were connected in parallel to channels 1 through 4 of a Gould Brush Strip Chart Recorder (SCR) with a bandwidth from dc to 100 Hz. The chart speed was either 5 mm/s or 25 mm/s. Timing and thunder records were also displayed on the SCR, as discussed later.

The sensing of the magnetic fields due to lightning was accomplished using a system of two vertical orthogonal loops mounted on top of the MLL and directionally aligned to sense the S-N and W-E components of the horizontal magnetic field. The signals from the loop antennas were integrated and amplified with a 3 db bandwidth

from 1 kHz to about 1.5 MHz and were normally fed into two DWRs. However, for the purpose of this experiment, only the signal due to the W-E component of the magnetic field was fed into a DWR to be digitized and recorded on one of the channels of the chopped lower beam of the oscilloscopes, the other being used to display the UTL voltage, as we shall discuss. The magnetic field signals were not recorded on either the SCR or on the ITR.

2.3.2 Voltage Measurements

With the exception of the north and south end poles, the 460 m, 5-span UTL was identical to standard Tampa Electric Company (TECO) single-phase 7,620/13,000 V grounded-wye primary lines. In Figure 2.2 the location of the UTL and the MLL were shown in detail, and important parameters of the UTL were listed in Table 2.1. The impulse insulation level of the end poles was made in excess of 250 kV by using 25 kV-class insulators, unbonded wood crossarms and fiberglass guy insulators. Provision was made for the connection of a 10 kV lightning arrestor on the north-end pole, but none was ever used. A protective gap of 40 cm was also installed at the north end to limit the maximum lightning impulse voltage on the line to about 250 kV. At the south end a driven ground rod and a downlead were provided with plans for disconnecting the neutral and grounding the phase conductor. To measure the voltage induced in the top (phase) conductor, a downlead was provided at the north end, closest to the MLL. This downlead was terminated on the top plate of a specially designed parallel plate capacitor. The bottom plate of this capacitor was mounted on a square ground plane with 6 m sides, which

was in turn bonded to the true ground plane established for the MLL. The capacitor plate separation was 0.5 m. The electric field signal in the capacitor, generated by the voltage on the line, was sensed by a flat-plate antenna, very similar to the ones used for sensing the vertical field due to lightning, built into the bottom capacitor plate. This signal was transmitted through a coaxial cable, buried in the service trench, into the MLL to be integrated, amplified, and then recorded.

For the purpose of our experiment, the input to direct channel 6 of the ITR was the UTL voltage signal. In addition, for very close storms the electric field signal was disconnected from the most sensitive FM channel 4, and the UTL voltage recorded instead. For distant storms, the UTL signal was sometimes recorded on FM channel 1.

As noted previously, the line voltage was also displayed on the oscilloscopes. The input to channel 6 of the ITR was connected in parallel to the input of a Biomation 805 DWR. The output of the DWR was connected to one of the channels of the chopped lower beams, displayed at two different sensitivities on the oscilloscope screens, and permanently recorded on the film, together with vertical electric field and the W-E magnetic field.

In instances of very close lightning, the line voltage was also connected to channel 4 of the SCR in place of the electric field.

2.3.3 Lightning Location

As discussed in Section 1.2.2 the ground strike point of a lightning return stroke is determined only when the leader comes

within tens of meters of the ground and initiates the attachment process. In order to correlate the remotely measured fields with the lightning characteristics, it is important to know the ground strike point. With this goal in mind, a network of five TV cameras was employed to record lightning in the vicinity of the UTL. Continuous videotape records were obtained during active thunderstorm periods. The field of view of each TV was calibrated in degrees. The MLL was equipped with a dynamic microphone which sensed the thunder due to lightning. This signal was amplified and recorded on channel 5 of the SCR. The time difference between the electric field record and the thunder from an individual lightning was used to determine the distance between the MLL and the ground strike point.

The south-east corner of the roof of the MLL was equipped with a plastic dome. During a thunderstorm "run" an observer was positioned under this dome, and a visual identification of the lightning and its location was made. The observer's comments were recorded on the audio channel of a videotape recorder located at the MLL and independently on an Audio Cassette Recorder (ACR). Comments judged particularly important were also written on the SCR paper in real time. The ACR proved very valuable, since, during a run, changes in equipment settings were sometimes not recorded in the data book and only a verbal record on the ACR was available.

If a particular flash was seen on at least two TVs, triangulation was used to determine the location of the ground strike point. The time-to-thunder and the observer's comments were then used as a check on the location. If the flash was seen only on one TV, the thunder record was used to locate the ground strike point,

and the observer's comments were used as a check. The ground strike points of all flashes located for this study were seen on at least one TV.

2.3.4 Relative Timing

In order to locate a ground flash, accurate relative timing had to be maintained between the various pieces of data. The time signals recorded on the field and voltage records were derived from a Time Code Generator (TCG) in the MLL. The TCG was periodically synchronized to WWV time. The TCG output was recorded in the FM mode on channel 7 of the ITR. It was also used to drive light-emitting diodes (LEDs) positioned on the edge of the oscilloscope screens to be recorded on film and to provide the time display for the TV monitor and videotape at the MLL. Hence, there were no problems of relative timing associated with the records on ITR, SCR, film, and the videotape recorded by the TV located at the MLL site. However, each of the four remotely switchable TVs was equipped with its own TCG located at each remote site. All four TCGs were periodically synchronized to the WWV time signal. However, failures of individual TCGs occurred due to excessive heat and humidity, line voltage surges, and circuit-breaker operations, so that there were instances when all TCGs were not synchronized. In spite of these problems, however, the correlation of most of the TV records was possible.

2.4 The Data Base

The data presented in this thesis were taken from three separate thunderstorms in the vicinity of the MLL and the UTL in the Tampa Bay area during the summer of 1979. In Section 2.3 it was pointed out that a complete dataset consists of three essential elements: the electromagnetic field due to lightning, the line voltage, and the location of the ground strike point. From an initial review of the records, it was found that on three days of the 1979 storm season, the field and voltages were simultaneously recorded, and the TV network was operational. Various elements of the dataset were subsequently extracted from recordings made on those three days. We now describe in detail the process of data selection for any particular day.

2.4.1 Flash Selection

The first step in the data extraction was to make a general survey of the field and voltage records to determine if there were good data on the film and on the instrumentation tape. When it was determined that good waveforms could be obtained, all the TV tapes were scanned, and lists of times and angles were made for each flash seen on the screen. The next step involved looking through the strip-chart records to see if there were identifiable thunder records and observer comments for the flashes seen on the TVs. Hard copies were made from the TV tapes for each flash and a copy of the thunder record was made. The flash was identified by the Universal Time (UT) of its occurrence.

The audio cassette recorded during the storm was played back to get an idea about the storm in general and to note any changes in equipment gain settings not recorded in the data book. At the end of this phase it was possible to tell whether the ground strike point of a flash could be located, either by triangulation if records were obtained from more than one TV, or by using one TV and the thunder record. As noted previously, all the flashes selected for this study were seen on at least one TV.

2.4.2 Field and Voltage Records

The next step in the analysis was to look through the simultaneously triggered field and voltage records on film and make hard copies on a microfilm copier. These records were all on a time base of 200 μs full-scale. The final step to completing the database was to obtain the field and voltage waveforms from the continuous instrumentation tape records and photograph them on polaroid film. The time base for these could be varied from 200 ms to 40 μs full-scale depending on the chosen sampling rate. During this stage of data extraction, some of the flashes which could be located were eliminated from the dataset because of the absence of field and voltage records. The final list of flashes which emerged at the end of this phase were those which could be located and for which field and voltage records were available.

2.4.3 Location and Calibration

If a flash was seen on two TVs, the angles of the flash from each TV were measured from the calibrated screen, and triangulation

was used to find the location of the ground strike point. If the time to thunder at the MLL was also available, the distance of the flash from the MLL was estimated by assuming that the velocity of the sound in that environment was 345 m/s. This distance estimate and the observer's comments were used to check on the strike point obtained from the TV triangulation. However, if the flash was seen on only one TV, the angle from that TV was used together with the distance from the MLL obtained by thunder ranging, to locate the ground strike point. In that case, the observer's comments were used as a check.

Let us first discuss the calibration of the triggered records obtained from the film. As can be seen from Figure 2.3, the vertical electric field and the line voltage signals obtained from the respective antennas were integrated and passed through the delay line which is essentially as a 2 MHz low-pass filter and then connected to the Biomation DWRs. The outputs from the DWRs were used to display the waveforms on the oscilloscope. The electric field antennas were mounted on top of the MLL. This resulted in enhancing the electric field at the actual antenna plate relative to the vertical electric field at the ground, which led to the addition of an "enhancement factor" in all the field waveform calibrations. Thus, we have the following calibration formulae for the film records:

$$E_{gr} = \frac{a \times F \times S \times 2.6 \times K_E}{R} \qquad (2.1)$$

and,

$$V_{TL} = a \times F \times S \times 2.6 \times K_V \times d \qquad (2.2)$$

where,

a = number of divisions on the grid

F = scope sensitivity (V/division on grid)

S = biomation sensitivity (V full scale/V)

2.6 = attenuation due to delay line

$K_{E(V)}$ = combined calibration constant of antenna and integrator system (V/m per V)

R = enhancement factor

d = parallel-plate capacitor spacing (m)

The instrumentation tape calibrations for the electric field records obtained from FM and direct channels are given by

$$E_{gr} = \frac{a \times F \times S \times K_{FM}}{R} \tag{2.3}$$

and,

$$E_{gr} = \frac{a \times F \times S \times K_{dir}}{R} \tag{2.4}$$

where,

$K_{FM(dir)}$ = combined calibration constant for antenna integrator, and recording system (V/m per V)

a,F,S,R = as defined in Equations (2.1) and (2.2)

The calibration formula for the voltage records obtained from the direct tape channel is

$$V_{TL} = a \times F \times S \times 2.6 \times K_V \times d \tag{2.5}$$

which is exactly the same as Equation (2.2).

2.5 An Example

We shall illustrate the process of gathering the pertinent data for this study by discussing in detail one fairly typical flash. The flash being discussed occurred at 190610 Universal Time (UT) on July 15, 1979, during designated run #79196TR27 (run #27 at the MLL which was recorded on day 196 of the year 1979).

2.5.1 Location

From an initial survey of the strip-chart records it was found that at 190610 UT there was a ground flash with possibly two or three strokes and about 23 seconds to thunder. The observer's visual identification of the flash written in real-time on the strip-chart identified the location at 125° with respect to North (0°). A reproduction of the strip-chart record with the comments made in real-time is shown in Figure 2.4.

The TV records for run # 79196TR27 indicated that the TV camera located at the MLL registered a flash with two strokes at 190610 UT. From the calibrated TV screen the location of the ground strike point was found to be at 120° from true North. One of the remote TVs, designated TV2S, registered a three-stroke flash at 190610 UT, with a bearing from TV2S to the ground strike point of 141° from true North. Using the information obtained from the two TVs, an intersection point was defined as shown in Figure 2.5. The ground strike point determined from the TV intersection is located 120° from true North at a distance of 8.8 km from the MLL. The 120° location angle agrees very well with the rough visual angle of 125° obtained from

Figure 2.4. Six-channel strip-chart record for the 190610 flash during run #79196TR27, showing four channels of electric field signals, one channel of thunder, and one of time-code.

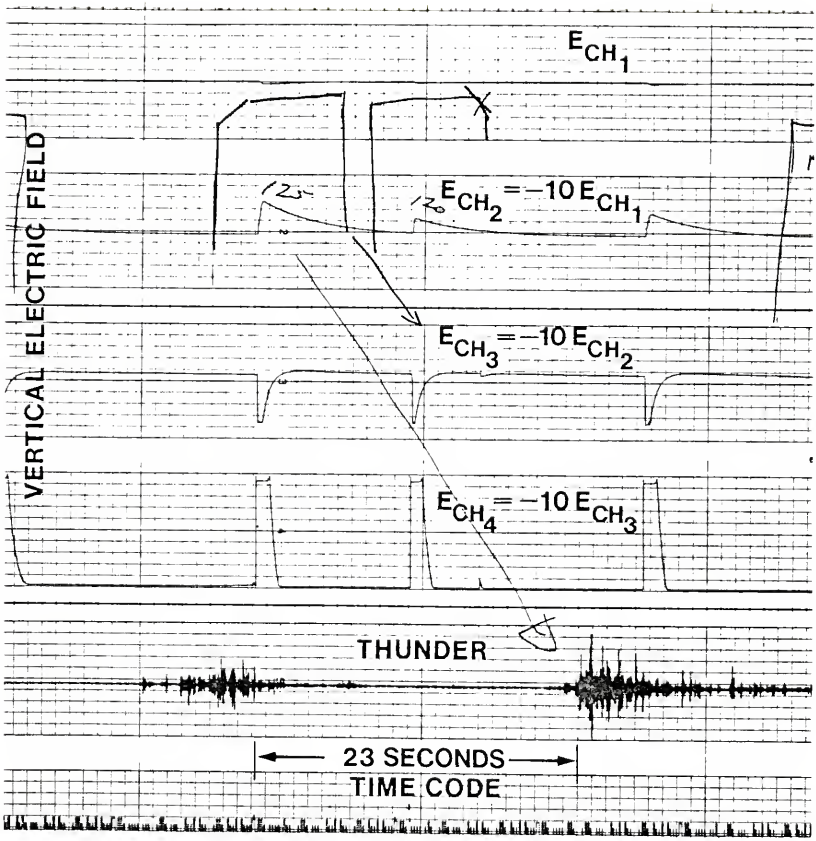
E_{CH_1}
$E_{CH_2} = -10\,E_{CH_1}$
$E_{CH_3} = -10\,E_{CH_2}$
$E_{CH_4} = -10\,E_{CH_3}$
VERTICAL ELECTRIC FIELD
THUNDER
23 SECONDS
TIME CODE

Figure 2.5. Location of the ground strike point for the 190610 flash during run #79196TR27 using the bearings from TV1E and TV2S.

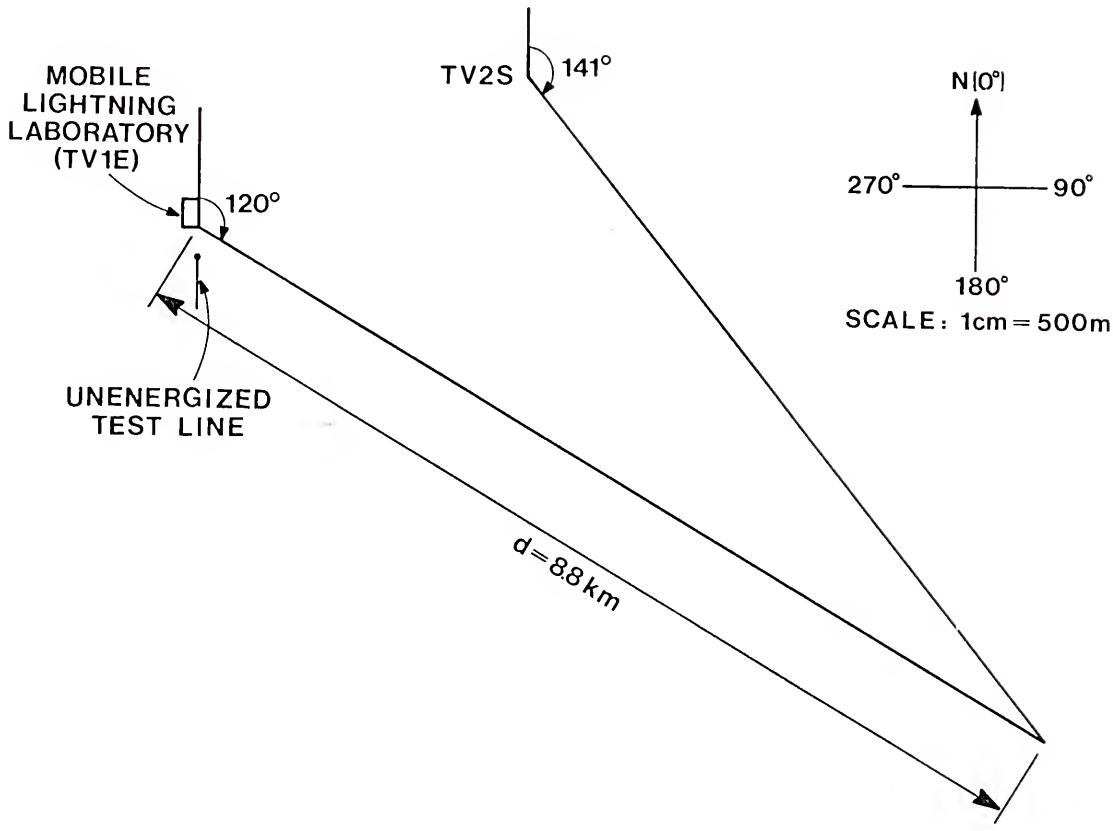
MOBILE
LIGHTNING
LABORATORY
(TV1E)
120°
TV2S
141°
N(0°)
270°
90°
180°
SCALE: 1cm = 500m
UNENERGIZED
TEST LINE
d=8.8km

the observer's comments. The distance obtained by thunder ranging is found to be 8 km, again in reasonable agreement with the location distance obtained from the TV intersection.

2.5.2 Film Records

At 190610 UT, film records were available from both the oscilloscopes. The trigger threshold was such that the film recorded two strokes. Reproductions of the 200 μs full-scale records obtained from both the films are shown in Figures 2.6(a) and (b). The magnetic field for the first stroke is saturated on both records. Scales for the vertical electric field and the test-line voltage are also shown in the figure.

2.5.3 Instrumentation Tape Records

The vertical electric field records for the 190610 flash obtained from one FM and one direct channel of the ITR are shown in Figure 2.7 on a scale of 20 ms/div. Records from the direct channel, in the vicinity of the fast field changes, at time-scales ranging from 40 μs/div to 4 μs/div, indicated that each of the three fast changes was a return stroke. For comparison with the film records, we show the waveforms of the vertical electric field and the test-line voltage for all three strokes on a time scale of 8 μs/div in Figure 2.8. The calibration for the electric field from the first stroke has been adjusted for saturation inside the isolation amplifier through which the electric field signal is recorded on the direct channel.

Figure 2.6(a). Records of the vertical electric and horizontal magnetic fields and the test-line voltages obtained from the left oscilloscope film for the 190610 flash during run #79196TR27. The electric field is on a scale of 120 V/m per division and the voltage scale is 65 kV/division. All records are 200 μs full-scale. The relative displacement in time between the vertical electric field and the voltage records is due to different pre-trigger delay settings on the respective Biomation recorders.

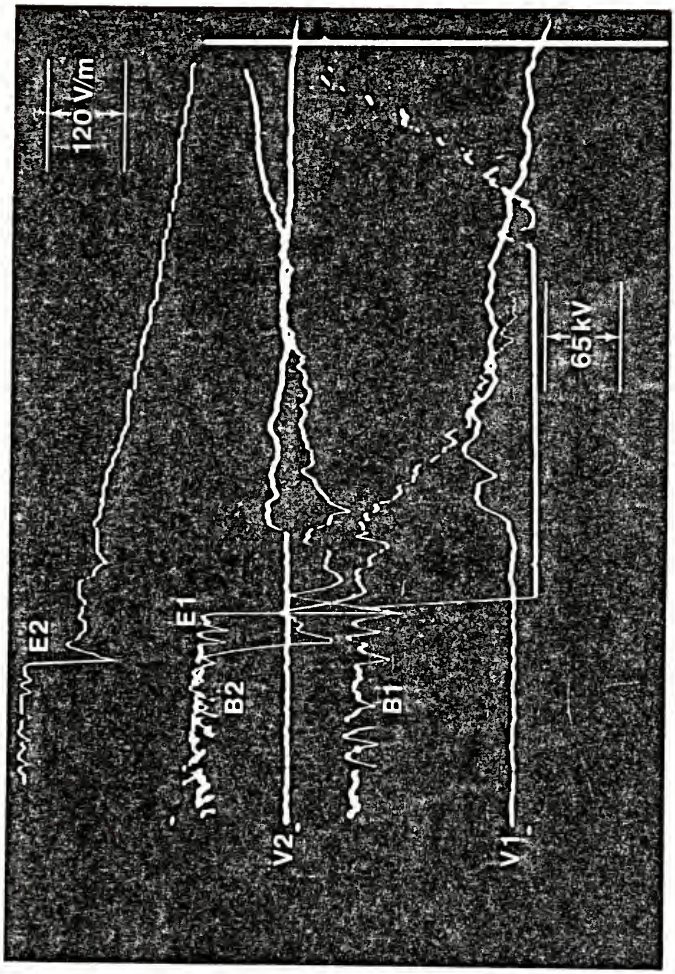
120 V/m
E2
E1
B2
B1
V2
V1
65 kV
20μs

Figure 2.6(b). Records of the vertical electric and horizontal magnetic fields and the test-line voltages obtained from the right oscilloscope film for the 190610 flash during run #79196TR27. The electric field is on a 600 V/m per division scale, and the voltage scale is 165 kV/division. All records are 200 μs full-scale. The relative displacement in time between the vertical electric field and the voltage records is due to different pre-trigger delay settings on the respective Biomation recorders.

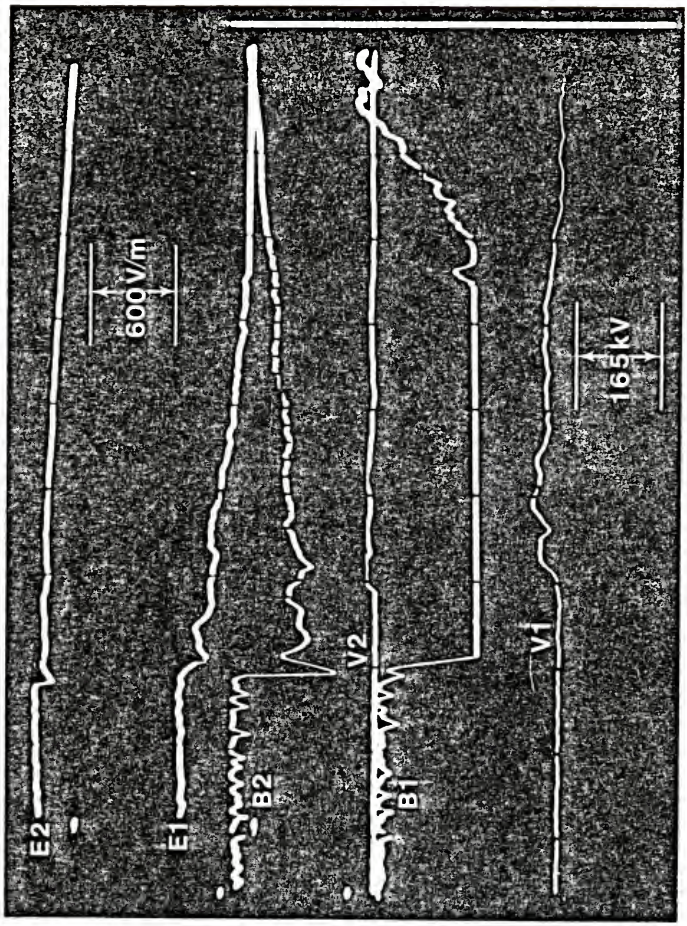
E2
E1
600 V/m
B2
V2
B1
V1
165 kV
20μs

Figure 2.7. Vertical electric field record for the whole flash obtained from instrumentation tape for the 190610 flash during run #79196TR27. The FM channel sensitivity is 870 V/m per division and direct channel is 90 V/m per division. Both records are 200 ms full-scale.

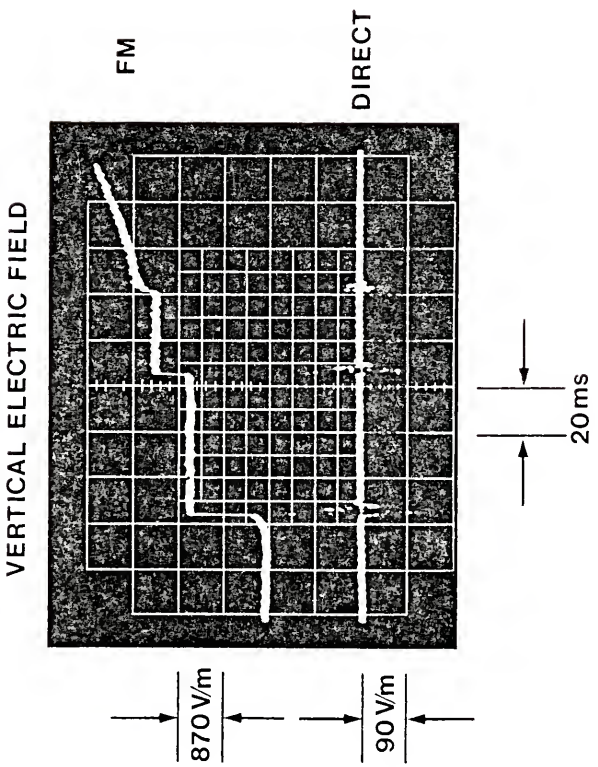
VERTICAL ELECTRIC FIELD
FM
DIRECT
870 V/m
90 V/m
20 ms

Figure 2.8. Vertical electric field and test-line voltages for all three return strokes of the flash obtained from the direct channels of the instrumentation tape recorder for the 190610 flash during run #79196TR27. The electric field and voltage scales are shown for each stroke. All records are 80 μs full-scale. The relative displacement in time between the electric field and the voltage records is due to the positioning of the record and reproduce heads of the Instrumentation Tape Recorder.

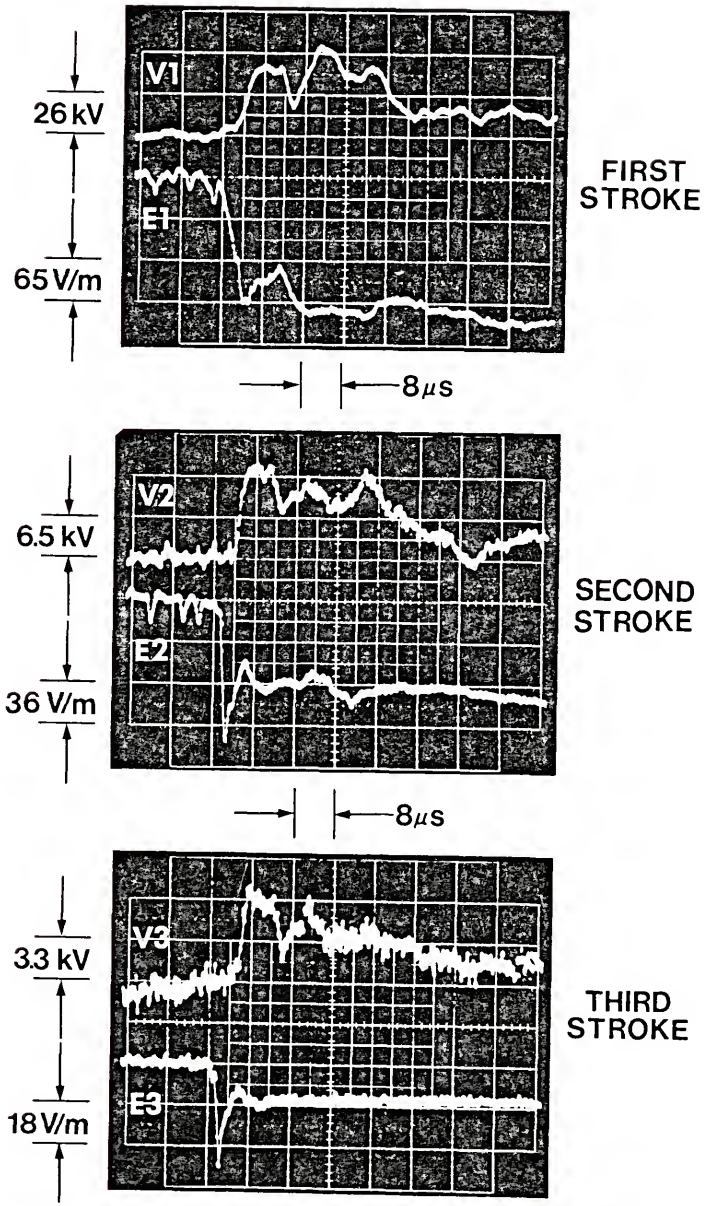
V1
E1
26 kV
65 V/m
8μs
FIRST STROKE
V2
E2
6.5 kV
36 V/m
8μs
SECOND STROKE
V3
E3
3.3 kV
18 V/m
THIRD STROKE

2.5.4 Conclusions

Comparing Figures 2.6 and 2.8, we note that the third return stroke in the flash is missing from the film records because it was below the trigger threshold. If continuous data were not taken on the ITR, this flash may have been characterized as a two-stroke flash rather than a three-stroke one. Another point to note is the fact that the voltage waveform measured from the direct tape channel falls to zero much faster than that measured off the film. This is due to the poor low-frequency response of the direct channel. For comparison purposes, we show in Figure 2.9 voltage waveform records on two tape channels, one FM and one direct, for the single stroke flash at 192238 UT during run #79199TR31. As noted in Section 2.3.1 the FM channel has a frequency response from about dc to 500 kHz (-6 db). As can be seen, the direct channel record is less noisy, but has a much faster decay characteristic; the peak voltage measured on each record is essentially the same.

In Table 2.2 the initial peak values obtained from the various film and tape records for the example being discussed are summarized. The values obtained from the measurements differ by about ±10%, well within the desired accuracy. This difference is attributed to several factors. As noted in Section 2.3, the oscilloscope records, the FM and the direct channels of the instrumentation tape recorder all have different bandwidths. In addition to the differences in waveform associated with the frequency response, there is error in measuring small deflections (see, for example, Figures 2.6(a) and (b)), particularly in the presence of noise.

Figure 2.9. Comparison between simultaneously recorded voltage signals on the direct and FM channels of the instrumentation tape recorder for a single stroke flash at 192238 UT during run #79199TR31.

LINE VOLTAGE FROM TAPE RECORDER

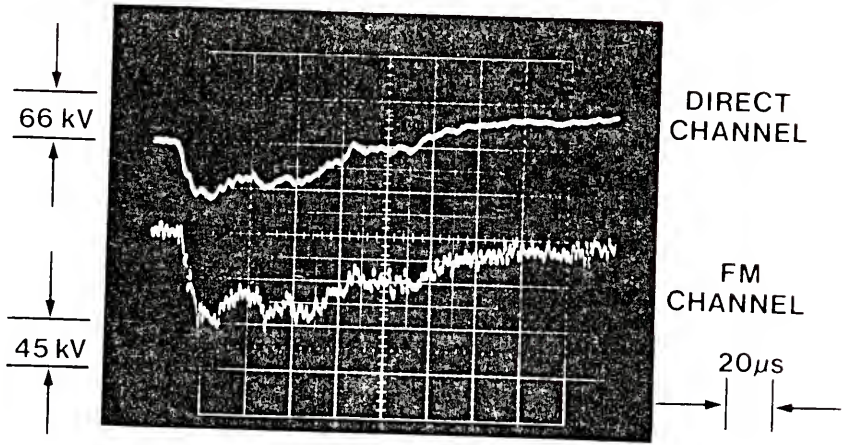

Table 2.2. Summary of the values of the vertical electric field initial radiation peak and peak test-line voltage obtained from oscillograms made via Biomation waveform recorders and replay of instrumentation tape records for the flash at 190610 UT during run #79196TR27.

	VERTICAL ELECTRIC FIELD (V/m)			TEST-LINE VOLTAGE (kV)		
	OSCILLOSCOPE		TAPE	OSCILLOSCOPE		TAPE
STROKE #	LEFT	RIGHT	DIRECT	LEFT	RIGHT	DIRECT
1	-191.4	-184.3	-188.0	+41.6	+51.2	+55.4
2	-136.7	-124.3	-120.6	+15.8	+21.5	+15.2
3	------	------	-47.5	-----	-----	+7.3

2.6 Data Analysis

As described in the earlier sections of this chapter, the data base accumulated for this thesis was put together from thunderstorms on three separate days. In Tables 2.3(a), (b), and (c) we list the flashes used in this study for each of these three days. This table gives the location of the strokes from the MLL in polar coordinates as illustrated in Figure 2.5 and the time interval between strokes. The values derived for the initial peak vertical electric field and the peak line voltage from the oscillograms and instrumentation tape records as outlined in the previous section, are also listed. In addition, from available 40 μs full-scale instrumentation tape records, risetimes for the electric field and the voltage were measured and have also been tabulated.

Analysis of the vertical electric field records will first be used to show that the sample of selected lightning is not unusual. Pertinent parameters will be plotted and compared with statistics on lightning in Florida and in the other areas of the world. The data obtained for first strokes will be analyzed separately from that obtained for subsequent strokes. The next step will be to plot various statistics related to the voltage waveforms and compare them with available data from other studies. Finally, we shall illustrate the relationship between the peak line voltage normalized to the initial peak vertical electric field as a function of the angle of the ground strike point around the line.

Table 2.3(a). List of flashes studied in this thesis from thunderstorms on July 15, 1979, run #79196TR27, and salient measurements made from the vertical electric field and induced voltage records. The location of the ground strike point from the Mobile Lightning Laboratory is given. The letter F or S given with each stroke number indicates whether the stroke has been classified classified as a first (F) or as a subsequent (S) stroke.

UNIVERSAL TIME	STROKE NUMBER	TIME INTERVAL (ms)	LOCATION FROM MLL R (km)	LOCATION FROM MLL θ (deg)	VERTICAL ELECTRIC FIELD PEAK (V/m)	VERTICAL ELECTRIC FIELD RISETIME (μs) 0-peak	VERTICAL ELECTRIC FIELD RISETIME (μs) 10%-90%	TEST LINE VOLTAGE PEAK (kV)	TEST LINE VOLTAGE RISETIME (μs) 0-peak	TEST LINE VOLTAGE RISETIME (μs) 10%-90%
185204	1 F	250	5.4	120	-260.0	5.81	2.19	+66.0	5.30	3.46
	2 S		"	"	-131.6	7.61	3.48	+39.6	4.00	3.24
185237	1 F		5.0	82	-98.7	4.65	2.71	-10.6	5.51	4.86
185244	1 F	70	5.0	90	-230.4	4.65	2.84	+22.4, -26.4	5.30	3.78
	2 S		"	"	-145.6	2.45	0.90	+5.3, -3.3	1.62	1.08
185300	1 F		5.0	87	-131.6	3.61	1.42	+5.3, -5.0	2.05	0.86
185337	1 F	180	2.5	124	-434.4	9.94	8.39	+152.0	6.16	4.22
	2 F		4.0	98	-89.1	1.81	1.03	+22.5	5.84	4.54
185354	1 F	28	4.0	88	-100.5	7.74	2.84	+4.3, -7.9	2.92	2.05
	2 S		"	"	-29.6	5.55	2.19	+0.7, 0	---	---
185421	1 F		4.5	94	-131.2	3.23	1.42	+7.9, -4.6	3.24	1.84

Table 2.3(a)--continued.

UNIVERSAL TIME	STROKE NUMBER	TIME INTERVAL (ms)	LOCATION FROM MLL R (km)	LOCATION FROM MLL θ (deg)	VERTICAL ELECTRIC FIELD PEAK (V/m)	VERTICAL ELECTRIC FIELD RISETIME (μs) 0-peak	VERTICAL ELECTRIC FIELD RISETIME (μs) 10%-90%	TEST LINE VOLTAGE PEAK (kV)	TEST LINE VOLTAGE RISETIME (μs) 0-peak	TEST LINE VOLTAGE RISETIME (μs) 10%-90%
185725	1 F		4.5	89	-117.8	5.29	3.48	+6.6, -4.6	6.05	5.08
	2 S	52	"	"	-129.7	6.97	3.09	+5.6, -6.6	3.57	2.49
	3 S	102	"	"	-29.2	3.79	2.32	0, 0	---	---
	4 S	132	"	"	-38.4	3.23	1.42	+0.8, -1.3	3.03	2.16
	5 S	68	"	"	-43.9	4.77	1.29	+2.0, -2.3	0.97	0.32
	6 S	68	"	"	-73.1	2.45	1.55	+3.6, -4.3	3.89	2.81
	7 S	110	"	"	-47.5	4.52	2.58	+2.0, -3.3	2.49	1.73
185758	1 F		5.9	107	-118.0	5.29	1.94	+18.7	5.95	3.57
185842	1 F		5.8	102	-106.2	4.77	1.16	+12.5	5.62	3.57
	2 S	40	"	"	-58.5	3.10	1.81	+4.6	3.89	2.92
	3 S	52	"	"	-120.7	5.42	2.58	+12.1	5.95	4.28
	4 S	156	"	"	-65.8	4.77	1.94	+7.3	5.84	4.32
185906	1 F		6.2	128	-64.1	5.94	2.97	+17.8	5.08	3.35
	2 S	66	"	"	-37.5	5.03	2.19	+11.1	7.24	5.62
	3 S	54	"	"	-25.6	1.16	0.59	+4.6	2.38	1.08
	4 S	30	"	"	-19.2	5.03	3.15	+4.3	3.35	2.49
185947	1 F		4.9	79	-132.0	8.13	3.74	-13.8	8.0	6.92

Table 2.3(a)--continued.

UNIVERSAL TIME	STROKE NUMBER		TIME INTERVAL (ms)	LOCATION FROM MLL R (km)	LOCATION FROM MLL θ (deg)	VERTICAL ELECTRIC FIELD PEAK (V/m)	VERTICAL ELECTRIC FIELD RISETIME (μs) 0-peak	VERTICAL ELECTRIC FIELD RISETIME (μs) 10%-90%	TEST LINE VOLTAGE PEAK (kV)	TEST LINE VOLTAGE RISETIME (μs) 0-peak	TEST LINE VOLTAGE RISETIME (μs) 10%-90%
190004	1	F		5.5	94	-105.0	6.06	3.74	+8.3, -5.9	4.54	3.24
	2	S	84	"	"	-65.8	2.71	1.29	+5.3, -1.0	3.87	3.35
	3	S	48	"	"	-54.8	2.48	1.42	+3.0, -1.3	2.27	1.30
	4	S	106	"	"	-29.2	3.35	1.24	0, 0	---	---
	5	S	58	"	"	-23.8	5.68	4.77	+1.3, -1.0	2.05	1.51
	6	S	26	"	"	-20.1	1.68	0.98	+1.0, -0.7	1.73	0.80
	7	S	32	"	"	-47.5	4.52	2.32	+2.5, -1.4	3.24	2.16
	8	S	22	"	"	-27.4	3.05	1.50	+2.1, -0.7	4.22	3.35
190146	1	F		6.2	101	-65.8	3.74	1.94	+8.3	4.86	3.68
190214	1	F		5.0	110	-158.2, -295.8*	4.0	1.73	+24.0, +38.6*	5.95	4.54
	2	S	44	"	"	-27.4, -19.2*	3.95	1.47	+3.3, +1.3*	5.19	3.35
	3	S	148	"	"	-73.1	4.9	2.84	+9.9	4.80	3.68
190546	1	F		9.0	126	-107.0	---	---	+20.8	---	---
	2	S	---	"	"	-85.0	---	---	+12.6	---	---
190610	1	F		8.8	120	-187.9	4.77	3.30	+49.4	4.11	2.92
	2	S	56	"	"	-127.2	3.02	0.95	+17.5	2.49	1.62
	3	S	36	"	"	-47.5	2.84	1.11	+7.3	1.84	1.29
190620	1	F		8.0	115	-67.6	3.30	1.42	+10.9	5.51	3.35
190652	1	F		7.6	157	-96.3	4.65	1.81	+32.9	7.14	4.76
	2	S	36	"	"	-111.7	2.45	1.42	+32.9	3.24	1.62
	3	S	15	"	"	-41.1	2.12	0.77	+11.2	2.49	1.62

Table 2.3(a)--continued

UNIVERSAL TIME	STROKE NUMBER	TIME INTERVAL (ms)	LOCATION FROM MLL R (km)	LOCATION FROM MLL θ (deg)	VERTICAL ELECTRIC FIELD PEAK (V/m)	VERTICAL ELECTRIC FIELD RISETIME (μs) 0-peak	VERTICAL ELECTRIC FIELD RISETIME (μs) 10%-90%	TEST LINE VOLTAGE PEAK (kV)	TEST LINE VOLTAGE RISETIME (μs) 0-peak	TEST LINE VOLTAGE RISETIME (μs) 10%-90%
190704	1 F	102	8.3	125	-88.0	5.03	3.10	+19.5	6.49	4.76
	2 F		5.2	112	-67.3	2.32	0.90	+8.9	2.81	1.73
190821	1 F	76	9.3	138	-68.6	5.63	4.0	+9.2	8.11	5.29
	2 F	168	7.3	153	-106.8	3.95	2.30	+39.8	2.27	1.41
	3 S	88	"	"	-43.0	4.31	3.15	+10.2	2.49	1.73
	4 S		"	"	-71.9	4.59	1.81	+16.0	2.59	1.69
190833	1 F	44	7.0	109	-107.4	3.79	2.14	+17.4	5.08	2.92
	2 S	104	"	"	-54.8	1.68	0.34	+8.3	4.22	3.24
	3 S	104	"	"	-78.2	3.23	1.42	+12.3	4.11	3.24
	4 S		"	"	-30.6	2.58	0.83	+2.6	1.62	1.34
190924	1 F	140	9.0	136	-37.2	4.95	3.30	+7.9	2.70	1.51
	2 S	96	"	"	-56.6	6.06	3.48	+12.5	6.38	5.84
	3 S		"	"	-30.2	3.05	1.10	+6.3	2.59	1.08
191024	1 F	92	9.3	128	-208.7	7.35	6.32	+50.1	8.00	5.08
	2 S	28	"	"	-65.5	3.87	2.25	+15.2	2.49	1.51
	3 S	34	"	"	-36.6	3.87	3.23	+7.3	5.51	4.43
	4 S	42	"	"	-36.6	4.0	2.19	+6.9	7.35	5.62
	5 S		"	"	-43.9	3.74	1.94	+9.2	6.81	5.19
191107	1 F	108	10.4	120	-165.0	7.79	2.71	+36.0	7.57	4.22
	2 S	76	"	"	-43.9	4.26	3.30	+7.6	5.84	3.46
	3 S	76	"	"	-45.7	2.76	1.42	+8.6	5.51	3.78
	4 S		"	"	-40.2, -27.4*	3.23	0.98	+6.6, +9.6*	4.32	3.14

Table 2.3(a)--continued.

UNIVERSAL TIME	STROKE NUMBER	TIME INTERVAL (ms)	LOCATION FROM MLL R (km)	LOCATION FROM MLL θ (deg)	VERTICAL ELECTRIC FIELD PEAK (V/m)	VERTICAL ELECTRIC FIELD RISETIME (μs) 0-peak	VERTICAL ELECTRIC FIELD RISETIME (μs) 10%-90%	TEST LINE VOLTAGE PEAK (kV)	TEST LINE VOLTAGE RISETIME (μs) 0-peak	TEST LINE VOLTAGE RISETIME (μs) 10%-90%
191137	1 F		8.3	136	-179.5, -278.2*	5.16	4.26	+48, +68.8*	5.30	4.54
	2 S	38	"	"	-47.5	4.26	2.97	+11.9	4.97	6.38
	3 S	34	"	"	-43.9	3.09	1.29	+13.5	7.03	5.51
	4 S	28	"	"	-32.9	2.32	1.16	+7.6	7.89	5.30
	5 S	100	"	"	-110.9	2.06	0.77	+34.9	7.78	6.05
191214	1 F		11.0	124	-170.0	4.46	1.81	+36.5	8.43	3.89
	2 S	70	"	"	-42.5	4.77	2.45	+7.5	3.83	2.16
	3 S	26	"	"	-43.9	3.41	1.68	+9.6	2.92	1.62
191308	1 F		10.2	123	-114.0	4.9	1.68	+21.5	4.00	3.03
	2 F	76	8.3	150	-54.8	2.79	1.03	+19.8	6.59	4.76
	3 F	72	9.0	147	-47.5	3.54	2.25	+11.9	2.49	1.41
	4 S	44	"	"	-32.9	2.32	1.55	+7.3	3.35	2.05
	5 S	44	"	"	-27.4	2.97	1.47	+7.3	2.38	2.59
	6 S	48	"	"	-69.5	3.74	2.19	+20.1	2.92	1.62
191354	1 F		11.0	134	-88.0	2.84	1.94	+27.2	8.00	5.73
	2 S	48	"	"	-49.4	4.5	2.45	+11.9	4.26	2.70
	3 S	60	"	"	-96.3	5.68	3.10	+21.6	4.43	2.59
	4 S	64	"	"	-46.6	3.54	2.66	+10.2	3.78	2.53
	5 S	52	"	"	-28.3	2.23	1.68	+6.9	3.57	2.27
191406	1 F		9.3	112	-33.7	4.83	2.01	+6.3	2.92	2.05
191416	1 F		8.6	115, 120*	-67.0, -91.0*	6.19	4.72	+11.9, +15.2*	7.03	5.95
	2 S	52	"	120	-38.4	3.66	2.17	+5.6	3.89	1.84

Table 2.3(a)--continued.

UNIVERSAL TIME	STROKE NUMBER	TIME INTERVAL (ms)	LOCATION FROM MLL R (km)	LOCATION FROM MLL θ (deg)	VERTICAL ELECTRIC FIELD PEAK (V/m)	VERTICAL ELECTRIC FIELD RISETIME (μs) 0-peak	VERTICAL ELECTRIC FIELD RISETIME (μs) 10%-90%	TEST LINE VOLTAGE PEAK (kV)	TEST LINE VOLTAGE RISETIME (μs) 0-peak	TEST LINE VOLTAGE RISETIME (μs) 10%-90%
191605	1 F	166	9.7	130	-75.9	3.61	1.73	+18.5	6.81	5.19
	2 F		11.0	125	-34.7	5.81	3.82	+8.9	8.21	6.38
191631	1 F		12.4	130	-38.4	5.29	2.71	+11.9	6.92	4.86
191711	1 F	48	10.4	131	-80.1	6.45	3.23	+19.8	4.76	2.77
	2 S	104	"	"	-51.2	2.27	0.90	+8.9	2.16	0.91
	3 S	160	"	"	-107.8	4.90	3.48	+26.4	6.05	4.43
	4 S		"	"	-25.6	2.58	1.81	+5.3	2.27	0.97
192112	1 F	36	9.0	122	-42.9	3.74	2.19	+10.6	3.35	2.81
	2 S	40	"	"	-42.8	2.58	1.47	+11.2	4.11	2.16
	3 S	92	"	"	-56.7	5.16	2.58	+15.2	5.51	4.43
	4 S	148	"	"	-56.7	4.05	2.06	+13.9	4.86	3.78
	5 S		"	"	-34.7	2.06	0.70	+5.6	3.35	2.27

*Two peaks within 200 μs probably due to two channels to ground.

Table 2.3(b). List of flashes studied in this thesis from thunderstorms on July 18, 1979, run #79199TR31, and salient measurements made from the vertical electric field and induced voltage records. The location of the ground strike point from the Mobile Lightning Laboratory is given. The letter F or S given with each stroke number indicates whether the stroke has been classified as a first (F) or as a subsequent (S) stroke.

UNIVERSAL TIME	STROKE NUMBER		TIME INTERVAL (ms)	LOCATION FROM MLL R (km)	LOCATION FROM MLL θ (deg)	VERTICAL ELECTRIC FIELD PEAK (V/m)	VERTICAL ELECTRIC FIELD RISETIME (μs) 0-peak	VERTICAL ELECTRIC FIELD RISETIME (μs) 10%-90%	TEST LINE VOLTAGE PEAK (kV)	TEST LINE VOLTAGE RISETIME (μs) 0-peak	TEST LINE VOLTAGE RISETIME (μs) 10%-90%
170455	1	F		10.6	8	-64.9	4.93	3.60	-34.3	6.16	4.11
	2	S	58	"	"	-46.5	4.27	2.53	-28.8	5.73	4.22
	3	S	72	"	"	-49.7	3.07	1.92	-19.9	7.03	4.97
	4	S	152	"	"	-32.6	1.53	0.93	-8.6	4.97	3.78
	5	S	68	"	"	-55.7	2.20	1.20	-19.7	5.62	4.86
171407	1	F		13.5	54	-40.2	5.0	3.27	-11.2	6.70	5.51
	2	S	160	"	"	-28.0	2.27	1.47	-5.3	1.62	0.43
	3	S	60	"	"	-20.1	0.93	0.48	-4.3	4.43	1.41
184041	1	F		8.7	160	-31.3	3.60	1.28	+11.6	3.89	2.05
	2	S	104	"	"	-70.7	4.05	1.68	+20.8	4.86	1.94
	3	S	76	"	"	-30.0	1.15	0.45	+9.4	3.14	1.62
	4	S	132	"	"	-33.2	1.43	1.28	+10.5	3.35	1.73
184244	1	F		6.7	105	-82.3	8.53	3.33	+13.5	8.22	5.19
	2	S	71	"	"	-20.2	5.5	3.47	+3.2	4.76	3.57
	3	F	63	8.6	114	-44.2	5.07	3.07	+7.5	6.49	3.78
	4	S	40	"	"	-29.3	4.13	1.47	+5.7	4.43	2.49
	5	S	44	"	"	-36.4	4.4	2.53	+6.5	3.57	2.38
	6	S	67	"	"	-40.6	4.4	1.9	+8.3	4.65	3.14
	7	S	66	"	"	-27.4	3.6	1.5	+5.9	4.86	3.03
	8	S	77	"	"	-30.1	4.4	1.55	+4.7	4.22	2.92

Table 2.3(b)--continued.

UNIVERSAL TIME	STROKE NUMBER		TIME INTERVAL (ms)	LOCATION FROM MLL R (km)	LOCATION FROM MLL θ (deg)	VERTICAL ELECTRIC FIELD PEAK (V/m)	VERTICAL ELECTRIC FIELD RISETIME (μs) 0-peak	VERTICAL ELECTRIC FIELD RISETIME (μs) 10%-90%	TEST LINE VOLTAGE PEAK (kV)	TEST LINE VOLTAGE RISETIME (μs) 0-peak	TEST LINE VOLTAGE RISETIME (μs) 10%-90%
184122	1	F		4.3	140	-90.1	6.0	3.9	+44.9	10.27	6.27
	2	S	22	"	"	-18.3	1.8	0.75	+3.6	2.27	1.19
	3	S	34	"	"	-56.5	5.0	2.08	+18.8	3.46	2.38
	4	S	226	"	"	-107.7	4.67	2.13	+37.3	4.65	2.49
	5	S	44	"	"	-42.7	2.53	0.75	+12.9	4.22	2.53
	6	S	68	"	"	-20.6	0.93	0.29	+4.6	2.05	1.19
	7	S	28	"	"	-24.8	1.2	0.4	+5.0	2.85	1.62
184600	1	F		1.2	90	-434.0	9.87	5.07	+35.7, -43.6	4.76	3.14
184642	1	F		4.7	155	-76.8	7.6	4.2	+39.6	10.48	6.92
184841	1	F		6.6	120	-75.5	3.2	2.08	+16.5	5.08	2.92
	2	F	120	6.9	126	-85.5	5.47	2.35	+21.4	5.41	3.14
	3	F	168	6.7	117	-80.2	3.73	1.87	+17.8	5.41	2.70
	4	S	44	"	"	-44.9	3.25	1.07	+7.9	3.14	1.62
	5	S	252	"	"	-117.2	4.0	2.0	+21.0	3.78	2.27
	6	S	32	"	"	-32.6	2.93	0.93	+5.3	2.81	1.73
	7	S	250	"	"	-85.3	5.33	2.13	+15.7	5.19	2.77
	8	S	295	"	"	-51.9	3.6	1.33	+7.7	3.35	1.84
	9	S	430	"	"	-45.8	2.6	1.33	+8.4	3.57	2.27

Table 2.3(b)--continued.

UNIVERSAL TIME	STROKE NUMBER	TIME INTERVAL (ms)	LOCATION FROM MLL R (km)	LOCATION FROM MLL θ (deg)	VERTICAL ELECTRIC FIELD PEAK (V/m)	VERTICAL ELECTRIC FIELD RISETIME (μs) 0-peak	VERTICAL ELECTRIC FIELD RISETIME (μs) 10%-90%	TEST LINE VOLTAGE PEAK (kV)	TEST LINE VOLTAGE RISETIME (μs) 0-peak	TEST LINE VOLTAGE RISETIME (μs) 10%-90%
184905	1 F		6.9	136	-71.3	3.47	2.13	+18.9	5.19	2.59
	2 S	44	"	"	-48.0	3.61	1.8	+11.0	3.57	1.95
	3 S	22	"	"	-23.0	3.2	1.0	+5.5	3.68	2.70
	4 S	48	"	"	-44.0	4.8	1.8	+8.7	4.00	2.75
	5 S	64	"	"	-29.1	2.13	0.59	+6.6	3.68	2.27
	6 S	54	"	"	-33.9	2.27	0.67	+7.9	4.00	2.38
	7 S	54	"	"	-47.5	3.25	1.8	+14.5	4.22	2.27
	8 S	18	"	"	-21.9	3.87	2.8	+4.3	4.65	3.35
184929	1 F		6.7	122	-88.0	---	---	+22.0	---	---
	3 S	---	"	"	-30.1	---	---	+4.9	---	---
190018	1 F		3.7	119.0	-144.0	5.87	3.33	+27.7	8.22	4.97
	2 S	60	"	"	-393.0	5.28	2.0	+91.2	6.70	4.76
	3 S	24	"	"	-53.4	5.07	2.67	+8.9	3.57	2.38
	4 S	444	"	"	-166.4	3.6	2.13	+32.6	5.95	3.24
	5 S	68	"	"	-23.9	4.53	3.4	+4.5	4.11	3.14
	6 S	128	"	"	-23.9	4.05	3.07	+4.3	8.00	4.86
	7 S	32	"	"	-78.7	3.55	1.47	+16.7	4.00	2.81
	8 S	82	"	"	-65.3	3.2	1.92	+13.9	3.72	1.79
	9 S	96	"	"	-85.3	2.8	2.13	+16.0	3.68	1.84
	10 S	116	"	"	-31.9	5.0	2.4	+5.6	4.97	3.89
	11 S	20	"	"	-107.7	3.25	1.2	+16.7	6.16	2.59
	12 S	32	"	"	-69.5	3.87	2.0	+12.0	3.68	2.16
190159	1 F		3.6	109	-161.3	6.8	4.13	+71.3	5.29	3.78
192340	1 F		4.1	252	-82.3	6.0	3.95	+13.9	4.97	3.37

Table 2.3(c). List of flashes studied in this thesis from thunderstorms on July 27, 1979, run #79208TR44, and salient measurements made from the vertical electric field and induced voltage records. The location of the ground strike point from the Mobile Lightning Laboratory is given. The letter F or S given with each stroke number indicates whether the stroke has been classified as a first (F) or as a subsequent (S) stroke.

UNIVERSAL TIME	STROKE NUMBER	TIME INTERVAL (ms)	LOCATION FROM MLL R (km)	LOCATION FROM MLL θ (deg)	VERTICAL ELECTRIC FIELD PEAK (V/m)	VERTICAL ELECTRIC FIELD RISETIME (μs) 0-peak	VERTICAL ELECTRIC FIELD RISETIME (μs) 10%-90%	TEST LINE VOLTAGE PEAK (kV)	TEST LINE VOLTAGE RISETIME (μs) 0-peak	TEST LINE VOLTAGE RISETIME (μs) 10%-90%
220135	1 F	---	12.3	185	-73.0	---	---	+28.9	---	---
	2 S		"	"	-72.3	---	---	+20.6	---	---
	3 S	---	"	"	-21.2	---	---	+5.8	---	---
	4 S	---	"	"	-25.9	---	---	+6.6	---	---
220149	1 F	---	10.6	180	-38.7	---	---	+13.2	---	---
	2 S		"	"	-28.5	---	---	+9.1	---	---
220319	1 F	74	10.3	175	-24.7	2.19	1.16	+7.0	4.0	2.0
	2 S	456	"	"	-70.2	2.06	1.55	+26.0	2.4	1.8
	3 S		"	"	-42.5	2.84	1.55	+15.0	3.2	2.0
220339	1 F		20.4	185	-24.2	1.89	1.55	+10.1	6.4	3.2
220410	1 F	120	6.1	180	-45.4	2.26	1.68	+17.2	2.8	1.2
	2 F	210	5.6	185	-55.6	1.42	1.03	+33.0	1.6	1.0
	3 S		"	"	-27.3	2.06	1.29	+13.2	2.8	2.2
220502	1 F		4.8	211	-99.5	2.40	1.40	+43.6	7.2	5.2
220525	1 F		10.1	180	-43.7	1.94	1.16	+16.4	2.8	1.8
			10.6	190+						

Table 2.3(c)--continued.

UNIVERSAL TIME	STROKE NUMBER	TIME INTERVAL (ms)	LOCATION FROM MLL R (km)	LOCATION FROM MLL θ (deg)	VERTICAL ELECTRIC FIELD PEAK (V/m)	VERTICAL ELECTRIC FIELD RISETIME (μs) 0-peak	VERTICAL ELECTRIC FIELD RISETIME (μs) 10%-90%	TEST LINE VOLTAGE PEAK (kV)	TEST LINE VOLTAGE RISETIME (μs) 0-peak	TEST LINE VOLTAGE RISETIME (μs) 10%-90%
220547	1 F		11.2	190	-49.9	2.58	2.06	+18.1	6.0	5.6
220603	1 F		5.7	244	-98.0	1.80	1.16	+27.8	8.0	6.4
220623	1 F		11.2	190	-21.7	1.94	1.55	+7.8	2.8	1.6
220631	1 F		11.5	194	51.2	1.83	0.65	+23.6	2.0	1.6
220651	1 F		8.2	190	-83.4	3.35	2.19	+35.6	7.2	4.4
	2 S	248	"	"	-58.2	0.97	0.39	+16.8	2.8	1.8
	3 S	60	"	"	-28.3	0.65	0.39	+8.4	2.4	1.0
	4 S	94	"	"	-25.5	1.55	1.10	+8.4	2.0	1.6
	5 S	36	"	"	-54.8	1.55	0.52	+18.6	2.8	1.8
	6 S	44	"	"	-31.6	0.91	0.45	+9.9	1.6	1.0
	7 S	84	"	"	-40.6	1.42	0.77	+13.7	4.4	2.8
	8 S	92	"	"	-41.2	1.42	1.03	+13.5	3.6	1.4
	9 S	120	"	"	-45.1	1.03	0.52	+11.6	2.4	1.0
	10 S	92	"	"	-76.8	2.06	0.97	+25.8	3.2	1.6
	11 S	52	"	"	-19.3	0.77	0.39	+7.2	2.4	1.2
	12 S	196	"	"	-53.8	1.48	1.16	+22.1	3.2	1.6
	13 S	144	"	"	-19.9	0.84	0.65	+5.9	2.0	2.0
	14 S	92	"	"	-35.2	0.97	0.65	+11.0	2.8	1.2
220745	1 F		7.6	210	-93.6	2.19	1.16	+34.7	7.6	6.4
	2 S	96	"	"	-48.7	2.84	2.19	+12.4	4.8	2.8
	3 S	172	"	"	-68.0	3.10	1.94	+19.7	8.0	6.6
	4 S	160	"	"	-44.3	2.71	1.42	+11.2	2.4	1.6

Table 2.3(c)--continued.

UNIVERSAL TIME	STROKE NUMBER	TIME INTERVAL (ms)	LOCATION FROM MLL R (km)	LOCATION FROM MLL θ (deg)	VERTICAL ELECTRIC FIELD PEAK (V/m)	VERTICAL ELECTRIC FIELD RISETIME (μs) 0-peak	VERTICAL ELECTRIC FIELD RISETIME (μs) 10%-90%	TEST LINE VOLTAGE PEAK (kV)	TEST LINE VOLTAGE RISETIME (μs) 0-peak	TEST LINE VOLTAGE RISETIME (μs) 10%-90%
220832	1 F		7.5	196	-74.5	3.48	1.42	+26.5	6.8	4.0
	2 S	32	"	"	-65.9	1.55	0.77	+18.1	1.6	1.2
	3 S	84	"	"	-82.5	3.48	2.97	+26.8	4.0	3.2
	4 S	24	"	"	-30.2	0.77	0.45	+7.6	2.0	1.6
220919	1 F		10.2	211	-67.1	3.35	1.94	+17.8	5.6	3.6
	2 S	44	"	"	-78.8	2.65	2.19	+22.0	3.2	2.0
220920	1 F		7.5	211	-93.4	3.35	2.58	+32.4	9.6	6.4
	2 S	48	"	"	-20.1	0.77	0.32	+3.3	8.8	3.6
	3 S	52	"	"	-25.4	1.55	1.03	+5.3	2.0	1.6
221003	1 F		13.3,9.5	205+	-64.6	3.35	2.58	+24.3	4.4	3.8
	2 F	68	8.4	"	-51.5	4.26	2.06	+14.5	3.6	2.8
	3 S	100	"	"	-69.9	1.16	0.39	+14.9	1.6	1.2
	4 S	136	"	"	-74.7	2.58	1.42	+15.1	2.8	1.6
	5 S	88	"	"	-25.0	0.65	0.39	+5.8	2.0	1.6
	6 S	144	"	"	-29.0	1.16	0.58	+5.6	2.0	1.6
	7 S	80	"	"	-21.9	1.42	0.71	+5.3	1.6	1.4
	8 S	40	"	"	-33.0	1.10	0.77	+6.4	0.8	0.6
	9 S	12	"	"	-20.1	0.84	0.52	+4.3	1.6	1.2
	10 S	32	"	"	-45.4	1.35	0.77	+9.9	1.6	1.4
	11 S	112	"	"	-32.6	1.16	0.77	+7.3	1.2	0.8

Table 2.3(c)--continued.

UNIVERSAL TIME	STROKE NUMBER	TIME INTERVAL (ms)	LOCATION FROM MLL R (km)	LOCATION FROM MLL θ (deg)	VERTICAL ELECTRIC FIELD PEAK (V/m)	VERTICAL ELECTRIC FIELD RISETIME (μs) 0-peak	VERTICAL ELECTRIC FIELD RISETIME (μs) 10%-90%	TEST LINE VOLTAGE PEAK (kV)	TEST LINE VOLTAGE RISETIME (μs) 0-peak	TEST LINE VOLTAGE RISETIME (μs) 10%-90%
221031	1 F		9.8	215	-83.5	5.16	3.35	+25.0	9.2	7.2
	2 S	32	"	"	-32.9	1.94	1.29	+6.9	1.6	0.8
	3 S	344	"	"	-91.2	4.13	2.52	+24.6	6.8	4.8
	4 S	24	"	"	-48.6	1.03	0.52	+14.0	6.4	4.4
	5 S	100	"	"	-43.0	1.42	0.77	+8.1	1.6	0.8
	6 S	248	"	"	-53.3	1.03	0.71	+8.4	1.6	0.8
	7 S	52	"	"	-26.5	1.03	0.35	+5.0	1.2	0.8
221055	1 F		9.3	195	-49.2	4.39	3.55	+22.7	4.0	3.4
	2 F	102	6.0	195	-54.6	3.29	2.45	+15.2	4.0	2.0
	3 S	48	9.3	195	-38.9	2.32	1.68	+9.9	4.0	3.2
221124	1 F		12.0	200	-55.6	5.55	4.13	+20.9	6.0	3.6
	2 S	84	"	"	-66.2	4.00	3.10	+14.8	4.8	3.2
	3 S	74	"	"	-58.1	2.97	2.06	+16.5	2.4	1.4
	4 S	60	"	"	-44.9	0.65	0.45	+10.2	1.4	0.8
	5 S	120	"	"	-66.2	1.03	0.52	+12.5	1.6	0.8

Table 2.3(c)--continued.

UNIVERSAL TIME	STROKE NUMBER	TIME INTERVAL (ms)	LOCATION FROM MLL R (km)	LOCATION FROM MLL θ (deg)	VERTICAL ELECTRIC FIELD PEAK (V/m)	VERTICAL ELECTRIC FIELD RISETIME (μs) 0-peak	VERTICAL ELECTRIC FIELD RISETIME (μs) 10%-90%	TEST LINE VOLTAGE PEAK (kV)	TEST LINE VOLTAGE RISETIME (μs) 0-peak	TEST LINE VOLTAGE RISETIME (μs) 10%-90%
221157	1 F		8.8	200	-84.3, -25.7*	3.87, 2.06*	1.68, 1.55*	+25.8, +12.2*	2.4	1.6
	2 S	52	"	"	-82.8	3.61	2.71	+20.6	2.4	1.2
	3 F	76	11.6	201	-50.7	2.06	1.68	+16.9	2.8	2.0
	4 S	112	"	"	-38.5	2.97	2.00	+9.0	2.8	2.0
	5 S	64	"	"	-60.8	1.42	0.84	+21.7	2.0	1.2
	6 S	40	"	"	-25.6	1.68	1.16	+7.3	2.0	0.8
	7 S	168	"	"	-32.4	1.42	0.52	+8.6	2.0	1.6
	8 S	56	"	"	-48.2	1.55	0.77	+11.2	1.6	1.0
	9 S	12	"	"	-37.1	1.10	0.52	+11.6	2.0	1.2
	10 S	92	"	"	-19.5	1.29	0.65	+5.3	1.2	0.8
	11 S	152	"	"	-26.1	0.90	0.39	+6.9	2.0	1.2
	12 S	60	"	"	-26.2	1.48	0.90	+8.8	1.6	1.0
	13 S	136	"	"	-32.0	2.64	1.42	+7.9	1.6	0.8
	14 S	76	"	"	-48.5	1.61	0.65	+14.5	2.8	1.6
221241	1 F		11.0	211	-72.1	4.64	1.81	+20.9	7.2	6.0
	2 S	32	"	"	-40.0	3.35	2.58	+13.4	4.0	3.2
	3 S	112	"	"	-87.1	6.19	4.90	+43.6	10.4	5.2

Table 2.3(c)--continued.

UNIVERSAL TIME	STROKE NUMBER		TIME INTERVAL (ms)	LOCATION FROM MLL R (km)	LOCATION FROM MLL θ (deg)	VERTICAL ELECTRIC FIELD PEAK (V/m)	VERTICAL ELECTRIC FIELD RISETIME (μs) 0-peak	VERTICAL ELECTRIC FIELD RISETIME (μs) 10%-90%	TEST LINE VOLTAGE PEAK (kV)	TEST LINE VOLTAGE RISETIME (μs) 0-peak	TEST LINE VOLTAGE RISETIME (μs) 10%-90%
221331	1	F		10.0	198	-45.3	5.29	3.87	+12.2	7.6	4.8
	2	S	64	"	"	-66.2	2.84	1.68	+20.3	2.0	1.4
	3	S	148	"	"	-32.8	2.84	2.06	+7.7	2.8	1.8
	4	S	48	"	"	-21.9	1.55	0.77	+4.6	1.2	0.8
	5	S	180	"	"	-49.2	1.16	0.65	+9.9	1.6	0.8
	6	S	40	"	"	-32.0	1.03	0.32	+7.5	1.6	1.2
	7	S	24	"	"	-38.5	1.29	0.45	+12.8	1.6	1.2
	8	S	180	"	"	-41.6	1.81	0.77	+12.5	2.0	1.0
	9	S	144	"	"	-48.2	1.48	0.90	+14.2	1.8	1.2
221450	1	F		11.8	205	-48.5	5.16	4.26	+12.9	4.8	3.6
	2	S	50	"	"	-40.7	4.06	2.97	+11.2	3.2	2.8
	3	F	76	13.5	205	-40.7	3.23	2.58	+12.5	8.8	3.6
	4	S	160	"	"	-20.4	3.42	1.94	+5.6	1.6	1.2
	5	S	46	"	"	-19.4	2.71	0.77	+3.3	5.6	3.6
	6	S	94	"	"	-21.0	1.16	0.32	+5.0	6.4	4.0
	7	S	56	"	"	-24.3	1.42	0.45	+5.0	4.4	3.6
	8	S	140	"	"	-29.5	1.81	0.65	+8.8	6.4	3.2
221919	1	F		11.0	193	-36.2	---	---	+12.4	---	---
	2	S	---	"	"	-61.1	---	---	+16.5	---	---
	3	F	---	6.1	195	-89.1	---	---	+34.6	---	---
	4	S	---	"	"	-40.4	---	---	+12.4	---	---
	5	S	---	"	"	-81.1	---	---	+25.0	---	---
	6	S	---	"	"	-34.1	---	---	+12.4	---	---
	7	S	---	"	"	-31.9	---	---	+10.0	---	---
	8	S	---	"	"	-32.4	---	---	+5.6	---	---

Table 2.3(c)--continued.

UNIVERSAL TIME	STROKE NUMBER	TIME INTERVAL (ms)	LOCATION FROM MLL R (km)	LOCATION FROM MLL θ (deg)	VERTICAL ELECTRIC FIELD PEAK (V/m)	VERTICAL ELECTRIC FIELD RISETIME (μs) 0-peak	VERTICAL ELECTRIC FIELD RISETIME (μs) 10%-90%	TEST LINE VOLTAGE PEAK (kV)	TEST LINE VOLTAGE RISETIME (μs) 0-peak	TEST LINE VOLTAGE RISETIME (μs) 10%-90%
222843	1 F		2.5	229	-217.0	5.60	3.82	+60.8	8.0	5.6
	2 S	136	"	"	-69.5	4.52	1.68	+17.2	8.0	6.2
	3 S	152	"	"	-47.9	1.55	0.65	+8.0	8.0	6.4
	4 S	68	"	"	-66.2	2.45	1.03	+12.5	7.6	6.4
	5 S	128	"	"	-34.1	1.16	0.65	+5.9	6.8	4.0
222909	1 F		6.6	268	-67.7	4.00	3.23	+10.2	8.4	4.8
	2 S	40	"	"	-29.3	1.68	0.77	+3.3	8.8	5.2
	3 S	40	"	"	-58.7	4.39	2.97	+7.0	2.8	1.6
223010	1 F		5.5	243	-39.9	3.87	1.94	+7.7	7.6	6.4
	2 F	200	5.5	240	-74.2	3.23	1.68	+15.0	8.0	6.8
	3 S	44	"	"	-40.5	2.38	0.77	+5.0	7.2	5.6
	4 S	96	"	"	-76.9	5.55	2.58	+14.7	9.2	7.4
223119	1 F		8.1	231	-61.4	3.48	2.71	+15.8	9.6	7.6
	2 S	56	"	"	-76.2	1.94	1.55	+16.2	10.0	6.8
	1 F	100	4.4	293	-82.3	6.45	3.10	-23.8	11.2	4.4
223324	1 F		5.5	230	-49.5	2.71	1.16	+7.4	6.8	6.0
223651	1 F		5.1	273	-79.1	---	---	+12.4	---	---
	2 S	---	"	"	-38.9	---	---	+5.8	---	---
	3 S	---	"	"	-68.1	---	---	+9.1	---	---
	4 S	---	"	"	-41.0	---	---	+5.8	---	---
	5 S	---	"	"	-28.0	---	---	+5.0	---	---

Table 2.3(c)--continued.

UNIVERSAL TIME	STROKE NUMBER	TIME INTERVAL (ms)	LOCATION FROM MLL R (km)	LOCATION FROM MLL θ (deg)	VERTICAL ELECTRIC FIELD PEAK (V/m)	VERTICAL ELECTRIC FIELD RISETIME (μs) 0-peak	VERTICAL ELECTRIC FIELD RISETIME (μs) 10%-90%	TEST LINE VOLTAGE PEAK (kV)	TEST LINE VOLTAGE RISETIME (μs) 0-peak	TEST LINE VOLTAGE RISETIME (μs) 10%-90%
223815	1 F		7.0	246	-34.3	4.13	2.58	+5.0	16.8	11.6
	2 S	108	"	"	-31.4	4.52	2.84	+4.4	13.2	12.4
	3 S	146	"	"	-34.4	2.97	2.32	+4.0	4.8	3.2
	4 S	104	"	"	-36.6	1.94	1.16	+4.2	5.6	2.0
223917	1 F		6.5	253,261+	-37.0	4.64	2.71	+8.3	22.0	19.6
	2 F	66	7.0	269	-95.1	3.48	1.29	-13.2, +6.6	4.0	2.0
	3 F	98	6.5	259	-79.7	3.61	1.81	-5.0, +7.3	1.2	1.2
	4 S	66	"	"	-86.6	4.77	3.48	-5.3, +8.6	1.0	0.8
	5 S	108	"	"	-85.1	6.06	3.23	-4.6, +8.6	1.2	1.0
	6 S	100	"	"	-56.9	2.45	1.16	-4.0, +5.0	1.6	1.2
224014	1 F		6.5	261	-88.9	4.13	3.23	-7.9, +7.6	7.2	2.4
	2 S	56	"	"	-87.4	3.74	3.23	-7.6, +5.6	4.0	3.2
	3 S	28	"	"	-34.2	1.68	0.77	-3.2, +3.0	1.6	1.6
	4 S	320	"	"	-86.8	3.35	1.03	-8.6, +6.6	2.0	1.4
224251	1 F		8.1	254	-30.3	5.81	2.45	-0.9, +3.3	5.4	2.8
	2 F	116	7.2	288	-87.1	3.35	2.71	-19.0	7.2	3.6
224313	1 F		10.0	285	-39.3	5.29	3.10	-8.3, +2.3	8.0	5.2
	2 S	180	"	"	-36.1	3.35	1.55	-7.9, +2.0	4.0	2.4
	3 S	48	"	"	-16.5	0.77	0.26	-2.5, +1.2	1.6	0.8
224453	1 F		9.5	269	-58.8	1.94	1.16	-7.9, +1.7	3.2	0.8
	2 F	84	"	282	-68.8	1.68	1.16	-10.1, +2.6	1.4	0.8

Table 2.3(c)--continued.

UNIVERSAL TIME	STROKE NUMBER	TIME INTERVAL (ms)	LOCATION FROM MLL R (km)	LOCATION FROM MLL θ (deg)	VERTICAL ELECTRIC FIELD PEAK (V/m)	VERTICAL ELECTRIC FIELD RISETIME (μs) 0-peak	VERTICAL ELECTRIC FIELD RISETIME (μs) 10%-90%	TEST LINE VOLTAGE PEAK (kV)	TEST LINE VOLTAGE RISETIME (μs) 0-peak	TEST LINE VOLTAGE RISETIME (μs) 10%-90%
224520	1 F		9.5	282	-71.7	4.77	2.97	-16.5, +1.3	10.4	5.0
	2 S	40	"	"	-26.5	2.06	1.03	-4.6, +1.7	7.2	5.6
	3 S	66	"	"	-90.9	2.58	1.61	-17.2, +2.6	9.2	3.2
	4 S	74	"	"	-36.2	1.81	1.29	-6.6	4.8	2.8
	5 S	24	"	"	-34.8	1.68	0.65	-5.0, +1.3	2.0	1.6
	6 S	24	"	"	-33.4	1.55	0.77	-4.6, +1.0	2.8	1.4
	7 S	294	"	"	-82.6	2.84	1.81	-11.9, +5.3	4.8	2.0
	8 S	58	"	"	-28.4	1.68	0.90	-5.3, +1.3	4.8	3.2
	9 S	170	"	"	-23.4	1.55	0.90	-4.1, +1.0	7.2	3.2
224612	1 F		11.5	270	-104.0	8.00	4.26	-15.8, +6.6	8.4	4.4
	2 S	58	"	"	-60.3	3.23	2.45	-8.6, +5.2	4.0	2.8
	3 S	22	"	"	-23.8	2.58	1.42	-4.3, +1.3	2.8	2.0
	4 S	48	"	"	-28.7	1.68	0.39	-4.9, +1.7	6.8	5.4
	5 S	58	"	"	-15.8	0.90	0.52	-3.0	16.0	10.4
	6 S	24	"	"	-28.5	1.03	0.52	-4.8	5.2	4.0
	7 S	204	"	"	-32.9	1.94	1.29	-4.9, +1.3	2.8	2.2
	8 S	152	"	"	-26.3	1.81	1.16	-3.3, +1.7	4.8	3.6
224645	1 F		8.8	283	-112.1	4.39	2.84	-25.1, +5.3	5.6	3.2
	2 S	26	"	"	-35.7	1.68	0.90	-7.0	4.8	1.6
	3 S	28	"	"	-77.7	1.68	0.90	-15.3	7.2	3.6
	4 S	28	"	"	-20.1	0.77	0.39	-2.0, +1.0	2.4	1.2

Table 2.3(c)--continued.

UNIVERSAL TIME	STROKE NUMBER	TIME INTERVAL (ms)	LOCATION FROM MLL R (km)	LOCATION FROM MLL θ (deg)	VERTICAL ELECTRIC FIELD PEAK (V/m)	VERTICAL ELECTRIC FIELD RISETIME (μs) 0-peak	VERTICAL ELECTRIC FIELD RISETIME (μs) 10%-90%	TEST LINE VOLTAGE PEAK (kV)	TEST LINE VOLTAGE RISETIME (μs) 0-peak	TEST LINE VOLTAGE RISETIME (μs) 10%-90%
224738	1 F	26	8.0	267	-110.7	2.97	1.61	-13.2, +7.3	4.8	4.8
	2 S		"	"	-22.3	2.97	2.06	-2.3, +1.3	2.8	1.6
224739	1 F	40	17.0	269	-19.8	2.45	1.42	-2.6, +1.0	3.2	2.0
	2 S		"	"	-32.1	2.32	1.81	-8.3, +2.6	4.0	3.2

+Two channels to ground.

*Two peaks within 200 μs probably due to two channels to ground.

2.6.1 Analysis of Vertical Electric Field Records

In Figures 2.10 and 2.11 we plot histograms of the location of the various strokes used in the analysis. In Figure 2.10 we plot the number of strokes at various angles from the MLL, 0° being true North. In Figure 2.11 we plot the number of strokes occurring at various ranges from the MLL. The shaded data in Figures 2.10 and 2.11, and in all other figures involving first stroke parameters, represent subsequent strokes which have a new channel to ground and are classified as first strokes, as discussed in Chapter I. Figure 2.10 shows that there are strikes in all four quadrants around the test-line, although there is relatively less lightning in the first quadrant (0° - 90°) and the fourth quadrant (260° - 360°). This is partly because of the positioning of the TV network and partly due to operation problems associated with the remote TVs. Figure 2.11 indicates that we have data on strokes at distances from about 1 km to about 20 km from the line. The range at which the TVs can register a flash limits the range of the measured data because the data set was limited to those flashes which could be seen on at least one TV monitor.

A total of 90 flashes have been analyzed in this thesis. In Figure 2.12(a) we plot a histogram of the number of strokes in a flash; Figure 2.12(b) shows a cumulative distribution function derived from the histogram. The average number of strokes per flash is 3.8 with a standard deviation of 3.0; the median value is 3, and the most probable value is 1. A histogram of the time interval between successive strokes in a multiple-stroke flash is shown in Figure 2.13(a). The associated cummulative frequency distribution is

Figure 2.10. Number of strokes in the analyzed data plotted as a function of the angle from the Mobile Lightning Laboratory. The shaded data indicate subsequent strokes which have been classified as first strokes.

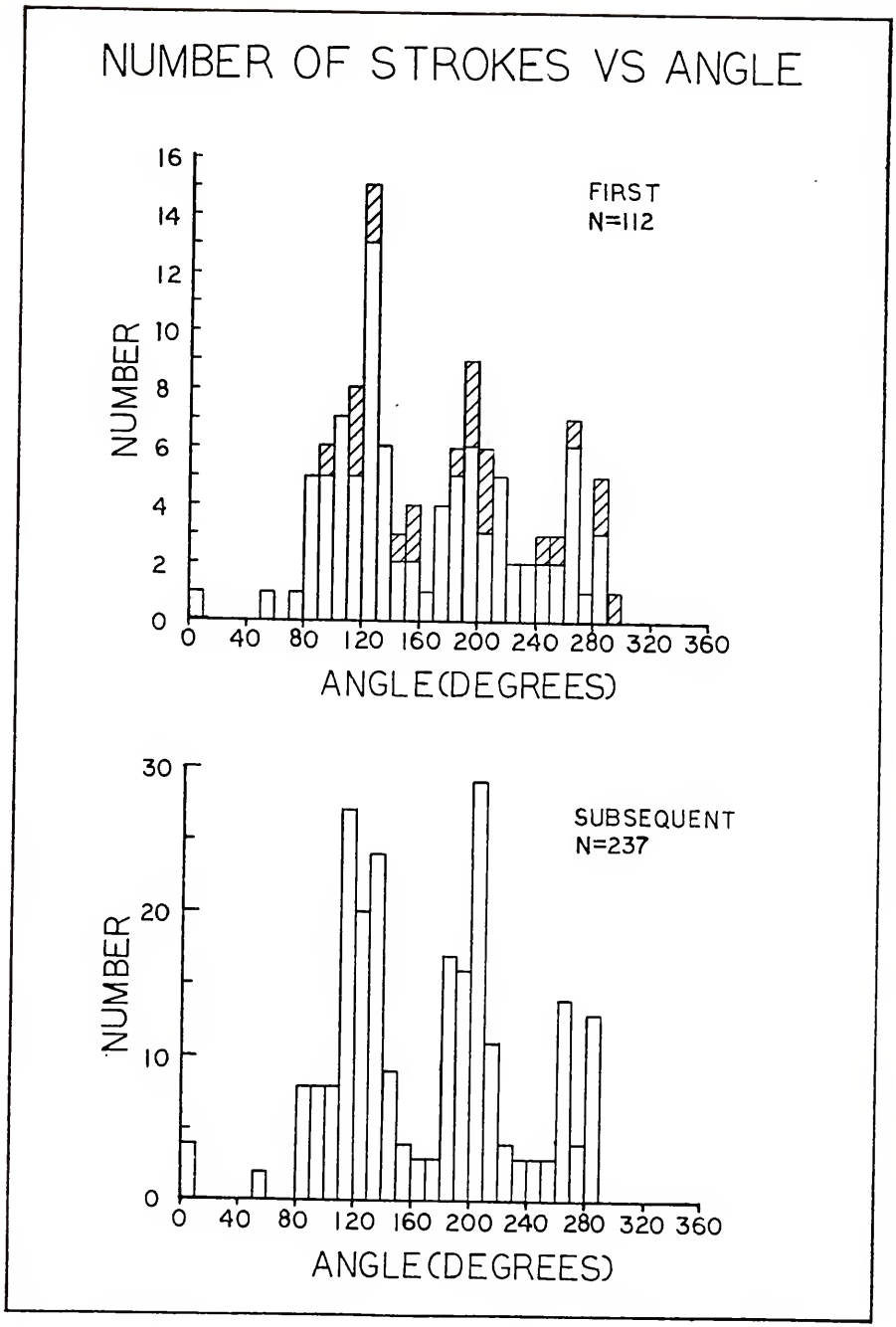
NUMBER OF STROKES VS ANGLE
FIRST
N=112
NUMBER
0
2
4
6
8
10
12
14
16
0 40 80 120 160 200 240 280 320 360
ANGLE(DEGREES)
SUBSEQUENT
N=237
NUMBER
0
10
20
30
0 40 80 120 160 200 240 280 320 360
ANGLE(DEGREES)

Figure 2.11. Number of strokes in the analyzed data plotted as a function of the distance from the Mobile Lightning Laboratory. The shaded data indicate subsequent strokes which have been classified as first strokes.

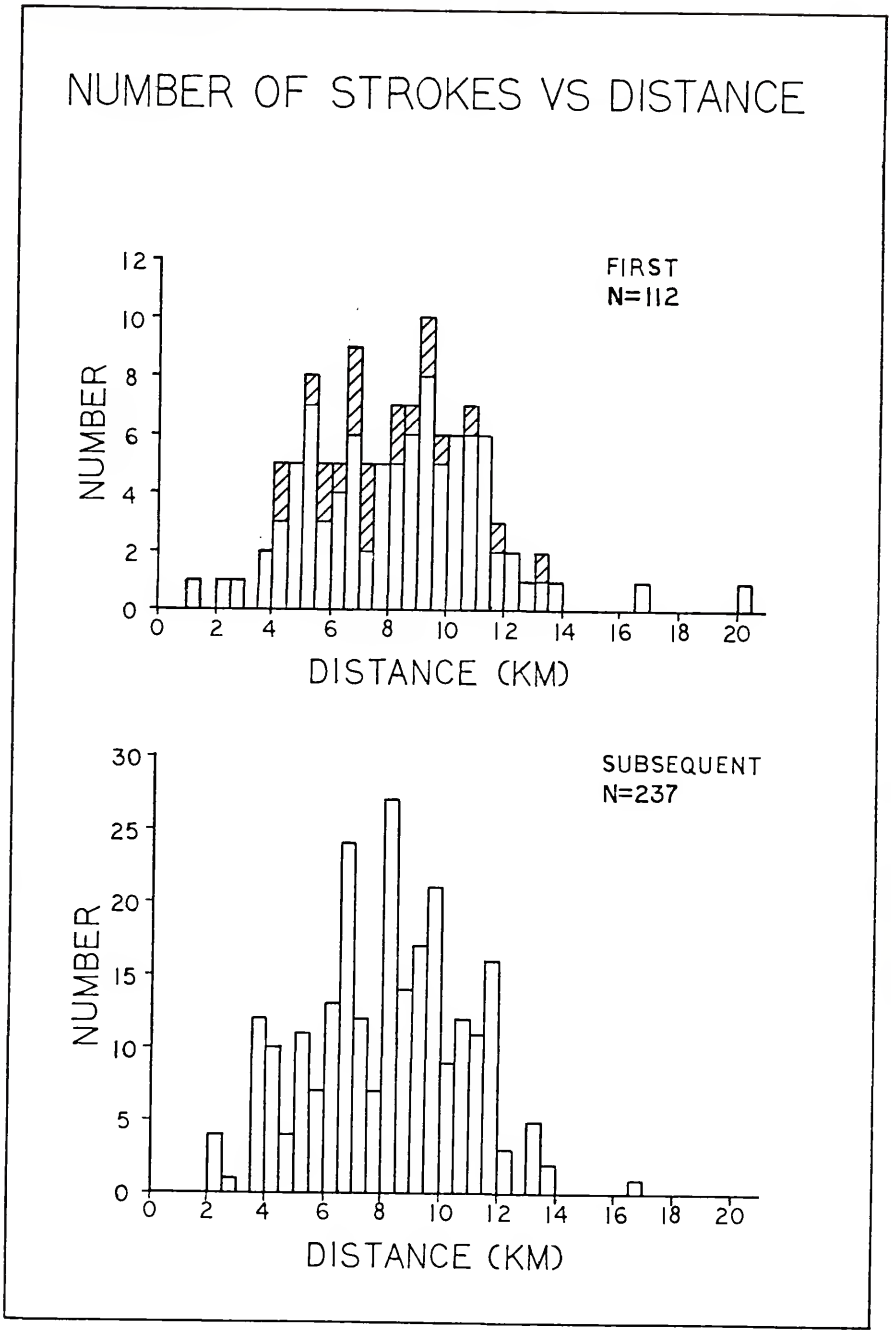
NUMBER OF STROKES VS DISTANCE
FIRST
N=112
NUMBER
DISTANCE (KM)
SUBSEQUENT
N=237
NUMBER
DISTANCE (KM)

Figure 2.12(a). Histogram showing the number of strokes per flash for the data analyzed. The mean is 3.8 with a standard deviation of 3.0. The median is 3.

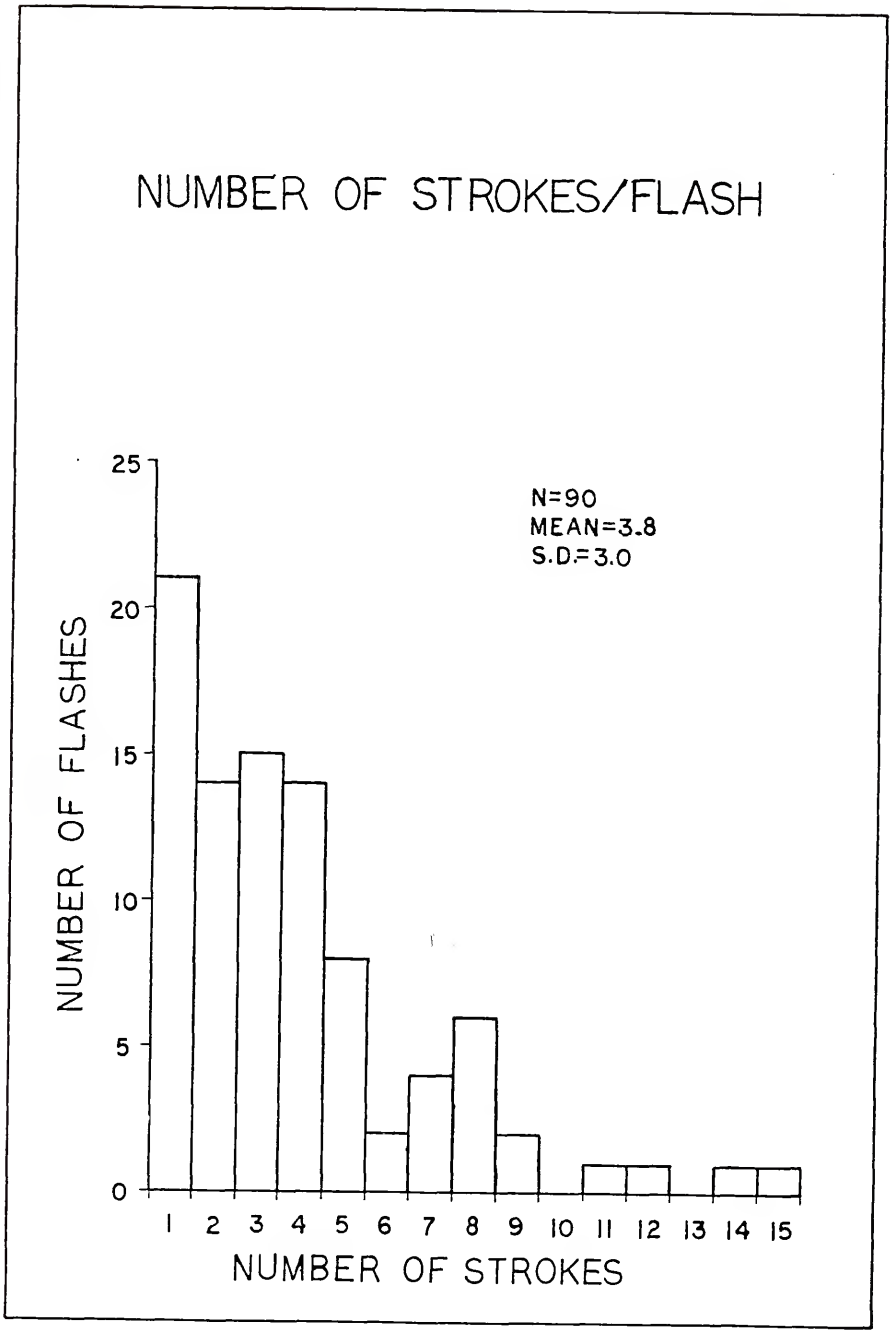
NUMBER OF STROKES/FLASH
N=90
MEAN=3.8
S.D.=3.0
NUMBER OF FLASHES
25
20
15
10
5
0
1 2 3 4 5 6 7 8 9 10 11 12 13 14 15
NUMBER OF STROKES

Figure 2.12(b). Cumulative distribution function for the number of strokes per flash showing the correlation between data obtained in this thesis and other studies.

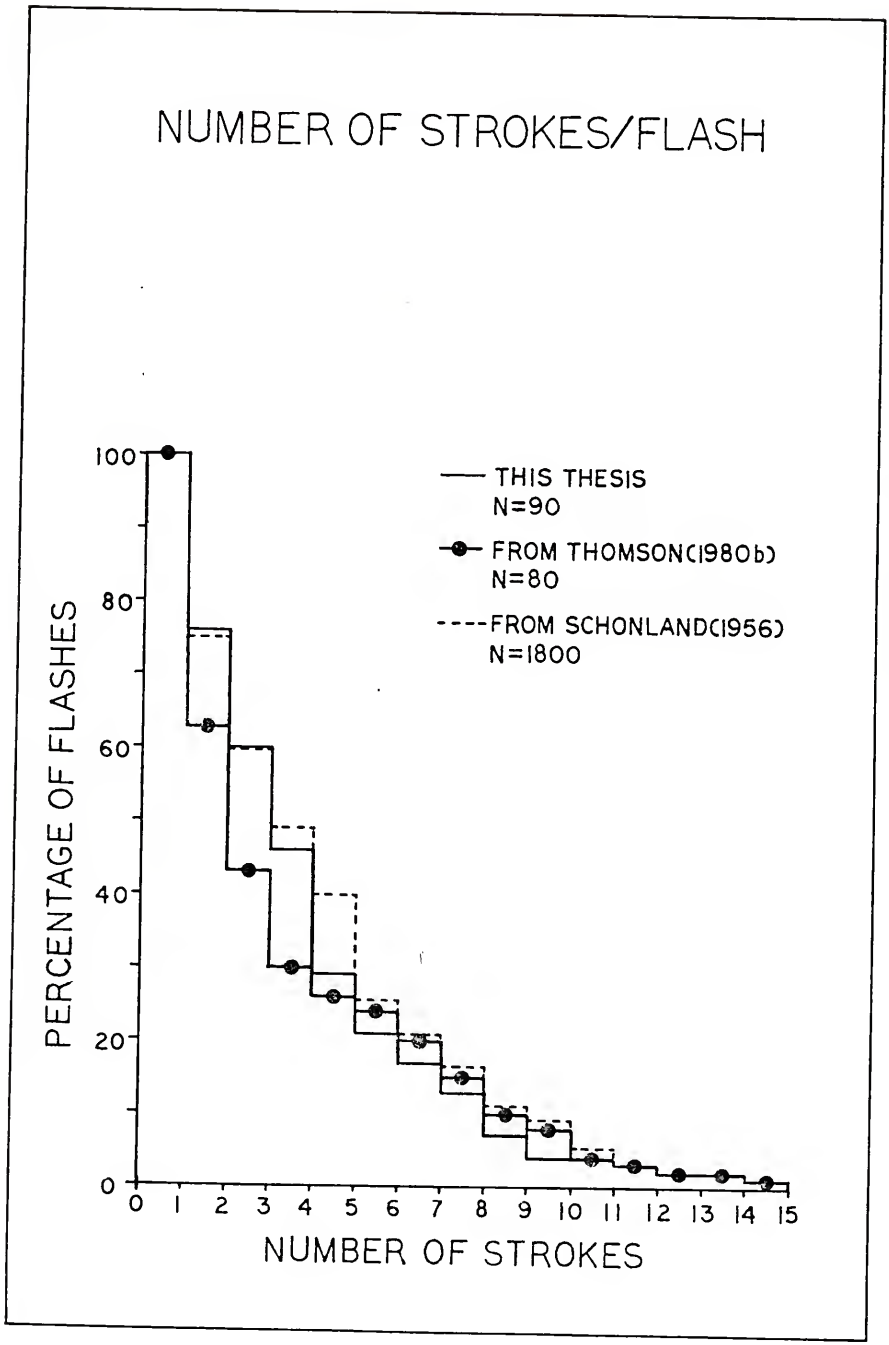
NUMBER OF STROKES/FLASH
THIS THESIS
N=90
FROM THOMSON(1980b)
N=80
FROM SCHONLAND(1956)
N=1800
PERCENTAGE OF FLASHES
100
80
60
40
20
0
0 1 2 3 4 5 6 7 8 9 10 11 12 13 14 15
NUMBER OF STROKES

Figure 2.13(a). Histogram of time intervals between successive return strokes in a flash.

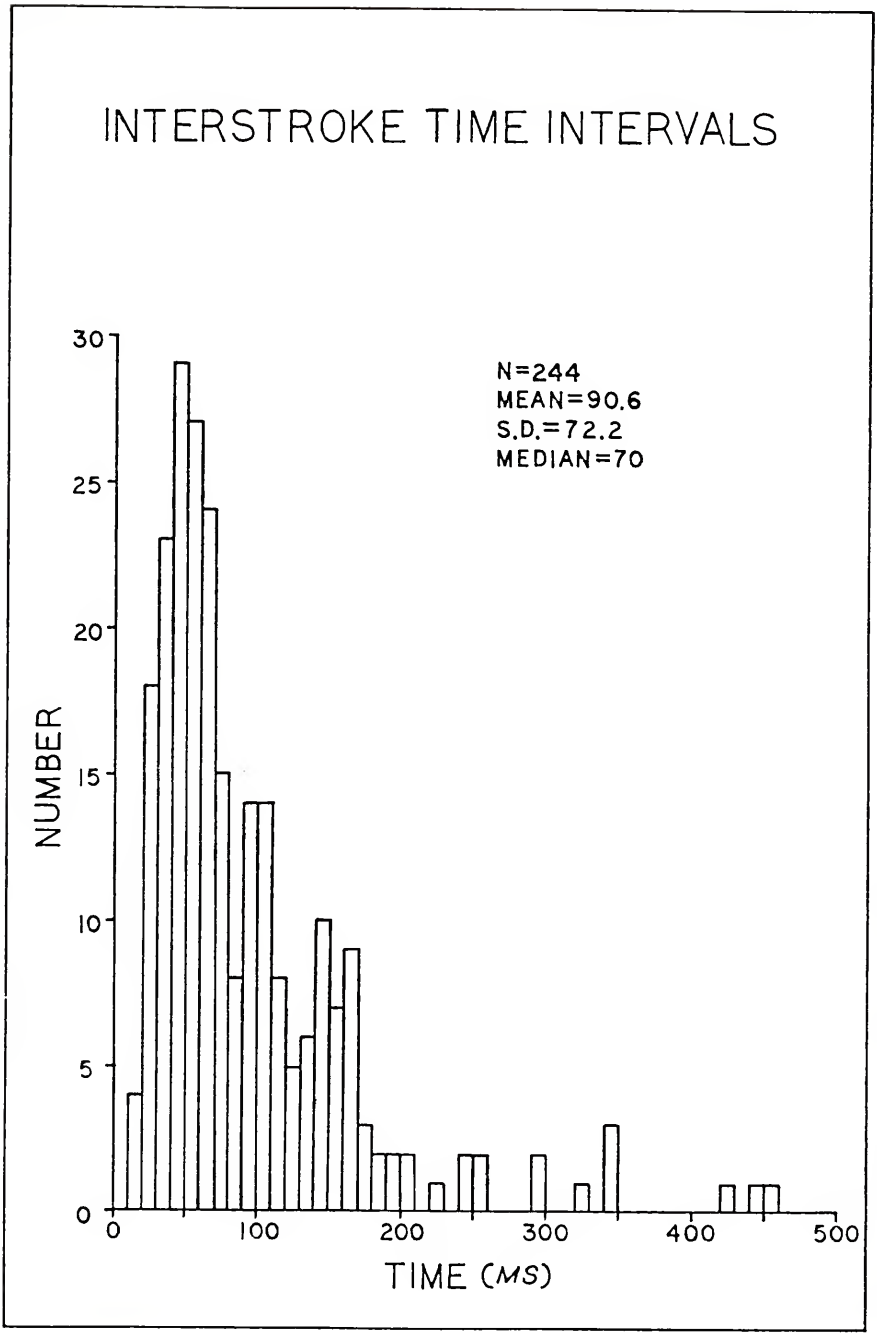
INTERSTROKE TIME INTERVALS
N=244
MEAN=90.6
S.D.=72.2
MEDIAN=70
NUMBER
30
25
20
15
10
5
0
0
100
200
300
400
500
TIME (MS)

Figure 2.13(b). Cumulative distribution function for interstroke time intervals showing the correlation between data obtained in this thesis and other studies.

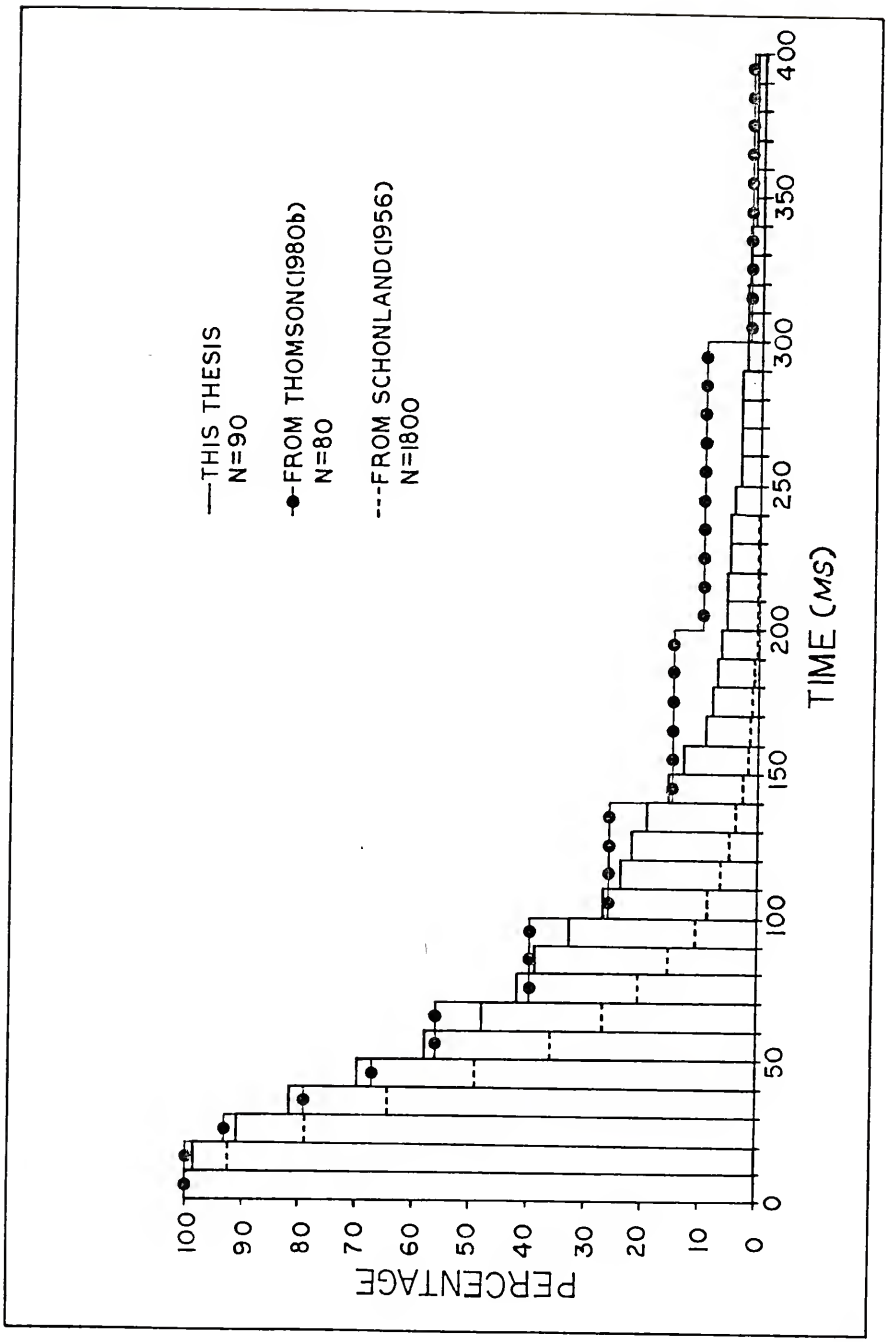
—THIS THESIS
N=90
-●-FROM THOMSON(1980b)
N=80
---FROM SCHONLAND(1956)
N=1800
PERCENTAGE
0
10
20
30
40
50
60
70
80
90
100
0
50
100
150
200
250
300
350
400
TIME (MS)

given in Figure 2.13(b). The mean for this distribution is 90 ms with 72 ms as the standard deviation; the median is 70 ms, with the most probable values between 40 and 60 ms. In Figures 2.12(b) and 2.13(b) the data presented here are compared with those given by Schonland (1956) and Thomson (1980a).

The parameters plotted in Figures 2.12(a) and (b), and in Figures 2.13(a) and (b) were obtained from continuous instrumentation tape records which were examined at various time-scales ranging from 400 ms to 40 μs full-scale. Thomson (1980b) has presented a summary of data on the number of strokes per flash and the interstroke time interval measured by various researchers all over the world using various techniques which include records of fields on a slow time-scale, optical data, and measurements made from closed-circuit video tape records. The technique used here is less prone to error than any technique used before. From Table 1 in Thomson (1980b) it can be seen that there is considerable spread in the values of the mean number of strokes per flash and mean interstroke time interval as reported in the literature. The mean number of strokes per flash ranges from a low value of 2.1 (Brantley et al., 1975) to a high of 6 (Kitagawa et al., 1962). The mean interstroke interval ranges from 38 ms (McCann, 1944) to 150 ms (Takeuti, 1965). The statistics presented in Figures 2.12(a) and 2.13(a) give values which are within the range of those presented in the literature. In another paper, Thomson (1980a) has given a cumulative distribution function for the number of strokes per flash for 80 lightning flashes in Papua, New Guinea. Schonland (1956) also gives such a distribution due to 1800 flashes over a long period of time in South Africa. In Figures

2.12(b) and 2.13(b) these two distributions are also redrawn and indicate reasonable agreement with the data presented in this thesis. Anderson and Eriksson (1980) report a mean of 2.5 strokes per flash computed from 638 flashes. However, over half the number of flashes in their data have a single stroke. They also report a median value of 50 ms for their interstroke time interval distribution. A summary of the flash statistics listed in Table 2.4 indicates that the sample of flashes analyzed in this thesis is fairly typical of worldwide lightning.

We shall now discuss various statistical parameters of interest related to the return stroke field change. We analyze first and subsequent strokes separately. As discussed in Chapter I, in this thesis we define a "first" stroke as one which is associated with a new channel to ground, as seen on the TV monitors. However, as mentioned earlier, the data points associated with these strokes will be shaded in the histograms, so that they may be readily identified. There are 22 such events out of a total of 112 first strokes.

The initial peak in the vertical electric field at ground is essentially due to the radiation component of the total electric field and can be identified readily at all but very close (under 500 m) distances from the lightning channel. Figure 2.14(a) shows a plot of this electric peak field as a function of distance from the MLL. This initial peak may be normalized to a distance of 100 km using an inverse distance relationship as discussed by Lin et al. (1979). In Figure 2.14(b) we show histograms for the normalized peak for 112 first strokes: the mean is 6.2 V/m and the standard deviation is 3.4

Table 2.4. Summary of flash statistics from selected studies.

	NUMBER	MEAN	S.D.	MEDIAN
STROKES PER FLASH				
This thesis (Figure 2.12(a))	90	3.8	3.0	3
Thomson (1980a)	80	3.5	3.2	3
Brantley et al. (1975)	119	2.1	1.6	2
	86	2.9	2.1	3
Kitagawa et al. (1962)	87	6	-	-
Schonland (1956)	1800	4.1	3.1	4
INTERSTROKE TIME INTERVAL (ms)				
This thesis (Figure 2.13(a))	244	90	72	70
Thomson (1980a)	202	90	97	60
Brantley et al. (1975)	133	116	107	85
	161	114	77	91
Takeuti (1965)	160	150	146	89
Schonland (1956)	1500	63	50	50
McCann (1944)	83	38	36	26

Figure 2.14(a). Peak vertical electric field for first and subsequent strokes, plotted as a function of distance from the Mobile Lightning Laboratory. The dashed and solid lines represent the peak radiation field inverse distance relationship for first and subsequent strokes, respectively.

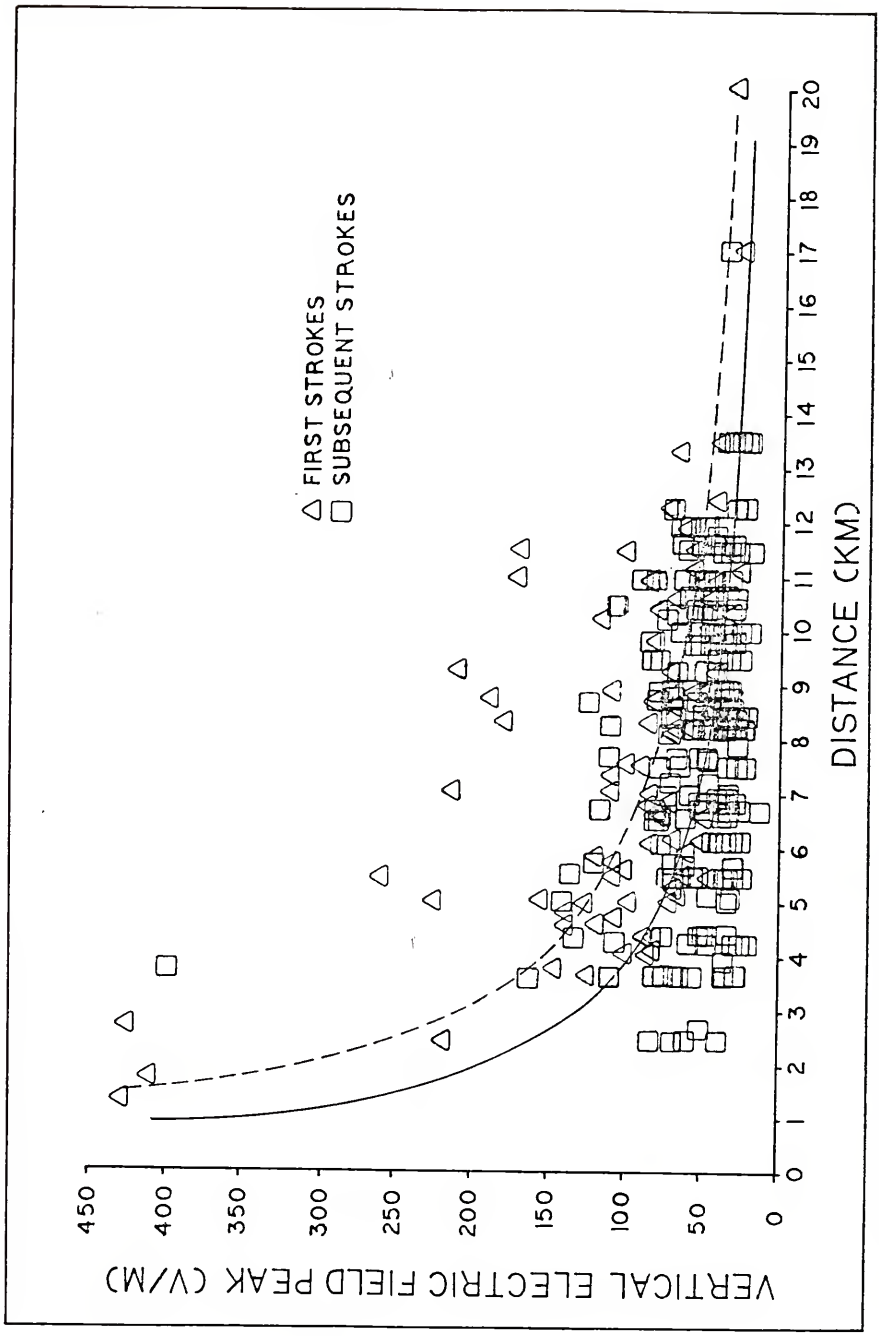
VERTICAL ELECTRIC FIELD PEAK (V/M)
450
400
350
300
250
200
150
100
50
0
0 1 2 3 4 5 6 7 8 9 10 11 12 13 14 15 16 17 18 19 20
DISTANCE (KM)
△ FIRST STROKES
□ SUBSEQUENT STROKES

Figure 2.14(b). Peak vertical electric field of the return stroke normalized to 100 km. For 112 first strokes the mean is 6.2 V/m with a standard deviation of 3.4 V/m; without the shaded data the mean for 90 first strokes is 6.5 V/m with a standard deviation of 3.5 V/m. For 237 subsequent strokes, the mean and standard deviation are 3.8 V/m and 2.2 V/m, respectively.

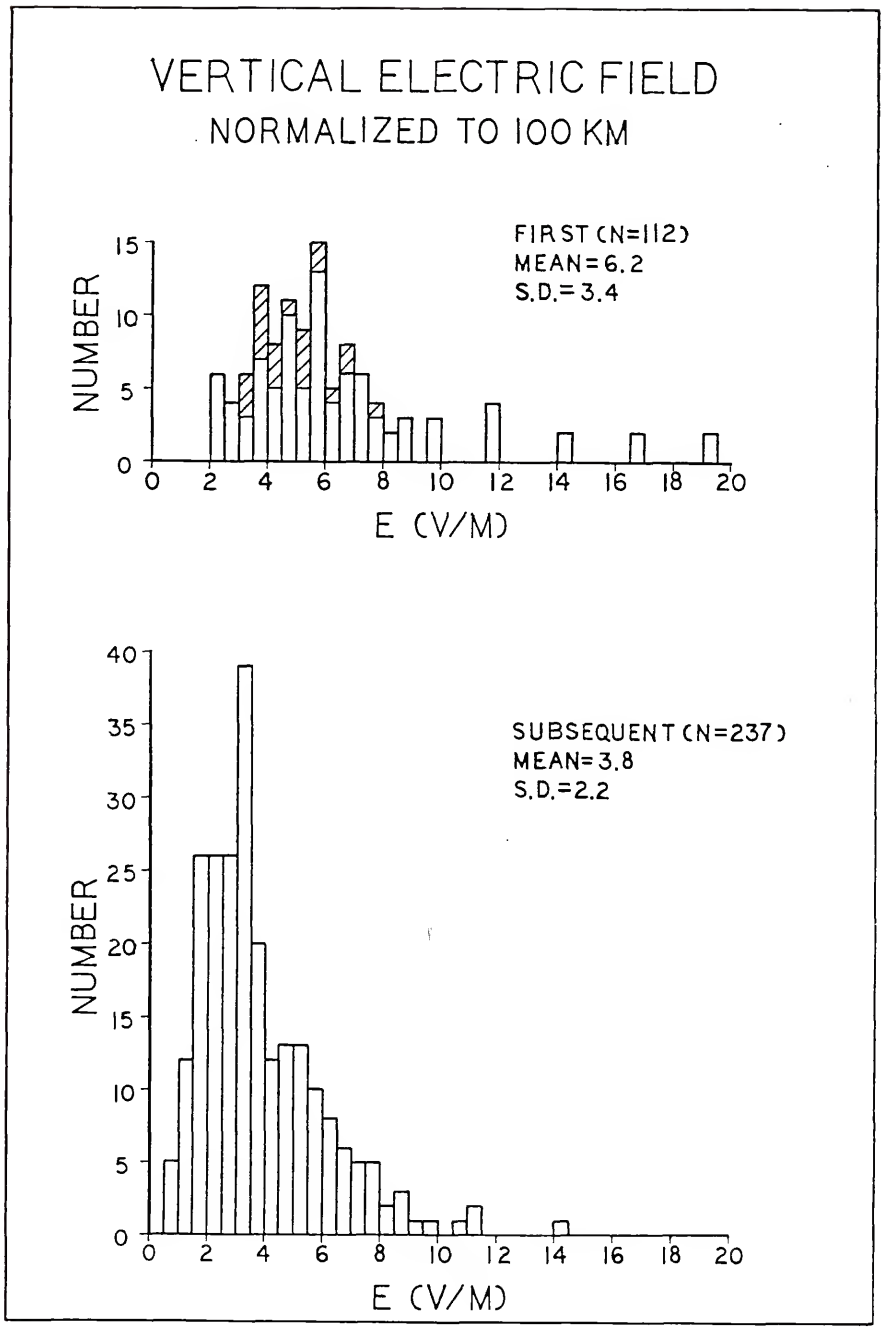
VERTICAL ELECTRIC FIELD
NORMALIZED TO 100 KM
FIRST (N=112)
MEAN=6.2
S.D.=3.4
NUMBER
E (V/M)
SUBSEQUENT (N=237)
MEAN=3.8
S.D.=2.2
NUMBER
E (V/M)

V/m. Eliminating the shaded data points leads to a mean of 6.5 V/m with a standard deviation of 3.5 V/m for 90 first strokes. For 237 subsequent strokes the mean is 3.8 V/m with a standard deviation of 2.2 V/m. Tiller et al. (1976) reported a mean of 9.9 V/m with a standard deviation of 6.8 V/m for 75 first strokes; for 163 subsequent strokes the mean and standard deviation were reported to be 5.7 V/m and 4.5 V/m respectively. McDonald et al. (1979) studied two night storms in Florida, one over the Gulf, the other over the Atlantic. The Atlantic storm had a vertical electric field peak distribution which gave a mean and standard deviation of 5.4 V/m and 2.1 V/m, respectively, for 54 first strokes, and 3.6 V/m and 1.3 V/m, respectively, for 119 subsequent strokes. Much larger means were reported for the Gulf storm: 10.2 V/m for first strokes and 5.4 V/m for subsequent strokes. Taylor (1963) reported a mean value of 4.8 V/m for 47 first strokes measured in Oklahoma. Lin et al. (1979) have presented the normalized values of the initial vertical electric field as measured simultaneously at two stations, one within 15 km of the lightning, and the other either 50 km or 200 km away. Their reported mean values at the close station for first and subsequent strokes are 6.4 V/m and 4.7 V/m, respectively. They show that the average normalized value measured at the distant station for the same data is smaller than that measured at the close station as a result of attenuation due to propagation over lossy earth. To summarize, the values for the vertical electric field peak normalized to 100 km given in this thesis agree very well with the extant data.

We now focus on the various parameters associated with the rise of the initial vertical electric field to its peak value. For the

sake of consistency all risetime measurements reported in this thesis have been made from the direct channel records obtained from the instrumentation tape on a time-scale of 40 μs full-scale. When such records were not available, no risetime measurements were made. The error involved in determining the zero is estimated to be about ±0.5 μs in most cases. A further error in measurement is estimated at about ±0.1 μs. In Figure 2.15 we present histograms for the zero-to-peak risetimes of the vertical electric field. The distribution for 105 first strokes has a mean of 4.4 μs with a standard deviation of 1.8 μs; for 220 subsequent strokes the mean is 2.8 μs with 1.5 μs as the standard deviation. Eliminating the shaded data gives a mean of 4.6 μs with 1.8 μs as the standard deviation for 84 first strokes. In a Pennsylvania study, Fisher and Uman (1972) found a mean zero-to-peak risetime from 200 μs full-scale records of 3.6 μs with a standard deviation of 1.8 μs for 26 first strokes; for 26 subsequent strokes the mean was 3.1 μs with a standard deviation of 1.9 μs. All these strokes were within 25 km of the measuring station. For storms in the area around the Kennedy Space Center, Florida, Lin and Uman (1973) using 100 μs full-scale records reported a mean zero-to-peak risetime of 4.0 μs with a standard deviation of 2.2 μs for 12 first strokes. For 83 subsequent return strokes, the mean and standard deviation were reported to be 1.2 μs and 1.1 μs, respectively. Data reported for two close storms around Gainesville, Florida, by Tiller et al. (1976) give a mean zero-to-peak risetime measured from 200 μs full-scale and 100 μs full-scale records for 120 first strokes as 3.3 μs with 1.0 μs as the standard deviation; for 163 subsequent return strokes

Figure 2.15. Distribution of the zero-to-peak risetime of the vertical electric field. For 105 first strokes the mean and standard deviation are 4.4 μs and 1.8 μs, respectively; for 220 subsequent strokes, 2.8 μs and 1.5 μs, respectively. Without the shaded data the mean for 84 first strokes is 4.6 μs with a standard deviation of 1.8 μs.

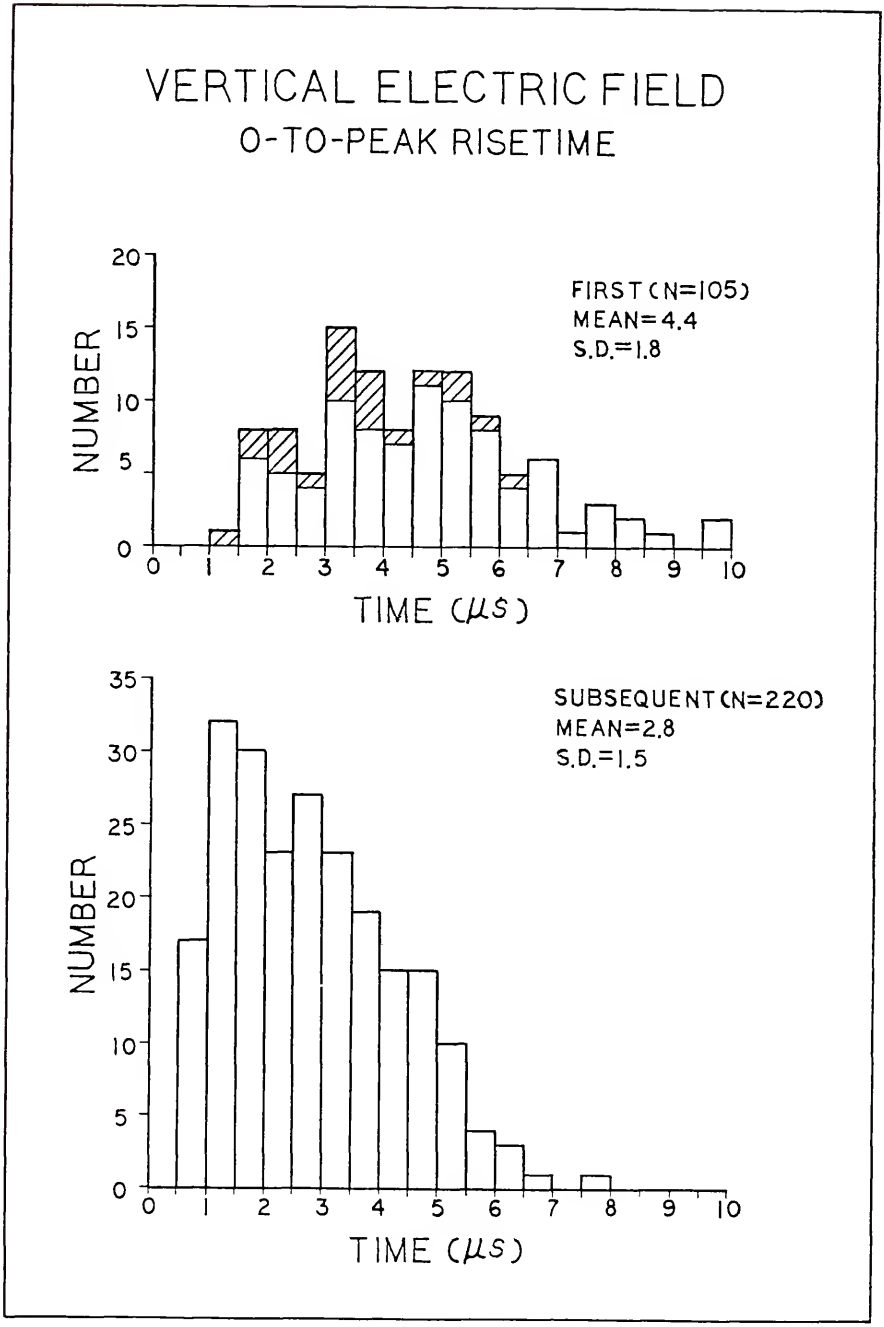
VERTICAL ELECTRIC FIELD
0-TO-PEAK RISETIME
FIRST (N=105)
MEAN=4.4
S.D.=1.8
NUMBER
TIME (μs)
SUBSEQUENT (N=220)
MEAN=2.8
S.D.=1.5
NUMBER
TIME (μs)

the mean zero-to-peak risetime was reported as 2.3 μs with a standard deviation of 0.9 μs. For the two-station electric field data reported by Lin et al. (1979) and recorded on time-scales from 40 μs to 200 μs full-scale, the mean vertical electric field zero-to-peak risetime as measured at the close station for 80 first strokes was found to be 2.5 μs with a standard deviation of 1.3 μs. For 142 subsequent strokes the mean and standard deviation were found to be 1.6 μs and 0.8 μs, respectively. For the same data, the mean risetimes measured at the far station are much larger due to the degradation in the front due to propagation. To conclude, the distributions of zero-to-peak risetimes for first and subsequent return strokes analyzed in this thesis are in agreement with those reported elsewhere in the literature. Differences in the reported values can be attributed to the different time scales of measurement.

It is difficult to define the exact zero field value, especially due to the tape recorder noise. The 10%-90% risetime is therefore a more meaningful parameter to measure than the zero-to-peak risetime. In Figure 2.16 we present histograms of the vertical electric field 10%-90% risetimes. For 105 first strokes, the distribution of the vertical electric field 10%-90% risetime was found to have a mean of 2.6 μs with a standard deviation of 1.2 μs; for 220 subsequent strokes, the mean and standard deviation were found to be 1.5 μs and 0.9 μs, respectively. Eliminating the shaded data, we find a mean of 2.7 μs with a standard deviation of 1.2 μs for 84 first strokes. There appear to be no data on the 10%-90% risetime of the vertical electric field reported in the literature. However, the values shown in Figure 2.16 are in

Figure 2.16. Distribution of the 10%-to-90% risetime of the vertical electric field. For 105 first strokes mean and standard deviation are 2.6 μs and 1.2 μs, respectively; for 220 subsequent strokes, 1.5 μs and 0.9 μs, respectively. Without the shaded data the mean is 2.7 μs with a standard deviation of 1.2 μs for 84 first strokes.

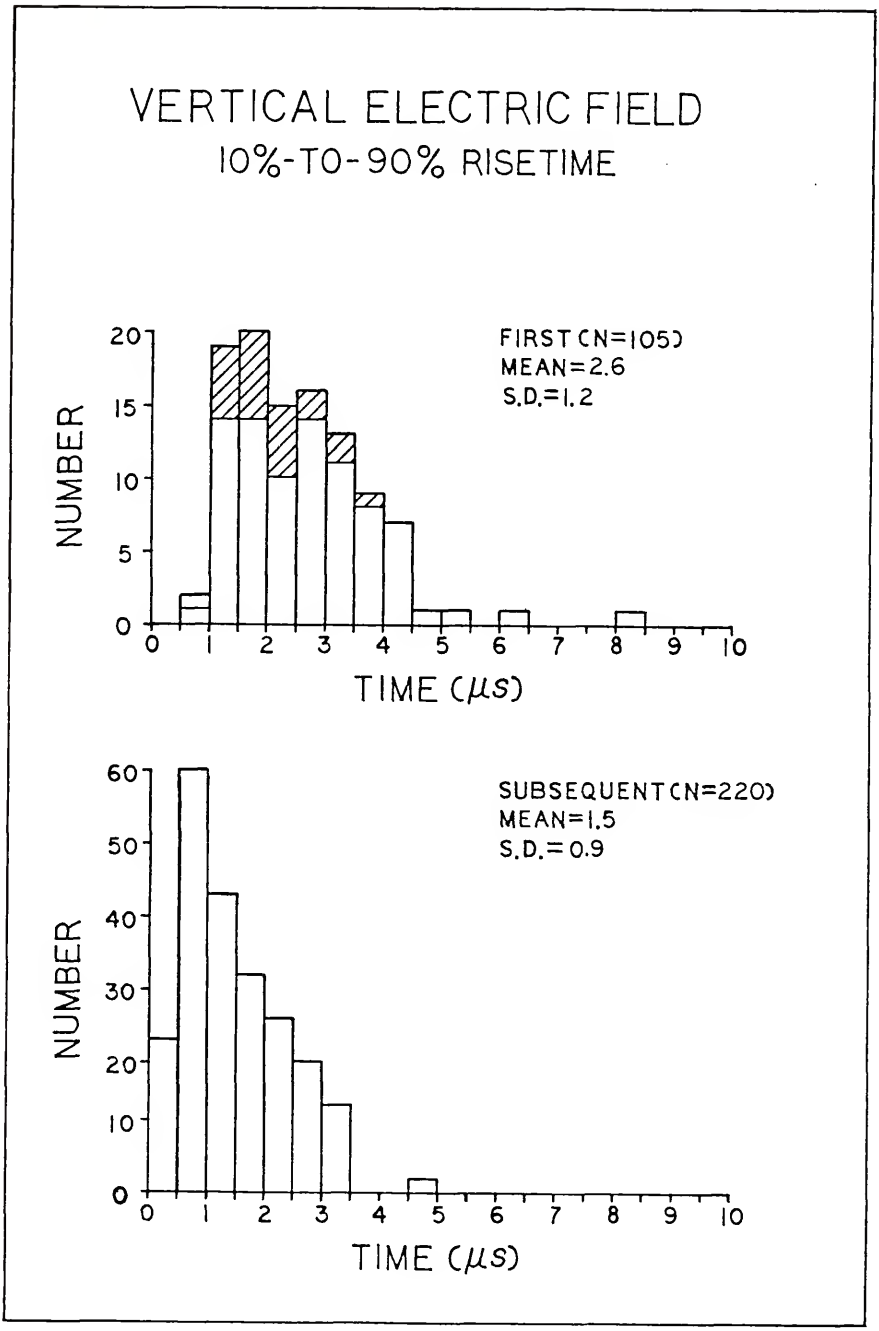
VERTICAL ELECTRIC FIELD
10%-TO-90% RISETIME
FIRST (N=105)
MEAN=2.6
S.D.=1.2
NUMBER
TIME (μs)
SUBSEQUENT (N=220)
MEAN=1.5
S.D.=0.9
NUMBER
TIME (μs)

conformity with the data on zero-to-peak risetimes reported in this thesis and elsewhere, as discussed in the previous paragraph.

Weidman and Krider (1978) have suggested that the initial wavefront of the vertical electric field due to a return stroke may be decomposed into two parts: a slow initial front, followed by a fast rise to peak. The fast portion of the wavefront is responsible for the maximum rate-of-change and hence it is a parameter of prime importance in all engineering studies. From a study of 125 strokes propagating about 50 km over sea water, Weidman and Krider (1980) have reported a mean of 90 ns and a standard deviation of 40 ns for the 10%-90% risetime of the fast portion of the wavefront. Interestingly, they report that both first and subsequent return stroke fields have about the same maximum rate-of-change. However, the fast portion of the wavefront is severely degraded as a result of propagation over land. For example, they found that the mean 10%-90% risetime of the fast transition for 29 strokes which struck sea water over a distance of 10-35 km but which propagated over only 3 km of land was 201 ns, more than twice the mean obtained when there was no propagation over land. In Figure 2.17 we plot histograms for the 10%-90% risetime of the fast transitions for data presented in this thesis. The mean is 970 ns and the standard deviation is 680 ns for 102 first strokes. Without the shaded data points the mean is 1010 ns with a standard deviation of 710 ns for 82 first strokes. For 217 subsequent strokes, the mean and standard deviation are 610 ns and 270 ns, respectively. All propagation in our data is over land with distances ranging from about 1 km to 20 km as shown in Figure 2.11.

Figure 2.17. Distribution of the 10%-to-90% risetime of the fast transition in the vertical electric field. For 102 first strokes the mean and standard deviation are 0.97 μs and 0.68 μs, respectively; for 217 subsequent strokes, 0.61 μs and 0.27 μs, respectively. Without the shaded data the mean is 1 μs with a standard deviation of 0.70 μs for 82 first strokes.

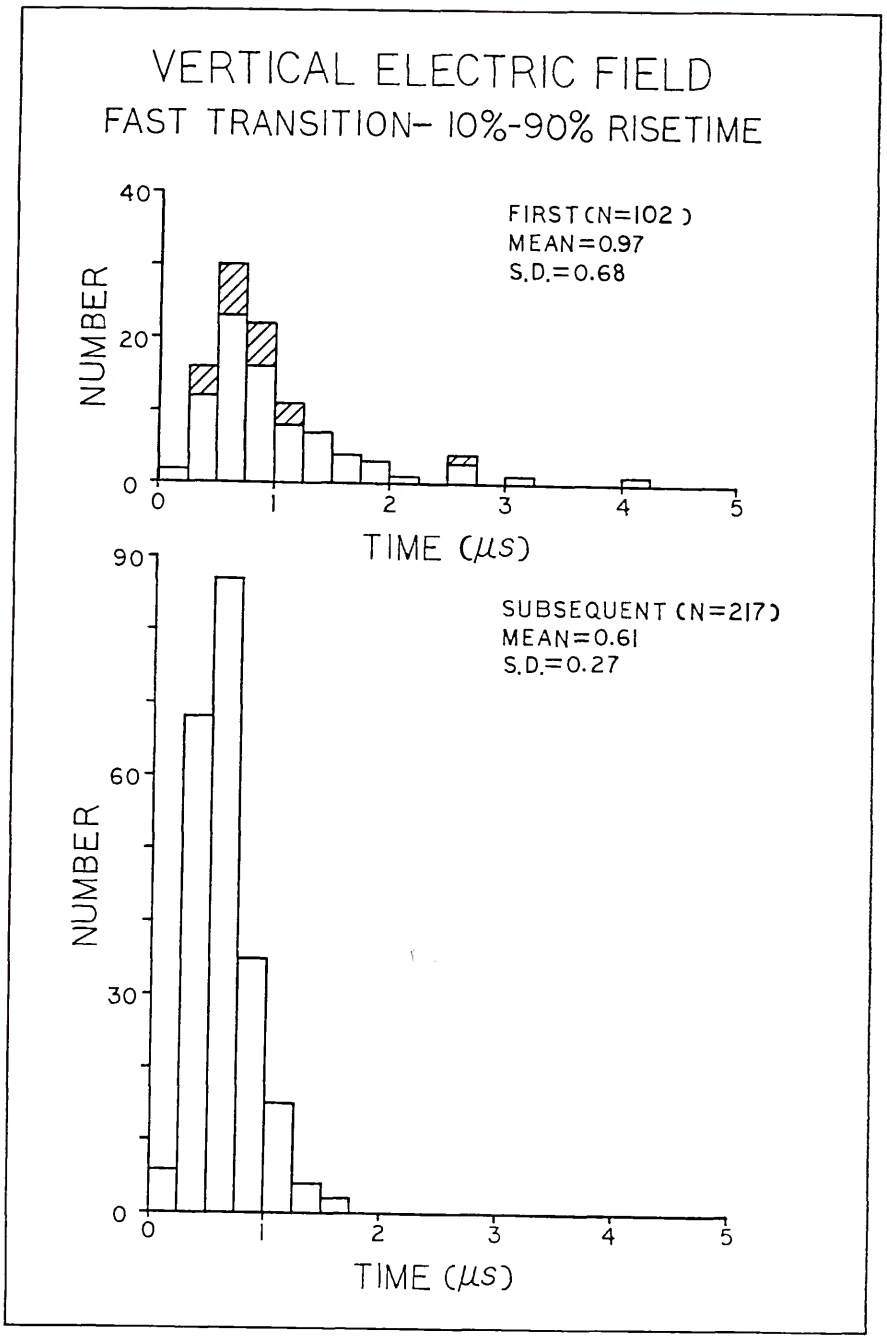
VERTICAL ELECTRIC FIELD
FAST TRANSITION- 10%-90% RISETIME
FIRST (N=102)
MEAN=0.97
S.D.=0.68
NUMBER
TIME (μs)
SUBSEQUENT (N=217)
MEAN=0.61
S.D.=0.27
NUMBER
TIME (μs)

In Figure 2.18 we plot a histogram for the duration of the slow initial front of the vertical electric field, for 105 first strokes. The mean and standard deviation were computed to be 2.9 μs and 1.3 μs, respectively. Removing the shaded data, we obtain a mean of 3.0 μs and a standard deviation of 1.3 μs for 83 first strokes. Weidman and Krider (1978) have reported a mean of about 4 μs for 152 first strokes, which is close to the mean found in this thesis. Another parameter of interest is the amplitude of the slow front expressed as a percentage of the associated return stroke peak vertical electric field. From Figure 2.19 we see that the mean for the data presented in this thesis is 28 percent for 105 first strokes, the standard deviation being 15 percent. Elimination of the shaded data leads to a mean of 27 percent and a standard deviation of 15 percent for 83 first strokes. Weidman and Krider (1978) reported a mean of about 44 percent with a standard deviation of 20 percent for 34 first strokes. It should be borne in mind that the data presented in Figures 2.17, 2.18, and 2.19 are for return strokes which propagate over ground for distances ranging from 1 km and 20 km. The data presented by Weidman and Krider (1978) were for strokes propagating over 30 to 50 km of sea water. Hence, the relatively large values of the risetime associated with the fast field change of the vertical electric fields measured in this thesis can easily be understood.

A summary of the return stroke vertical electric field statistics is given in Table 2.5. Comparisons with statistics reported in the literature indicate that the lightning return strokes studied in this thesis are not unusual.

Figure 2.18. Distribution of the duration of the slow initial front in the first stroke vertical electric field. For 105 first strokes the mean is 2.9 μs with a standard deviation of 1.3 μs; without the shaded data the mean and standard deviation are 3.0 μs and 1.3 μs, respectively for 83, first strokes.

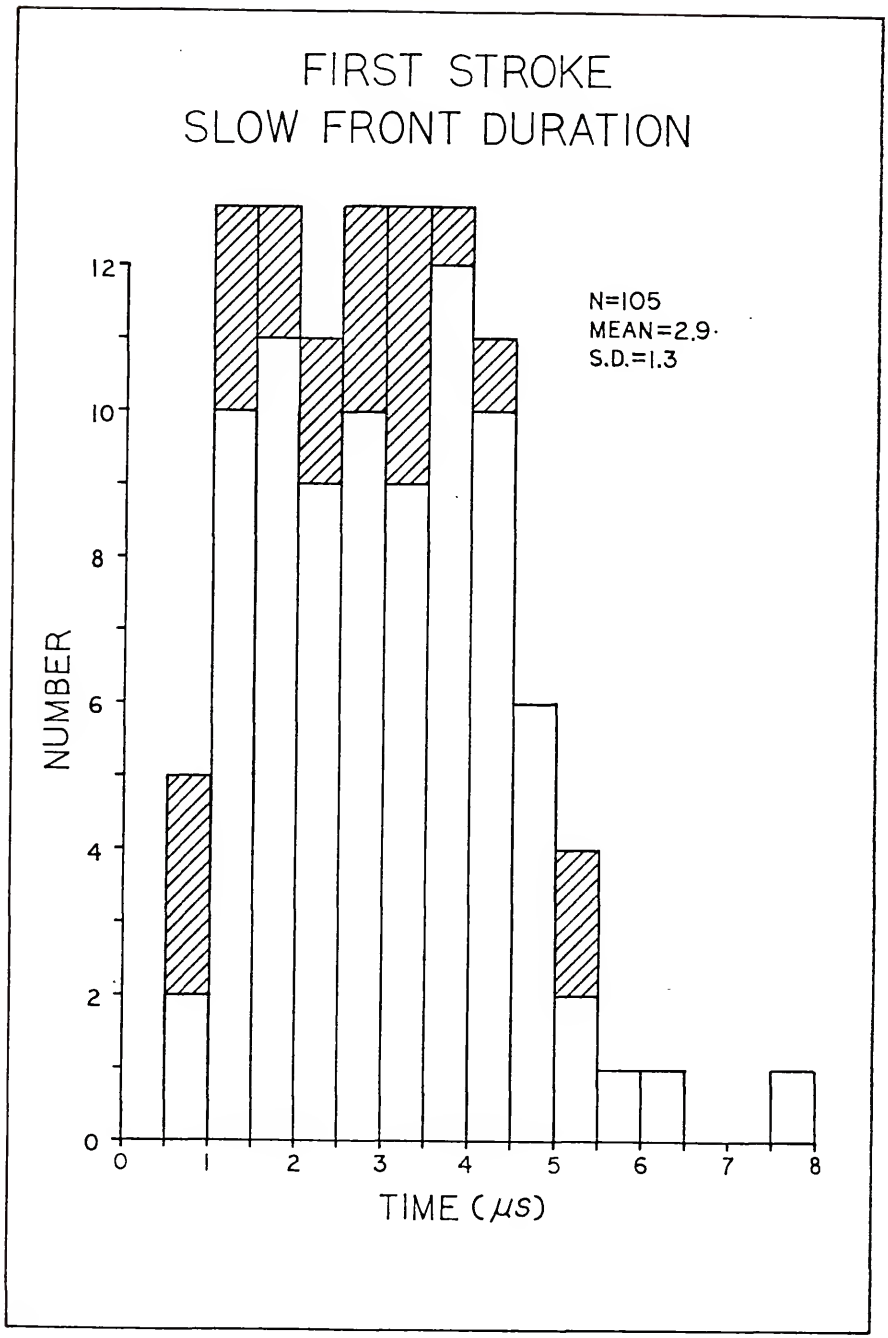
FIRST STROKE
SLOW FRONT DURATION
N=105
MEAN=2.9
S.D.=1.3
NUMBER
0
2
4
6
8
10
12
0
1
2
3
4
5
6
7
8
TIME (μs)

Figure 2.19. Distribution of the first stroke slow initial front amplitude as a percentage of the peak vertical electric field. For 105 first strokes the mean is 28% with a standard deviation of 15%; without the shaded data, the mean is 27% with a 15% standard deviation for 83 first strokes.

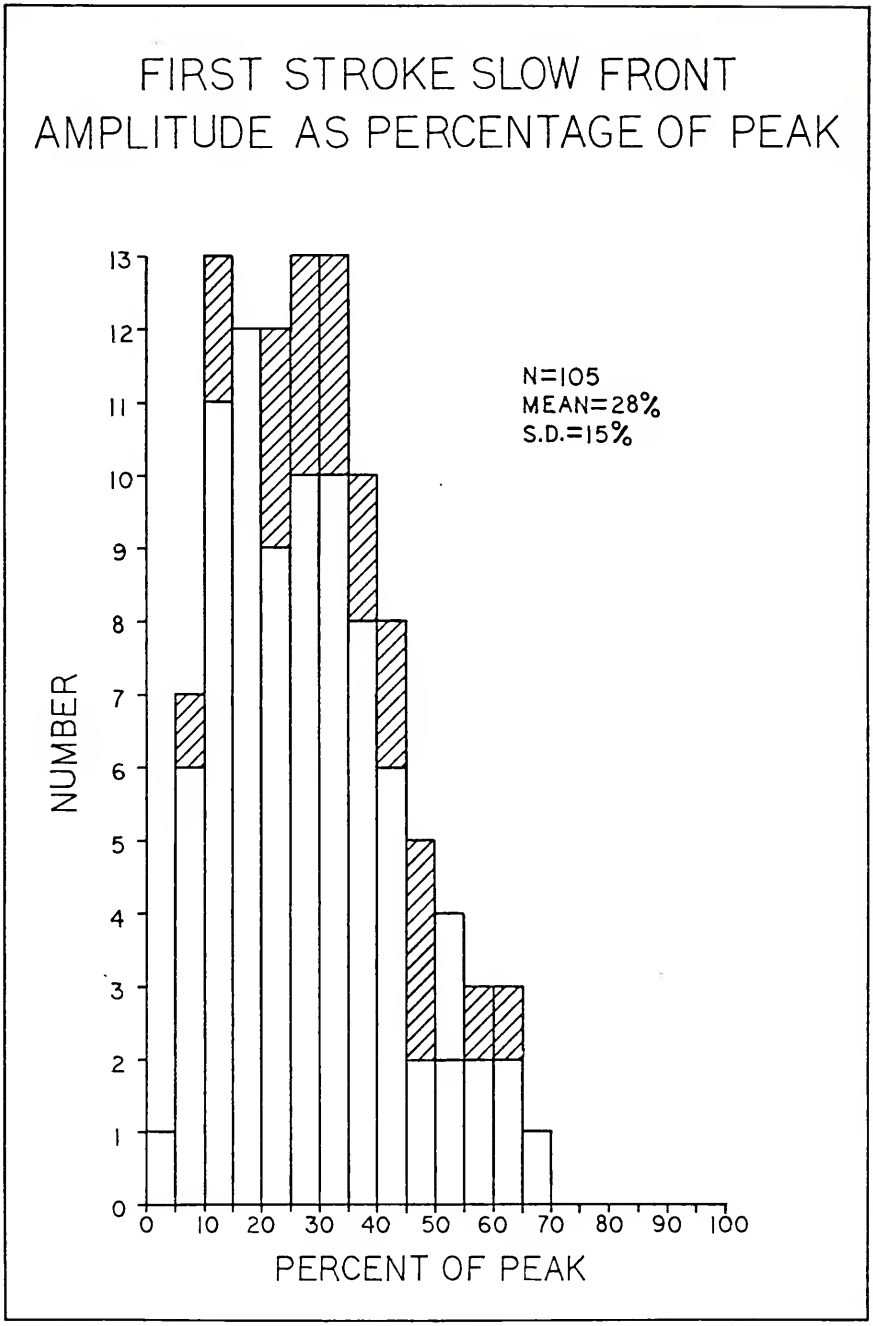
FIRST STROKE SLOW FRONT
AMPLITUDE AS PERCENTAGE OF PEAK
N=105
MEAN=28%
S.D.=15%
NUMBER
0
1
2
3
4
5
6
7
8
9
10
11
12
13
0
10
20
30
40
50
60
70
80
90
100
PERCENT OF PEAK

Table 2.5. Summary of return stroke vertical electric field statistics from selected studies.

	FIRST STROKES			SUBSEQUENT STROKES		
	N	MEAN	S.D.	N	MEAN	S.D.
Vertical Electric Field peak normalized to 100 km (V/m)						
This Thesis (Figure 2.14(b))	112	6.2	3.4	237	3.8	2.2
Lin et al. (1979)	80	6.4	---	142	4.7	---
McDonald et al. (1979)	54	5.4	2.1	119	3.6	1.3
	52	10.2	3.5	153	5.4	2.6
Tiller et al. (1976)	75	9.9	6.8	163	5.7	4.5
Taylor (1963)	47	4.8	---	---	---	---
Vertical Electric Field zero-to-peak risetime (μs)						
This Thesis (Figure 2.15)	105	4.4	1.8	220	2.8	1.5
Lin et al. (1979)	80	2.5	1.3	142	1.6	0.8
Tiller et al. (1976)	120	3.3	1.0	163	2.3	0.9
Lin and Uman (1973)	12	4.0	2.2	83	1.2	1.1
Fisher and Uman (1972)	26	3.6	1.8	26	3.1	1.9
Vertical Electric Field 10%-90% risetime (μs)						
This Thesis (Figure 2.16)	105	2.6	1.2	220	1.5	0.9
Vertical Electric Field Fast Transition 10%-90% risetime (ns)						
This Thesis (Figure 2.17)	102	970	680	217	610	270
Weidman and Krider (1980)	125	90	40	---	---	---
Vertical Electric Field slow ramp duration (μs)						
This Thesis (Figure 2.18)	105	2.9	1.3	---	---	---
Weidman and Krider (1978)	152	4.0	1.7	---	---	---

Table 2.5--continued.

	FIRST STROKES			SUBSEQUENT STROKES		
	N	MEAN	S.D.	N	MEAN	S.D.
Vertical Electric Field - Slow Ramp amplitude as percent of peak						
This Thesis (Figure 2.19)	105	28	15	---	---	---
Weidman and Krider (1978)	34	40	20	---	---	---

2.6.2 Analysis of Voltage Records

Theories of the induced voltage mechanism as presented by Wagner and McCann (1942), Golde (1954), Lundholm (1957), Rusck (1958), Chowdhuri (1960), and Singarajah (1971) make the assumption that the line voltage is induced only by coupling of the vertical electric field produced by nearby lightning. Thus, induced line voltages produced by the nearby negative return strokes to ground would always be of positive polarity, as discussed in Chapter I. Since in previous studies the inducing electric or magnetic fields produced by lightning were never measured in the vicinity of the line on which the voltage measurements were made, the validity of the above assumption was never put to test. We will now present some of the interesting aspects related to the induced voltages measured in this thesis. In particular, we shall show that the induced voltage may be either positive or negative in polarity for the same value of the vertical electric field peak, the polarity and amplitude of the voltage being a strong function of the location of the ground strike point. It follows that the coupling cannot be due to the vertical electric field only.

In Figure 2.20 we plot the peak measured voltage as a function of distance from the MLL for first and subsequent strokes. Peak voltages induced by first strokes vary from +150 kV to -40 kV; for subsequent strokes, the values range from +90 kV to -30 kV. In Figure 2.21 we show the distribution of the absolute value of the peak induced voltage on the line. For 112 first strokes we find a mean of 22.6 kV with a standard deviation of 22.4 kV. For 237 subsequent strokes, the mean and standard deviation of the

Figure 2.20. Peak induced voltage on the test-line for first and subsequent strokes as a function of the distance of the stroke from the Mobile Lightning Laboratory.

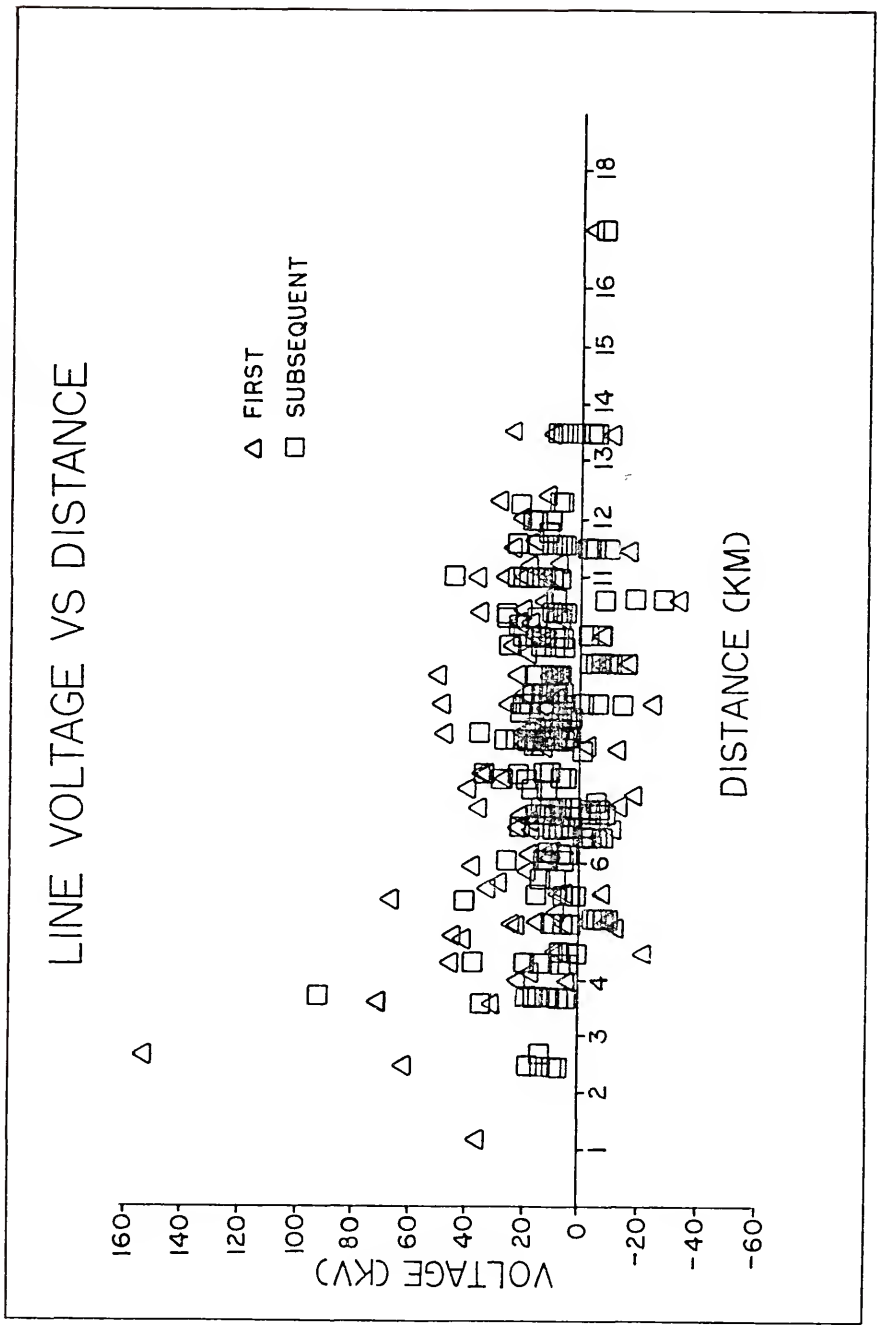
LINE VOLTAGE VS DISTANCE
FIRST
SUBSEQUENT
VOLTAGE (KV)
DISTANCE (KM)
160
140
120
100
80
60
40
20
0
-20
-40
-60
1
2
3
4
6
11
12
13
14
15
16
18

Figure 2.21. Distribution of peak induced voltage on the test line. For 112 first strokes the mean and standard deviation are 22.6 kV and 22.4 kV, respectively; for 237 subsequent strokes, 10.8 kV and 9.0 kV, respectively.

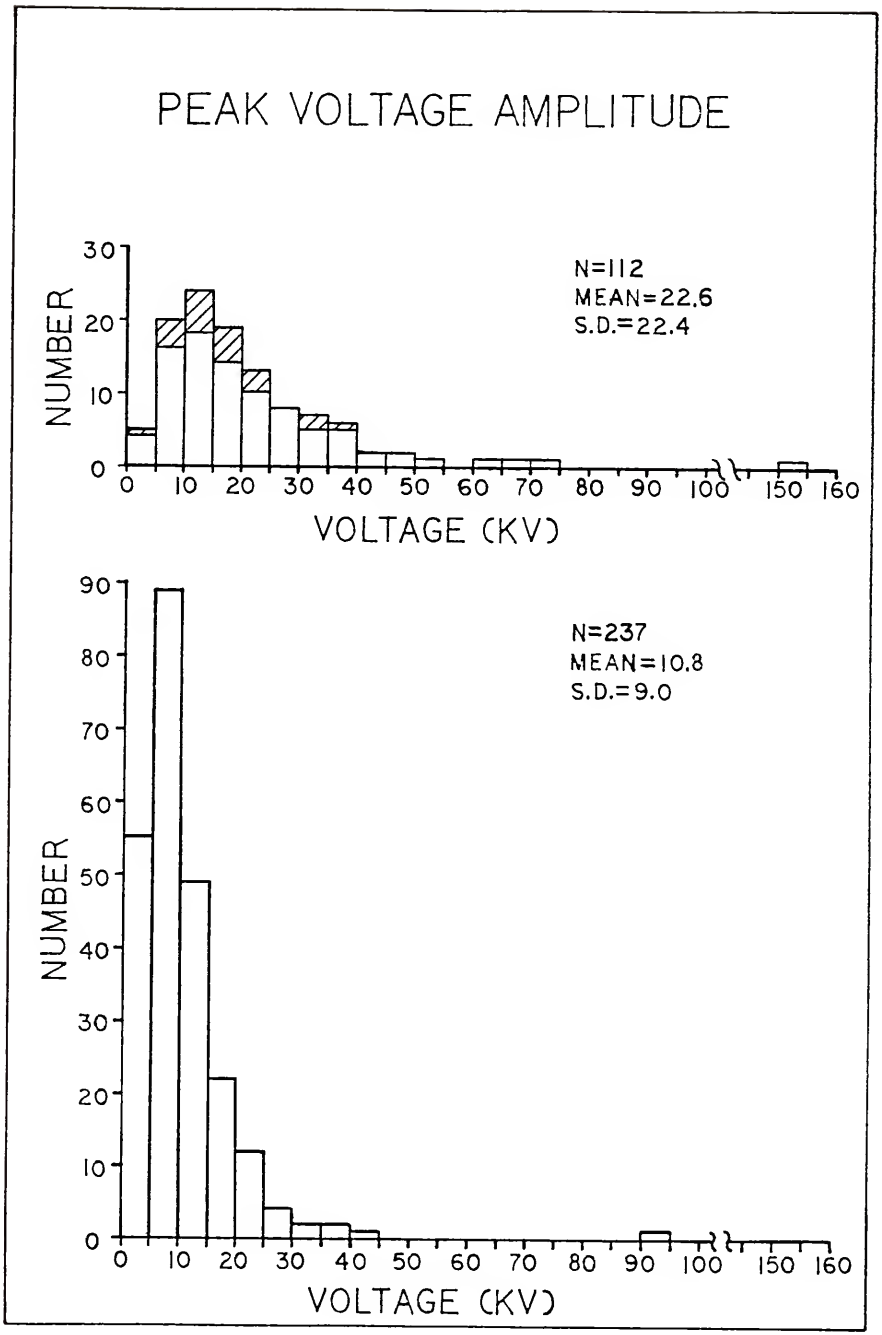
PEAK VOLTAGE AMPLITUDE
N=112
MEAN=22.6
S.D.=22.4
NUMBER
VOLTAGE (KV)
N=237
MEAN=10.8
S.D.=9.0
NUMBER
VOLTAGE (KV)

distribution were 10.8 kV and 9.0 kV, respectively. Eliminating the shaded data, we find a mean of 23.9 kV with a standard deviation of 24.4 kV for 90 first strokes. Before comparing this data with other studies, we take one more look at Figure 2.20 and note that most of the voltages measured in this thesis were induced by lightning return strokes which were between about 4 and 12 km distant. Further, the continuous records obtained from the instrumentation tape recorder limit the lowest measurable voltage to the channel noise level, estimated to be about 1 kV.

Measurements of overvoltages on the specially instrumented 9.9 km test line in South Africa, reported by Eriksson and Meal (1982) and by Eriksson et al. (1982), were made with a trigger threshold of about 12 kV. The most common type of surge measured in that study was found to be of positive polarity, or the "classical induced" type. It is interesting to note that the data given by Eriksson and Meal (1982) indicate a significant number of positive surges (7 out of 21) attributed to a direct strike on the line. Further, a small percentage of the surges exhibit a negative polarity and are not attributed to direct strikes. Out of a total of 281 surges measured by Eriksson et al. (1982), 32 which produced "good quality overvoltage recordings" were located accurately by triangulation. Most of these surges were produced by return strokes within about 1 km from the line. The peak voltage for these 32 records has a mean of 45 kV with a standard deviation of 35 kV, and there does not appear to be any strong dependence of the peak voltage on the distance from the line. It is not very clear whether the voltage recordings are always due to the first return stroke, though we may

presume that to be the case. Voltages induced on overhead lines due to triggered lightning have been reported by Hamelin et al. (1979). The mean peak voltage measured on the 2.1 km telecommunication line was 1 kV for lightning 1.4 km from the line. A mean of 74 kV was reported on the 260 m medium voltage line for lightning 50 m away. We conclude that the peak voltages measured on our test line are much larger than the values reported by other researchers.

In Appendix D we present a histogram of measured induced voltages during a one hour and thirty minute period during which a storm passed very close to the line. Since the TV network was not operating during this period, no flashes were located. However, some of the voltages induced on the line during this period were due to flashes which were closer to the line than those presented in this thesis. Figure D.1 shows several voltages greater than 250 kV. This does not appear to be reasonable since the line was designed to spark-over at 250 kV. Thus, either the spark-over gap was improperly set or there was an error in the voltage calibration so that the actual voltages are smaller in peak amplitude than the measured values indicate.

Figure 2.22 shows the distributions of the zero-to-peak risetime of the induced voltage waveforms measured in this thesis. All risetime measurements have been made on a time-scale of 40 μs full-scale. The error in determining the zero is estimated at ±0.5 μs in most cases. A further error in measurement once the zero is defined is estimated at ±0.1 μs. For 105 voltages induced by first strokes, the mean was 6.0 μs with a standard deviation of 3.8 μs. Without the shaded data, the mean

Figure 2.22. Distribution of the zero-to-peak risetime of the induced voltage on the test-line. For 105 first strokes the mean and standard deviation are 6.0 μs and 3.8 μs, respectively; for 218 subsequent strokes, 4.0 μs and 2.3 μs, respectively.

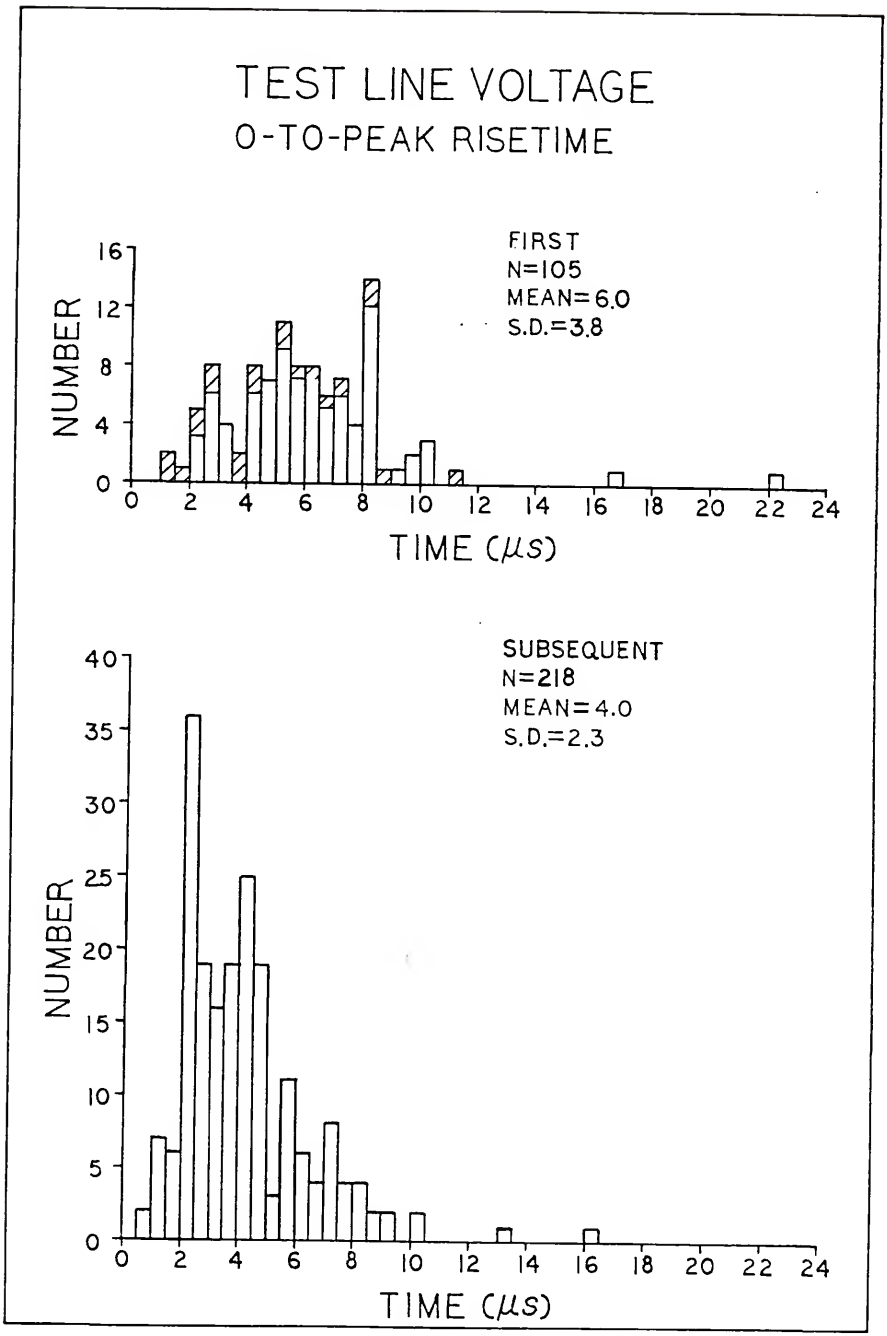
TEST LINE VOLTAGE
0-TO-PEAK RISETIME
FIRST
N=105
MEAN=6.0
S.D.=3.8
NUMBER
TIME (μs)
SUBSEQUENT
N=218
MEAN=4.0
S.D.=2.3
NUMBER
TIME (μs)

was 6.3 μs with 4.0 μs as the standard deviation for 84 first strokes. For 218 voltages induced by subsequent strokes, the mean and standard deviation were found to be 4.0 μs and 2.3 μs, respectively. Due to the errors involved in determining the zero and the peak of the waveforms in the presence of noise it is more meaningful to talk about the 10%-90% risetimes shown in Figure 2.23. For 105 first stroke induced voltages the mean was 4.0 μs with 3.2 μs as the standard deviation. Without the shaded data points, the mean was 4.2 μs and the standard deviation 3.4 μs for 84 first strokes. For 218 subsequents, the mean and standard deviation were 2.6 μs and 1.7 μs, respectively.

Comparing Figures 2.16 and 2.23, we can conclude that, on the average, the value of the 10%-90% risetime of the vertical electric field is smaller than that of the induced voltage. A similar conclusion may be drawn with regard to the zero-to-peak risetimes. However, there is considerable spread in the ratio of the 10%-90% risetime of the voltage to that of the simultaneously recorded vertical electric field. This distribution is shown in Figure 2.24: the most likely value of the ratio is between one and two. A summary of induced voltage statistics presented here is given in Table 2.6.

2.6.3 Correlation Between the Voltage and Field Records

The most interesting aspect of the induced voltages on the unenergized test line measured in this thesis is the fact that the polarity of the induced voltage was found to be either positive or negative for the same value of the peak vertical electric field.

Figure 2.23. Distribution of the 10%-to-90% risetime of the induced voltage on the test-line. For 105 first strokes the mean and standard deviation are 4.0 μs and 3.2 μs, respectively; for 218 subsequent strokes, 2.6 μs and 1.7 μs, respectively.

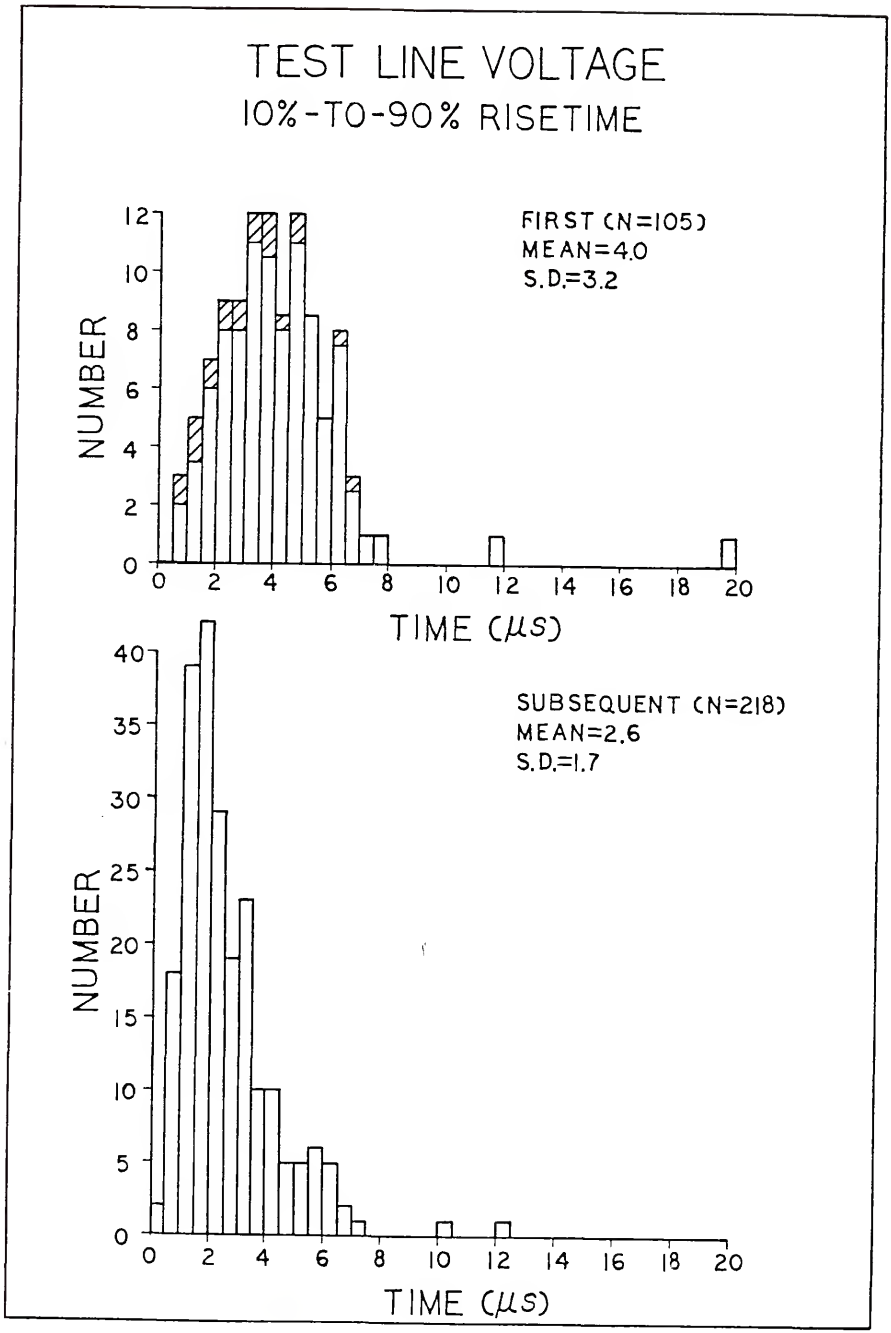
TEST LINE VOLTAGE
10%-TO-90% RISETIME
FIRST (N=105)
MEAN=4.0
S.D.=3.2
NUMBER
TIME (μs)
SUBSEQUENT (N=218)
MEAN=2.6
S.D.=1.7
NUMBER
TIME (μs)

Figure 2.24. Ratio of the 10%-to-90% risetime of the induced voltage to the 10%-to-90% risetime of the simultaneously recorded vertical electric field.

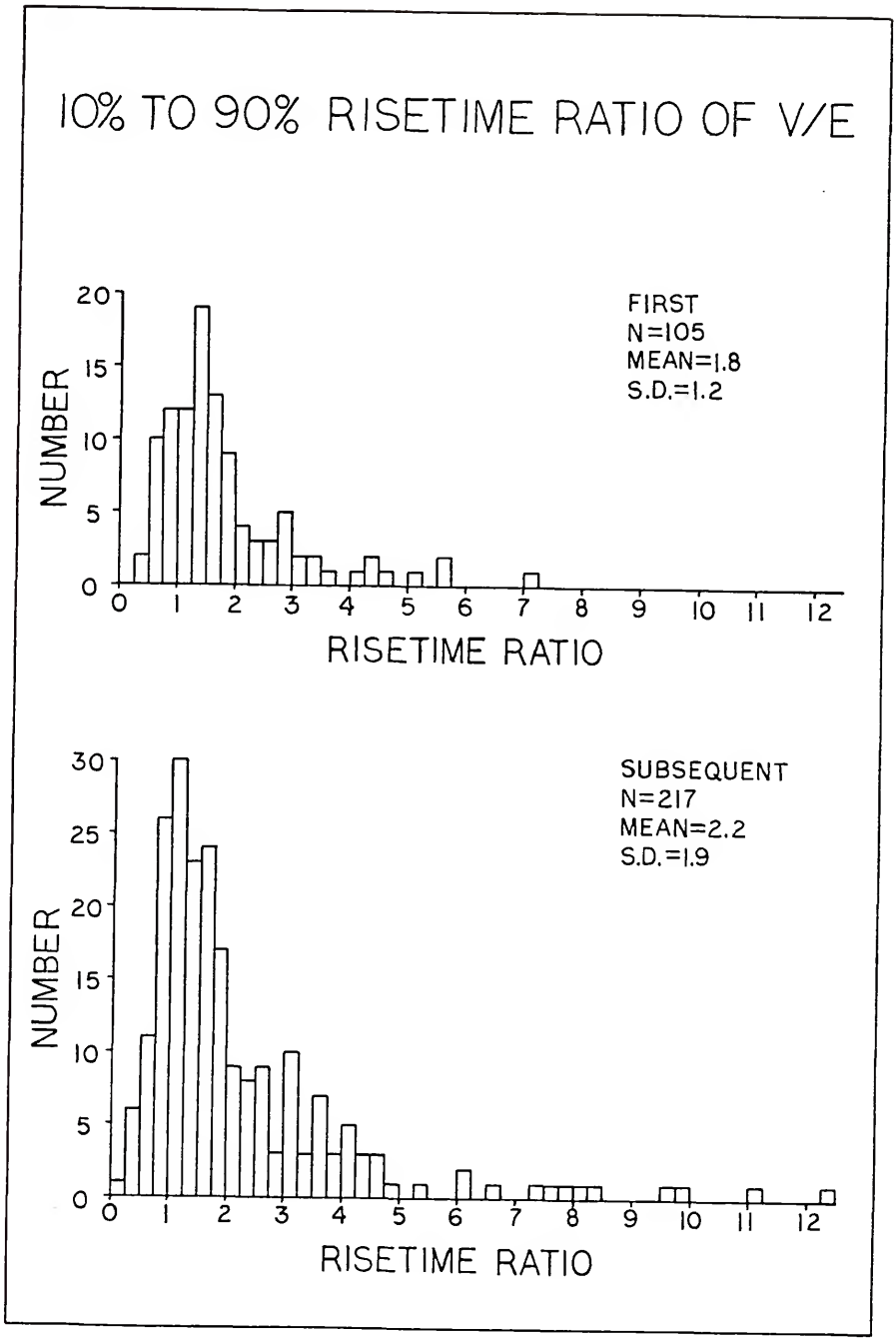
10% TO 90% RISETIME RATIO OF V/E
FIRST
N=105
MEAN=1.8
S.D.=1.2
NUMBER
RISETIME RATIO
SUBSEQUENT
N=217
MEAN=2.2
S.D.=1.9
NUMBER
RISETIME RATIO

Table 2.6. Summary of induced voltage statistics.

	FIRST STROKES			SUBSEQUENT STROKES		
	N	MEAN	S.D.	N	MEAN	S.D.
Test Line Voltage peak amplitude (kV) (Figure 2.21)	112	22.6	22.4	237	10.8	9.0
Test Line Voltage zero-to-peak risetime (μs) (Figure 2.22)	105	6.0	3.8	218	4.0	2.3
Test Line Voltage 10%-90% risetime (μs) (Figure 2.23)	105	4.0	3.2	218	2.6	1.7
Ratio of 10%-90% risetime of V to 10%-90% E risetime of E (Figure 2.24)	105	1.8	1.2	217	2.2	1.9

This is contradictory to the various theories associated with the concept of the classical induced surge. In Figure 2.25 this point is illustrated with the help of three subsequent return strokes which are at approximately the same distance from the line. The located position in each case is indicated in polar coordinates. Each of the three return strokes has about the same value of the peak vertical electric field peak as measured at the MLL, the measurement of line voltage being made at the northern end of the line. As can be seen clearly from the figure, the line voltages induced by essentially the same vertical electric field are remarkably different for the three return strokes. For the stroke due north of the line, the induced voltage waveform is of negative polarity. For the stroke due south of the line, the voltage is of positive polarity and has about the same peak amplitude as that induced by the stroke due north of the line. For the return stroke with its ground strike point perpendicular to the line, the induced voltage is buried in the tape recorder noise level and is very small in peak amplitude compared with the other two induced voltages. It therefore appears from the data that the coupling of the lightning electromagnetic field on the line cannot be satisfactorily described in terms of the vertical electric field alone. In fact, from Figure 2.25 there are strong indications that the dominant driving function for the induced voltage is probably the horizontal component of the electric field and not its vertical component. The horizontal electric field component for a perfectly conducting ground plane is directly related to the horizontal magnetic field, as discussed in the next Chapter. Similar conclusions have been drawn by Koga et al. (1981) who report

Figure 2.25. Induced voltages on the test line and vertical electric field due to lightning for return strokes at three different locations.

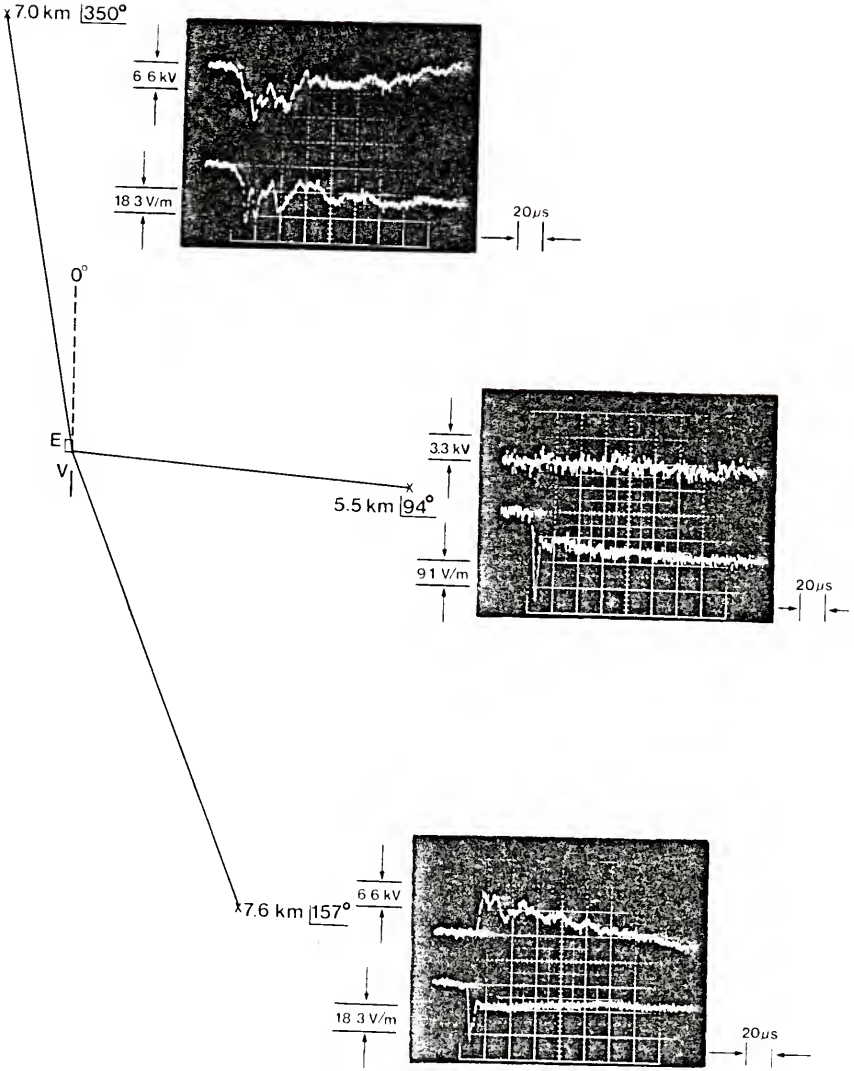
7.0 km 350°
6.6 kV
18.3 V/m
20μs
0°
E
V
5.5 km 94°
3.3 kV
9.1 V/m
20μs
7.6 km 157°
6.6 kV
18.3 V/m
20μs

surges of opposite polarities measured simultaneously at two ends of a telephone cable. However, they did not have the locations of lightning ground strike points in their study.

To investigate further the relationship between the induced voltage and the location of the ground strike point the following was done. The peak value of the induced voltage was first normalized to the simultaneously recorded peak vertical electric field. This normalization was done in an attempt to remove the distance and return stroke current dependence. The value of V/E, or the normalized voltage, was plotted as a function of the angle around the test line. The strokes are grouped together in 10° intervals. The mean and standard deviation of the values of V/E within the angle range were computed. In Figure 2.26 these values are plotted for first strokes; Figure 2.27 shows the relationship for subsequent strokes. The circled point represents the mean, the vertical bars represent the value of the standard deviation on each side of the mean, and the number of strokes within that angle range is shown with each point. It is clear from these figures that the normalized voltage V/E has a strong dependence on the angle around the line. The values for first strokes are not significantly dif-ferent from those for subsequent strokes. This is not surprising, since the voltage has been normalized with respect to stroke severity. The curves exhibit a positive peak at around 180°, go through zero around 90° and 270°, and exhibit a negative peak around 0°.

In this section, we have examined the relationship between the lightning return stroke field, the line voltage, and the location of the ground strike point. We have found that the induced voltage is

Figure 2.26. Ratio of initial peak induced voltage to initial peak vertical electric field for first strokes vs. angle of the lightning ground strike point from the Mobile Lightning Laboratory; the circled point represents the mean and the vertical bars represent the standard deviation for the indicated number of points in each 10° interval.

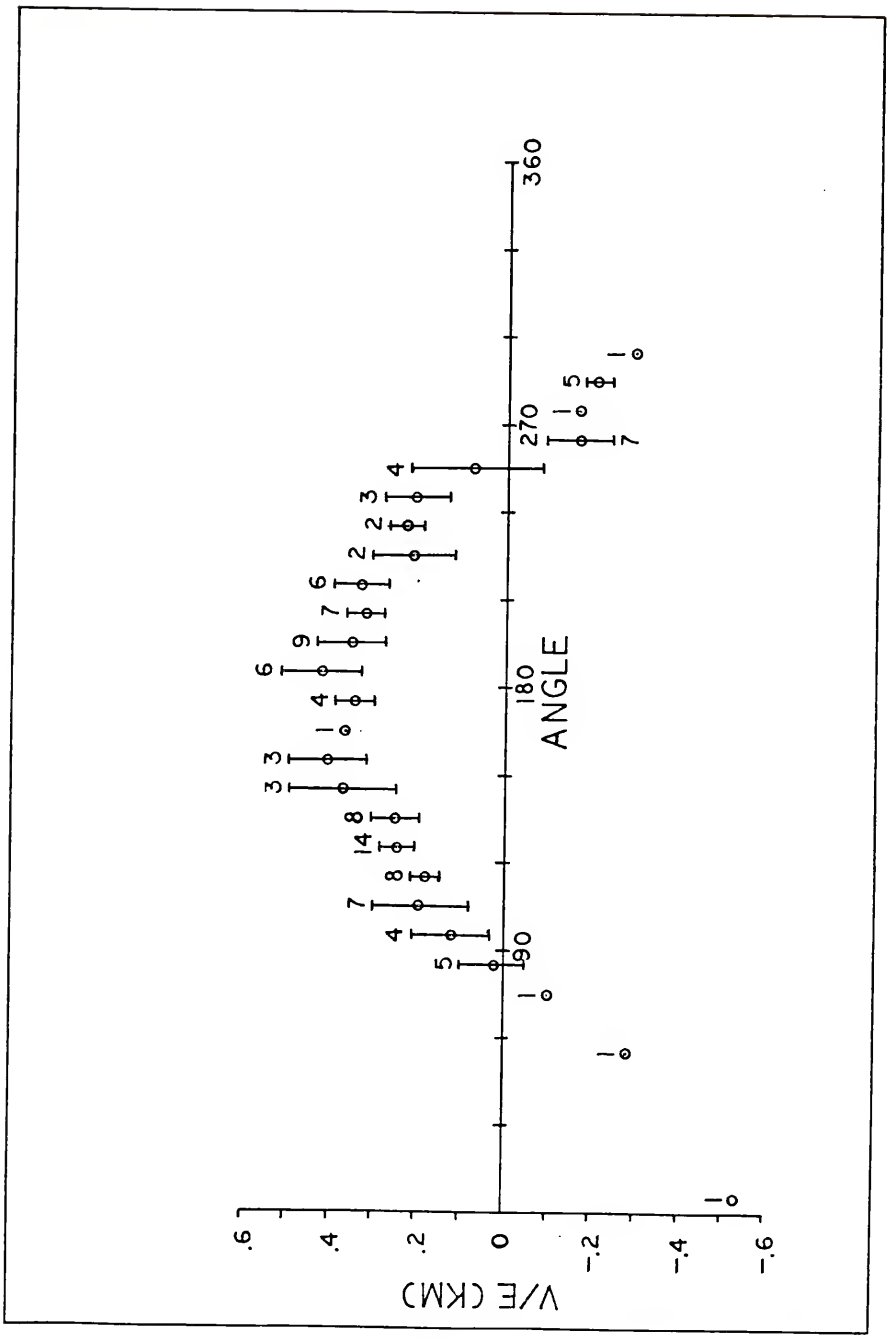
V/E (KM)
.6
.4
.2
0
-.2
-.4
-.6
ANGLE
90
180
270
360

Figure 2.27. Ratio of initial peak induced voltage to initial peak vertical electric field for subsequent strokes vs. angle of the lightning ground strike point from the Mobile Lightning Laboratory; the circled point represents the mean and the vertical bars represent the standard deviation for the indicated number of points in each 10° interval.

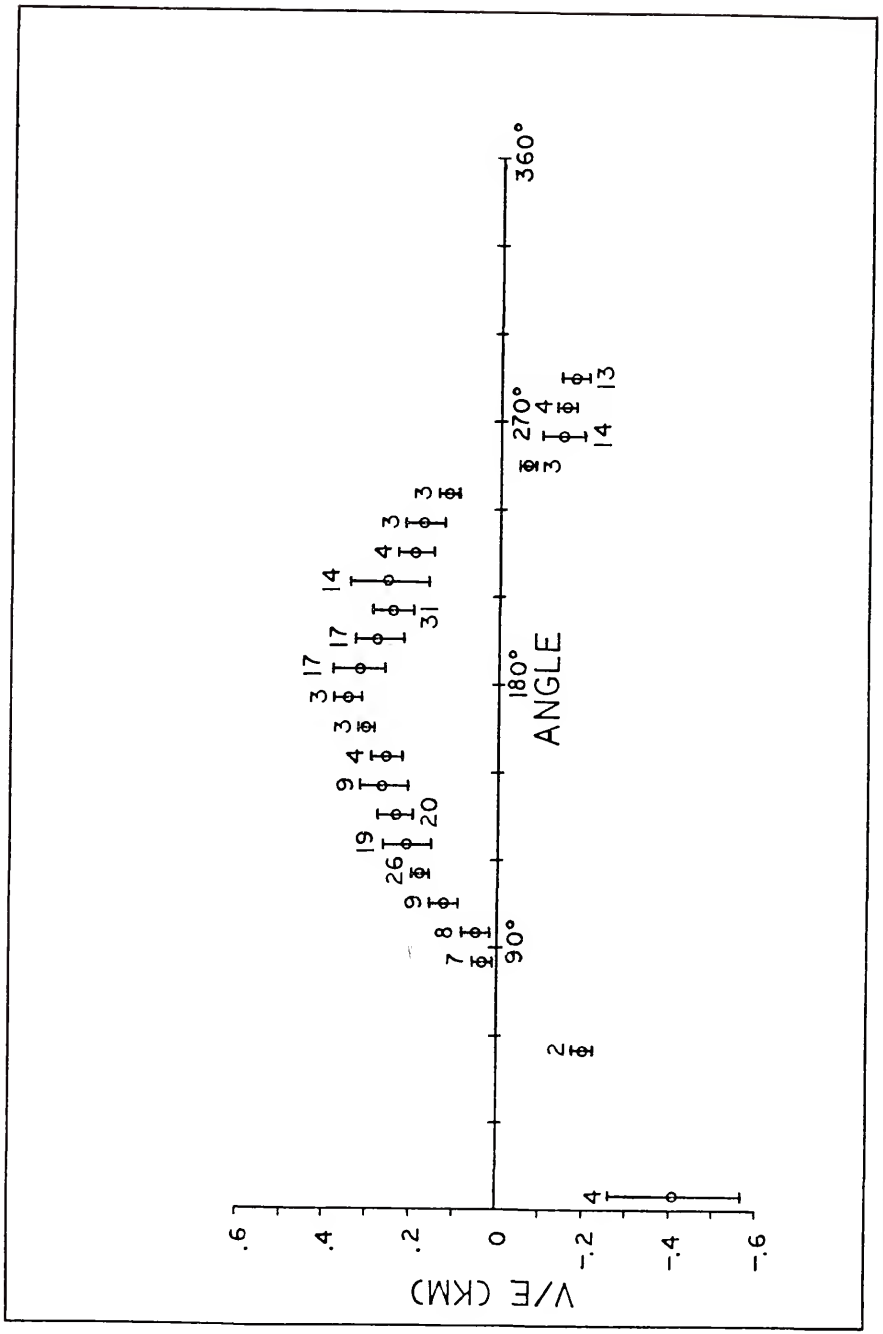
V/E (KM)
.6
.4
.2
0
-.2
-.4
-.6
90°
180°
270°
360°
ANGLE
2
7 8 6 26 19 20 9 4 3 17 17 14 31 4 3 3
5 3 4 14 13
4

at its maximum, when the return stroke is "end-on" the line, the induced effects being much smaller for return strokes perpendicular to the line. We have also found that for strokes in the first and fourth quadrants around the line, the induced voltage waveform is of negative polarity; strokes in the second and third quadrants produce the classical induced surge of positive polarity. Let us examine these results. It appears from Figure 2.25 that there is no obvious relationship between the induced voltage and the vertical electric field, since essentially the same vertical electric field illuminating the line can give rise to widely differing voltages. Since, for a negative return stroke, the vertical electric field always points into the ground, the horizontal electric field produced by the finite ground conductivity is along the direction of propagation and points towards the lightning. For a return stroke due north of the line, the lightning electromagnetic field would be propagating along the line and away from the north end measuring point. However, for a stroke due south, the field would be propagating along the line and toward the measuring point. For both these cases, the vertical electric field along the line would be in the same direction, and hence if the vertical electric field coupling were dominant, only positive polarity voltages would be produced. However, the component of the horizontal electric field along the line would be in opposite directions. If the coupling produced by the horizontal electric field were dominant, it would explain why voltages of either polarity are induced. This would also explain why the induced voltage for strokes due east or west of the line is

rather small, because the component of the horizontal electric field along the line would be very small in that case.

Given the fact that negative induced surges measured on the unenergized test line for this thesis are almost as likely to occur as positive induced surges, why is it that measurements of induced surges made over the years on various types of lines indicate a predominance of positive waveforms? To answer this question, we note that in most instances, the measurements are made on long lines which are part of the network and the voltage is not measured at the "end". In the previous paragraph we noted that the induced voltage would have a negative polarity only if the lightning electromagnetic field propagates along the line and away from the end at which the voltage is measured. If the measurement is made in the middle of the line, the lightning electromagnetic field is always propagating along the line and towards the measuring station, and hence the induced surge is always of positive polarity. The South African 9.9 km test line was equipped with one measuring station at one end, and another measuring station in the middle. However, the data presented by Eriksson and Meal (1982) and by Eriksson et al. (1982) are drawn only from the station in the middle of the line. Hence, it is not surprising that their records indicate the classical induced surge. The experimental setup used in the French experiment given in Hamelin et al. (1979) is such that only positive surges would be measured. However, results from the recent Japanese study on a telephone cable shield presented by Koga et al. (1981) and discussed earlier show simultaneous induced surges of negative and positive polarity

measured at the two ends of their 1 km line. This is in keeping with the physical arguments presented in this section.

In the next chapter we shall mathematically formulate the problem of computing induced line voltages from a knowledge of the inducing fields. In Chapter IV calculated waveforms will be compared with all available data.

CHAPTER III

THEORETICAL ANALYSIS

3.1 Introduction

In Chapter I the various theories used to explain induced power-line voltages were outlined, e.g., Lundholm (1957), Rusck (1958), Chowdhuri (1966), and Singarajah (1971). These theories lead to induced surges which are only of positive polarity. The theory presented by Leteinturier et al. (1980) and Djebari et al. (1981), which includes the effects of the imperfectly conducting ground plane, was used by the French to make limited comparisons between their theoretically calculated waveshapes and the measured waveform of the current at one end of their 2.1 km test line. It was pointed out in Chapter I that the major drawback of their theory was the use of a very simple model for the lightning current. Further, their calcu-lations were performed only for times greater than 2 μs when the fields do not vary rapidly. In addition, their experimental setup was such that it excluded any measurements of induced surges of negative polarity. No general calculations were done which predicted induced line surges of negative polarity. The recent Japanese study reported by Koga et al. (1981) clearly shows measured induced surges of negative and positive polarity on their test line. Although some general calculations are presented, no direct comparison between

their theory and their data could be made because of lack of information on stroke locations. Furthermore, they do not present any calculation which shows negative induced surges on their line.

In Chapter II, simultaneous measurements of the return stroke vertical electric field and the induced voltage on a specially constructed unenergized power line were discussed. It is clear from the data that the "classical induced" surge of positive polarity is almost as likely to be induced on our 460 m test-line as a surge of negative polarity. Furthermore, it was indicated that the polarity of the surge was dependent on the location of the ground strike point. There are strong indications from the data that the horizontal electric field coupling is the predominant factor responsible for the induced voltage. The reasons for the existence of a horizontal electric field component at the line will now be investigated.

(a) Assuming an infinitely conducting ground plane and a vertical lightning channel, the horizontal electric field at ground is zero; however there is a finite horizontal field at line height, which is approximately 10 m above the ground. This horizontal electric field may be predicted using the return stroke model of Master et al. (1981). However, for a 10 m altitude this horizontal electric field is too small to produce the measured voltages.

(b) More often than not, the lightning return stroke channel from cloud to ground is not perfectly straight and vertical as assumed in the various return stroke models, but exhibits a certain tortuosity on a scale from about 1 m to over 1 km (e.g., Evans and Walker, 1963; Hill, 1968). A dipole with an arbitrary orientation in

space would result in different electric and magnetic fields at the line height compared to that due to a vertical dipole at the same point. However, data analyzed by Hill (1968) indicate that the direction of sections of lightning channels are randomly distributed. For segment lengths studied (between 5 m and 70 m) and total channel lengths analyzed (between 1 km and 4.3 km) the mean absolute value of the channel direction change was 16°. The reported random distribution of the parameters governing channel tortuosity indicate that the net effect of the complete lightning channel is such that it can be modeled as vertical. This is because the random distribution of tortuosity cannot, on average, provide a large effect in any particular direction. It is in fact this argument which accounts for the good agreement between measured data and theory as presented by Lin et al. (1979, 1980).

Data presented on the measured test-line voltages in this thesis for lightning at some fixed distance and angle from the MLL do not indicate a wide range of variability. This further indicates that the channel shape is not a critical factor in producing the horizontal electric field. In fact, the averaged data on the peak line voltage normalized to the vertical electric field peak as shown in Figures 2.26 and 2.27 indicate very little spread, and hence we argue again that the straight vertical channel for lightning is a good approximation to an actual lightning channel.

(c) Using an argument that the ground is a good, but not a perfect conductor, a horizontal electric field may be computed from the vertical component at ground, based on the wavetilt of the propagating electromagnetic wave. This method gives the correct

waveshape and reasonable amplitudes for the theoretically calculated voltages, as discussed later.

The first part of this chapter will be devoted to the investigation of the horizontal electric field produced by mechanisms (a) and (c) outlined above. The latter half of the chapter will be devoted to the derivation of the transmission-line coupling equations, and a discussion of their numerical solution. It will be shown that the total voltage at any point on an overhead line may be derived from a knowledge of the incident horizontal electric field at all interior points and the incident vertical electric field at the ends of the line and at the measuring point. Listings of FORTRAN codes used to obtain the various solutions are given in Appendix C.

3.2 Electric and Magnetic Fields Illuminating the Test-Line

3.2.1 The Return Stroke Model

The word "model" as used in this thesis may be defined as a mathematical construct of the properties of physical phenomenon which can be used as a convenient tool to further the understanding of that phenomenon. The lightning return stroke has been subject of various models for over four decades. An important objective of most of these models is to be able to describe the electric and magnetic fields produced by the return stroke. This field description is arrived at from a knowledge of the current in the channel. The modeling of the current itself has been accomplished to varying degrees of sophistication, e.g., Strawe (1979), Price and Pierce (1977), Little (1978), Bruce and Golde (1941), Dennis and Pierce

(1964), Uman and McLain (1970), Lin et al. (1980), and Master et al. (1981).

The lightning return stroke model of Lin et al. (1980) is the only available model consistent with measured data on electric and magnetic fields. The model currents are derived from data recorded simultanously at two recording stations on the ground, one within 15 km of the lightning and the other at 50 or 200 km. The model postulates the existence of the following three current components in a straight, vertical return stroke channel above a perfectly conducting earth:

(a) a short upward-propagating pulse of current associated with the electrical breakdown at the return stroke wavefront and responsible for the peak current; the pulse propagating up at a constant velocity v;

(b) a uniform current, which may already be flowing in the channel as leader current, or may begin to flow soon after the commencement of the return stroke; and

(c) a "corona" current, caused by the neutralization of the charge stored around the leader channel, and discharged by the passage of the return stroke wavefront.

The parameters defining these three current components are derived from the measured two-station fields and are discussed in detail by Lin et al. (1980).

Although the model of Lin et al. (1980) was primarily applicable to subsequent return strokes, it proved reasonably successful at modeling the first stroke two-station electric and magnetic fields measured at ground level reported by Lin (1978). However, Schonland

et al. (1935) reported that the peak luminosity of the first return stroke channel decreased with height above the ground. Recent observations reported by Jordan and Uman (1980) show a marked decrease in peak luminosity with height for subsequent strokes as well. These observations indicate that the breakdown pulse current [(i) in the previous paragraph] should be attenuated as it propagates up the channel. This attenuation would not substantially alter the electric and magnetic fields measured at ground level; however, it would significantly alter the fields measured at an altitude. This extension of the model of Lin et al. (1980) to predict fields at altitudes and bring the model currents in closer conformity with reported observations was carried out as an integral part of this thesis and was reported by Master et al. (1981). This model can be used to compute the electric and magnetic fields in the vicinity of any overhead power line. The fields may then be coupled onto the line in order to produce the induced voltage.

3.2.2 Electromagnetic Field Calculation

In Figure 3.1 we indicate the geometry of the return stroke channel. The "image" channel will be used to simulate the effect of the perfectly conducting ground plane (see Stratton, 1941, pgs. 577-582). Due to the cylindrical symmetry of the problem about the return stroke channel, the solution for the electric and magnetic fields at any general point P (r, ϕ, z) will be obtained using a cylindrical coordinate system with the origin at the point at which the return stroke makes contact with the earth. The complete channel from cloud to ground is split into small channel

Figure 3.1. Geometry for field computations based on the model of Master et al. (1981).

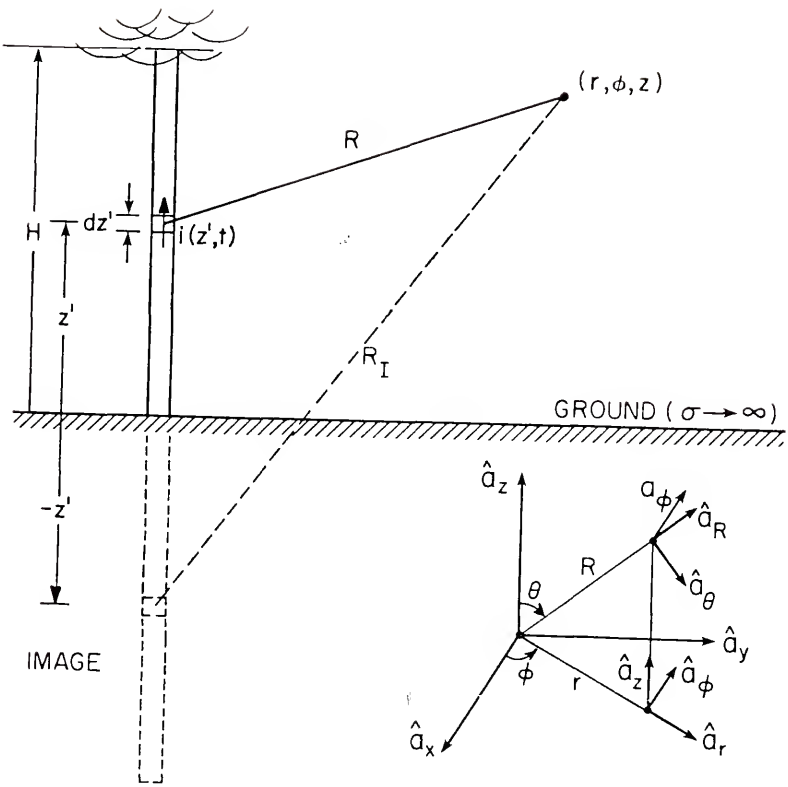
(r,φ,z)
R
H
dz'
i(z',t)
z'
R_I
GROUND (σ→∞)
-z'
IMAGE
â_z
a_φ
â_R
R
â_θ
θ
â_y
φ
r
â_z
â_φ
â_x
â_r

sections or current dipoles. The electric and magnetic fields at point P (r, ϕ, z) produced by a small dipole located at the origin and carrying a current $i(t)$ have been derived in Appendix A. Equations (A.35), (A.36) and (A.37) written for a general dipole of length dz' and at height z', carrying a current $i(z', t)$ are reproduced below.

$$B_\phi(r,\phi,z,t) = \frac{\mu_0 dz'}{4\pi}\left[\frac{r}{cR^2}\ \frac{\partial i(z',t-\frac{R}{c})}{\partial t} + \frac{r}{R^3}\ i(z',t-\frac{R}{c})\right] \qquad (3.1)$$

$$E_r(r,\phi,z,t) = \frac{dz'}{4\pi\varepsilon_0}\left[\frac{3r(z-z')}{R^5}\int_0^t i(z',\tau-\frac{R}{c})d\tau + \frac{3r(z-z')}{cR^4}\ i(z',t-\frac{R}{c})\right.$$

$$\left. + \frac{r(z-z')}{c^2R^3}\ \frac{\partial i(z',\tau-\frac{R}{c})}{\partial t}\right] \qquad (3.2)$$

$$E_z(r,\phi,z,t) = \frac{dz'}{4\pi\varepsilon_0}\left[\frac{2(z-z')^2-r^2}{R^5}\int_0^t i(z',\tau-\frac{R}{c})d\tau\right.$$

$$\left. + \frac{2(z-z')^2-r^2}{cR^4}\ i(z',t-\frac{R}{c}) - \frac{r^2}{c^2R^3}\ \frac{\partial i(z',t-\frac{R}{c})}{\partial t}\right] \qquad (3.3)$$

where, μ_0 is the permeability and ε_0 the permittivity of air (or vacuum), and all geometrical factors are illustrated in Figure 3.1. The current $i(z,t)$ represents the currents derived from the models presented by Lin et al. (1980) and Master et al. (1981) described in Section 3.2.1. The first terms in Equations (3.2) and (3.3) are generally called the electrostatic field; the second terms in Equations (3.1), (3.2) and (3.3) are known as the induction terms;

and the remaining terms which involve the time-derivative of the current are called the radiation terms.

To obtain the electric and magnetic fields at P (r, ϕ, z) due to the lightning return stroke, we have to sum the field contributions due to each individual dipole in the channel. We note that at any time the complete field is due to contributions from various dipoles from the real and the image channels, each dipole carrying a different current which depends on its position, on the channel, and with respect to the field point.

The computation of the time-varying electric and magnetic field components based on the model of Master et al. (1981) is performed on a digital computer. A listing of the FORTRAN code is given in Appendix C. As input, the user specifies the parameters of the return stroke model current, the coordinates of the field point, and the total time for which the field description is desired. The program output gives the electric and magnetic field components and the waveform of the current at ground. The current waveform at ground due to a typical subsequent return stroke which was modeled by Lin et al. (1980) and Master et al. (1981) is shown in Figure 3.2. The electric and magnetic field components at a range of 3 km from the channel and an altitude of 10 m above ground produced by this current are shown in Figure 3.3.

3.2.3 Wavetilt Formulation

If the earth were a perfect conductor, a propagating electromagnetic wave would have no tangential electric field component at the earth's surface. However, if the earth has a finite

Figure 3.2. Typical subsequent return stroke current at ground. The three current components of the model are also indicated.

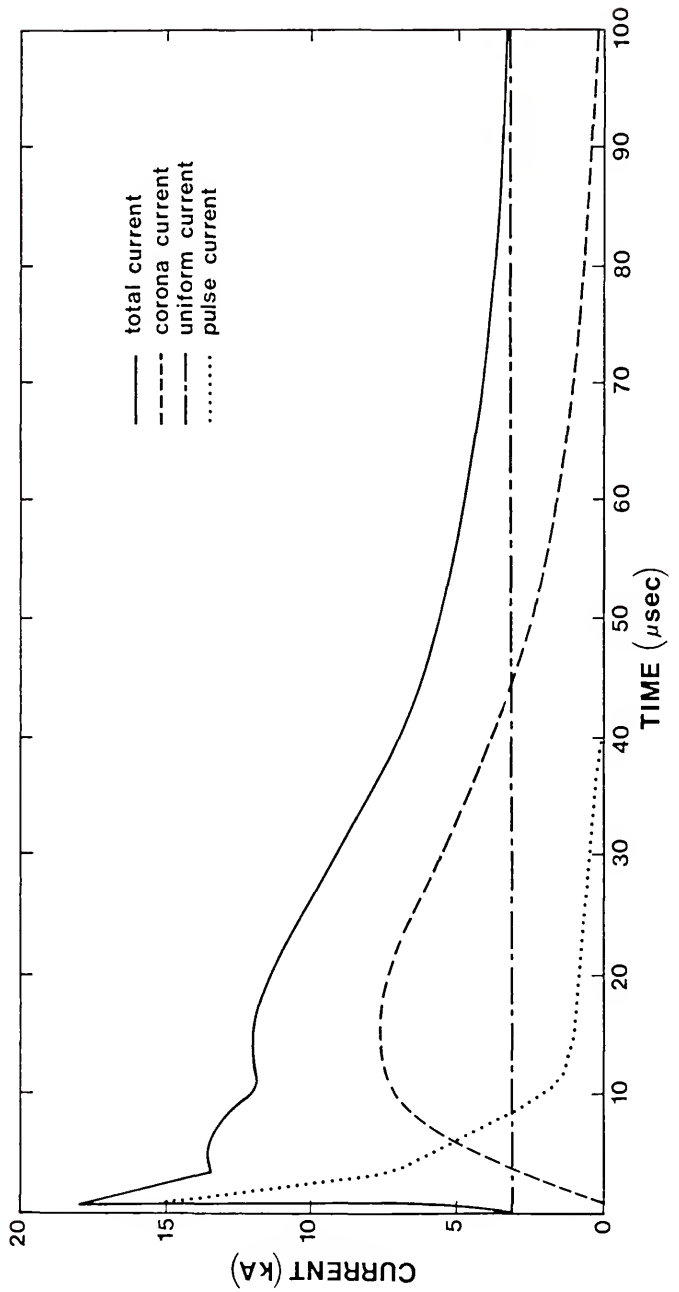
total current
corona current
uniform current
pulse current
CURRENT (kA)
TIME (μsec)
0
5
10
15
20
10
20
30
40
50
60
70
80
90
100

Figure 3.3. Electric and magnetic fields produced by a typical subsequent return stroke at a distance of 3 km from the channel at an altitude of 10 m.

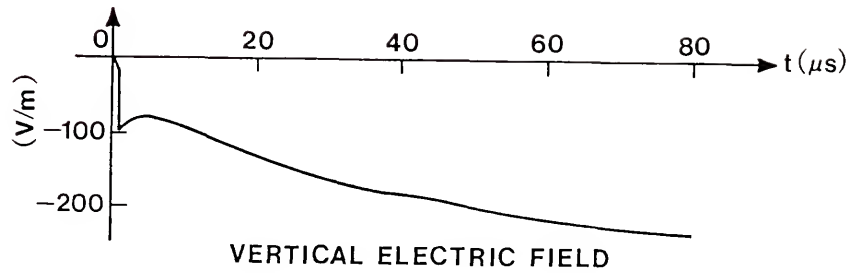

VERTICAL ELECTRIC FIELD

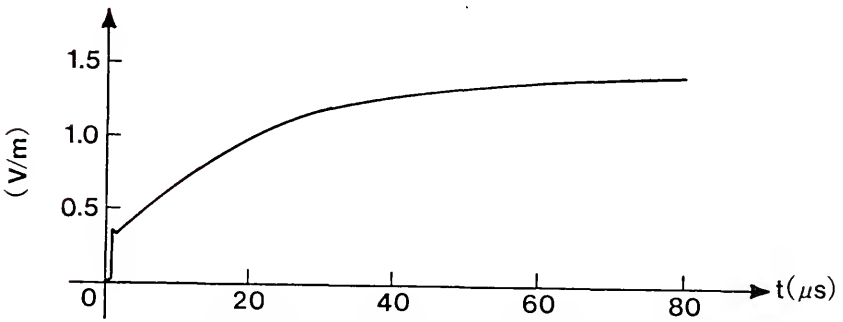

HORIZONTAL ELECTRIC FIELD

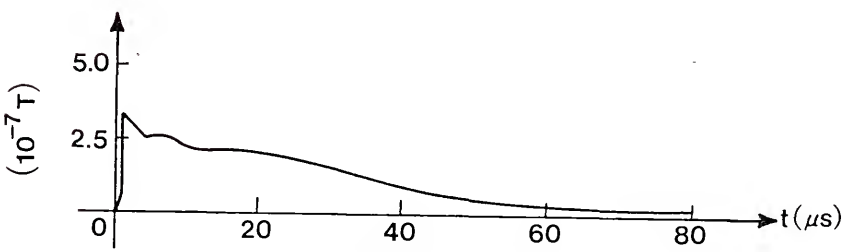

MAGNETIC FIELD

conductivty, a propagating electromagnetic wave has a non-zero net tangential electric field along the direction of propagation. This is because the tangential component of the propagating magnetic field at the ground induces a current density in the ground, which for a finite conductivity produces a tangential electric field at the surface. The classical research associated with the understanding of this phenomenon has been credited mainly to Zenneck (1907), Sommerfeld (1909, 1926), and Norton (1935, 1936, 1937). An interesting historical perspective is given in Chapter II of Wait (1962). Special mention must be made of the work reported by Carson (1926) which was concerned with propagation in overhead wires with ground return. For a moderately good, flat, homogenous ground, the wavetilt function relating the Fourier transform of the vertical electric field to that of the horizontal electric field at ground may be adequately approximated by (e.g. Wait, 1962; Vance, 1977)

$$W(j\omega) = \frac{E_H(j\omega)}{E_V(j\omega)} = \frac{1}{\sqrt{\varepsilon_r + \sigma/j\omega\varepsilon_0}} \tag{3.4}$$

where

E_H - horizontal electric field

E_V - vertical electric field

W - wavetilt

ε_r - relative permittivity of the soil

σ - soil conductivity

ε_0 - permittivity of air (or vacuum)

The main approximations involved in arriving at the above formulation are the following: (a) the incident wave is a radiation field with

its electric field vector in the plane defined by the direction of propagation and the normal to the ground, and (b) the angle of incidence is near grazing to the flat earth's surface. Both these approximations are reasonable for the data reported in this thesis. Approximation (a) will be further investigated later.

From Equation (3.4) we note that the horizontal electric field may be obtained from the vertical electric field and a knowledge of the ground parameters ε_r and σ. For a radiation field in air (or vacuum), the vertical electric field and the horizontal magnetic field are related by the free space impedance. Due to this fact, Equation (3.4) may also be used to determine the horizontal electric field from the horizontal magnetic field.

An obvious way to proceed would be to Fourier Transform the vertical electric field and then obtain the Fourier Transform of the horizontal component in accordance with Equation (3.4). Inverse transforming the results gives $E_H(t)$. For any real waveform this would involve using the Discrete Fourier Transform (DFT) and the Fast Fourier Transform (FFT) technique. A more direct approach will be adopted here. Since the vertical electric field may be obtained in a piecewise linear form, the ramp response of W(s) can be used to obtain the horizontal field in the time-domain without resorting to the transform-inverse transform process.

Let us consider a vertical electric field signal as being represented by its piecewise linear version as shown in Figure 3.4. Without any loss of generality let us assume that there are only four linear segments as shown. The start point of any segment j is given by the coordinates (t_j, E_{V_j}) and the end point by $(t_{j+1}, E_{V_{j+1}})$.

Figure 3.4. Example of a piecewise linear vertical electric field due to a return-stroke.

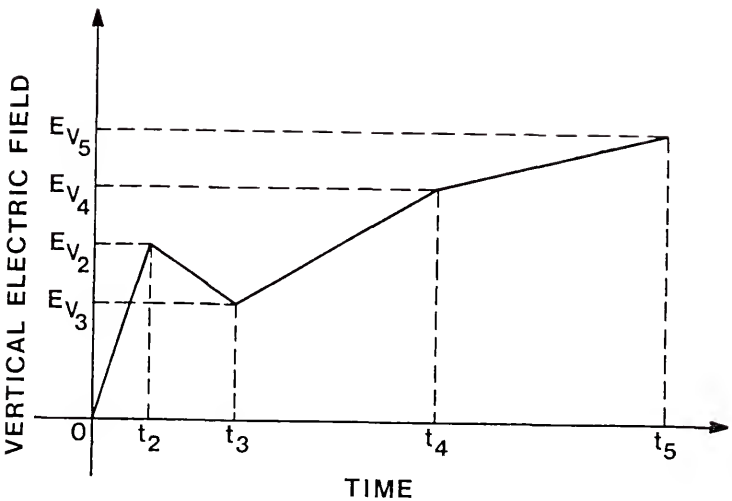
VERTICAL ELECTRIC FIELD
E_{V_5}
E_{V_4}
E_{V_2}
E_{V_3}
0
t_2
t_3
t_4
t_5
TIME

Thus, an m-segment representation will be defined by m+1 points. Further, it will be assumed that outside the time interval given by $[t_1, t_{m+1}]$ the vertical electric field is zero. Therefore, from Figure 3.4, an analytical expression for $E_V(t)$ may be written down as follows,

$$E_V(t) = \frac{E_{V_2}}{t_2} \cdot t \cdot u(t) + \left[-\frac{E_{V_2}}{t_2} + \frac{E_{V_3} - E_{V_2}}{t_3 - t_2}\right] \cdot (t-t_2) \cdot u(t-t_2)$$

$$+ \left[-\frac{E_{V_3} - E_{V_2}}{t_3 - t_2} + \frac{E_{V_4} - E_{V_3}}{t_4 - t_3}\right] \cdot (t-t_3) \cdot u(t-t_3)$$

$$+ \left[-\frac{E_{V_4} - E_{V_3}}{t_4 - t_3} + \frac{E_{V_5} - E_{V_4}}{t_5 - t_4}\right] \cdot (t-t_4) \cdot u(t-t_4)$$

$$+ \left[-\frac{E_{V_5} - E_{V_4}}{t_5 - t_4} \cdot (t-t_5) - E_{V_5}\right] \cdot u(t-t_5) \qquad (3.5)$$

where u(t) is the unit step function.

It can be seen that each term in Equation (3.5) represents a ramp, except for the last term which is a step, due to the fact that the field waveform in Figure 3.4 terminates at a finite non-zero value.

At this point, a digression is necessary in order to determine the ramp and step response of W(s) as given in Equation 3.4. For a ramp input, i.e.

$$E_V(t) = m\ t\ u(t) \tag{3.6}$$

we have,

$$E_H(s) = \frac{1}{\sqrt{\varepsilon_r + \sigma/s\varepsilon_0}} \cdot \frac{m}{s^2}$$

$$E_H(s) = \frac{m}{\sqrt{\varepsilon_r}} \cdot \frac{1}{s^{3/2}(s + \sigma/\varepsilon_0 \varepsilon_r)^{1/2}} \tag{3.7}$$

Using a table of Inverse Laplace Transforms (e.g. Abramovitz and Stegun, 1968), we have from Equation (3.4)

$$E_H(t) = \frac{m}{\sqrt{\varepsilon_r}} \cdot t \cdot e^{-pt} [I_0(pt) + I_1(pt)] \cdot u(t) \tag{3.8}$$

where

$p = \sigma/2\varepsilon_0 \varepsilon_r$

I_0, I_1 - modified Bessel's Functions of the first kind of the zeroth and first order respectively.

Similarly for a step input,

$$E_V(s) = k\ u(t) \tag{3.9}$$

we obtain

$$E_H(s) = \frac{k}{\sqrt{\varepsilon_r}} \frac{1}{s^{1/2}(s + \sigma/e_0 \varepsilon_r)^{1/2}} \tag{3.10}$$

and thus,

$$E_H(t) = \frac{k}{\sqrt{\varepsilon_r}} e^{-pt} I_0(pt) \cdot u(t) \tag{3.11}$$

To summarize, for a ramp vertical electric field given by Equation (3.6), the horizontal electric field is given in the time-domain by Equation (3.8). Similarly, the step in Equation (3.9) leads to a solution given by Equation (3.11). Using these results we return to the waveform shown in Figure 3.4 and given analytically by Equation (3.5). For that vertical electric field, the horizontal electric field is given by,

$$E_H(t) = \frac{1}{\sqrt{\varepsilon_r}} \cdot \frac{E_{V_2}}{t_2} \cdot t \cdot e^{-pt}[I_0(pt) + I_1(pt)]u(t)$$

$$+ \frac{1}{\sqrt{\varepsilon_r}} \left[- \frac{E_{V_2}}{t_2} + \frac{E_{V_3} - E_{V_2}}{t_3 - t_2}\right] \cdot (t-t_2) \cdot e^{-p(t-t_2)}$$

$$\cdot [I_0(p(t-t_2)) + I_1(p(t-t_2))]u(t-t_2)$$

$$+ \frac{1}{\sqrt{\varepsilon_r}} \left[- \frac{E_{V_3} - E_{V_2}}{t_3 - t_2} + \frac{E_{V_4} - E_{V_3}}{t_4 - t_3}\right] \cdot (t-t_3) \cdot e^{-p(t-t_3)}$$

$$\cdot [I_0(p(t-t_3)) + I_1(p(t-t_3))]u(t-t_3)$$

$$+ \frac{1}{\sqrt{\varepsilon_r}} \left[- \frac{E_{V_4} - E_{V_3}}{t_4 - t_3} + \frac{E_{V_5} - E_{V_4}}{t_5 - t_4}\right] \cdot (t-t_4) \cdot e^{-p(t-t_4)}$$

$$\cdot [I_0(p(t-t_4)) + I_1(p(t-t_4))]u(t-t_4)$$

$$+\frac{1}{\sqrt{\varepsilon_r}}\left[-\frac{E_{V_5}-E_{V_4}}{t_5-t_4}\right]\cdot(t-t_5)\cdot e^{-p(t-t_5)}$$

$$\cdot\left[I_0(p(t-t_5))+I_1(p(t-t_5))\right]u(t-t_5)$$

$$+\frac{1}{\sqrt{\varepsilon_r}}\left[-E_{V_5}\right]\cdot e^{-p(t-t_5)}\cdot I_0(p(t-t_5))\cdot u(t-t_5) \qquad (3.12)$$

It has therefore been analytically demonstrated that for a piecewise linear vertical electric field waveform given in the time-domain by Equation (3.5), a horizontal field waveform may be derived, also in the time-domain, in accordance with Equation (3.12). For example, let us determine the horizontal field from the wavetilt for the vertical electric field waveform given in Figure 3.3. In Figure 3.5 we show the digitized version of the vertical electric field, and the derived horizontal electric field for ground parameters given by $\varepsilon_r = 10$ and $\sigma = 10^{-3}$ mhos/m.

One of the assumptions underlying the wavetilt formulation as given by Equation (3.4) is its restriction to radiation fields. It is therefore applicable to only the radiation component of the total electric field. However, in Figure 3.5 the wavetilt formulation was applied to the complete vertical electric field. We now provide justification for that procedure. In Figure 3.6 we show the piecewise-linear version of the vertical electric radiation field at a distance of 3 km from the channel. This field is obtained by determining the complete field at 100 km (which is essentially all radiation) and extrapolating it to 3 km using an inverse distance

Figure 3.5. Piecewise-linear version of the vertical electric field given in Figure 3.3 and the derived horizontal field for $\varepsilon_r = 10$ and $\sigma = 10^{-3}$ mhos/m.

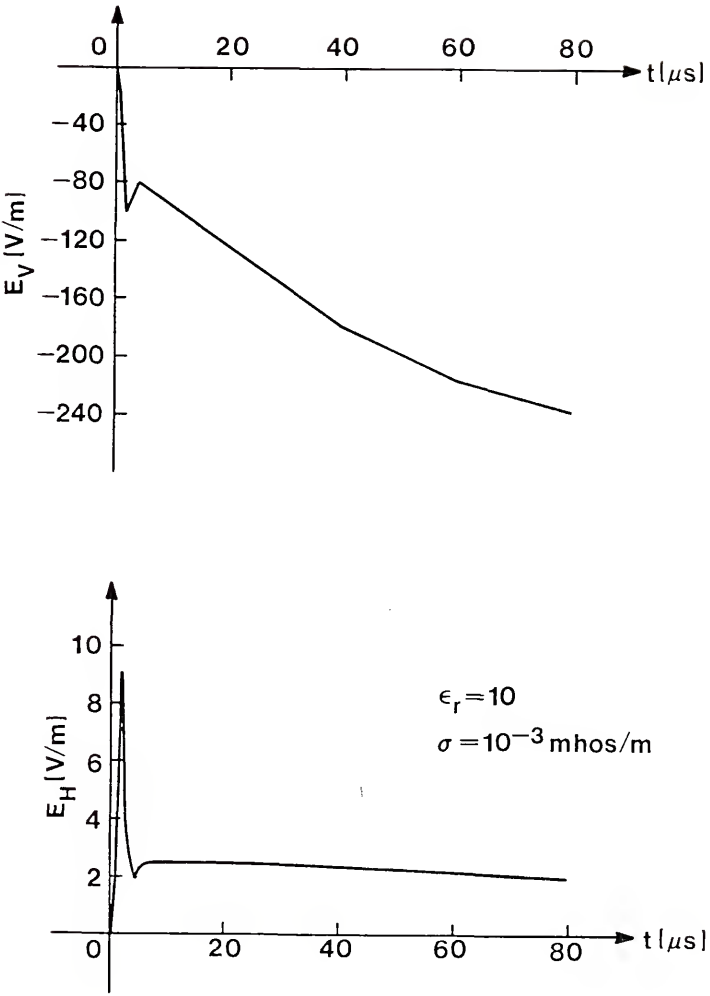
0
20
40
60
80
t [μs]
−40
−80
−120
−160
−200
−240
E_V [V/m]
10
8
6
4
2
0
E_H [V/m]
ε_r = 10
σ = 10^−3 mhos/m

Figure 3.6. Piecewise-linear version of the vertical electric field calculated at 100 km and extrapolated to 3 km and the derived horizontal field for $\varepsilon_r = 10$ and $\sigma = 10^{-3}$ mhos/m.

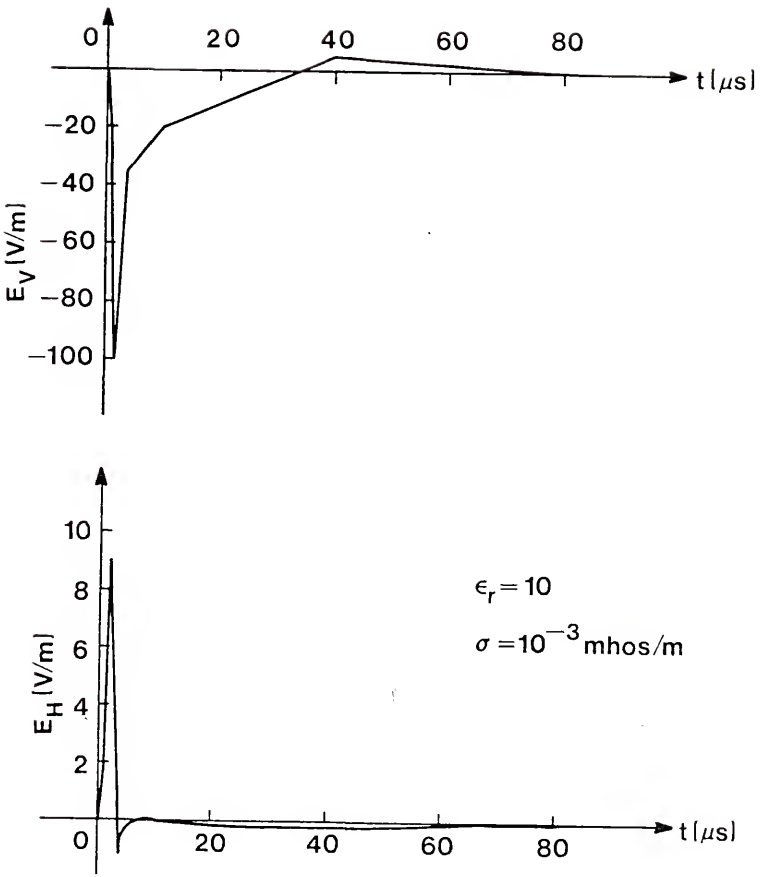
0
20
40
60
80
t [μs]
−20
−40
−60
−80
−100
E_V [V/m]
10
8
6
4
2
0
E_H [V/m]
ε_r = 10
σ = 10^−3 mhos/m
20
40
60
80
t [μs]

relationship, in accordance with standard practice. In Figure 3.6 the horizontal electric field derived from this radiation field is shown for $\varepsilon_r = 10$ and $\sigma = 10^{-3}$ mhos/m. A comparison between Figures 3.5 and 3.6 indicates that the peak horizontal field is essentially the same in both instances. This result is not very surprising, since from Equation (3.12) it is clear that the peak horizontal field occurs at a time which corresponds approximately to the time at which the vertical electric field has the maximum slope. However, the horizontal electric field shown in Figure 3.6 decays to zero at a much faster rate than that shown in Figure 3.5. As discussed earlier, the wavetilt formulation may also be applied to the magnetic field of the radiated wave. The resultant horizontal electric field derived from the radiation magnetic field would be identical to that shown in Figure 3.6. In Figure 3.7 we show the results of applying the formulation to the complete magnetic field. Again, the peak horizontal field is the same. However, its decay back to zero is not as fast as that in Figure 3.6 but is faster than that of the horizontal electric field shown in Figure 3.5 because of the absence of the electrostatic component in the magnetic field. Calculations of the horizontal field were also performed using the vertical fields at 200 m. Again, the peak value of the horizontal electric field derived from the complete vertical electric field is essentially the same as that obtained from the radiation waveform alone. However, the error involved in the horizontal field decay back to zero is larger at 200 m than at 3 km due to the presence of a larger electrostatic component. To summarize, we conclude, that the wavetilt formulation may be applied to the complete vertical electric

Figure 3.7. Piecewise linear version of the magnetic field given in Figure 3.3 and the derived horizontal electric field for $\varepsilon_r = 10$ and $\sigma = 10^{-3}$ mhos/m.

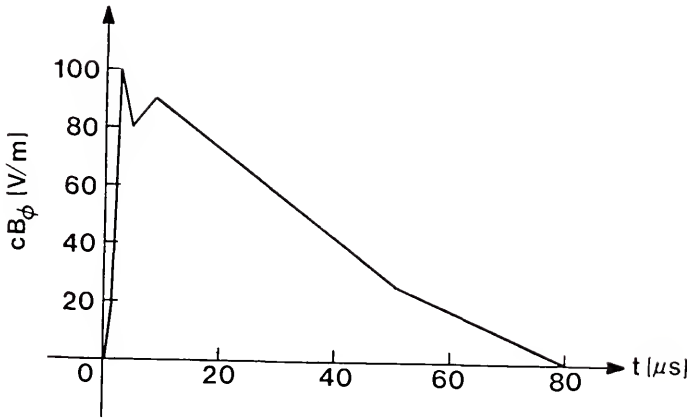
100
80
60
40
20
0
20
40
60
80
t [μs]
cB_φ [V/m]

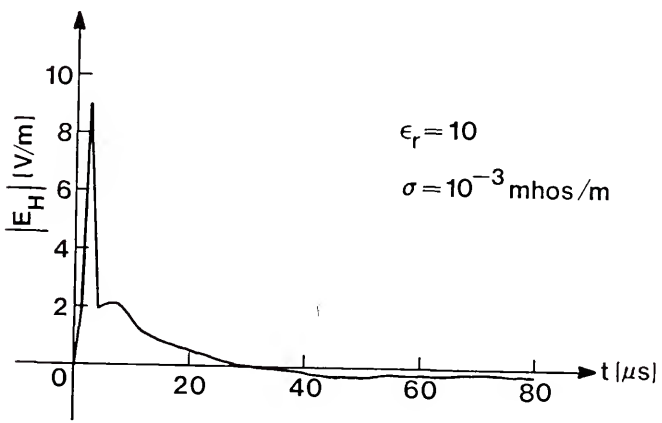
10
8
6
4
2
0
20
40
60
80
t [μs]
|E_H| [V/m]
ε_r = 10
σ = 10^−3 mhos/m

field or the complete magnetic field waveforms without much error in the initial peak although small errors may occur later. However, the only measurements of the magnetic field were made on the triggered system on a time scale of 200 μs full-scale as discussed in Chapter II, and do not provide sufficient resolution for accurate analysis, and hence the complete vertical electric field waveform will be used in this thesis.

We have explained how the vertical and horizontal components of the electric field may be derived in the vicinity of a power line using the model of Master et al. (1981) with the assumption that the ground is a perfect conductor. Effects of an imperfectly conducting ground plane may then be incorporated as a perturbation to the field solution derived for a perfectly conducting ground. Either the vertical electric field predicted by the model, or the vertical field directly measured near the line, may be used to compute the horizontal field due to the ground tilt. In this thesis, we shall do both: we shall first present a sequence of calculated line voltages for various ground conditions using model electric fields. We shall then use the measured vertical electric field near the test-line to compute a voltage waveform to be compared with the simultaneously measured voltage. For ground conductivities lower than 10^{-2} mhos/m, the horizontal electric field computed from the wavetilt is much larger than that obtained from the model of Master et al. (1981) for a line height of 10 m. For example, from Figures 3.5 and 3.6, $\sigma = 10^{-3}$ mhos/m leads to a horizontal field peak of 9 V/m whereas from Figure 3.3 we find an initial peak of only 0.4 V/m. Calculations indicate that for lightning over sea-

water (σ = 1 mhos/m; ε_r = 80) the peak horizontal electric field calculated from the wavetilt is of the same order of magnitude as that calculated from the model of Master et al. (1981). For such high conductivities, both horizontal fields would have to be taken into account. Even for 10^{-2} mhos/m, the value of the horizontal field after the initial peak derived from the wavetilt is of the same order of magnitude as the value derived from the model of Master et al. (1981). However, in this thesis we shall only use the horizontal electric field derived from the wavetilt formula and the vertical electric field. We now proceed to the coupling analysis to determine how these fields induce the line voltages.

3.3 Induced Line Voltage

In this section we discuss how the electromagnetic field generated by nearby lightning is coupled onto an overhead power line. We shall first derive the coupled differential equations for the line voltages and currents, starting with Maxwell's Equations in the time domain. These differential equations will then be converted into a set of difference equations which can be solved on a digital computer.

3.3.1 Theoretical Model

The heights above ground, at the poles and midspans, for both the conductors of our unenergized test-line have been given in Table 2.1. From these values we find average heights at the pole and at midspan for each conductor, and hence determine an average value of

the sag for each conductor. The average height of the line is then computed using the following engineering approximation,

$$h = h_p - \frac{2}{3} s$$

where,

h = effective height of the line

h_p = height of the line at the pole

s = sag

This leads to the following values which will be used in this study,

h_1 = 9.8 m -- height of phase (top) conductor

h_2 = 7.6 m -- height of neutral (bottom) conductor.

The phase and neutral conductors were of the same type, with diameters equal to 8 mm. We have now completely defined the geometry of the unenergized test-line. We have to determine the response of this line when it is excited by a transient electromagnetic field due to nearby lightning. This field is, in general, a non-uniform electromagnetic field.

The solution to this problem was first obtained in the frequency domain by Taylor et al. (1965), and a more convenient form of this solution was presented by Smith (1973). Whitescarver (1969) started with the solution given by Taylor et al. (1965) and modified it according to the formulation given by Putzer (1968). He then used these results to make frequency-domain comparisons between the theory and his experimental results. The frequency-domain solution was transformed by Perala (1974) into a form more suitable for computer simulation. This solution indicated that the transmission line

problem could be solved completely in terms of the tangential electric field at the conductor boundaries and the vertical electric field at the end points of the line, and the vertical electric field at the calculation point. A general time-domain solution to the problem was presented recently by Agrawal et al. (1980). The various assumptions underlying the solution were more closely examined. A computational scheme was outlined using finite-difference techniques.

For the sake of completeness, we shall derive the Telegrapher's Equations for the two-conductor line under study, using a perfectly conducting ground as the reference conductor. The equations will be formulated in the time-domain. The approach adopted will parallel that used by Agrawal et al. (1980). It is important to note that most of the earlier studies conducted with the specific purpose of understanding induced voltages on power lines, i.e. Lundholm (1957), Rusck (1958), Chowdhuri (1966), and Singarajah (1971), did not follow the approach indicated below, but assumed that the line voltage was due to the vertical electric field coupling alone.

In Figure 3.7 we show the two-conductor test line above a perfectly conducting ground. The effect of finite ground conductivity will be introduced later. Let $\bar{E}(x,y,z,t)$ and $\bar{H}(x,y,z,t)$ be the total electric and magnetic field in the vicinity of the line. However, due to the orientation of the axes, $y = 0$ for all points on the line and hence we omit the y dependence; the time dependence will be suppressed for brevity. To derive the first Telegrapher's Equation we apply Faraday's Law to the top phase conductor over the region shown by dotted lines in Figure 3.7. Since,

Figure 3.8. The two conductor test-line above a perfectly conducting earth.

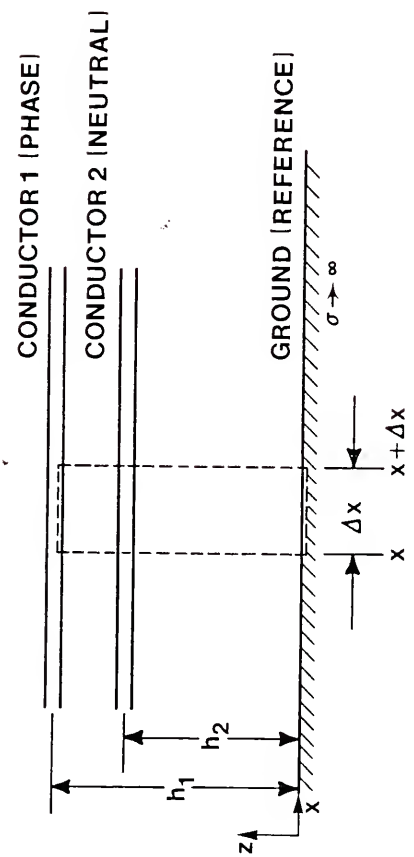
CONDUCTOR 1 (PHASE)
CONDUCTOR 2 (NEUTRAL)
GROUND (REFERENCE)
$\sigma \to \infty$
h_2
h_1
z
x
x
Δx
$x+\Delta x$

$$\oint \overline{E} \cdot \overline{dl} = -\frac{\partial}{\partial t} \iint \overline{B} \cdot \overline{ds}, \tag{3.13}$$

$$\int_0^{h_1} \{E_z(x + \Delta x, z) - E_z(x,z)\}dz - \int_x^{x+\Delta x} E_x(x,h_1)dx = \frac{\partial}{\partial t} \int_x^{x+\Delta x} \int_0^{h_1} B_y(x,z)dz\, dx \tag{3.14}$$

where we have made use of the boundary condition

$$E_x(x,0) = 0 \tag{3.15}$$

Dividing each term in Equation (3.14), by Δx, and taking the limit as $\Delta x \to 0$ we have

$$\frac{\partial}{\partial x} \int_0^{h_1} E_z(x,z)dz - E_x(x,h_1) = \frac{\partial}{\partial t} \int_0^{h_1} B_y(x,z)dz \tag{3.16}$$

At this point it is convenient to split the complete field into two components (a) "incident" field due to lightning, which would be present in the absence of conductors and (b) "scattered" field due to the current and voltage induced in the conductor by the incident field. Thus,

$$\begin{aligned} E_z &= E_z^i + E_z^s \\ E_x &= E_x^i + E_x^s \\ B_y &= B_y^i + B_y^s \end{aligned} \tag{3.17}$$

where the superscripts i and s represent the incident and the scattered components of the total field. Substituting these into Equation (3.16), we obtain

$$\frac{\partial}{\partial x} \int_0^{h_1} E_z^s(x,z)dz - \frac{\partial}{\partial t} \int_0^{h_1} B_y^s(x,z)dz - E_x(x,h_1)$$

$$= -\frac{\partial}{\partial x} \int_0^{h_1} E_z^i(x,z)dz + \frac{\partial}{\partial t} \int_0^{h_1} B_y^i(x,z)dz \qquad (3.18)$$

This equation is exact. However, we shall now make an assumption that the scattered fields are transverse magnetic. This is a valid assumption since the diameter of the conductor ($\sim$ 1 cm) is very small compared to the line height ($\sim$ 10 m). This ensures that the following two properties hold (Stratton, 1941, pg. 352). (a) the scattered voltage is single valued in the transverse plane, and defined by

$$V_1^s(x) = -\int_0^{h_1} E_z^s(x,z)dz \qquad (3.19)$$

and (b) the scattered magnetic flux can be directly related to the inductances per unit length of the line,

$$\int_0^{h_1} B_y^s(x,z)dz = L_{11}I_1(x) + L_{12}I_1(x) \qquad (3.20)$$

where,

L_{11} -- self-inductance of the phase conductor

and L_{12} -- mutual inductance between the phase and the neutral conductor

We note that in Equation (3.20) we have not used any superscript on the currents because there are only scattered currents. Substituting Equations (3.19) and (3.20) into Equation (3.18),

$$\frac{\partial V_1^s(x)}{\partial x} + \frac{\partial}{\partial t}\{L_{11}I_1(x) + L_{12}I_1(x)\} + E_x(x,h_1)$$

$$= \frac{\partial}{\partial x}\int_0^{h_1} E_z^i(x,z)dz - \frac{\partial}{\partial t}\int_0^{h_1} B_y^i(x,z)dz \qquad (3.21)$$

If we apply Equation (3.13) to the incident component of the fields, we obtain

$$\frac{\partial}{\partial x}\int_0^{h_1} E_z^i(x,z)dz - \frac{\partial}{\partial t}\int_0^{h_1} B_y^i(x,z)dz = E_x^i(x,h_1) \qquad (3.22)$$

where we have again used the boundary condition given in Equation (3.15). The total electric field parallel to the line, $E_x(x,h_1)$ in Equation (3.21), is related to the scattered current, and produces a voltage drop per unit length along the line. This relation may be expressed in the frequency domain using an impedance per unit length of the line. The internal inductance of the conductor is generally negligible, and hence we shall assume that the relation between $E_x(x,h_1)$ and $I(x)$ is purely resistive.

$$E_x(x,h_1) = R_{11}I_1(x) + R_{12}I_2(x) \qquad (3.23)$$

where R_{11} and R_{12} are the self and mutual resistance per unit length for conductor 1. Substituting Equations (3.22) and (3.23) into Equation (3.21), we get the first Telegrapher's Equation for our line,

$$\frac{\partial V_1^s(x)}{\partial x} + \frac{\partial}{\partial t}[L_{1j}][I_j] + [R_{1j}][I_j] = E_x^i(x,h_1) \qquad (3.24)$$

A similar analysis for the neutral conductor leads to

$$\frac{\partial V_2^s(x)}{\partial x} + \frac{\partial}{\partial t}[L_{2j}][I_j] + [R_{2j}][I_j] = E_x^i(x,h_2) \qquad (3.25)$$

Equations (3.24) and (3.25) may be combined together into a matrix form,

$$\frac{\partial}{\partial x}[V^s(x)] + [R][I(x)] + [L]\frac{\partial}{\partial t}[I(x)] = [E_x^i(x,h)] \qquad (3.26)$$

To derive the second Telegrapher's Equation we start with Maxwell's formulation of Ampere's Law

$$\bar{\nabla} \times \bar{H} = \bar{J} + \frac{\partial \bar{D}}{\partial t} \qquad (3.27)$$

and integrate over a closed cylindrical surface of length Δx just outside the phase conductor. Using the Gauss Divergence Theorem,

$$\oint \bar{J}_1 \cdot \overline{dS} + \frac{\partial}{\partial t}\oint \bar{D}_1 \cdot \overline{dS} = 0 \qquad (3.28)$$

We have already made the assumption that the current in the wire flows parallel to its axis, and hence

$$\int_{\text{ends}} \bar{J} \cdot \overline{dS} = I_1(x + \Delta x) - I_1(x) \qquad (3.29)$$

If we assume that the air conductivity is negligible,

$$\int_{cyl} \overline{J} \cdot \overline{ds} = 0 \tag{3.30}$$

We substitute Equations (3.29) and (3.30) into Equation (3.28), divide by Δx, and take the limit as $\Delta x \to 0$,

$$\frac{\partial I_1(x)}{\partial x} + \frac{\partial Q_1(x)}{\partial t} = 0 \tag{3.31}$$

where Q_1 is the net free charge per unit length on the phase conductor, obtained from Gauss's Law,

$$\oint \overline{D}_1 \cdot \overline{dS} = Q_1 \tag{3.32}$$

Q_1 may be related to the capacitances per unit length of the line and the scattered voltages,

$$Q_1 = C_{11}V_1^s + C_{12}V_2^s \tag{3.33}$$

where,

C_{11} -- capacitance between phase conductor and ground,

C_{12} -- capacitance between phase and neutral conductors.

As shown in Agrawal et al. (1980), Equation (3.33) rests on the assumption that the scattered axial electric field E_x^s does not vary significantly along the x-direction. Substituting Equation (3.33) into Equation (3.31) we have the second Telegrapher's Equation,

$$\frac{\partial I_1(x)}{\partial x} + \frac{\partial}{\partial t}\,[C_{1j}][V_j^s(x)] = 0 \tag{3.34}$$

Similarly for the neutral conductor

$$\frac{\partial I_2(x)}{\partial x} + \frac{\partial}{\partial t} [C_{2j}][V_j^s(x)] = 0 \tag{3.35}$$

Combining Equations (3.34) and (3.35) into a matrix formulation leads to

$$\frac{\partial}{\partial x} [I(x)] + [C] \frac{\partial}{\partial t} [V^s(x)] = 0 \tag{3.36}$$

Equations (3.26) and (3.36) are the coupled set of first-order partial differential equations which may be solved for the variables $[I(x)]$ and $[V^s(x)]$. Note that the source term is present in only one equation. However, the boundary conditions at the ends of the line also involve a knowledge of the vertical electric field, as we shall see later. The current $[I(x)]$ represents the actual current which is flowing in the line. However $[V^s(x)]$ represents only the scattered voltage. Thus, instead of solving the Telegraphers' Equations for the currents and actual voltages on the line, we solve only for the currents and the scattered voltages. The advantage of this formulation will be discussed below. After obtaining the solution for the scattered voltage, the actual voltage at any point x on the line may be determined in accordance with Equations (3.17) and (3.19),

$$\begin{aligned} [V(x)] &= [V^s(x)] + [V^i(x)] \\ &= [V^s(x)] - [\int_0^h E_z^i(x,z)dz] \end{aligned} \tag{3.37}$$

We now transform Equations (3.26) and (3.36) into another form where the variables are the actual currents on the line and the total voltage. Let us substitute Equation (3.37) into Equation (3.26),

$$\frac{\partial}{\partial x}\left\{[V(x)] + \left[\int_0^h E_z^i(x,z)dz\right]\right\} + [R][I(x)]$$

$$+ [L]\frac{\partial}{\partial t}[I(x)] = [E_x^i(x,h)]$$

Hence,

$$\frac{\partial}{\partial x}[V(x)] + [R][I(x)] + [L]\frac{\partial}{\partial t}[I(x)] = [E_x^i(x,h)]$$

$$- \frac{\partial}{\partial x}\left[\int_0^h E_z^i(x,z)dz\right] \qquad (3.38)$$

From Equation (3.22) it is clear that the forcing terms in Equation (3.38) can be rewritten in terms of the incident magnetic field, so that

$$\frac{\partial}{\partial x}[V(x)] + [R][I(x)] + [L]\frac{\partial}{\partial t}[I(x)] = -\frac{\partial}{\partial t}\left[\int_0^h B_y^i(x,z)dz\right] \qquad (3.39)$$

Similarly Equation (3.36) may be transformed into

$$\frac{\partial}{\partial x}[I(x)] + [C]\frac{\partial}{\partial t}[V(x)] = -[C]\frac{\partial}{\partial t}\left[\int_0^h E_z^i(x,z)dz\right] \qquad (3.40)$$

We see that the forcing terms in Equations (3.39) and (3.40) are much more involved than the single term in the set of Equations (3.26) and (3.36). Furthermore, the forcing terms in Equations (3.39) and

(3.40) involve taking derivatives of the incident field, and hence, in general, are not efficient for computer simulation studies.

In this thesis the set of coupled differential equations given by Equations (3.26) and (3.36) will be used. The effect of the imperfectly conducting earth will be introduced in the formulation by using the horizontal electric field determined from the wavetilt. Furthermore, a resistance per unit length will be introduced to account for attenuation due to the ground. The calculation of the horizontal electric field from the vertical component was illustrated in Figures 3.5 and 3.6. We now present the theory to account for the per unit line resistance.

For a single conductor at height h located above earth which has finite conductivity, the impedance per unit length of the ground plane given by Vance (1977) is

$$Z_g = - \frac{j\gamma}{4\pi h \sigma} \cdot \frac{H_0^{(1)}(j\gamma 2h)}{H_1^{(1)}(j\gamma 2h)} \tag{3.41}$$

where

$$\gamma = \{ j\omega\mu_0 (\sigma + j\omega\varepsilon) \}^{1/2}$$

σ, ε - conductivity and permittivity of the ground.

Simplified versions of Equation (3.41) may be written as follows. If the earth is a good conductor to the extent that the displacement current term is negligible, then

$$Z_g = \frac{1 + j}{4\pi h \sigma \delta} \tag{3.42}$$

If the earth is a relatively poor conductor such that the skin depth is large compared to the height h,

$$Z_g = \frac{\omega\mu_o}{8} + j\omega\frac{\mu_o}{2\pi}\log\frac{\delta}{\sqrt{2}\,\gamma_o h} \tag{3.43}$$

where

$$\delta = 1/(\pi f \mu_o \sigma)^{1/2}$$

$$\gamma_o = 1.7811$$

Consider a ground plane with $\sigma = 10^{-4}$ mhos/m and $\varepsilon_r = 3$. Then, at 1 MHz,

$$\delta = 1/(\pi \times 10^6 \times 4\pi \times 10^{-7} \times 10^{-4})^{1/2} = 50$$

For h = 10 m and using Equation (3.43) we obtain

$$Z_g = 0.99 + j\omega\, 6.01 \times 10^{-8} \tag{3.44}$$

Thus we see that the impedance in this case is almost purely resistive. The resistance per meter of the copper conductor is negligible compared to the 1 Ohm/m calculated in Equation (3.44). On the other hand the inductance per unit length of a conductor 10 m above ground is about two orders of magnitude larger than that due to the earth conductivity.

3.3.2 Computer Solution

The coupled differential equations given by Equations (3.26) and (3.36) will now be converted into a set of difference equations using

the point-centered finite-difference technique. We shall not dwell on the existence and uniqueness of the solutions to these equations; the interested reader is referred to Lax (1958). The difference formulation of Equation (3.26) centered about the point (x,t) is,

$$\left[\frac{V(x + \Delta x/2,t) - V(x - \Delta x/2,t)}{\Delta x}\right] + [R][I(x,t)]$$

$$+ [L]\left[\frac{I(x,t + \Delta t/2) - I(x,t - \Delta t/2)}{\Delta t}\right] = [E_s(x,t)] \qquad (3.45)$$

where the source term for conductor j is given by

$$E_{sj}(x,t) = E_x^i(x,h_j,t) \qquad (3.46)$$

Similarly, Equation (3.36) may be written as

$$\left[\frac{I(x + \Delta x/2,t) - I(x - \Delta x/2,t)}{\Delta x}\right]$$

$$+ [C]\left[\frac{V(x,t + \Delta t/2) - V(x,t - \Delta t/2)}{\Delta t}\right] = 0 \qquad (3.47)$$

Note that in Equations (3.45) and (3.47) we have dropped the superscript on the scattered voltage V^s for notational brevity.

Let us introduce the following notation:

$$V_k^n = [V\{(k - 1)\Delta x,\ (n - 1)\Delta t\}]$$

$$I_k^n = [I\{(k - \tfrac{1}{2})\Delta x,\ (n - \tfrac{1}{2})\Delta t\}]$$

$$V_{s_k}^n = [V_s\{(k - \frac{1}{2})\Delta x,\ (n - \frac{1}{2})\Delta t\}]$$

where,

$n = 1,2,3, \ldots\ldots n_{max}+1$; (time count)

$k = 1,2,3, \ldots\ldots k_{max}+1$; (position count)

and,

$k_{max}\Delta x = L \equiv$ total line length;

$n_{max}\Delta t = T \equiv$ total time of interest.

Hence, Equation (3.45) becomes

$$\frac{V_{k+1}^{n+1} - V_k^{n+1}}{\Delta x} + [R]\frac{I_k^{n+1} + I_k^n}{2} + [L]\frac{I_k^{n+1} - I_k^n}{\Delta t} = \frac{V_{s_k}^{n+1} + V_{s_k}^n}{2} \qquad (3.48)$$

and Equation (3.47) gives

$$\frac{I_{k+1}^n - I_k^n}{\Delta x} + [C]\frac{V_{k+1}^{n+1} - V_{k+1}^n}{\Delta t} = 0 \qquad (3.49)$$

From Equations (3.48) and (3.49) we obtain

$$I_k^{n+1} = [\frac{L}{\Delta t} + \frac{R}{2}]^{-1}\{[\frac{L}{\Delta t} - \frac{R}{2}]I_k^n + \frac{V_{s_k}^{n+1} + V_{s_k}^n}{2} - \frac{V_{k+1}^{n+1} - V_k^{n+1}}{\Delta x}\} \qquad (3.50)$$

and

$$V_k^{n+1} = V_k^n + [\frac{C}{\Delta t}]^{-1}\frac{I_{k-1}^n - I_k^n}{\Delta x} \qquad (3.51)$$

The solution scheme presented in Equations (3.50) and (3.51) may be understood in terms of Figure 3.8 and the following algorithm:

Figure 3.9. Solution scheme for the coupled set of first-order transmission-line equations.

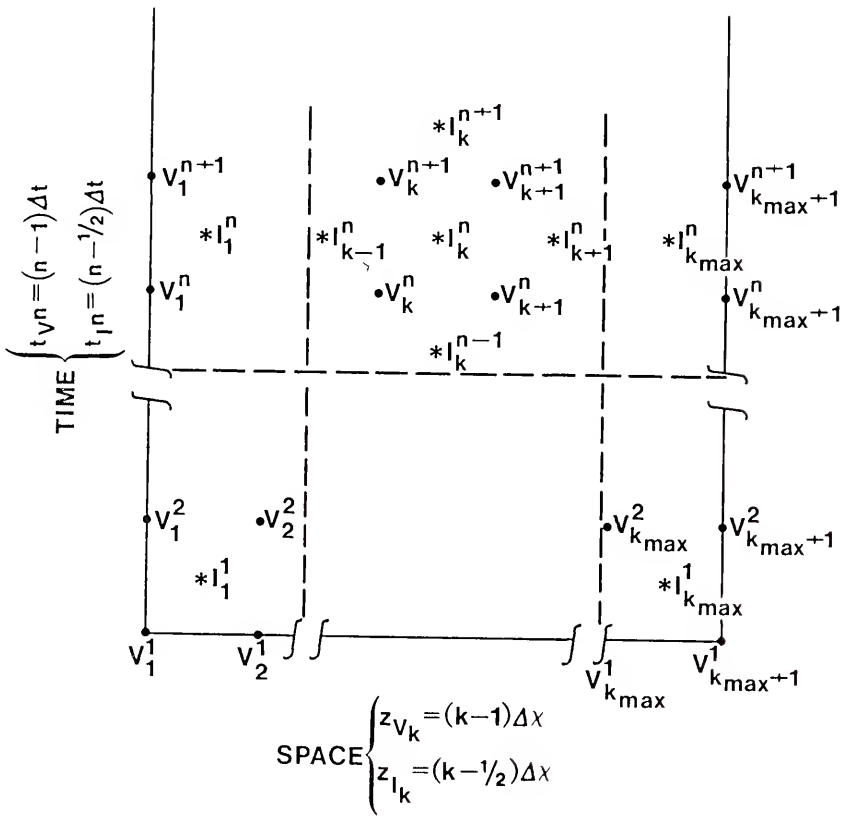
TIME
$t_{V^n} = (n-1)\Delta t$
$t_{I^n} = (n-1/2)\Delta t$
V_1^{n+1}
I_1^n
V_1^n
I_k^{n+1}
V_k^{n+1}
V_{k+1}^{n+1}
I_{k-1}^n
I_k^n
I_{k+1}^n
V_k^n
V_{k+1}^n
I_k^{n-1}
$V_{k_{max}+1}^{n+1}$
$I_{k_{max}}^n$
$V_{k_{max}+1}^n$
V_1^2
V_2^2
I_1^1
$V_{k_{max}}^2$
$V_{k_{max}+1}^2$
$I_{k_{max}}^1$
V_1^1
V_2^1
$V_{k_{max}}^1$
$V_{k_{max}+1}^1$
SPACE
$z_{V_k} = (k-1)\Delta x$
$z_{I_k} = (k-1/2)\Delta x$

1. Initialize the current array.
2. Define voltage at all nodes at n = 1 as zero.
3. Compute I_k^n for k = 1, 2, ... k_{max}.
4. Compute V_k^{n+1} for k = 2, 3, ... k_{max}.
5. Compute V_1^{n+1}, $V_{k_{max}+1}^{n+1}$ from boundary conditions.
6. Store information for plots.
7. Do steps 3 through 6 for n = 1, ... n_{max}.

The solution proceeds sequentially, within each step of the do-loop we solve for one row of current and the next row of voltage, as shown in above diagram.

A close look at Equation (3.51) indicates that it cannot be used for points k = 1 and k = k_{max}+1, i.e. the end points. That is not very surprising since these two points define the boundaries of the transmission line. Solutions to the voltages at these end points are determined by the terminations between various conductors and between the conductors and ground. With reference to Figure 3.8 we note that the current is not known at the boundary, but is known at points $\Delta x/2$ and $3\Delta x/2$ inside the boundary. To determine the current at the end we assume that currents at these two closest nodes and the current at the end itself can be approximated by a parabolic curve at each time t. Using the coefficients of that fit the value of $\partial I/\partial x$ may be obtained and then plugged directly into Equation (3.36) to determine the end voltage. We illustrate this procedure by determining the voltage at x = 0, for some time step. We have,

$$I = ax^2 + bx + c \tag{3.52}$$

where a, b, c will be determined.

If I_1^n and I_2^n define the currents at points $x = \Delta x/2$ and $x = 3\Delta x/2$, and if I_o^n denotes current at $x = 0$, then

$$\left.\frac{\partial I}{\partial x}\right|_{x=0} = \frac{1}{3\Delta x}\{9I_1^n - I_2^n - 8I_o^n\} \tag{3.53}$$

Let us assume that the termination network at $x = 0$ is a parallel R-C network. This more general termination as opposed to a purely resistive termination and will be needed to simulate the effect of the measuring capacitor at the north end of the unenergized test line. It is important to note that the scattered voltage used in our formulation in Equation (3.36) is not a physical real voltage. The boundary condition at the end of the line will therefore be in terms of the physical total voltage denoted by V_1^T,

$$I_o = -[G_L]V_1^T - [C_t]\frac{dV_1^T}{dt} \tag{3.54}$$

where $[G_L]$ and $[C_t]$ are the conductance and capacitance terminating matrices at $x = 0$ and

$$V_1^T = V_1 + V_1^i \tag{3.55}$$

and V_1^i represents the voltage due to the incident vertical electric field, and is given by

$$V_1^i = \left[- \int_0^h E_z^i(0,z)dz \right] \tag{3.56}$$

Substituting Equations (3.53), (3.54), and (3.55) into Equation (3.26) and writing it in a difference form we obtain

$$V_1^{n+1} = \left[C + \frac{4\Delta t}{3\Delta x} G_L + \frac{8}{3\Delta x} C_t\right]^{-1} \left\{\left[C - \frac{4\Delta x}{3\Delta x} G_L + \frac{8}{3\Delta x} C_t\right] V_1^n \right.$$

$$- \frac{\Delta t}{3\Delta x} (9I_1^n - I_2^n) - \frac{4\Delta t}{3\Delta x} [G_L] (V_1^{i\,n+1} + V_1^{i\,n})$$

$$\left. - \frac{8}{3\Delta x} [C_t] (V_1^{i\,n+1} - V_1^{i\,n})\right\} \tag{3.57}$$

A similar analysis may be carried out to determine the voltage at x = L. In Figure 3.10 we show an equivalent circuit for a single-conductor line above ground. Note that at the ends of the line, the vertical electric field is needed; at all other points only the horizontal electric field is required for a solution of the Telegraphers' Equations for the scattered voltage and current.

To summarize, the solution to the currents and scattered voltages on the line may be obtained from the knowledge of the horizontal electric field along the conductors and the vertical electric fields at the two ends. However, to determine the actual voltage physically present at any point along the line, knowledge of the vertical electric field at that point is also required as in Equations (3.55) and (3.56).

Figure 3.10. Circuit diagram for a single-conductor line above a ground plane. To solve the Telegraphers' Equations for the scattered voltage and current in the line the horizontal electric field is required at all points along the line and the vertical electric field is needed only at the ends.

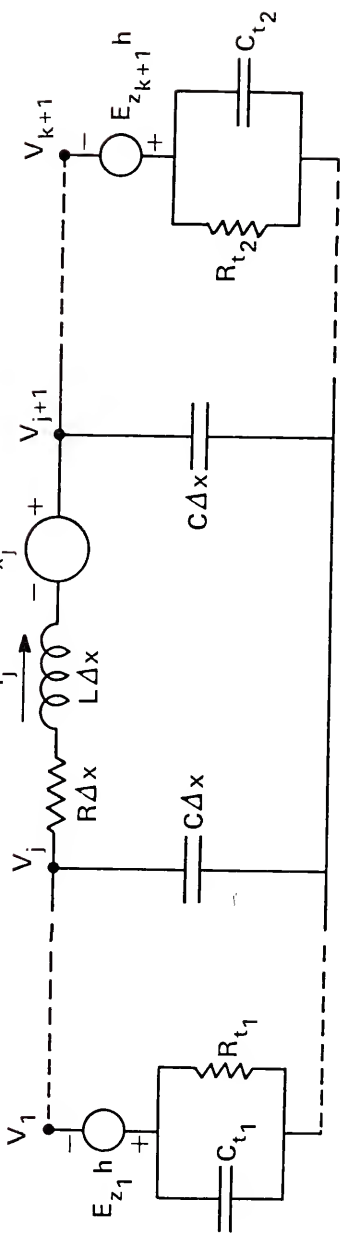
V_1
$E_{z_1}h$
R_{t_1}
C_{t_1}
V_j
$R\Delta x$
I_j
$L\Delta x$
$E_{x_j}\Delta x$
V_{j+1}
$C\Delta x$
$C\Delta x$
V_{k+1}
$E_{z_{k+1}}h$
R_{t_2}
C_{t_2}

CHAPTER IV

RESULTS

4.1 Introduction

In this chapter we present calculations based on the theory presented in Chapter III. First, we derive typical voltages which would be measured on the short test line for various soil conditions, using typical waveforms for the return stroke vertical electric field derived from the model of Lin et al. (1980) and Master et al. (1981). Second, we perform similar calculations for a 5 km long line. Finally, we use some of the data presented in Chapter II on simultaneously measured vertical electric fields and induced voltages on the 460 m test line to make comparisons between the theory and the data on a case-by-case basis.

4.2 Short Line

In this section, we calculate induced voltage waveforms on a short line produced by a typical return stroke at various locations for a range of earth parameters and line terminations. The overhead line is chosen to be a 500 m single-phase 13 kV distribution line, identical in construction to the actual test line described in

Chapter II. The line is assumed to have a North-South orientation. The bottom neutral wire is grounded at the North end in a 20 Ohm resistance, and at the South end in a 60 Ohm resistance. The voltage is calculated at the North end of the phase wire. Calculations indicate that the presence of the terminated neutral wire reduces the value of the voltage on the phase wire by about 20%, without making any significant changes in its waveshape. However, when the neutral wire is left open-circuited, there is no reduction in the voltage on the phase wire. To illustrate the range of possible voltage waveforms and their sensitivity to stroke location, earth parameters, and line terminations, calculations will be performed:

(i) for the case where the phase wire is open-circuited (10^6 Ohms) at both ends and for the case where both ends of the phase wire are terminated in 500 Ohm resistances;

(ii) for lightning at three distances from the line: 200 m, 1 km, and 5 km. For each of these distances, we choose five locations for the ground strike point at various bearings from the line; and,

(iii) for four soil conditions: $\sigma = 10^{-2}$ mhos/m with $\varepsilon_r = 15$; $\sigma = 10^{-3}$ mhos/m with $\varepsilon_r = 8$; $\sigma = 10^{-4}$ mhos/m with $\varepsilon_r = 3$; and, $\sigma = 10^{-5}$ mhos/m with $\varepsilon_r = 3$.

It was shown in Chapter III that the induced voltage at either end of the line may be determined from a knowledge of the incident vertical electric field at the ends and the incident horizontal electric field along the line. The first step, therefore, is to determine the vertical electric fields at the ends of the line. In this study, we shall use the typical subsequent return stroke, with a 18 kA peak current, modeled by Lin et al. (1980) and Master et al.

(1981). Since the waveform of the vertical electric field measured at two close distances, typically under 3 km, varies considerably, the vertical electric fields to be used at the two ends of the line have been computed directly from the model. For each of these two vertical electric fields, a horizontal electric field component is calculated using the wavetilt formulation described in Chapter III. An average horizontal field waveshape is then computed. The component of this average horizontal field along the line is used with a 1/D extrapolation as the source function along the line, the calculated vertical electric fields being used as the source functions at the two ends. This procedure will be adopted for studies with lightning at 200 m and at 1 km from the line. For lightning at 5 km, the source functions will be determined by using a 1/D extrapolation for the calculated vertical and horizontal electric fields at 5 km. As discussed in Chapter III, it will be assumed here that the horizontal electric field produced by the wavetilt is the only horizontal source driving the line.

For a conductivity of 10^{-2} mhos/m, the ground is a reasonably good conductor, with a skin depth at 1 MHz equal to 5 m. Hence, the resistance per unit length introduced into the transmission line formulation, as discussed in Chapter III, will be calculated from Equation (3.42) and is about 0.2 Ohms/m at 1 MHz. For conductivities lower than 10^{-3} mhos/m, Equation (3.43) is used, giving a resistance per unit length of about 1 Ohm/m at 1 MHz. From Equations (3.42) and (3.43) it is clear that the resistance per unit length is frequency dependent. However, we shall use fixed values, determined at 1 MHz, in the time-domain calculations.

The calculations of the induced voltage waveforms for various conditions are shown in Figures 4.1 through 4.12. In each figure the soil parameters σ and ε_r are indicated and so is the distance of the lightning from the line. In all cases, voltages are calculated at the North end of the line shown by a 'V' and the ground strike point is indicated by an asterisk (*). The waveforms drawn with a solid line are for the case in which the line is open-circuited at both ends; the waveforms drawn with dashed lines are obtained when the line is terminated in 500 Ohms at both ends. The factor 'x a' used on some of the waveforms indicates that the waveform shown is 'a' times the actual waveform; that is, the actual waveform is 'a' times smaller than that shown on the figure. The distance in km and the bearing of the ground strike points from the North end of the line are as follows:

(i) 0.2 km A: 0.20|0° ; B: 0.20|90° ; C: 0.32|143°
D: 0.54|158° ; E: 0.70|180°

(ii) 1 km A: 1.00|0° ; B: 1.00|90° ; C: 1.03|104°
D: 1.12|117° ; E: 1.50|180°

(iii) 5 km A: 5.00|0° ; B: 5.00|45° ; C: 5.01|93°
D: 5.11|136° ; E: 5.50|180°

Several features of the waveforms shown in Figures 4.1 through 4.12 are discussed below.

(a) In Figures 4.1 through 4.12 time t = 0 corresponds to the time at which the propagating lightning fields illuminate the first section of the line. Thus some of the waveforms exhibit a time delay. For example, in Figure 4.1, the voltages for lightning at

Figure 4.1. Calculated voltage waveforms at the North end of the 500 m overhead line for lightning 200 m from the line for $\sigma = 10^{-2}$ mhos/m and $\epsilon_r = 15$. The solid lines represent the calculated waveforms when the line is open-circuited at both ends. The dotted lines represent the calculated waveforms for the line terminated in 500 Ω at each end. The factor 'x a' on any waveform indicates that the waveform shown is 'a' times the actual waveform. The ground strike points are indicated by asterisks (*).

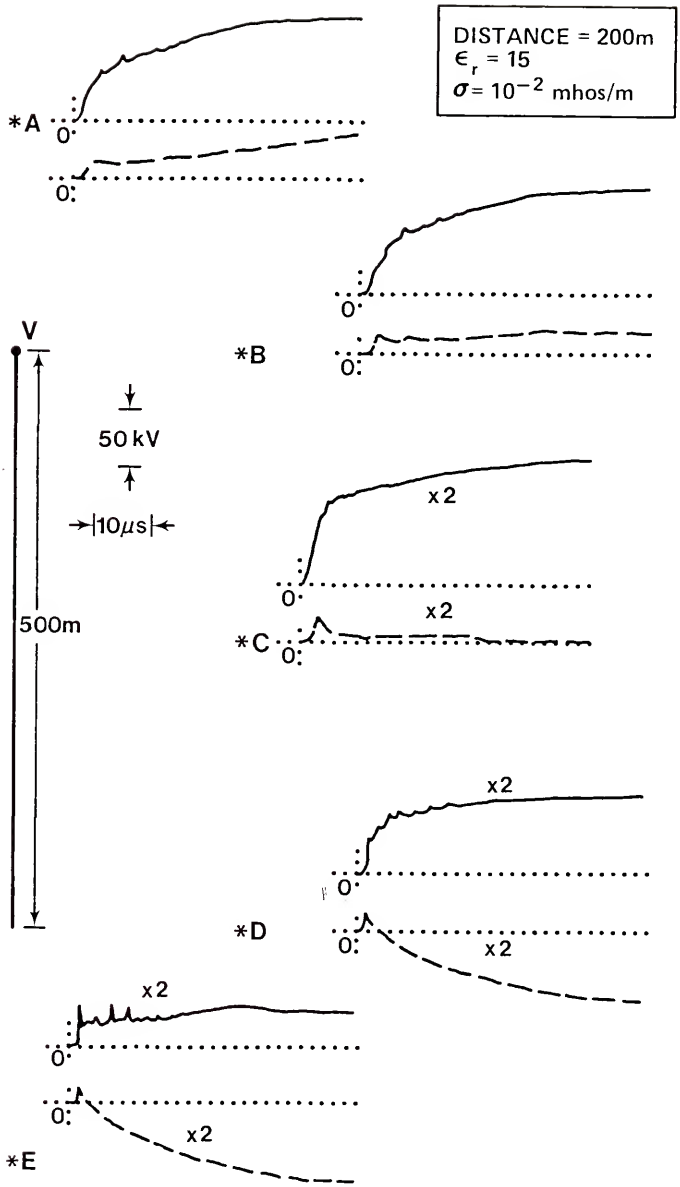
DISTANCE = 200m
ϵ_r = 15
σ = 10^{-2} mhos/m
*A
0
0
V
50 kV
10μs
500m
*B
0
0
x2
*C
0
x2
0
x2
*D
0
x2
x2
0
0
x2
*E

Figure 4.2. Calculated voltage waveforms at the North end of the 500 m overhead line for lightning 200 m from the line for $\sigma = 10^{-3}$ mhos/m and $\varepsilon_r = 8$. The solid lines represent the calculated waveforms when the line is open-circuited at both ends. The dotted lines represent the calculated waveforms for the line terminated in 500 Ω at each end. The factor 'x a' on any waveform indicates that the waveform shown is 'a' times the actual waveform. The ground strike points are indicated by asterisks (*).

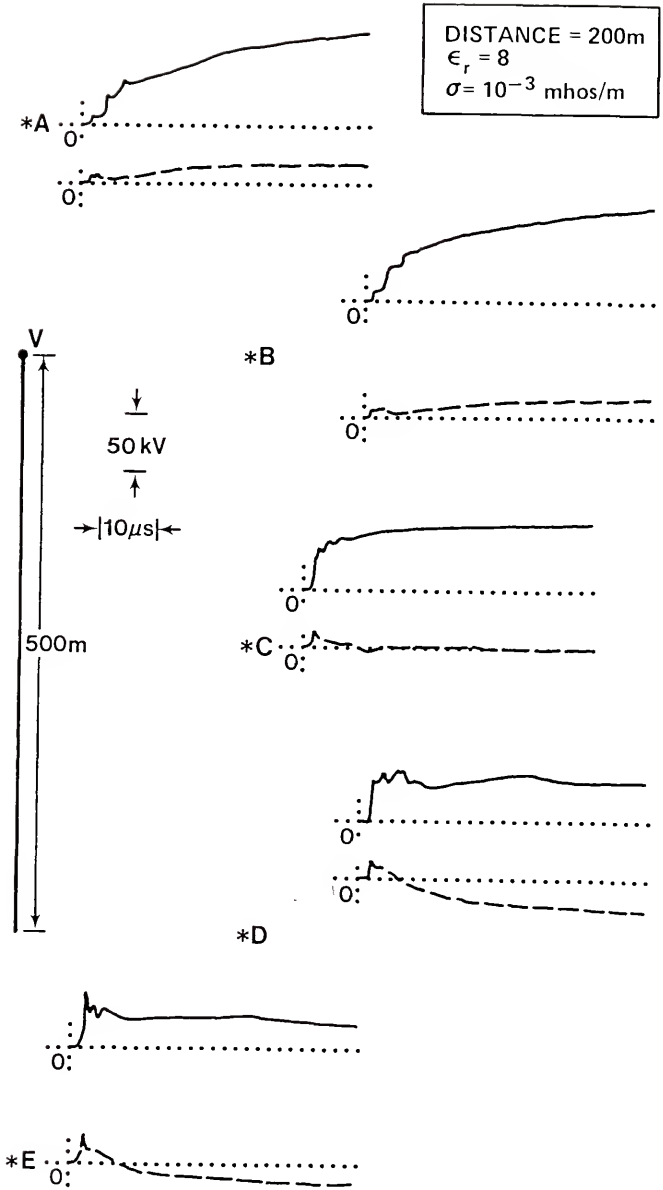
DISTANCE = 200m
$\epsilon_r = 8$
$\sigma = 10^{-3}$ mhos/m
*A
0
0
*B
0
0
V
50 kV
10μs
500m
*C
0
0
0
0
*D
0
*E
0

Figure 4.3. Calculated voltage waveforms at the North end of the 500 m overhead line for lightning 200 m from the line for $\sigma = 10^{-4}$ mhos/m and $\varepsilon_r = 3$. The solid lines represent the calculated waveforms when the line is open-circuited at both ends. The dotted lines represent the calculated waveforms for the line terminated in 500 Ω at each end. The factor 'x a' on any waveform indicates that the waveform shown is 'a' times the actual waveform. The ground strike points are indicated by asterisks (*).

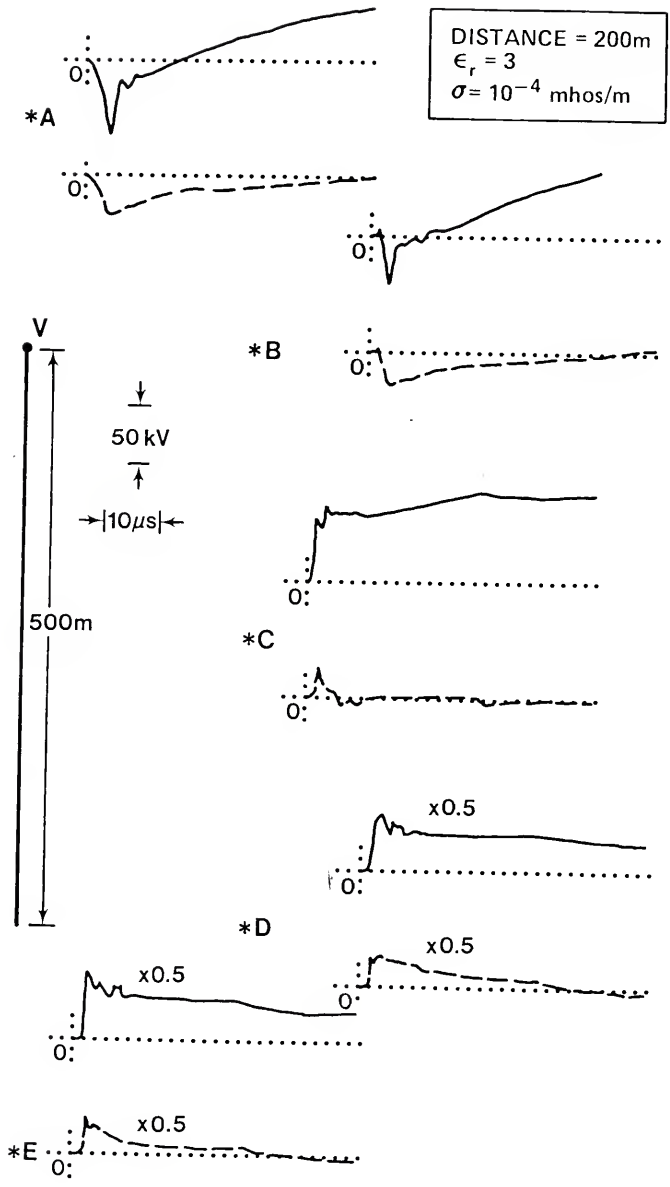
DISTANCE = 200m
$\epsilon_r = 3$
$\sigma = 10^{-4}$ mhos/m
*A
0
0
0
V
*B
50 kV
10μs
500m
0
*C
0
x0.5
0
*D
x0.5
x0.5
0
0
*E
x0.5
0

Figure 4.4. Calculated voltage waveforms at the North end of the 500 m overhead line for lightning 200 m from the line for $\sigma = 10^{-5}$ mhos/m and $\varepsilon_r = 3$. The solid lines represent the calculated waveforms when the line is open-circuited at both ends. The dotted lines represent the calculated waveforms for the line terminated in 500 Ω at each end. The factor 'x a' on any waveform indicates that the waveform shown is 'a' times the actual waveform. The ground strike points are indicated by asterisks (*).

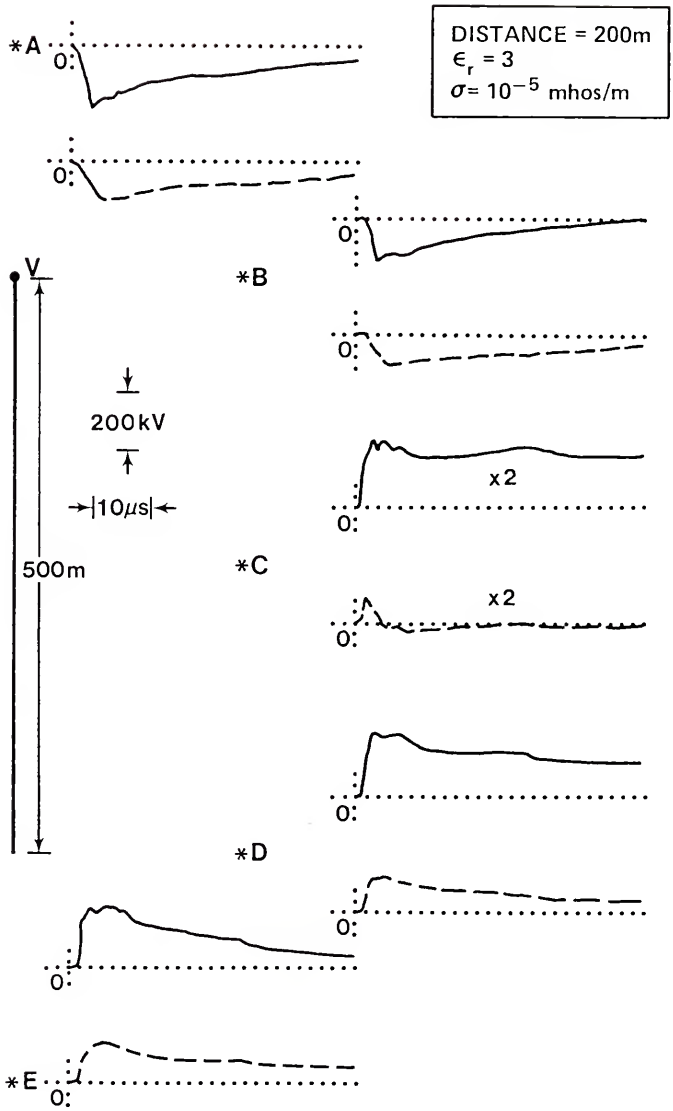
DISTANCE = 200m
ϵ_r = 3
σ= 10^{-5} mhos/m
*A
0
*B
V
200kV
10μs
500m
x2
*C
x2
*D
*E

Figure 4.5. Calculated voltage waveforms at the North end of the 500 m overhead line for lightning 1 km the line for $\sigma = 10^{-2}$ mhos/m and $\varepsilon_r = 15$. The solid lines represent the calculated waveforms when the line is open-circuited at both ends. The dotted lines represent the calculated waveforms for the line terminated in 500 Ω at each end. The factor 'x a' on any waveform indicates that the waveform shown is 'a' times the actual waveform. The ground strike points are indicated by asterisks (*).

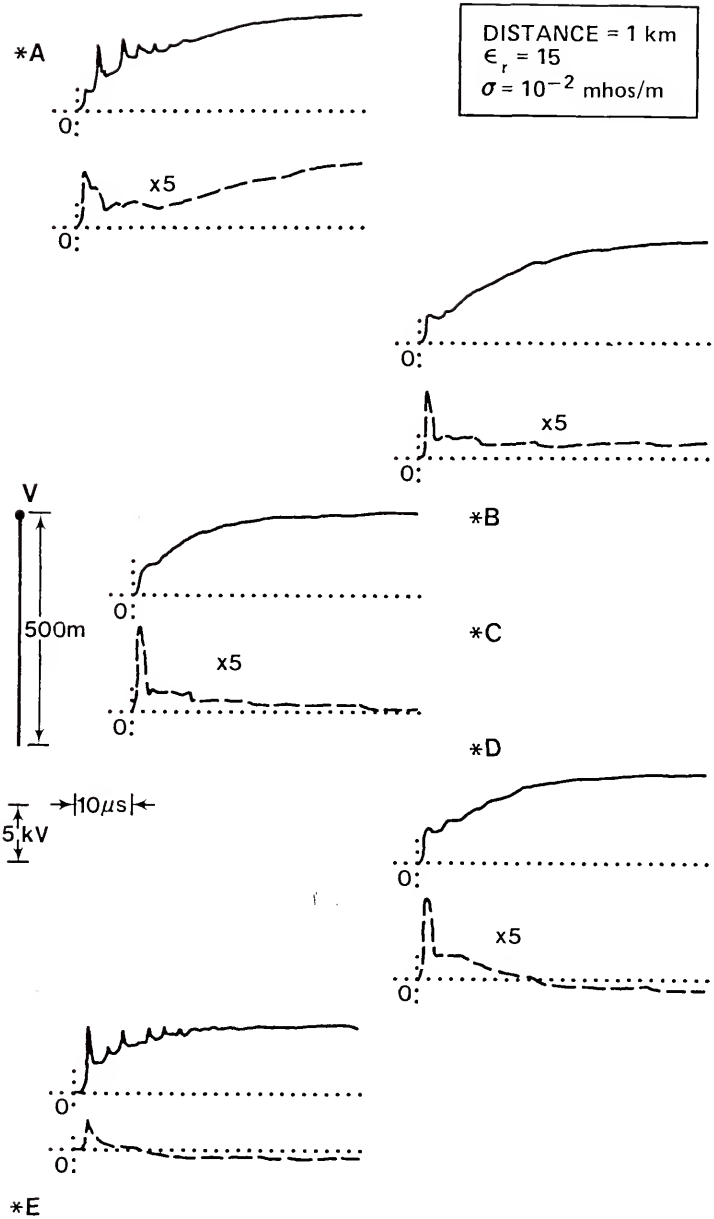
DISTANCE = 1 km
ϵ_r = 15
$\sigma = 10^{-2}$ mhos/m
*A
0
x5
0
*B
0
x5
0
V
500m
*C
0
x5
0
*D
0
x5
0
10μs
5 kV
0
0
*E

Figure 4.6. Calculated voltage waveforms at the North end of the 500 m overhead line for lightning 1 km from the line for $\sigma = 10^{-3}$ mhos/m and $\varepsilon_r = 8$. The solid lines represent the calculated waveforms when the line is open-circuited at both ends. The dotted lines represent the calculated waveforms for the line terminated in 500 Ω at each end. The factor 'x a' on any waveform indicates that the waveform shown is 'a' times the actual waveform. The ground strike points are indicated by asterisks (*).

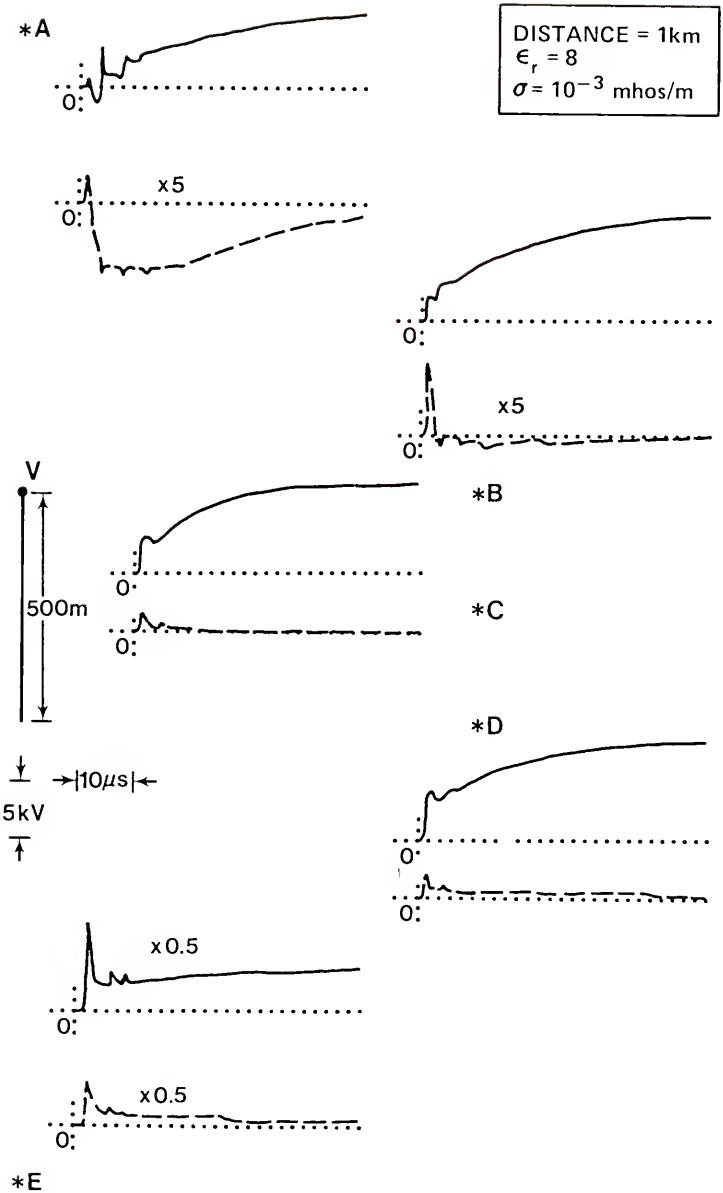
*A
0
DISTANCE = 1km
$\epsilon_r = 8$
$\sigma = 10^{-3}$ mhos/m
x5
0
0
x5
0
V
500m
*B
0
*C
0
*D
0
0
5kV
10μs
x0.5
0
x0.5
0
*E

Figure 4.7. Calculated voltage waveforms at the North end of the 500 m overhead line for lightning 1 km from the line for $\sigma = 10^{-4}$ mhos/m and $\epsilon_r = 3$. The solid lines represent the calculated waveforms when the line is open-circuited at both ends. The dotted lines represent the calculated waveforms for the line terminated in 500 Ω at each end. The factor 'x a' on any waveform indicates that the waveform shown is 'a' times the actual waveform. The ground strike points are indicated by asterisks (*).

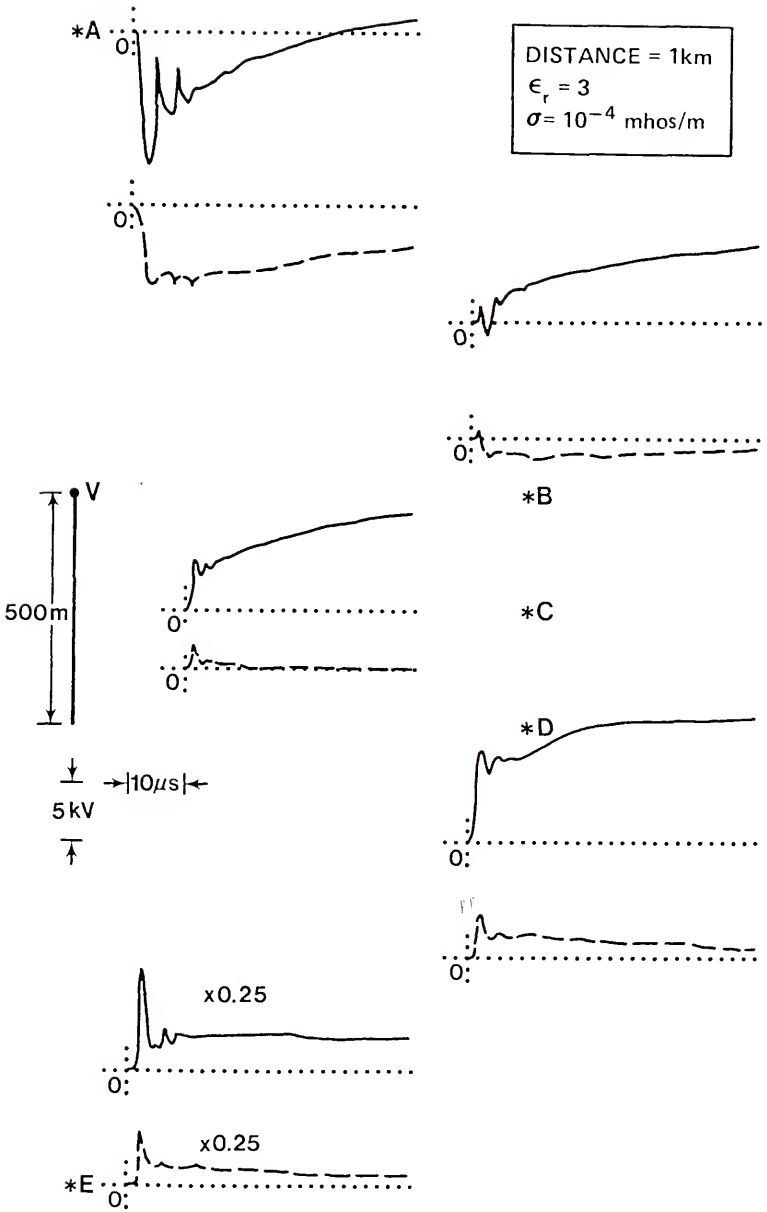
*A
0
DISTANCE = 1km
ϵ_r = 3
σ= 10^{-4} mhos/m
0
0
*B
V
500m
0
*C
0
*D
5kV
10μs
0
0
x0.25
0
x0.25
*E
0

Figure 4.8. Calculated voltage waveforms at the North end of the 500 m overhead line for lightning 1 km from the line for $\sigma = 10^{-5}$ mhos/m and $\varepsilon_r = 3$. The solid lines represent the calculated waveforms when the line is open-circuited at both ends. The dotted lines represent the calculated waveforms for the line terminated in 500 Ω at each end. The factor 'x a' on any waveform indicates that the waveform shown is 'a' times the actual waveform. The ground strike points are indicated by asterisks (*).

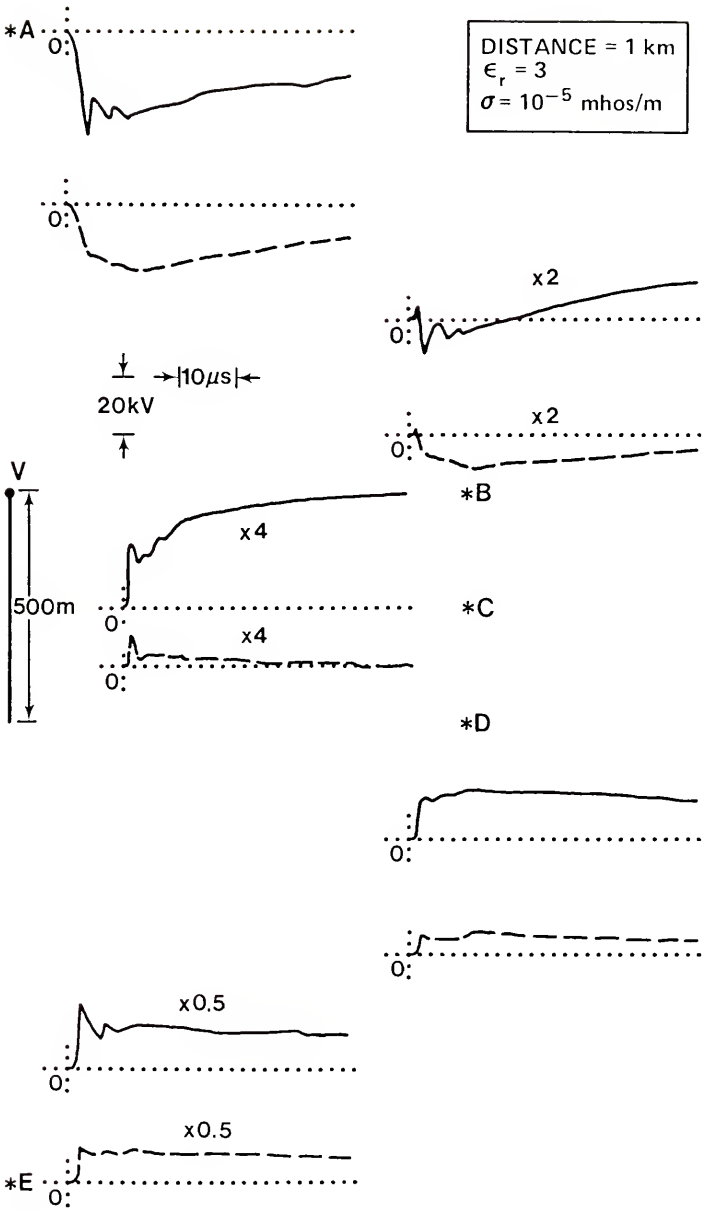
DISTANCE = 1 km
$\epsilon_r = 3$
$\sigma = 10^{-5}$ mhos/m
*A
0
x2
20kV
10μs
V
500m
x4
*B
*C
*D
x0.5
*E

Figure 4.9. Calculated voltage waveforms at the North end of the 500 m overhead line for lightning 5 km from the line for $\sigma = 10^{-2}$ mhos/m and $\varepsilon_r = 15$. The solid lines represent the calculated waveforms when the line is open-circuited at both ends. The dotted lines represent the calculated waveforms for the line terminated in 500 Ω at each end. The factor 'x a' on any waveform indicates that the waveform shown is 'a' times the actual waveform. The ground strike points are indicated by asterisks (*).

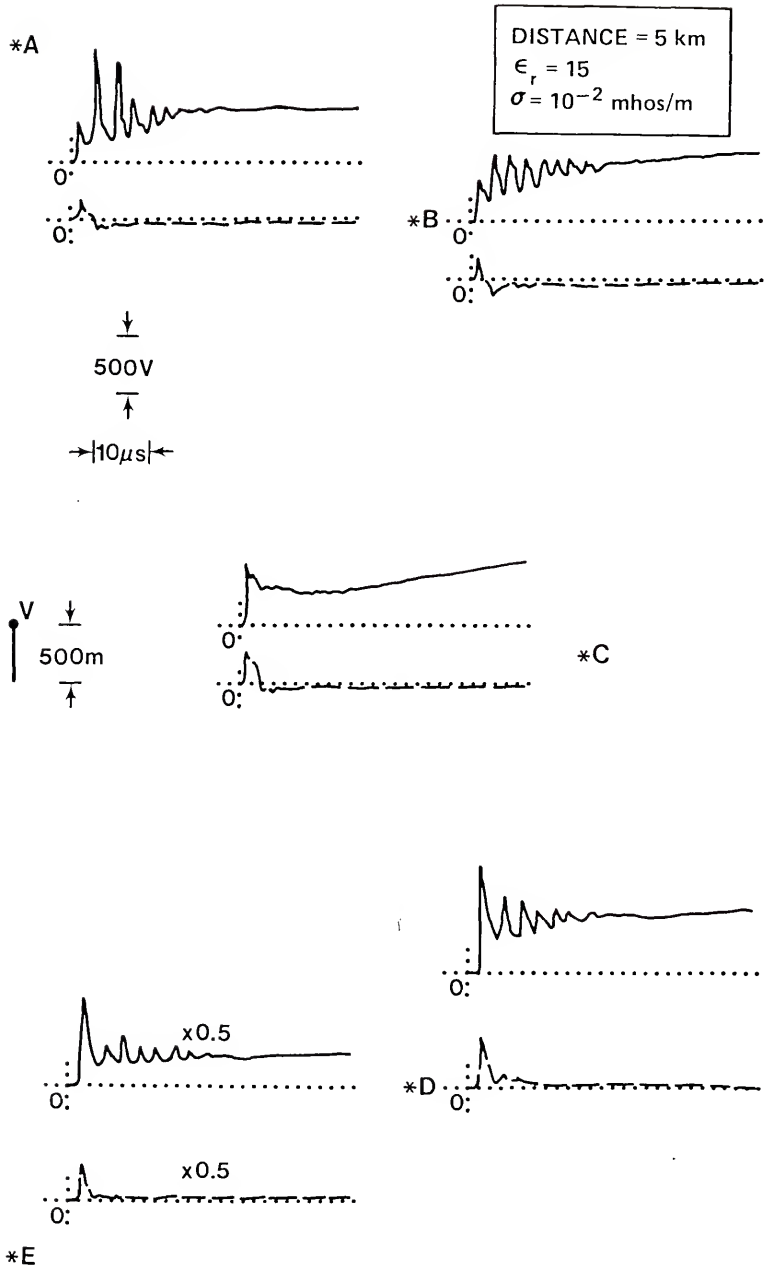
*A
DISTANCE = 5 km
ϵ_r = 15
σ = 10^{-2} mhos/m
0
0
*B
0
0
500V
10μs
V
500m
0
0
*C
0
*D
0
x0.5
0
x0.5
0
*E

Figure 4.10. Calculated voltage waveforms at the North end of the 500 m overhead line for lightning 5 km from the line for $\sigma = 10^{-3}$ mhos/m and $\epsilon_r = 8$. The solid lines represent the calculated waveforms when the line is open-circuited at both ends. The dotted lines represent the calculated waveforms for the line terminated in 500 Ω at each end. The factor 'x a' on any waveform indicates that the waveform shown is 'a' times the actual waveform. The ground strike points are indicated by asterisks (*).

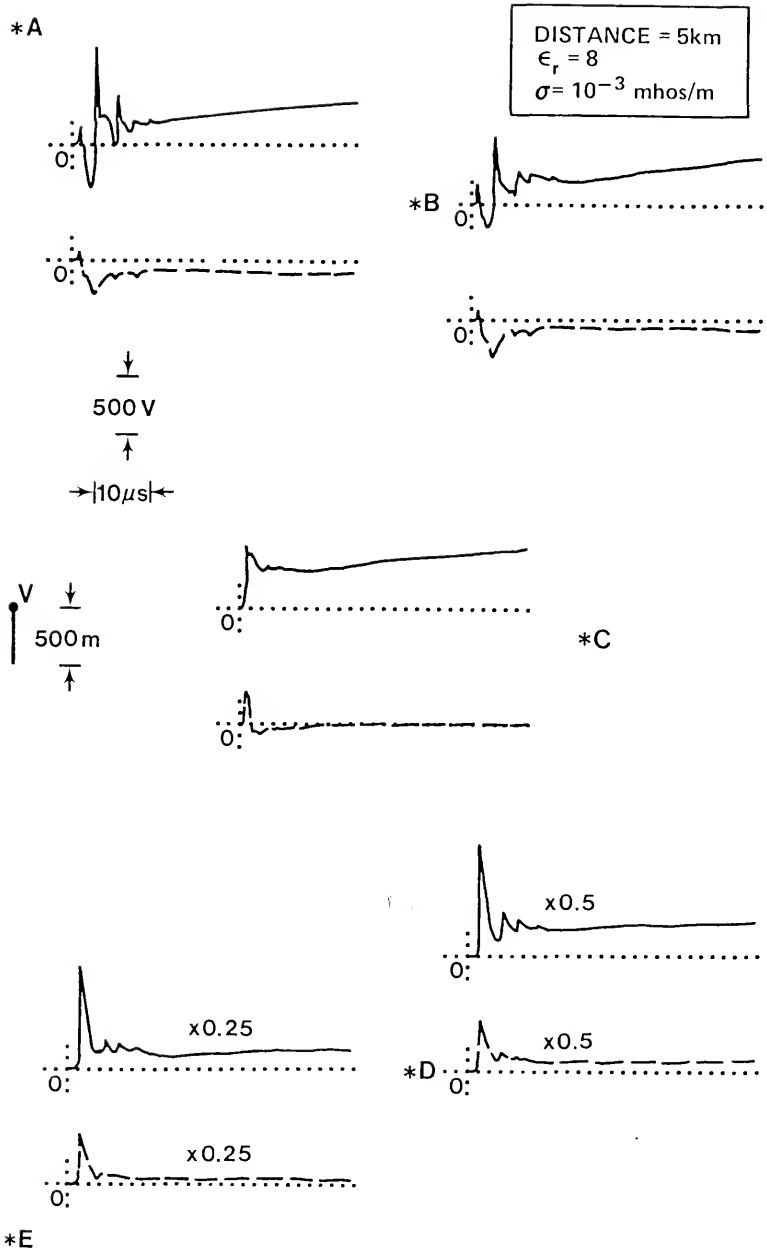
*A
DISTANCE = 5km
$\epsilon_r = 8$
$\sigma = 10^{-3}$ mhos/m
0
*B
500 V
10 μs
V
500 m
*C
x0.5
x0.25
*D
*E

Figure 4.11. Calculated voltage waveforms at the North end of the 500 m overhead line for lightning 5 km from the line for $\sigma = 10^{-4}$ mhos/m and $\varepsilon_r = 3$. The solid lines represent the calculated waveforms when the line is open-circuited at both ends. The dotted lines represent the calculated waveforms for the line terminated in 500 Ω at each end. The factor 'x a' on any waveform indicates that the waveform shown is 'a' times the actual waveform. The ground strike points are indicated by asterisks (*).

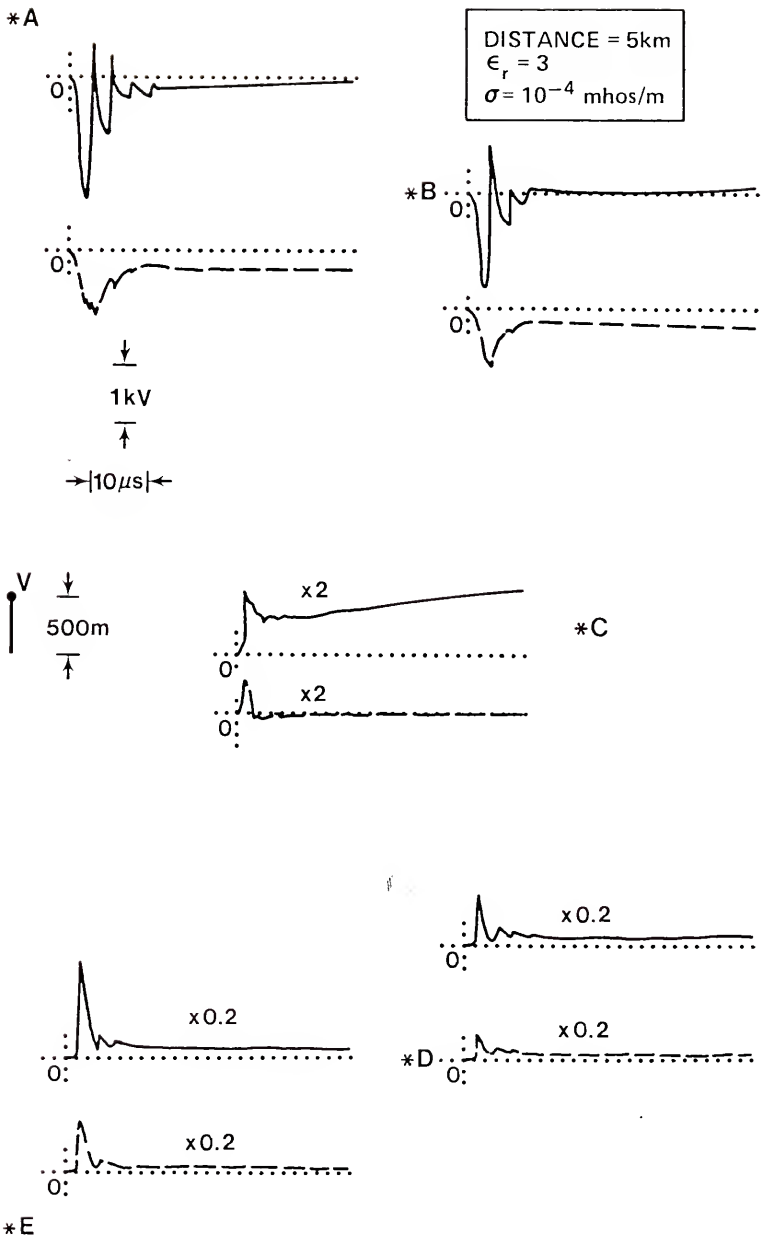
*A
0
0
1kV
10μs
DISTANCE = 5km
$\epsilon_r = 3$
$\sigma = 10^{-4}$ mhos/m
*B
0
0
V
500m
x2
0
x2
0
*C
x0.2
0
x0.2
0
*D
x0.2
0
x0.2
0
*E

Figure 4.12. Calculated voltage waveforms at the North end of the 500 m overhead line for lightning 5 km from the line for $\sigma = 10^{-5}$ mhos/m and $\varepsilon_r = 3$. The solid lines represent the calculated waveforms when the line is open-circuited at both ends. The dotted lines represent the calculated waveforms for the line terminated in 500 Ω at each end. The factor 'x a' on any waveform indicates that the waveform shown is 'a' times the actual waveform. The ground strike points are indicated by asterisks (*).

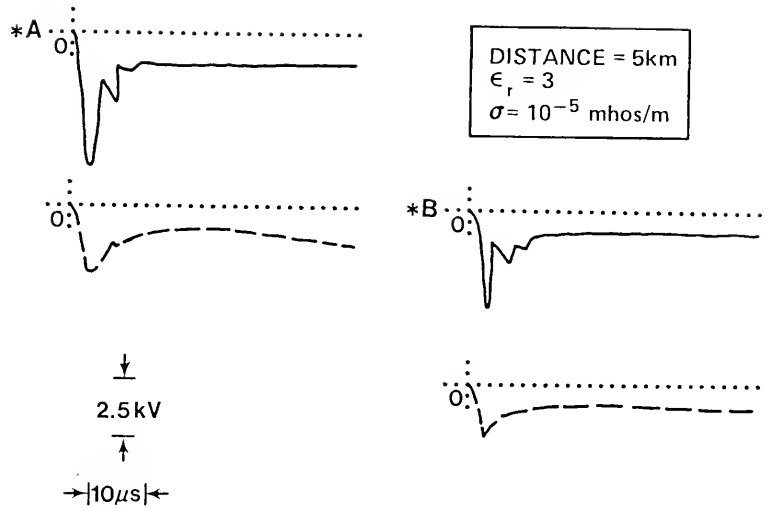
*A
0
0
DISTANCE = 5km
$\epsilon_r = 3$
$\sigma = 10^{-5}$ mhos/m
*B
0
0
2.5kV
10μs

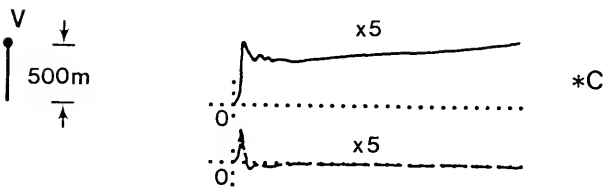
V
500m
x5
0
x5
0
*C

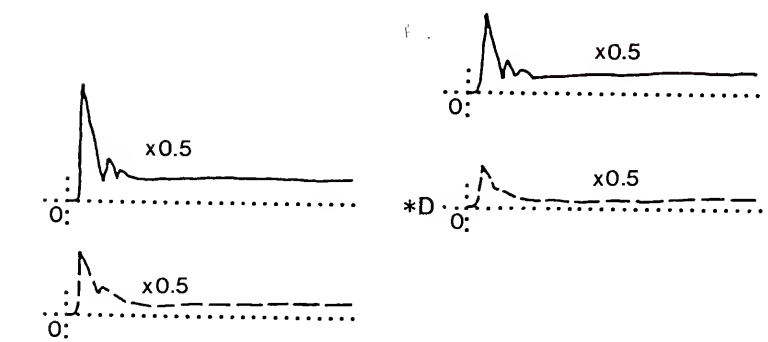
x0.5
0
x0.5
0
x0.5
0
x0.5
0
*D
*E

point A commence at t = 0; for lightning at point E, they commence after a time lag of 1.7 μs which corresponds to the travel time down the line.

(b) When the ground strike point is equidistant from the two ends of the line (i.e., at point C), the voltage waveform calculated for the open-circuited case is similar to the vertical electric field waveform. The waveforms for the terminated case, however, look more like the derivative of the vertical electric field. This behavior is exhibited for all distances and soil conditions, and is due to the fact that for point C, the voltage coupling is essentially due to the vertical electric field, and the line behaves like a classical vertical electric field antenna. However, there is some initial ripple in the open-circuit waveforms due to propagation and reflections along the finite line length. The ripple is stronger for lower conductivities, indicating that it is due to the horizontal electric field coupling.

(c) When the ground conductivity is high ($\sigma = 10^{-2}$ mhos/m), the voltage waveforms for the open-circuited case are similar for all ground strike points and look like the vertical electric field. However, the initial portion of the waveforms due to lightning at points A and E (i.e. parallel to the line) show significant oscillations due to the reflections produced by the coupling of the horizontal electric field. The oscillations appear to be very small at 200 m range because they are imbedded within the large electrostatic component of the vertical electric field. At 1 km and 5 km range, when the electrostatic field is weaker, these oscillations become more apparent.

(d) When soil conductivity is reduced to from 10^{-2} mhos/m to 10^{-3} mhos/m, the horizontal field coupling becomes comparable to the vertical field coupling and the voltage waveforms for the open-circuit case for lightning at point A become bipolar. As the conductivity is reduced further, to $\sigma = 10^{-4}$ mhos/m and $\sigma = 10^{-5}$ mhos/m, the horizontal field coupling becomes dominant and the voltage waveforms exhibit negative polarity for lightning at points A or B and positive polarity for lightning at points D or E. For lightning at point C, the induced voltage waveforms were discussed in (a).

(e) We note that in general the induced voltage on the line is a function of the vertical electric field coupling and the horizontal electric field coupling. The vertical electric field coupling tends to produce a voltage of positive polarity irrespective of the ground strike point, in conformity with the concept of a positive induced classical surge. However, the voltage produced by the horizontal electric field coupling is of negative polarity when the ground strike point is located such that the incident lightning electromagnetic field is propagating along the line and away from the calculation point (e.g., points A or B). For ground strike points located such that the incident lightning electromagnetic field is propagating along the line and toward the point at which the calculation is done, the horizontal electric field coupling produces a positive surge (e.g., points D or E). In addition to the location of the ground strike point, the horizontal coupling is determined by the soil parameters, the coupling being stronger for soils with lower conductivity. Thus, it can be seen that a negative induced surge may

be produced at one end of the line for soils for which the horizontal coupling is the dominant voltage producing mechanism.

(f) The magnitude of the peak induced voltage is also a function of the soil parameters, the peak amplitude being larger for poorer soils. For example, at a distance of 1 km and the ground strike point as E, the peak induced voltage for the open-circuit case is about 5 kV for $\sigma = 10^{-2}$ mhos/m and about 45 kV for $\sigma = 10^{-5}$ mhos/m. For the ground strike point at A the peak voltage is about 5 kV for $\sigma = 10^{-2}$ mhos/m, and about 40 kV at $\sigma = 10^{-5}$ mhos/m, in addition to reversing its polarity. This indicates that in areas where the soil has a low conductivity, the induced line voltages would be larger in peak amplitude. This is of special significance to the power industry because under poor soil conditions grounds on arrestors and transformers often have relatively high grounding resistances. Higher equipment failure has often been attributed to these higher grounding resistances. However, calculations presented here indicate that poor soil conductivities also lead to higher induced voltage amplitudes via horizontal field coupling, so that both effects may be responsible for arrestor and transformer failures.

Making comparisons between the calculations presented in this section, as shown in Figures 4.1 through 4.12, and the data on positive and negative induced voltages, as presented in Figure 2.25 of Chapter II, we conclude that the effective soil conductivity under which the data were recorded is in the range 10^{-4} to 10^{-5} mhos/m. If the soil conductivity were high ($\sigma \sim 10^{-2}$ mhos/m) the angular variation in the voltage polarity illustrated in Figures 2.26 and 2.7 would not have been observed on our 460 m test line.

4.3 Long Line

In this section, we present calculations of induced voltage waveforms on a 5 km long overhead line. The vertical electric field illuminating the line is obtained from the return stroke model of Lin et al. (1980) and Master et al. (1981) as discussed in the previous section, and the horizontal electric field is calculated from the wavetilt formulation. The overhead line is a single conductor identical to the short line discussed in the previous section, except for the missing neutral conductor. Again, the line is assumed to have a North-South orientation, with the North end short-circuited (1 Ohm), and the South end open-circuited (10^6 Ohm). Voltage waveforms are calculated at two points along the line: one at a distance of 2.2 km from the short-circuited North end, and the other at the open circuited South end. This seemingly peculiar configuration is chosen because it is representative of the 9.9 km South African test line (Eriksson and Meal, 1980) discussed previously. Calculated waveforms will be shown for two soil conditions: $\sigma = 10^{-2}$ mhos/m with $\varepsilon_r = 15$; and, $\sigma = 10^{-4}$ mhos/m with $\varepsilon_r = 3$. The ground strike point will be assumed to be 200 m or 1 km from the line. Three ground strike points are selected at three different bearings in each instance. The computation strategy is identical to that used for the short line, except for the fact that in this case, we also need the vertical electric field at the calculation point in the middle of the line.

Figures 4.13 through 4.16 show calculated voltage waveforms for various cases. In each figure, the soil parameters σ and ε_r are

Figure 4.13. Calculated voltage waveforms for a 5 km line for lightning 200 m from the line for $\sigma = 10^{-2}$ mhos/m and $\varepsilon_r = 15$. The solid lines represent the voltage waveform calculated for point V_1; the dotted lines represent the voltage waveform calculated for point V_2. Waveforms marked 'x a' indicate that the waveform shown is 'a' times the actual waveform. The location of the ground strike points are indicated by asterisks (*).

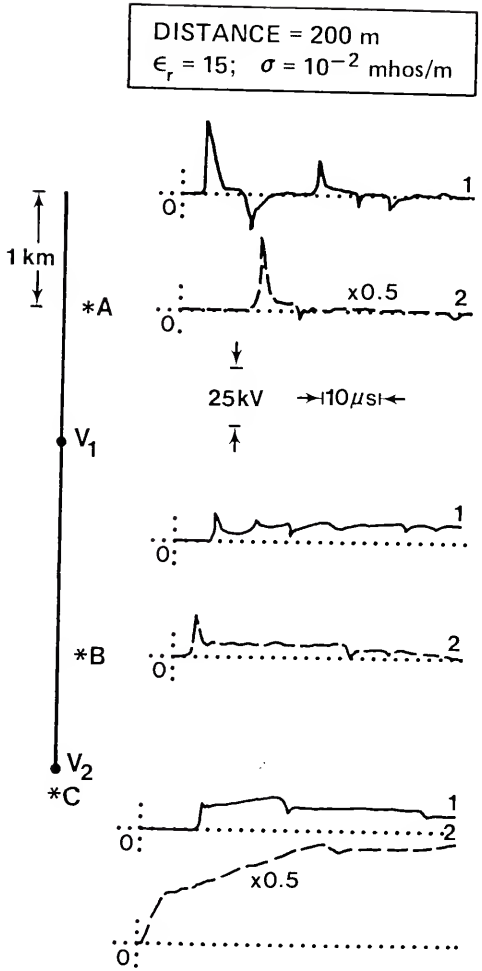
DISTANCE = 200 m
ϵ_r = 15; $\sigma = 10^{-2}$ mhos/m
1 km
*A
x0.5
25kV
10μs
V_1
*B
V_2
*C
0
1
2

Figure 4.14. Calculated voltage waveforms for a 5 km line for lightning 200 m from the line for $\sigma = 10^{-4}$ mhos/m and $\varepsilon_r = 3$. The solid lines represent the voltage waveform calculated for point V_1; the dotted lines represent the voltage waveform calculated for point V_2. Waveforms marked 'x a' indicate that the waveform shown is 'a' times the actual waveform. The location of the ground strike points are indicated by asterisks (*).

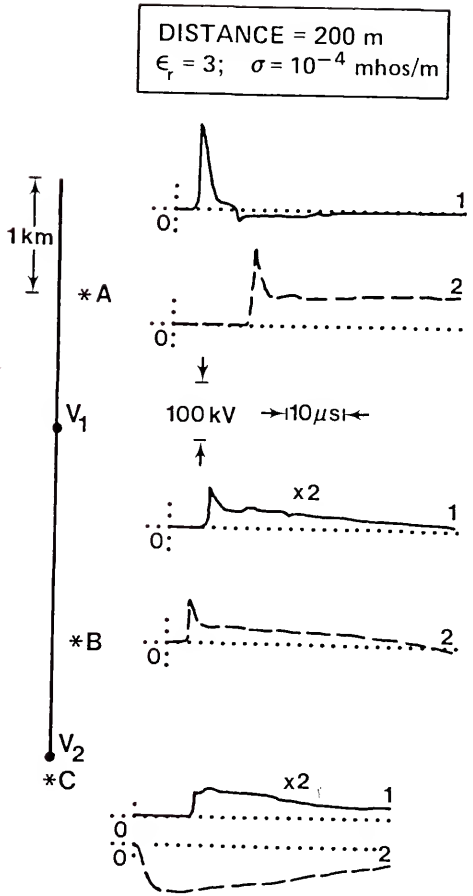
DISTANCE = 200 m
ϵ_r = 3; $\sigma = 10^{-4}$ mhos/m
1 km
*A
V_1
100 kV
10 μs
x2
*B
V_2
*C
0
1
2

Figure 4.15. Calculated voltage waveforms for a 5 km line for lightning 1 km from the line for $\sigma = 10^{-2}$ mhos/m and $\varepsilon_r = 15$. The solid lines represent the voltage waveform calculated for point V_1; the dotted lines represent the voltage waveform calculated for point V_2. Waveforms marked 'x a' indicate that the waveform shown is 'a' times the actual waveform. The location of the ground strike points are indicated by asterisks (*).

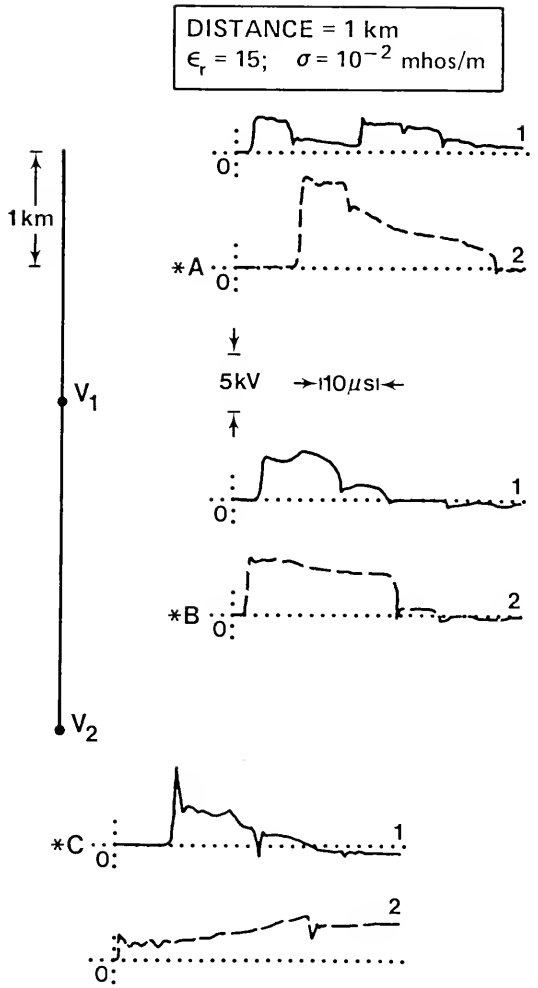
DISTANCE = 1 km
ϵ_r = 15; $\sigma = 10^{-2}$ mhos/m
1km
V_1
V_2
1
0
*A
2
5kV
110μsl
*B
*C

Figure 4.16. Calculated voltage waveforms for a 5 km line for lightning 1 km from the line for $\sigma = 10^{-4}$ mhos/m and $\varepsilon_r = 13$. The solid lines represent the voltage waveform calculated for point V_1; the dotted lines represent the voltage waveform calculated for point V_2. Waveforms marked 'x a' indicate that the waveform shown is 'a' times the actual waveform. The location of the ground strike points are indicated by asterisks (*).

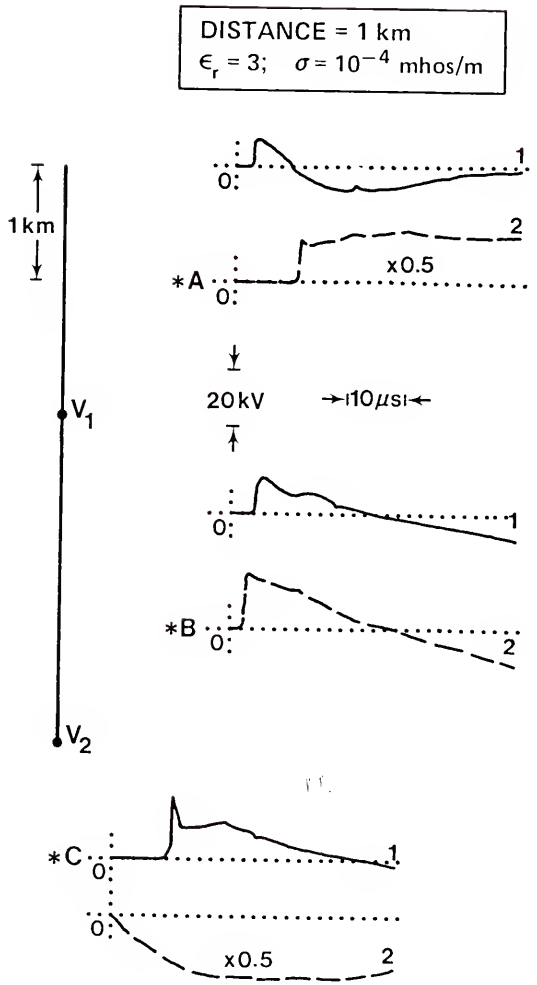
DISTANCE = 1 km
$\epsilon_r = 3$; $\sigma = 10^{-4}$ mhos/m
1km
V_1
V_2
0
1
2
*A
x0.5
20kV
10μs
*B
*C
x0.5

shown, the voltage points are indicated 'V_1' and 'V_2', and the ground strike points are shown by asterisks (*). The waveforms shown with bold lines and labeled '1' represent the induced voltages calculated at point V_1; the waveforms shown with dashed lines and labeled '2' are calculated at point V_2. The factor 'x a' used with some of the waveforms indicates that the waveform shown is 'a' times the actual waveform. The distance in km and the bearing of the ground strike points from the short-circuited North end are:

(i) 0.2 km A: 1.02|168.7° ; B: 4.00|177.1° ; C: 5.2|180°

(ii) 1 km A: 1.41|135° ; B: 4.12|166° ; C: 6.0|180°

We now note some of the interesting features of the voltage waveforms shown in Figures 4.13 through 4.16.

(a) Time t = 0 in Figures 4.13 through 4.16 correspond to the time at which the incident electromagnetic field due to lightning illuminates the closest section of the line. For example, for lightning at point C, there is no time delay associated with the calculation at point V_2. Point V_1 being 2.8 km away corresponds to a time delay of about 9 seconds.

(b) For the good ground ($\sigma = 10^{-2}$ mhos/m, $\varepsilon_r = 15$), the reflections in the voltage waveforms from the short-circuited and open-circuited ends of the line may be readily identified. Recall that a voltage pulse reflected from a short-circuited end reverses polarity, whereas it retains its polarity when reflected from an open-circuited end. For low ground conductivity ($\sigma = 10^{-4}$ mhos/m, $\varepsilon_r = 3$), these reflections are essentially damped out because of the resistance per unit length introduced into the transmission line formulation.

(c) All voltage waveforms calculated at V_1 for different soil conductivities and different ground strike points are of positive polarity. This is because V_1 being in the middle of the line, the lightning electromagnetic field is always travelling along the line towards V_1, as discussed under (d) in the previous section.

(d) For the low conductivity case ($\sigma = 10^{-4}$ mhos/m, $\varepsilon_r = 3$) the calculated voltage at V_2, for lightning at point C, is of negative polarity. This is in keeping with arguments presented in (c) above, and (d) in the previous section.

(e) The peak amplitude of the voltage surges is greater for poor soil conditions, because of the fact that there is more horizontal electric field coupling. The problems associated with this larger induced surge were discussed under (e) in the previous section.

Thirty-two good quality recordings reported by Eriksson et al. (1982) on the South African 9.9 km test line, as discussed previously, give an average induced voltage peak of 45 kV with a standard deviation of 35 kV. The configuration and termination of their line was similar to the 5 km line discussed in this section. Furthermore, the location of the calculation point V_1, with respect to the line length, as shown in Figures 4.13 through 4.16, is also close to the point at which measurements reported by Eriksson et al. (1982) were made. The locations of most of the ground strike points for their reported data (Figure 5 of Eriksson et al., 1982) may be represented by locations A and B in Figures 4.13 through 4.16. Though no direct comparisons can be made between the theory presented here and the South African data due to lack of electric or magnetic field measurements, there appears to be a general agreement between

the calculated peak voltage shown in Figures 4.13 through 4.16 and the data reported by Eriksson et al. (1982) for an effective ground conductivity of the order of 10^{-3} mhos/m. No conductivity measurements have been reported by Eriksson et al. (1982); however a value of 10^{-3} mhos/m is not unreasonable.

Similar calculations were also performed for the 2.1 km French telecommunication line reported by Hamelin et al. (1979) which was terminated in 500 Ohms at each end. Again, we find reasonably good agreement between measured and calculated peak voltages for an effective ground conductivity of the order of 10^{-2} mhos/m, a value which has been used by Djebari et al. (1981) as representative of their "wet ground" conditions.

4.4 Comparison of Measured Voltages with Theory

Pertinent data for simultaneously measured vertical electric field and induced test-line voltages due to nearby lightning are listed in Tables 2.3(a), (b), and (c). In this section, we use some of that data to make direct comparisons between the voltage measurements reported in this thesis and calculated voltage waveforms. We select six return strokes at various distances and angles from the North end of the line where the voltage measurement was made. The simultaneously measured vertical electric field is digitized and the horizontal electric field is determined from the wavetilt formulation. From the discussion in Section 4.1 it is clear that the effective ground conductivity in the vicinity of the test line must have been relatively low. Since no conductivity

measurements were made in the area at the time the data were recorded, we assume soil parameters to be $\sigma = 10^{-5}$ mhos/m and $\varepsilon_r = 3$ for the calculations. Though these values represent an unusually poor soil, the experience of the field engineers and line crews in the Tampa Bay area indicates that ground conditions are poor. The experience of the field crew also indicate vast differences in soil parameters for regions separated by a mere 100 m. During the summer of 1982, three years after the experiment, indirect conductivity measurements were made in the area in which the test-line voltage measurements were made. Measurements of the steady-state resistance to ground of a 1.25 cm diameter vertically driven ground rod were made at 1.5 m depth intervals between 1.5 m and 6.0 m. Using a formula given by Sunde (1968) we translated these ground rod resistance values to equivalent ground conductivities. Measurements indicate that the ground conductivity decreases with depth, the lowest value being about 10^{-3} mhos/m at a depth of about 6 m. This value is in agreement with the average effective conductivity derived from radio frequency propagation of lightning signals over 200 km of Florida soil by Serhan et al. (1980). However, a value between 10^{-4} and 10^{-5} mhos/m has to be used to reproduce the positive and negative polarity measured voltages. Since there are large local variations in the ground conductivity and the effective ground conductivity increases with depth in the area, as discussed above, these low values of conductivity may not be totally unreasonable.

The following strokes have been selected for this study and represent a selection of ground strike points all around the line. The range and bearing of the ground strike point from the North end

of the line, at which the voltage measurement was made, and the stroke identification are given.

(a) Range = 10.7 km; angle = 8°. Stroke #1 for the 170455 UT flash, during run #79199TR31.

(b) Range = 13.6 km; angle = 53°. Stroke #1 for the 171407 UT flash, during run #79199TR31.

(c) Range = 1.2 km; angle = 82°. Stroke #1 of the single stroke flash at 184600 UT, during run #79199TR31.

(d) Range = 5.5 km; angle = 92°. Stroke #2 for the 190004 UT flash, during run #79196TR27.

(e) Range = 5.8 km; angle = 104°. Stroke #1 for the 185842 UT flash, during run #79196TR27.

(f) Range = 10.2 km; angle = 175°. Stroke #2 for the 220319 UT flash, during run #79208TR44.

In Figures 4.17 through 4.22 we present direct comparisons between the data and theory. In each case, the vertical electric field obtained on 40 μs full-scale from the FM channel of the Instrumentation Tape Recorder is digitized. The wavetilt computer program listed in Appendix C is used to determine the horizontal electric field with the soil parameters assumed to be $\sigma = 10^{-5}$ mhos/m and $\varepsilon_r = 3$. These incident fields are then used in the coupling program (also listed in Appendix C) to determine the calculated voltages under various terminal conditions.

In Figures 4.17 through 4.22 we first show a piecewise-linear version of the measured vertical electric field, and the calculated horizontal electric field. The next waveform is that of the simultaneously measured voltage at the North end of the line obtained

Figure 4.17. Comparisons between data and theory for the first stroke in the 170455 UT flash during run #79199TR31 located at a range of 10.7 km and bearing of 8° from the North end of the line at which the voltage is measured. The top two traces are the measured vertical electric field and the calculated horizontal electric field for $\sigma = 10^{-5}$ mhos/m and $\varepsilon_r = 3$. The remaining traces show the measured voltage waveform (V_{meas}) and the calculated voltages when the South end is open-circuited (V_{OC}), short circuited to the 60 Ohm ground rod (V_{SC}), and terminated in 500 Ohms (V_M).

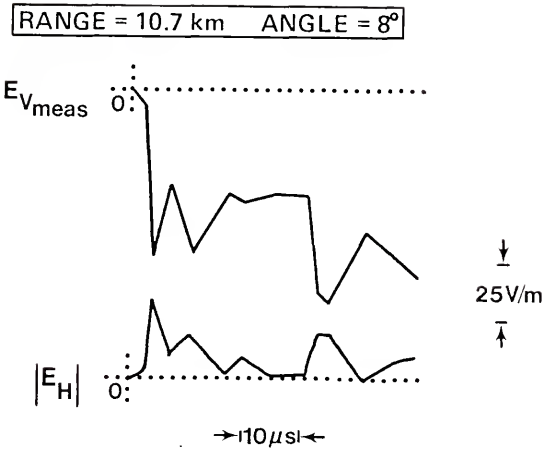
RANGE = 10.7 km ANGLE = 8°
$E_{V_{meas}}$
0
25V/m
$|E_H|$
0
10μs

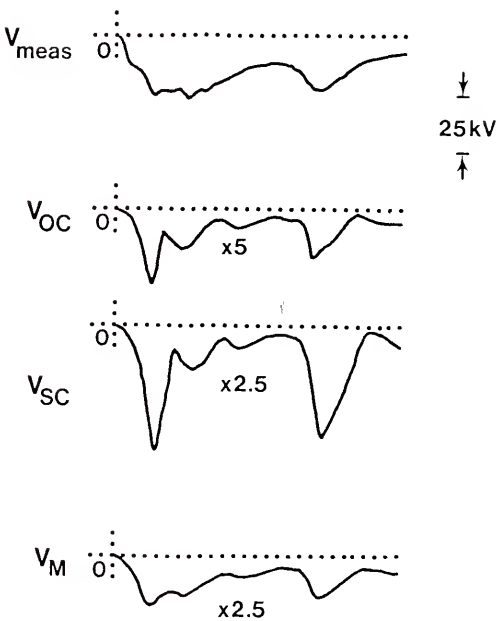
V_{meas}
0
25kV
V_{OC}
0
x5
V_{SC}
0
x2.5
V_M
0
x2.5

Figure 4.18. Comparisons between data and theory for the first stroke in the 171407 UT flash during run #79199TR31 located at a range of 13.6 km and bearing of 53° from the North end of the line at which the voltage is measured. The top two traces are the measured vertical electric field and the calculated horizontal electric field for $\sigma = 10^{-5}$ mhos/m and $\varepsilon_r = 3$. The remaining traces show the measured voltage waveform (V_{meas}) and the calculated voltages when the South end is open-circuited (V_{OC}), short circuited to the 60 Ohm ground rod (V_{SC}), and terminated in 500 Ohms (V_M).

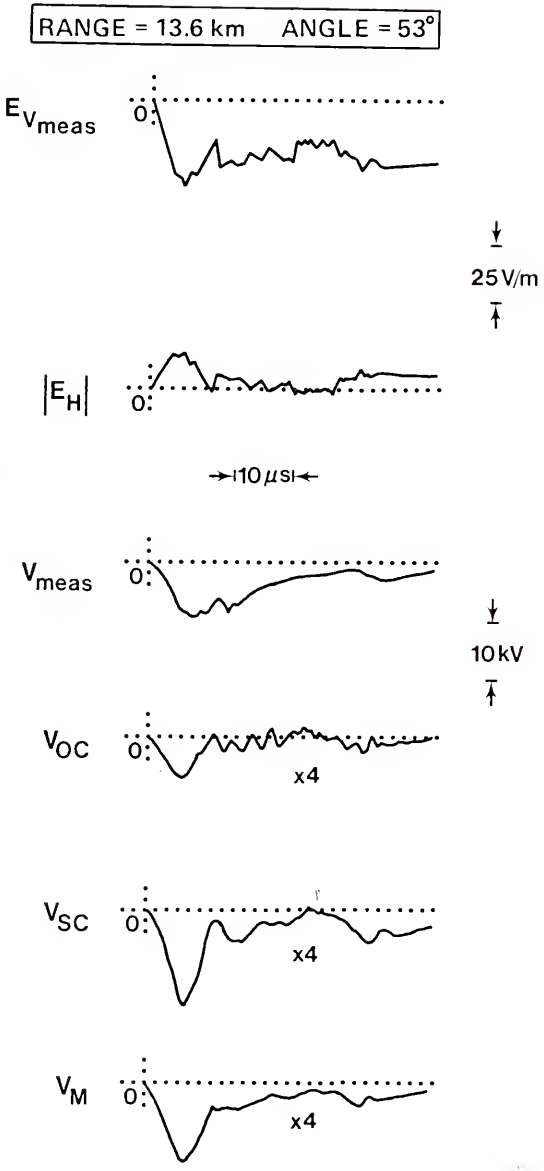
RANGE = 13.6 km ANGLE = 53°
$E_{V_{meas}}$
0
25 V/m
$|E_H|$
0
10 μs
V_{meas}
0
10 kV
V_{OC}
0
x4
V_{SC}
0
x4
V_M
0
x4

Figure 4.19. Comparisons between data and theory for the first stroke in the 184600 UT flash during run #79199TR31 located at a range of 1.2 km and bearing of 82° from the North end of the line at which the voltage is measured. The top two traces are the measured vertical electric field and the calculated horizontal electric field for $\sigma = 10^{-5}$ mhos/m and $\epsilon_r = 3$. The remaining traces show the measured voltage waveform (V_{meas}) and the calculated voltages when the South end is open-circuited (V_{OC}), short circuited to the 60 Ohm ground rod (V_{SC}), and terminated in 500 Ohms (V_M).

RANGE = 1.2 km ANGLE = 82°

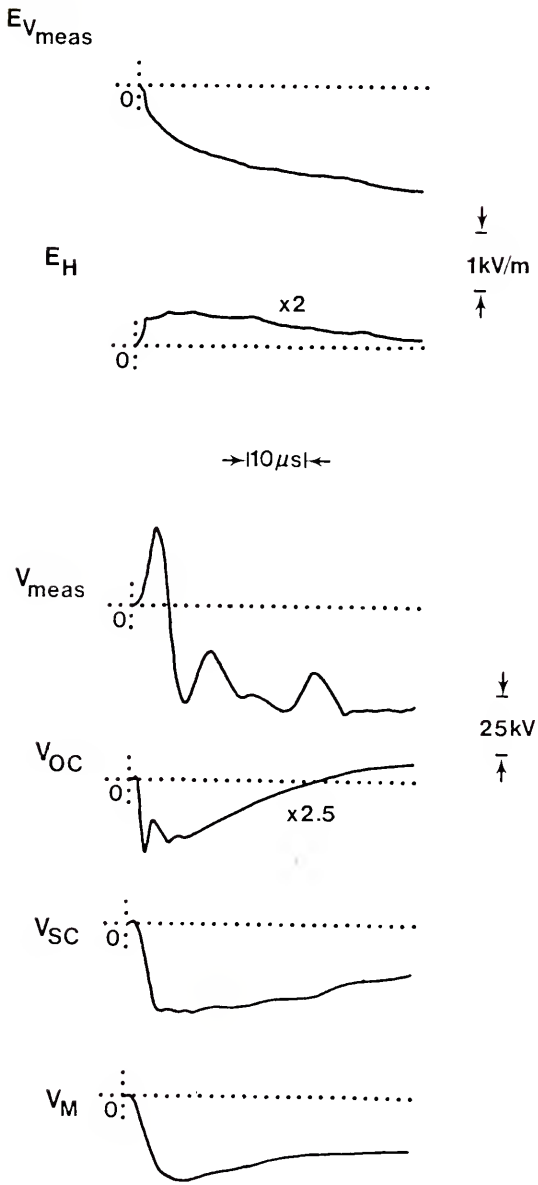

Figure 4.20. Comparisons between data and theory for the second stroke in the 190004 UT flash during run #79196TR27 located at a range of 5.5 km and bearing of 92° from the North end of the line at which the voltage is measured. The top two traces are the measured vertical electric field and the calculated horizontal electric field for $\sigma = 10^{-5}$ mhos/m and $\varepsilon_r = 3$. The remaining traces show the measured voltage waveform (V_{meas}) and the calculated voltages when the South end is open-circuited (V_{OC}), short circuited to the 60 Ohm ground rod (V_{SC}), and terminated in 500 Ohms (V_M).

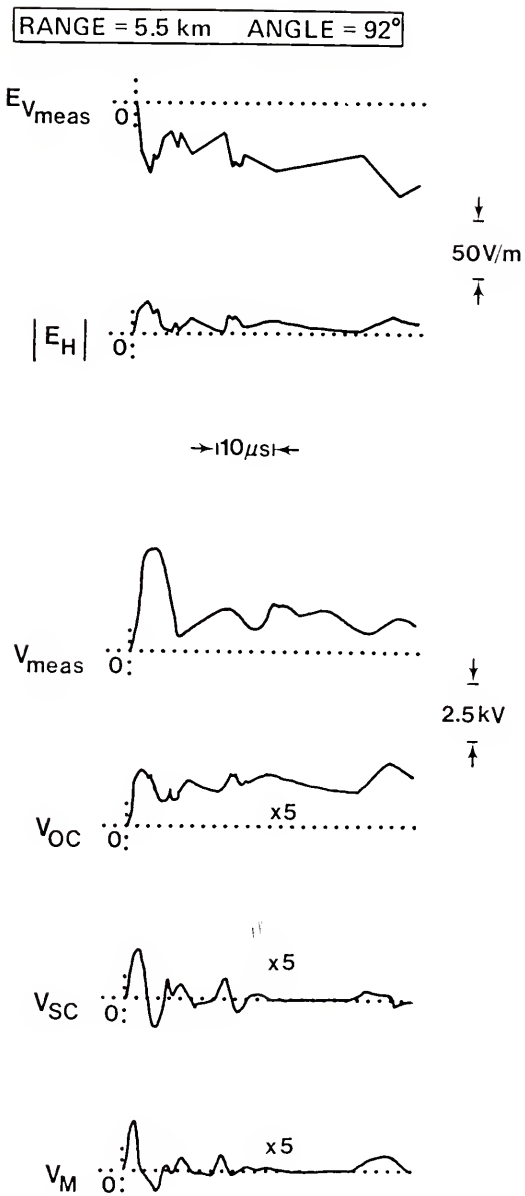
RANGE = 5.5 km ANGLE = 92°
$E_{V_{meas}}$
0
50V/m
$|E_H|$
0
110μs
V_{meas}
0
2.5kV
V_{OC}
0
x5
V_{SC}
0
x5
V_M
0
x5

Figure 4.21. Comparisons between data and theory for the first stroke in the 185842 UT flash during run #79196TR27 located at a range of 5.8 km and bearing of 104° from the North end of the line at which the voltage is measured. The top two traces are the measured vertical electric field and the calculated horizontal electric field for $\sigma = 10^{-5}$ mhos/m and $\varepsilon_r = 3$. The remaining traces show the measured voltage waveform (V_{meas}) and the calculated voltages when the South end is open-circuited (V_{OC}), short circuited to the 60 Ohm ground rod (V_{SC}), and terminated in 500 Ohms (V_M).

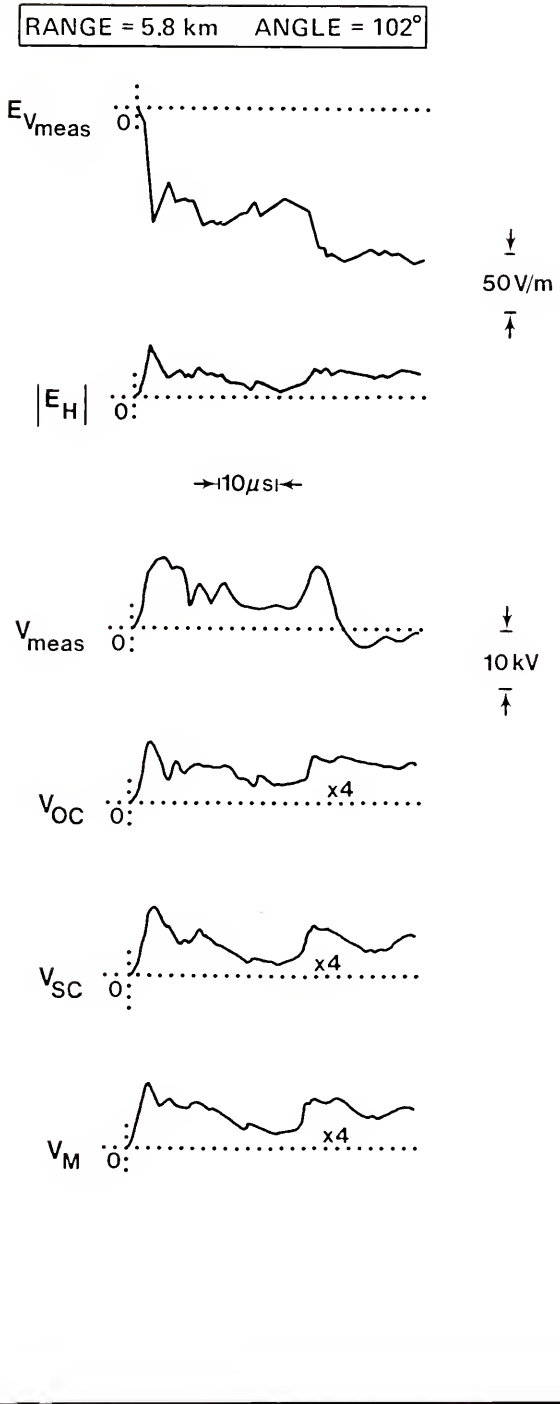
RANGE = 5.8 km ANGLE = 102°
$E_{V_{meas}}$
0
50 V/m
$|E_H|$
0
10 μs
V_{meas}
0
10 kV
V_{OC}
0
x4
V_{SC}
0
x4
V_M
0
x4

Figure 4.22. Comparisons between data and theory for the second stroke in the 220319 UT flash during run #79208TR44 located at a range of 10.2 km and bearing of 175° from the North end of the line at which the voltage is measured. The top two traces are the measured vertical electric field and the calculated horizontal electric field for $\sigma = 10^{-5}$ mhos/m and $\varepsilon_r = 3$. The remaining traces show the measured voltage waveform (V_{meas}) and the calculated voltages when the South end is open-circuited (V_{OC}), short circuited to the 60 Ohm ground rod (V_{SC}), and terminated in 500 Ohms (V_M).

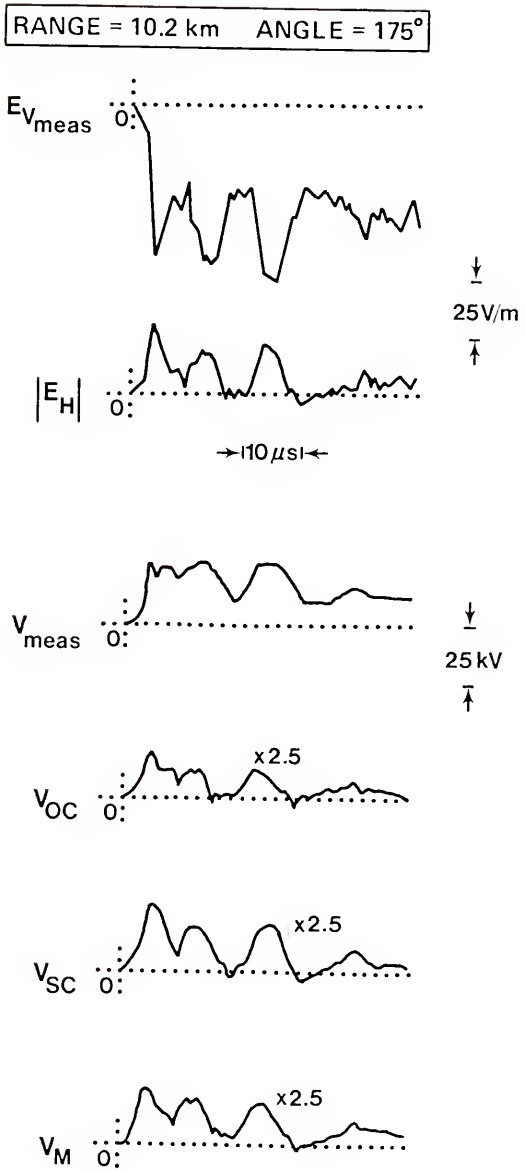
RANGE = 10.2 km ANGLE = 175°
$E_{V_{meas}}$
0
25V/m
$|E_H|$
0
10 μs
V_{meas}
0
25 kV
x2.5
V_{OC}
0
x2.5
V_{SC}
0
x2.5
V_M
0

from the electric field measurement inside the specially designed capacitor. This experimentally obtained waveform is compared with three calculated waveforms. The first calculated waveform labeled V_{OC} is obtained when the South end is left open-circuited (10^6 Ohms). From all available records of the experiment, it appears that this was the condition under which all measurements reported in this thesis were made. Calculated waveforms are also presented for the case in which the South end is clamped to the grounded 60 Ohm downlead (V_{SC}) and for the case when the South end is terminated in a 500 Ohm resistance (V_M).

In Figures 4.17 through 4.22, with the exception of Figure 4.19, the calculated waveform for the open-circuited case looks consistently reasonable compared to the measured waveform. However, there is a consistent discrepancy in peak amplitude: the calculated values are lower than the measured values by about a factor of 4. The waveforms for the matched case (South end terminated in 500 Ohms) also look very similar to the measured waveforms, except for the amplitude of the calculated waveform which is again lower than the measured amplitude by about a factor of 4. The waveforms calculated for the short-circuited case (South end terminated in 60 Ohms) still have features similar to the measured waveforms, however the agreement between theory and data is not as good as that obtained for the open-circuit or matched case, especially in Figures 4.17 and 4.18. In Figure 4.19 the agreement between theory and data is not very good for all three cases of the calculated waveform. The measured waveform is bipolar in nature with an initial positive excursion followed by an approximately equal negative excursion. The

calculated waveforms exhibit a very small positive excursion for the first 2 μs, after which the voltage is essentially negative. The amplitude of the negative peak in the calculated waveform for the open-circuited case is again about 4 times smaller than the negative peak in the data. The differences between the theory and data in this case may be attributed to return stroke channel tilt or tortuosity.

The consistent disagreement in the voltage amplitudes between the measured and calculated waveforms may be due to two principal reasons. It is conceivable that the calibration for the voltage is in error, especially the calibration constant associated with the measuring capacitor. This possibility was raised in Chapter II and in Appendix D. However, after a thorough check of the available records of the calibration, we can find no such error. Another possible source of error could be in the theory. In Chapter III the wavetilt formulation was used to compute the horizontal electric field from the vertical component. The formulation was applied to the complete vertical electric field instead of applying it to only the radiation component of the vertical electric field. This procedure was justified by the fact that essentially the same initial horizontal electric field would be obtained in either case. This, however, leads to the conclusion that the induction and electrostatic components in the vertical electric field do not make significant contributions to the horizontal electric field. It is possible that the induction and electrostatic components in the vertical electric field do give rise to a horizontal component which is determined in a manner different from the wavetilt formulation outlined in Chapter

III. If that were the case, the additional horizontal electric field would produce a greater coupling and hence lead to higher voltage amplitudes.

CHAPTER V

CONCLUSIONS

In this thesis we have presented data on the induced voltages measured on a specially constructed test-line and simultaneously recorded vertical electric fields due to return strokes, correlated with the location of the lightning ground strike point. For the 460 m test-line, the measured voltage waveforms exhibit a wide range of variability, depending on the location of the lightning ground strike point around the line. In particular, we presented data to show that when the ground strike point is along the imaginary line representing an extension of the test-line, the induced voltage is maximum. Furthermore, we indicated that similar lightning return strokes along this imaginary line could produce voltages of either polarity depending on the location of the ground strike point. For lightning along the perpendicular bisector to the line, the induced voltages were found to be relatively small in peak amplitude.

These data appear to be in conflict with most of the previously measured induced overvoltages which are of positive polarity, the so-called "classical induced" surge. Classical theories used to explain the induced surges on power lines couple only the vertical electric field due to lightning and produce only positive surges. It is obvious that the mechanism of induced voltage, at least on our test-line, is different because of the fact that measured induced surges are of either polarity.

We have therefore presented a new theory which can explain both positive and negative surges. Some of the elements of the theory have been developed over the years to determine coupling on wires produced by a nuclear electromagnetic pulse (NEMP) caused by a high-altitude nuclear explosion. However, the theory has never been applied to specifically study lightning induced power-line voltages.

Based on the new theory, we have calculated a wide range of voltage waveforms which would be measured on short and long lines under a broad range of conditions. We noted that as the ground conductivity decreased, the horizontal electric field coupling dominated, giving rise to induced voltages of negative or positive polarity depending on the location of the ground strike point.

Comparisons were made for individual voltage data and theoretically calculated waveforms with reasonable good results. However, we find a discrepancy in peak amplitude between the data and theory which is attributed to errors in measurement and/or flaws in the theory, as discussed below. Some general comparisons are also made between our theory and measurements made on a 9.9 km South African power line (Eriksson et al., 1982) and measurements made on a 2.1 km French telecommunication line (Hamelin et al., 1979). In both cases we find good agreement between theoretically obtained values and the reported data.

Some data on induced voltages produced by nearby stepped leaders together with simultaneous vertical electric field measurement are also presented. It is concluded that voltages induced on our test-line by nearby stepped leaders are about an order of magnitude lower than that induced by the following return stroke.

One of the basic problems underlying the theory presented in this thesis is the fact that even for very low values of ground conductivity, 10^{-5} mhos/m, the magnitude of the horizontal electric field is not large enough to produce the measured peak voltage magnitudes. Conductivities of the order of 10^{-3} to 10^{-4} mhos/m are generally considered the smallest reasonable values and, as noted in Chapter IV, 10^{-3} mhos/m was measured at the test-line three years after the experiment. On the other hand, the average measured peak voltages, 23 kV for first strokes and 11 kV for subsequent strokes, are an order of magnitude larger than those previously reported if we take into account that the average distance of lightning from the 460 m test-line is about 8 km, so there are some doubts about the validity of the voltage calibrations. Additional questions about the voltage measurements are raised in Appendix D.

Another apparent difficulty is associated with the absence of reflections in the experimental data. If the experimental test-line were indeed open-circuited at the south end, why are no reflections observed in the measured waveform? The answer to this question probably lies in the fact that there was sufficient damping of surges along the line such that the reflections were attenuated. We pointed out in Chapter III that the damping resistance is really frequency dependent with larger damping at high frequencies. However, in our time-domain calculations we determined a fixed value for the damping resistance at 10^6 Hz and used it for the complete time-domain return stroke waveform which has its frequency spectrum concentrated between 10^3 and 10^6 Hz. Thus we introduced additional damping at frequencies below 10^6 Hz and adequate damping for frequencies around 10^6 Hz. In

spite of this, calculated waveforms indicate identifiable reflections for normal values of conductivity, e.g., 10^{-3} mhos/m. This is again another fact which points to the validity of the low value of conductivity used in this thesis. As an alternative to the use of attenuation to eliminate reflections, if the south end of the test-line were somehow terminated in about 500 Ohms, the correlation between the measured and calculated waveforms would be good even at 10^{-4} mhos/m, except that the calculated peak amplitudes would be about an order of magnitude lower than those measured.

Obviously, a direct knowledge of the horizontal electric field at the surface of the earth is the missing link in our understanding of the experimental data. Since no horizontal electric fields due to lightning have been measured to date, we have had to resort to using the wavetilt formulation to compute a horizontal electric field from the measured vertical electric field. This theory may exhibit some errors, as discussed in Chapter III.

An experiment should be performed to measure the complete lightning electromagnetic field. The simultaneous measurement of the horizontal electric field, vertical electric field, and the horizontal magnetic field should be used to examine the assumptions made in this thesis and introduce correction terms wherever needed. The experimental set-up should be used to measure the complete lightning field in the presence of different soil conditions. Simultaneous measurement of the voltage on a test-line could also be recorded. Different terminations could be used at different times during a recording season in order to see any differences in the measured voltages. The coupling analysis presented in this thesis

could be directly applied to the test-line using the measured electric fields, thus providing a check of that portion of the theory.

APPENDIX A

ELECTRIC AND MAGNETIC FIELDS PRODUCED BY A VERTICAL DIPOLE ABOVE GROUND

The electric and magnetic fields at any arbitrary point in space due to a small isolated vertical dipole antenna may be derived in the time domain from Maxwell's Equations. For a homogenous, isotropic medium,

$$\bar{\nabla} \times \bar{B} = \mu\bar{J} + \mu\varepsilon \frac{\partial \bar{E}}{\partial t} \tag{A.1}$$

$$\bar{\nabla} \times \bar{E} = - \frac{\partial \bar{B}}{\partial t} \tag{A.2}$$

$$\varepsilon \bar{\nabla} \cdot \bar{E} = \rho \tag{A.3}$$

$$\mu \bar{\nabla} \cdot \bar{H} = 0 \ . \tag{A.4}$$

We will obtain the solution to Maxwell's equation in terms of scalar and vector potentials. Since $\bar{\nabla} \cdot \bar{B} = 0$, we may write

$$\bar{B} = \bar{\nabla} \times \bar{A} \ . \tag{A.5}$$

Substituting Equation (A.5) into Equation (A.2) we obtain,

$$\bar{\nabla} \times (\bar{E} + \frac{\partial \bar{A}}{\partial t}) = 0;$$

which leads to

$$\bar{E} + \frac{\partial \bar{A}}{\partial t} = -\bar{\nabla}\phi$$

$$\text{i.e.} \quad \bar{E} = -\bar{\nabla}\phi - \frac{\partial \bar{A}}{\partial t} \, . \tag{A.6}$$

Note that $\bar{A}$ and ϕ are arbitrary functions at this stage: they are to be determined.

Also, we have (using Equation (A.3)),

$$\bar{\nabla} \cdot (-\bar{\nabla}\phi - \frac{\partial \bar{A}}{\partial t}) = \frac{\rho}{\varepsilon}$$

$$\text{i.e.} \quad \nabla^2 \phi + \frac{\partial}{\partial t} (\bar{\nabla} \cdot \bar{A}) = -\frac{\rho}{\varepsilon} \tag{A.7}$$

From Equations (A.1), (A.5) and (A.6) we may write

$$\bar{\nabla} \times (\bar{\nabla} \times \bar{A}) = \mu \{\bar{J} + \varepsilon \frac{\partial}{\partial t} (-\bar{\nabla}\phi - \frac{\partial \bar{A}}{\partial t})\} \, ,$$

which when simplified gives

$$\bar{\nabla} (\bar{\nabla} \cdot \bar{A}) - \nabla^2 \bar{A} = \mu \bar{J} - \mu\varepsilon \bar{\nabla} \frac{\partial \phi}{\partial t} - \mu\varepsilon \frac{\partial^2 \bar{A}}{\partial t^2} \, . \tag{A.8}$$

We note that Equations (A.5) through (A.8) contain the same information as Equations (A.1) through (A.4). What we have done, in essence, is to transform the variables in the equations. To uniquely define the vector $\bar{A}$ we have to specify its curl and divergence. In Equation (A.5) we specified the curl of $\bar{A}$. We now specify its divergence as,

$$\bar{\nabla} \cdot \bar{A} = -\mu\varepsilon \frac{\partial \phi}{\partial t} \, , \tag{A.9}$$

since it leads to decoupling of the equations for ϕ and $\bar{A}$. Using Equation (A.9) into Equations (A.7) and (A.8) we obtain

$$\nabla^2 \phi - \mu\varepsilon \frac{\partial^2 \phi}{\partial t^2} = - \frac{\rho}{\varepsilon} \tag{A.10}$$

and

$$\nabla^2 \bar{A} - \mu\varepsilon \frac{\partial^2 \bar{A}}{\partial t^2} = - \mu \bar{J}. \tag{A.11}$$

Thus, we need to solve for $\bar{A}$ and ϕ from the above equations and then use Equations (A.5) and (A.6) to obtain the required expressions for the fields.

However, we do not really need to solve explicitly for ϕ since Equation (A.9) relates ϕ to $\bar{A}$ directly,

$$\phi = - \frac{1}{\mu\varepsilon} \int_{-\infty}^{t} (\bar{\nabla} \cdot \bar{A}) \, dt \, . \tag{A.12}$$

The solution to Equation (A.11) is

$$\bar{A}(\bar{R}, t) = \frac{\mu}{4\pi} \int_{V'} \frac{\bar{J}\left(\bar{R}', t - \frac{|\bar{R} - \bar{R}'|}{c}\right)}{|\bar{R} - \bar{R}'|} \, dV' \tag{A.13}$$

where $c^2 = \frac{1}{\mu\varepsilon}$ is the velocity of light in the medium, and the integral is taken over the source volume. The solution to Equation (A.11) obtained in Equation (A.13) may be verified by direct substitution.

Once $\bar{A}$ has been determined, the expressions for the fields may be written down using Equations (A.5), (A.6), and (A.12),

$$\bar{B}(\bar{R},t) = \bar{\nabla} \times \bar{A} \, , \tag{A.14}$$

$$\bar{E}(\bar{R},t) = -\frac{\partial \bar{A}}{\partial t} + c^2 \int_{-\infty}^{t} \bar{\nabla}(\bar{\nabla} \cdot \bar{A})\, dt \,. \qquad (A.15)$$

Equations (A.13), (A.14), and (A.15) will now be applied to the problem of a small dipole antenna carrying a current i(t). Consider the point P(r,ϕ,z) in Figure A.1 at which we need to determine the fields. Since the problem has cylindrical symmetry, we shall compute the electric and magnetic fields using a cylindrical coordinate system. Uman et al. (1975) have done the same problem in spherical coordinates. The first step is to determine the vector potential $\bar{A}$ of a dipole located at the origin of the coordinate system.

$$\bar{A}(R,t) = \left\{ \frac{\mu_o}{4\pi} \frac{i(o,t - \frac{R}{c})}{R} L \right\} \vec{a}_z = A_z(R,t)\vec{a}_z \qquad (A.16)$$

Using Equation (A.16) we obtain,

$$\bar{B}(r,\phi,z,t) = \bar{\nabla} \times \bar{A}$$

$$= \vec{a}_\phi \left\{ -\frac{\partial A_z}{\partial r} \right\}$$

$$\bar{B}(r,\phi,z,t) = -\left[\frac{\mu_o L}{4\pi} \frac{\partial}{\partial r} \left\{ \frac{i(t - \frac{R}{c})}{R} \right\} \right] \vec{a}_\phi \,. \qquad (A.17)$$

We have the following relationships,

$$r^2 = x^2 + y^2 \,;$$

and, $$R^2 = r^2 + z^2 \,. \qquad (A.18)$$

Figure A.1. Definition of the geometrical factors used in the derivation of the electric and magnetic fields at any arbitrary point due to a current carrying dipole at the origin.

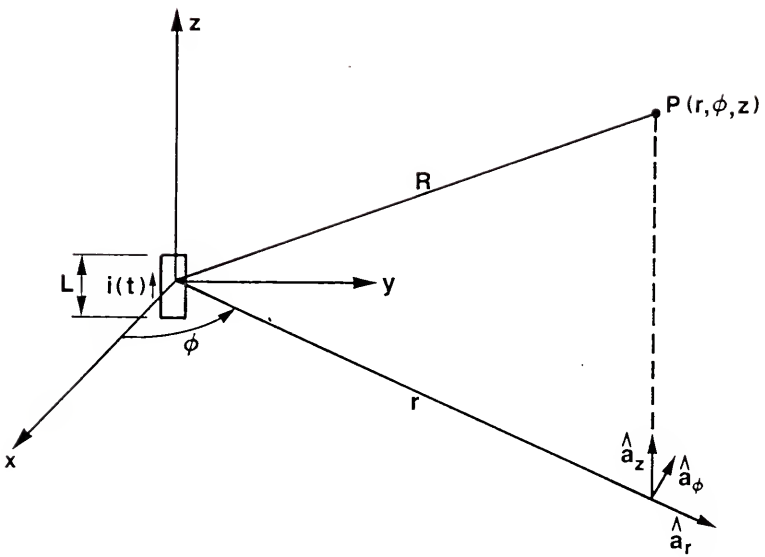
z
P (r,ϕ,z)
R
L
i(t)
y
ϕ
x
r
$\hat{a}_z$
$\hat{a}_\phi$
$\hat{a}_r$

Hence,

$$\frac{\partial}{\partial r}\left\{ i(t - \frac{R}{c}) \right\} = - \frac{r}{cR} \cdot i'(t - \frac{R}{c}) \ ;$$

and,

$$\frac{\partial}{\partial t}\left\{ i(t - \frac{R}{c}) \right\} = i'(t - \frac{R}{c}) \ ;$$

where primes denote derivative with respect to the whole argument, t - R/c. Hence,

$$\frac{\partial}{\partial r}\left\{ i(t- \frac{R}{c}) \right\} = - \frac{r}{cR} \frac{\partial}{\partial t} \ i(t- \frac{R}{c}) \ . \qquad (A.19)$$

Also,

$$\frac{\partial}{\partial r}(\frac{1}{R}) = - \frac{r}{R^3} \qquad (A.20)$$

Going back to Equation (A.17), we have

$$\bar{B}(r,\phi,z,t) = - \frac{\mu_o L}{4\pi}\left[\frac{1}{R} \frac{\partial i(t- \frac{R}{c})}{\partial r} + i(t- \frac{R}{c}) \frac{\partial}{\partial r}(\frac{1}{R}) \right] \vec{a}_\phi$$

Using Equations (A.19) and (A.20), we find

$$\bar{B}(r,\phi,z,t) = \frac{\mu_o L}{4\pi}\left[\frac{r}{cR^2} \frac{\partial i(t- \frac{R}{c})}{\partial t} + \frac{r}{R^3} \cdot i(t- \frac{R}{c}) \right] \vec{a}_\phi \qquad (A.21)$$

We now determine the expression for $\bar{E}$.

$$\bar{\nabla} \cdot \bar{A} = \frac{\partial A_z}{\partial z} = \frac{\mu_o L}{4\pi} \frac{\partial}{\partial z}\left\{ \frac{i(t- \frac{R}{c})}{R} \right\}$$

$$= \frac{\mu_o L}{4\pi}\left[\frac{1}{R} \frac{\partial i(t- \frac{R}{c})}{\partial z} - \frac{z}{R^3} \cdot i(t- \frac{R}{c}) \right] \qquad (A.22)$$

Since there is no ϕ-variation, the gradient operator becomes,

$$\bar{\nabla} = \vec{a}_r \frac{\partial}{\partial r} + \vec{a}_z \frac{\partial}{\partial z}$$

Thus,

$$\bar{\nabla}(\bar{\nabla} \cdot \bar{A}) = \frac{\mu_o L}{4\pi} \left[\frac{\partial}{\partial r} \left\{ \frac{1}{R} \frac{\partial i(t - \frac{R}{c})}{\partial z} \right\} - \frac{\partial}{\partial r} \left\{ \frac{z}{R^3} i(t - \frac{R}{c}) \right\} \right] \vec{a}_r$$

$$+ \frac{\mu_o L}{4\pi} \left[\frac{\partial}{\partial z} \left\{ \frac{1}{R} \frac{\partial i(t - \frac{R}{c})}{\partial z} \right\} - \frac{\partial}{\partial z} \left\{ \frac{z}{R^3} i(t - \frac{R}{c}) \right\} \right] \vec{a}_z \qquad (A.23)$$

Expanding Equation (A.23) we have,

$$\frac{\bar{\nabla}(\bar{\nabla} \cdot \bar{A})}{\frac{\mu_o L}{4\pi}} = \left[\frac{1}{R} \frac{\partial^2 i(t - \frac{R}{c})}{\partial r \, \partial z} + (-\frac{r}{R^3}) \frac{\partial i(t - \frac{R}{c})}{\partial z} \right.$$

$$\left. - z (-\frac{3r}{R^5}) i(t - \frac{R}{c}) - \frac{z}{R^3} \frac{\partial i(t - \frac{R}{c})}{\partial r} \right] \vec{a}_r$$

$$+ \left[\frac{1}{R} \frac{\partial i(t - \frac{R}{c})}{\partial z^2} + (-\frac{z}{R^3}) \frac{\partial i(t - \frac{R}{c})}{\partial z} - \frac{1}{R^3} i(t - \frac{R}{c}) \right.$$

$$\left. -z (-\frac{3z}{R^5}) \cdot i (t - \frac{R}{c}) - \frac{z}{R^3} \frac{\partial i(t - \frac{R}{c})}{\partial z} \right] \vec{a}_z \qquad (A.24)$$

We have from Equation (A.19)

$$\frac{\partial}{\partial r} \left\{ i(t - \frac{R}{c}) \right\} = - \frac{r}{cR} \frac{\partial i(t - \frac{R}{c})}{\partial t}$$

Similarly,

$$\frac{\partial}{\partial z} \left\{ i(t - \frac{R}{c}) \right\} = - \frac{z}{cR} \frac{\partial i(t - \frac{R}{c})}{\partial t} \qquad (A.25)$$

Using these relations, we have

$$\frac{\partial^2 i(t-\frac{R}{c})}{\partial z^2} = \frac{\partial}{\partial z}\left\{-\frac{z}{cR}\frac{\partial i(t-\frac{R}{c})}{\partial t}\right\}$$

$$= -\left[\frac{1}{cR}\frac{\partial i(t-\frac{R}{c})}{\partial t} + \frac{z}{c}\left(\frac{-z}{R^3}\right)\frac{\partial i(t-\frac{R}{c})}{\partial t} + \frac{z}{cR}\frac{\partial^2 i(t-\frac{R}{c})}{\partial z\,\partial t}\right]$$

$$= -\frac{1}{cR}\frac{\partial i(t-\frac{R}{c})}{\partial t} + \frac{z^2}{cR^3}\frac{\partial i(t-\frac{R}{c})}{\partial t} + \frac{z^2}{c^2R^2}\frac{\partial^2 i(t-\frac{R}{c})}{\partial t^2} \qquad (A.26)$$

Similarly, it may be shown that

$$\frac{\partial^2 i(t-\frac{R}{c})}{\partial r\,\partial z} = \frac{zr}{cR^3}\frac{\partial i(t-\frac{R}{c})}{\partial t} + \frac{zr}{c^2R^2}\frac{\partial^2 i(t-\frac{R}{c})}{\partial t^2}\,. \qquad (A.27)$$

Substituting Equations (A.19), (A.25), (A.26), and (A.27) into Equation (A.24), we find,

$$\frac{\bar{\nabla}(\bar{\nabla}\cdot\bar{A})}{\frac{\mu_o L}{4\pi}} = \left[\frac{1}{R}\left\{\frac{zr}{cR^3}\frac{\partial i(t-\frac{R}{c})}{\partial t} + \frac{zr}{c^2R^2}\frac{\partial^2 i(t-\frac{R}{c})}{\partial t^2}\right\} - \frac{r}{R^3}\left\{-\frac{z}{cR}\frac{\partial i(t-\frac{R}{c})}{\partial t}\right\}\right.$$

$$\left. + \frac{3zr}{R^5}\,i(t-\frac{R}{c}) - \frac{z}{R^3}\left\{-\frac{r}{cR}\frac{\partial i(t-\frac{R}{c})}{\partial t}\right\}\right]\vec{a}_r$$

$$+ \left[\frac{1}{R}\left\{\left(-\frac{1}{cR} + \frac{z^2}{cR^3}\right)\cdot\frac{\partial i(t-\frac{R}{c})}{\partial t} + \frac{z^2}{c^2R^2}\frac{\partial^2 i(t-\frac{R}{c})}{\partial t}\right\}\right.$$

$$\left. - \frac{z}{R^3}\left\{-\frac{z}{cR}\frac{\partial i(t-\frac{R}{c})}{\partial t}\right\} - \frac{1}{R^3}\,i(t-\frac{R}{c}) + \frac{3z^2}{R^5}\,i(t-\frac{R}{c})\right.$$

$$- \frac{z}{R^3} \left\{ - \frac{z}{cR} \frac{\partial i(t- \frac{R}{c})}{\partial t} \right\} \Big] \vec{a}_z$$

$$= \left[\frac{3rz}{R^5} i(t- \frac{R}{c}) + \frac{3rz}{cR^4} \frac{\partial i(t- \frac{R}{c})}{\partial t} + \frac{rz}{c^2R^3} \frac{\partial i(t- \frac{R}{c})}{\partial t^2} \right] \vec{a}_r$$

$$+ \left[\left(\frac{3z^2}{R^5} - \frac{1}{R^3} \right) . i(t- \frac{R}{c}) + \left(\frac{3z^2}{cR^4} - \frac{1}{cR^2} \right) . \frac{\partial i(t- \frac{R}{c})}{\partial t} \right.$$

$$\left. + \frac{z^2}{c^2R^3} \frac{\partial^2 i(t- \frac{R}{c})}{\partial t^2} \right] \vec{a}_z \qquad \text{(A.28)}$$

Hence we can write,

$$-\bar{\nabla}\phi = c^2 \int_{-\infty}^{t} \bar{\nabla}(\bar{\nabla} \cdot \bar{A}) \, dt$$

$$= \frac{L}{4\pi\varepsilon_o} \left[\left\{ \frac{3rz}{R^5} \int_o^t i(\tau- \frac{R}{c}) \, d\tau + \frac{3rz}{cR^4} i(t- \frac{R}{c}) + \frac{rz}{c^2R^3} \frac{\partial i(t- \frac{R}{c})}{\partial t} \right\} \vec{a}_r \right.$$

$$+ \left\{ \left(\frac{3z^2}{R^5} - \frac{1}{R^3} \right) \int_o^t i(\tau- \frac{R}{c}) d\tau + \left(\frac{3z^2}{cR^4} - \frac{1}{cR^2} \right) i(t- \frac{R}{c}) \right.$$

$$\left. \left. + \frac{z^2}{c^2R^3} \frac{\partial i(t- \frac{R}{c})}{\partial t^2} \right\} \vec{a}_z \right] \qquad \text{(A.29)}$$

Also, from Equation (A.16), we have

$$- \frac{\partial \bar{A}}{\partial t} = - \frac{L}{4\pi\varepsilon_o c^2} \left\{ \frac{1}{R} \frac{\partial i(t- \frac{R}{c})}{\partial t} \right\} \vec{a}_z \qquad \text{(A.30)}$$

In Equations (A.29) and (A.30) we have used the relation,

$$c^2 = \frac{1}{\mu_o \varepsilon_o} . \qquad \text{(A.31)}$$

Finally, we are in a position to write down the complete expression for $\vec{E}$ from Equation (A.15). For the sake of convenience we write

$$\vec{E} = E_r \vec{a}_r + E_z \vec{a}_z \tag{A.32}$$

where the components in Equation (A.32) may be obtained by substituting Equations (A.29) and (A.30) into Equation (A.15).

$$E_r(r,\phi,z,t) = \frac{L}{4\pi\varepsilon_o}\left[\frac{3rz}{R^5}\int_o^t i(\tau - \frac{R}{c})\,d\tau + \frac{3rz}{cR^4}\,i(t-\frac{R}{c}) + \frac{rz}{c^2R^3}\frac{\partial i(t-\frac{R}{c})}{\partial t}\right] \tag{A.33}$$

and

$$E_z(r,z,\phi,t) = \frac{L}{4\pi\varepsilon_o}\left[\left(\frac{2z^2-r^2}{R^5}\right)\int_o^t i(\tau - \frac{R}{c})\,d\tau + \left(\frac{2z^2-r^2}{cR^4}\right) i(t-\frac{R}{c}) - \frac{r^2}{c^2R^3}\frac{\partial i(t-\frac{R}{c})}{\partial t}\right] \tag{A.34}$$

Equations (A.21), (A.33) and (A.34) represent the field solution due to a small dipole at the origin. For our purpose, the dipole will lie along the z-axis at an arbitrary source coordinate z'. In that case, the solution is modified and may be written as,

$$B_\phi(r,\phi,z,t) = \frac{\mu_o L}{4\pi}\left[\frac{r}{cR^2}\cdot\frac{\partial i(z',t-\frac{R}{c})}{\partial t} + \frac{r}{R^3}\cdot i(z',t-\frac{R}{c})\right] \tag{A.35}$$

$$E_r(r,\phi,z,t) = \frac{L}{4\pi\varepsilon_o}\left[\frac{3r(z-z')}{R^5}\int_0^t i(z',\tau-\frac{R}{c})d\tau + \frac{3r(z-z')}{cR^4}\, i(z',t-\frac{R}{c})\right.$$

$$\left. + \frac{r(z-z')}{c^2R^3}\,\frac{\partial i(z',\tau-\frac{R}{c})}{\partial t}\right] \qquad (A.36)$$

$$E_z(r,\phi,z,t) = \frac{L}{4\pi\varepsilon_o}\left[\frac{2(z-z')^2-r^2}{R^5}\int_0^t i(z',\tau-\frac{R}{c})d\tau\right.$$

$$\left. + \frac{2(z-z')^2-r^2}{cR^4}\, i(z',t-\frac{R}{c}) - \frac{r^2}{c^2R^3}\,\frac{\partial i(z',t-\frac{R}{c})}{\partial t}\right] \qquad (A.37)$$

APPENDIX B

TEST LINE VOLTAGES INDUCED BY NEARBY STEPPED LEADERS

In this Appendix, data on voltages induced by nearby stepped leaders are presented. Simultaneously measured vertical electric field pulses due to the stepped leader will also be shown.

Figure B.1 shows the vertical electric field change produced by a single stroke flash which occurred at 185337 UT during run #79196TR27 on a time scale of 10 ms/div: both direct and FM channels are given. In Figure B.2 the location of the ground strike point is indicated.

Instrumentation tape records of the return stroke field change and the corresponding voltage on the unenergized test line are shown in Figure B.3 on a time scale of 200 μs full-scale. The peak voltage is about 150 kV and is of positive polarity. Sampling the continuous voltage and field records at a faster sampling rate and at increased sensitivity, we can look at the waveforms in detail, for about 50 μs preceeding the return stroke. In Figure B.4 this detail is shown on two expanded time scales: the top photograph at 8 μs/div and the bottom at 4 μs/div. The stepped leader pulses can be easily identified on the vertical electric field records. Corresponding line voltages can also be identified over the noise level of the tape channel.

Figure B.1. Vertical electric field change associated with the 185337 flash during run #79196TR27. The FM channel record has a sensitivity of 1.1 kV/m per division and the direct channel 90 V/m per division. Both traces are 100 ms full-scale.

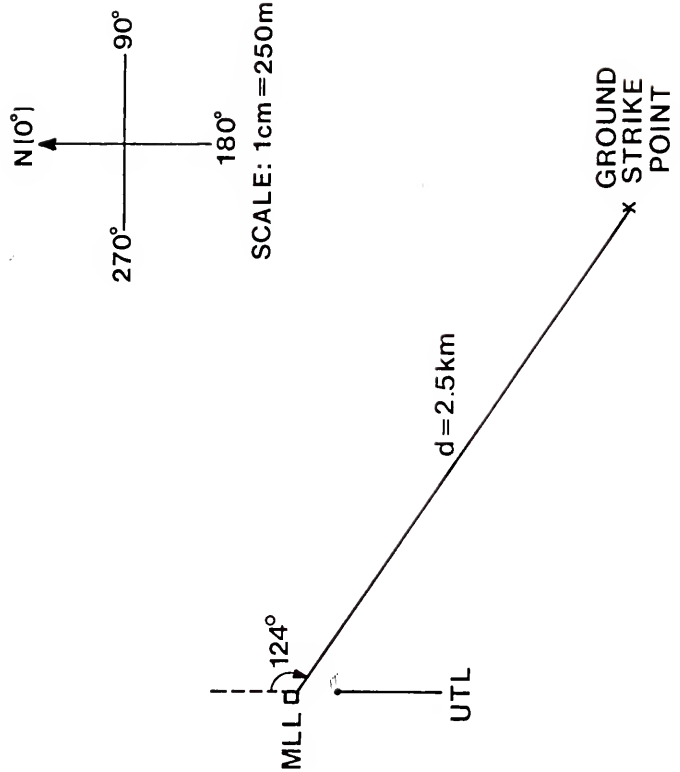
N(0°)
90°
180°
270°
SCALE: 1cm=250m
GROUND
STRIKE
POINT
d=2.5km
124°
MLL
UTL

Figure B.2. Location of the ground strike point of the 185337 flash during run #79196TR27.

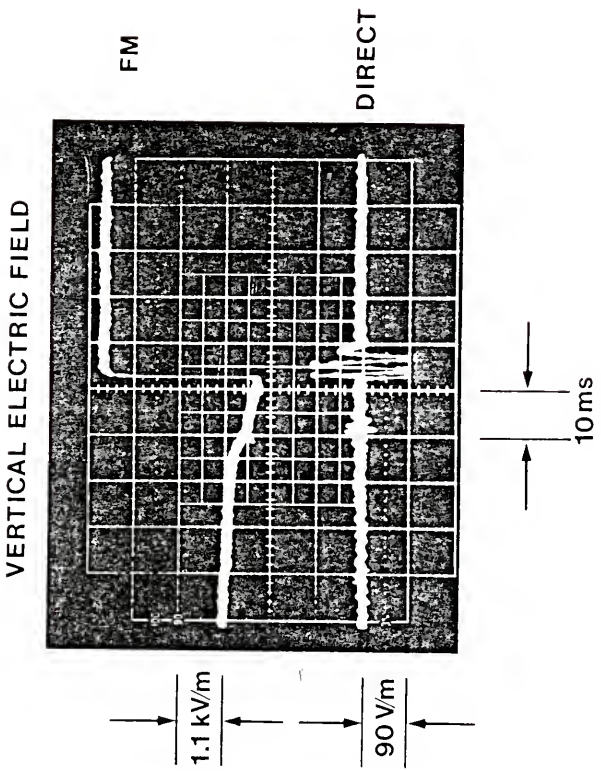
VERTICAL ELECTRIC FIELD
FM
DIRECT
1.1 kV/m
90 V/m
10 ms

Figure B.3. Simultaneous records of the induced voltage on the test-line and the vertical electric field for the return stroke at 185337 during run #79196TR27. The voltage scale is 65 kV/division and the vertical electric field 440 V/m per division. Both records are 200 μs full-scale. The voltage record is obtained from the direct channel and hence producesan accurate response for only about 50 μs.

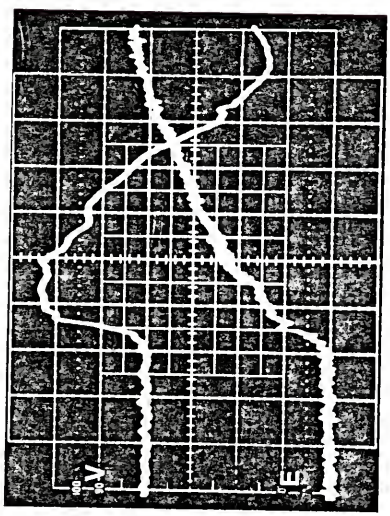
65 kV
440V/m
20μs

Figure B.4. Stepped leader induced voltages and simultaneously recorded vertical electric field for the 185337 flash during run #79196TR27. The top two traces are 8 μs/division, the bottom two traces 4 μs/division. The voltage scale is 6.5 kV per division, the vertical electric field 18 V/m per division.

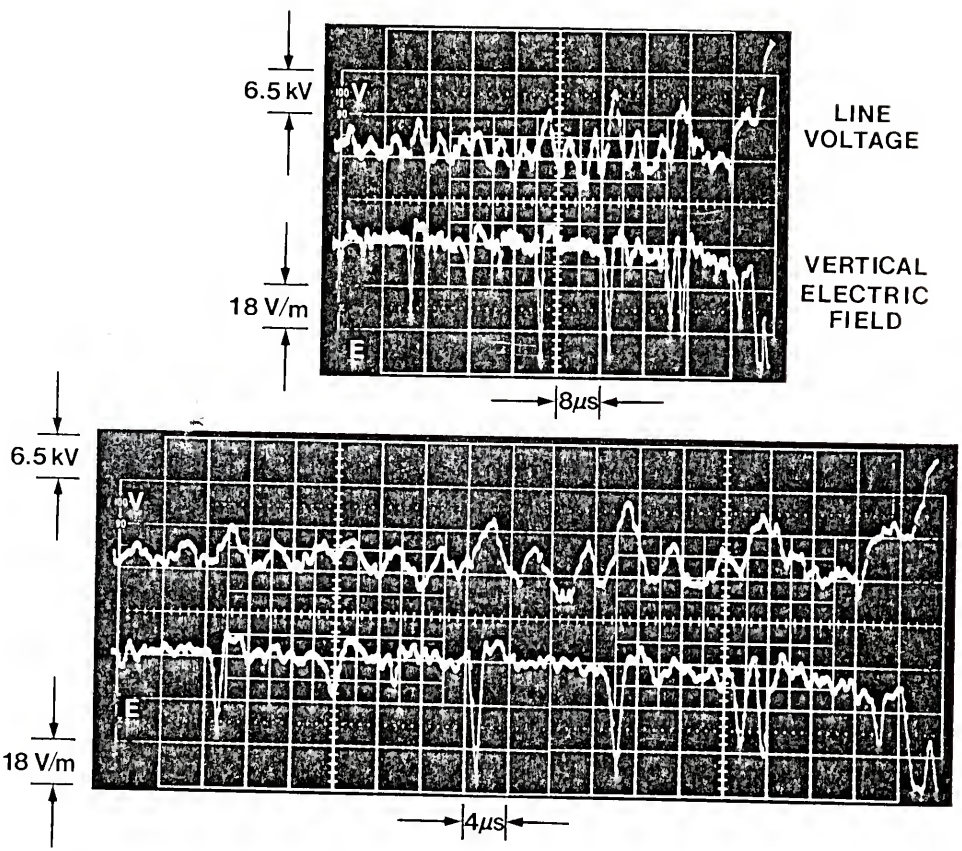
6.5 kV
18 V/m
LINE VOLTAGE
VERTICAL ELECTRIC FIELD
8μs
6.5 kV
18 V/m
4μs

The peak vertical electric field due to the stepped leader pulses is an order of magnitude lower than the return stroke radiation peak. This is in conformity with stepped leader electric field measurements reported by Krider et al. (1977). It is an interesting fact that the peak induced voltage on the UTL is also an order of magnitude lower i.e., about 13 kV, than that due to the following return stroke.

This method of trying to extract the stepped leader induced voltages was tried for several other strokes. However, in all cases, the induced line voltage was found to be buried below the channel noise level. Thus, it may be concluded that the peak voltage induced on the UTL by stepped leaders is an order of magnitude lower than that induced by the following return stroke. These data represent the first simultaneous recording of the voltages on an overhead line and the vertical electric field due to stepped leaders, and are in contradiction with calculated values of the order of 1 MV derived by Owa (1964), based on the pre-discharge theory put forth by Griscom (1958). This is not unexpected since the calculation by Owa (1964) assumed a stepped leader current of 100 kA, whereas modern measurements reported by Krider and Radda (1975) and by Krider et al. (1977) indicate a peak stepped leader current of the order of 1 kA.

APPENDIX C

COMPUTER PROGRAMS

In this Appendix we give FORTRAN listings of various computer codes which have been written as part of this dissertation. A brief note of their usage is also included.

C.1 Return Stroke Program

The user specifies the various parameters associated with the three component currents derived from two station field measurements as given by Lin et al. (1980). The field point is specified, and the printer and plotter format is also specified. As output the program gives the electric and magnetic field components at the field point and the return stroke current at ground for each time step. As an option, the electrostatic, induction, and radiation components of the fields may also be printed. A FORTRAN listing follows.

```
C
C       ****  LIGHTNING  RETURN  STROKE  PROGRAM  ***
C                    MANECK  J  MASTER
C
C
C     THIS PROGRAM COMPUTES THE HORIZONTAL ELECTRIC (EH), THE VERTICAL
C     ELECTRIC (EV), AND THE MAGNETIC (B) FIELDS DUE TO A LIGHTNING
C     RETURN STROKE AS MODELED BY MASTER ET AL. (1981). THE ORIGIN OF
C     THE CYLINDRICAL COORDINATE SYSTEM IS THE LIGHTNING GROUND STRIKE
C     POINT, THE CHANNEL HEIGHT IS H, AND THE FIELD POINT IS AT
C     (XA,YA,ZA). ALL VALUES ARE IN SI UNITS.
C
C     THE RETURN STROKE MODEL CURRENTS ARE:
C     (1) BREAKDOWN PULSE CURRENT -- PIECEWISE LINEAR SEGMENTS (ARRAYS
C     PI AND PT); EXPONENTIAL DECAY OF AMPLITUDE WITH HEIGHT (PDECAY);
C     CONSTANT UPWARD VELOCITY (V).
C     (2) UNIFORM CURRENT (CURU0)
C     (3) CORONA CURRENT (ALPHA,BETA,LAMBDA,CURC0)
C
C     OUTPUT OPTIONS:
C     (1) TLEN .LE. 0 THEN NO OUTPUT ON GOULD.  IF PLOTS ARE DESIRED
C     USE TLEN=5.0
C     (2) IOUTPT=1 PRODUCES LONG OUTPUT -- GIVES ELECTROSTATIC,
C     INDUCTION, AND RADIATION COMPONENTS OF ALL FIELDS AT EACH TIME
C     STEP; IOUTPT=2 PRODUCES SHORT OUTPUT -- GIVES ONLY TOTAL FIELD
C     VALUES AT EACH TIME STEP.
C
      REAL DT(1005),PI(21),PT(21),SLOPE(21),YINTCP(21)
      REAL EHEP(1005),EHIP(1005),EHRP(1005),EVEP(1005),EVIP(1005),
     1     EVRP(1005),BIP(1005),BRP(1005),EHEPR(1005),EHIPR(1005),
     2     EHRPR(1005),EVEPR(1005),EVIPR(1005),EVRPR(1005),BIPR(1005),
     3     BRPR(1005),EHP(1005),EVP(1005),BP(1005)
      REAL EHEC(1005),EHIC(1005),EHRC(1005),EVEC(1005),EVIC(1005),
     1     EVRC(1005),BIC(1005),BRC(1005),EHECR(1005),EHICR(1005),
     2     EHRCR(1005),EVECR(1005),EVICR(1005),EVRCR(1005),BICR(1005),
     3     BRCR(1005),EHC(1005),EVC(1005),BC(1005)
      REAL EHEU(1005),EHIU(1005),EVEU(1005),EVIU(1005),BIU(1005),
     1     EHEUR(1005),EHIUR(1005),EVEUR(1005),EVIUR(1005),BIUR(1005),
     2     EHU(1005),EVU(1005),BU(1005)
      REAL EH(1005),EV(1005),B(1005),TIME(1005)
      REAL CURP(10005),CURPD(10005),CURPI(10005),CURC(1005),CURU(1005),
     1     CURTOT(1005)
      REAL LAMBDA,MAXAE,MINDT,MAXDT
      INTEGER NTSTEP(21)
      COMMON EH,EV,B,CURTOT,TIME,TLEN,KSTOP
      LOGICAL IMAGE
```

```
C
 500  FORMAT('1',/,40X,'***   TIME  DOMAIN  OUTPUT   ***',////,5X,
     1       'TIME (SEC)',29X,'ELECTROSTATIC',6X,'INDUCTION',6X,
     2       'RADIATION',9X,'TOTAL',//)
 501  FORMAT(/,5X,1PE10.3,5X,'EH (V/M)',5X,'PULSE  ',5X,E10.3,7X,E10.3
     1       ,5X,E10.3,8X,E10.3,/,33X,'CORONA ',5X,E10.3,7X,E10.3,5X,
     2       E10.3,8X,E10.3,/,33X,'UNIFORM',5X,E10.3,7X,E10.3,23X,E10.3,
     3       /,33X,'TOTAL  ',55X,E10.3,/,20X,'EV (V/M)',5X,'PULSE  ',5X,
     4       E10.3,7X,E10.3,5X,E10.3,8X,E10.3,/,33X,'CORONA ',5X,E10.3,
     5       7X,E10.3,5X,E10.3,8X,E10.3/33X,'UNIFORM',5X,E10.3,7X,E10.3,
     6       23X,E10.3,/,33X,'TOTAL  ',55X,E10.3,/,23X,'B (T)',5X,
     7       'PULSE  ',22X,E10.3,5X,E10.3,8X,E10.3,/,33X,'CORONA ',22X,
     8       E10.3,5X,E10.3,8X,E10.3,/,33X,'UNIFORM',22X,E10.3,23X,E10.3
     9       ,/,33X,'TOTAL  ',55X,E10.3,/,17X,'CURRENT (A)',5X,'PULSE  '
     1       ,55X,E10.3,/,33X,'CORONA ',55X,E10.3,/,33X,'UNIFORM',55X,
     2       E10.3,/,33X,'TOTAL  ',55X,E10.3,//)
 502  FORMAT('1',///,10X,'THE FIELD POINT IS AT',/,15X,'XA = ',
     1    1PE9.2,' METRES',/,15X,'YA = ',E9.2,' METRES',/,15X,'ZA = ',
     2    E9.2,' METRES',/,15X,'WHERE (0.0,0.0,0.0) REPRESENTS THE ',
     3    'GROUND POINT OF THE VERTICAL LIGHTNING CHANNEL',/,10X,
     4    'THE SHORTEST DISTANCE FROM THE LIGHTNING CHANNEL TO THE ',
     5    'FIELD POINT IS = ',E9.2,' METRES',//)
 503  FORMAT(/,10X,'THE TOP OF THE LTG CHANNEL IS AT A HEIGHT OF ',
     1    'ZCHANL = ',1PE9.2,' METRES',/,10X,'THE VELOCITY OF PROPAGA',
     2    'TION FOR THE RETURN STROKE CURRENT IS V = ',E9.2,' METRES/',
     3    'SECOND',//)
 504  FORMAT(/,10X,'THE RETURN STROKE CURRENT COMPONENTS ARE AS ',
     1    'FOLLOWS :',//,15X,'(1) PULSE CURRENT - MADE UP OF ',I2,
     2    ' PIECEWISE LINEAR SEGMENTS',/,21X,'TIME (SEC)',5X,
     3    'CURRENT (A)',/,21X,1PE9.2,6X,E9.2,20(/,21X,E9.2,6X,E9.2))
 505  FORMAT('+',15X,'THE PULSE DECAYS EXPONENTIALLY WITH HEIGHT ABOVE'
     1    ,' GROUND WITH A DECAY CONSTANT PDECAY = ',1PE9.2,' METRES')
 506  FORMAT(/,15X,'(2) CORONA CURRENT - CURRENT PER UNIT LENGTH IS ',
     1    'I0*EXP(-Z/LAMBDA)*(EXP(-ALPHA*T)-EXP(-BETA*T)) A/M',/,20X,
     1    'CUR00 = ',1PE9.2,' A/M',/,20X,
     2    'LAMBDA = ',E9.2,' METRES',/,20X,'ALPHA = ',E9.2,' /SEC',/,
     3    20X,'BETA = ',E9.2,' /SEC',/,15X,'THE CORONA CURRENT AT ANY'
     4    ,' HEIGHT Z  IS TURNED ON ',E9.2,' SECS AFTER THE RETURN ',
     5    'STROKE WAVEFRONT HAS REACHED Z ',/)
 507  FORMAT(/,15X,'(3) UNIFORM CURRENT',/,20X,'CUR00 = ',1PE9.2,
     1    ' AMPS')
 508  FORMAT('1',//12X,'TIME (SEC)',5X,'HORZ ELEC FLD (V/M)',5X,'VERT '
     1    ,'ELEC FLD (V/M)',5X,'MAGNETIC FLD (T)',8X,'CURRENT (A)')
 509  FORMAT(/,11X,1PE10.3,8X,E10.3,14X,E10.3,14X,E10.3,12X,E10.3)
C
C      DEFINE INPUT PARAMETERS
C
       IOUTPT=2
```

```
      XA=15.0E+03
      YA=0.0
      ZA=0.0
      ALPHA=1.0E+05
      BETA=3.0E+06
      LAMBDA=1.5E+03
      CURC0=21.0C
      PDECAY=LAMDDA
      ZCHANL=7.5E+03
      V=1.0E+08
      NZ=75C0
      MINDT=1.0E-08
      MAXDT=4.0E-06
      TSTOP=99.0E-06
      CURU0=3.1E+03
      TLEN=5.0
C
      PI(1)=3.0E+03
      PI(2)=14.9E+03
      PI(3)=7.4E+03
      PI(4)=1.4E+03
      PI(5)=0.0
      PT(1)=1.0E-06
      PT(2)=1.1E-06
      PT(3)=3.7E-06
      PT(4)=11.0E-06
      PT(5)=40.0E-06
      NSEG=5
C
CC    COMPUTE CONSTANTS
C
      TSTEP=MINDT
      TCN=PT(1)
      NSTEP=TSTOP/TSTEP+0.5
      ZSTEP=ZCHANL/FLOAT(NZ)
      ECONST=0.5E+10
      DCONST=1.0E-07
      HZSTEP=ZSTEP/2.0
      C=2.997925E+08
      H1=1.0/V+1.0/C
      H2=ALPHA*H1-1.0/LAMBDA
      H3=BETA*H1-1.0/LAMDDA
      H9=-CURC0/ALPHA
      H10=CURC0/BETA
      H8=LAMBDA*(H10+H9)
      DSQ=XA*XA+YA*YA
      D=(DSQ)**0.5
      ZASQ=ZA*ZA
```

```
      CSQ=C*C
      RSQ=DSQ+ZASQ
      R=RSQ**0.5
      RFSQ=DSQ+(ZA-ZCHANL)*(ZA-ZCHANL)
      RIFSQ=DSQ+(ZA+ZCHANL)*(ZA+ZCHANL)
      RF=(RFSQ)**0.5
      RIF=(RIFSQ)**0.5
      RF3=RFSQ*RF
      RIF3=RIFSQ*RIF
      HEHU=ECONST*CURU0*D*(1.0/RF3-1.0/RIF3)
      HEVU=-ECONST*CURU0*((ZCHANL-ZA)/RF3 + (ZCHANL+ZA)/RIF3)
      HHU=HEHU*(R/C)
      HVU=HEVU*(R/C)
      HIBU=BCONST*(CURU0/D)*((ZA+ZCHANL)/RIF - (ZA-ZCHANL)/RF)
      TRETD=R/C
      TRETDC=TRETD+TJN
      ECONST=ECONST*HZSTEP
      BCONST=BCONST*HZSTEP
C
C     COMPUTE ARRAYS FOR BREAKDOWN PULSE CURRENT
C
      NSEG1=NSEG+1
      SLOPE(1)=PI(1)/PT(1)
      YINTCP(1)=0.0
      SLOPE(NSEG1)=0.0
      YINTCP(NSEG1)=0.0
      NTSTEP(1)=PT(1)/TSTEP +0.5
      NTSTEP(NSEG1)=TSTOP/TSTEP +0.5
C
      DO 10 J=2,NSEG
      SLOPE(J)=(PI(J)-PI(J-1))/(PT(J)-PT(J-1))
      YINTCP(J)=PI(J)-PT(J)*SLOPE(J)
      NTSTEP(J)=PT(J)/TSTEP + 0.5
   10 CONTINUE
C
      CURP(1)=0.0
      CURPD(1)=0.0
      CURPI(1)=0.0
      NSTART=2
      DO 12 J=1,NSEG
      NSTOP=NTSTEP(J) + 1
      SJ=SLOPE(J)
           DO 11 I=NSTART,NSTOP
           T=TSTEP*FLOAT(I-1)
           CURP(I)=SLOPE(J)*T + YINTCP(J)
           SCURP=CURP(I)+CURP(I-1)
           CURPI(I)=CURPI(I-1)+(SCURP*TSTEP*0.5)
           CURPD(I)=SJ
```

```
   11       CONTINUE
        NSTART=NSTOP + 1
   12   CONTINUE
        NSTOP=NSTEP
        DO 13 I=NSTART,NSTOP
        CURP(I)=0.0
        CURPD(I)=0.0
        CURPI0=CURPI(I-1)
        CURPI(I)=CURPI0
   13   CONTINUE
C
        WRITE(6,502)XA,YA,ZA,D
        WRITE(6,503)ZCHANL,V
        WRITE(6,504)NSEG,(PT(I),PI(I),I=1,NSEG)
        WRITE(6,505)PDECAY
        WRITE(6,506)CURC0,LAMBDA,ALPHA,BETA,TON
        WRITE(6,507)CURU0
C
        DO 23 I=1,1005
C
        EHEPR(I)=0.0
        EHIPR(I)=0.0
        EHRPR(I)=0.0
        EVEPR(I)=0.0
        EVIPR(I)=0.0
        EVRPR(I)=0.0
        BIPR(I)=0.0
        BRPR(I)=0.0
C
        EHECR(I)=0.0
        EHICR(I)=0.0
        EHRCR(I)=0.0
        EVECR(I)=0.0
        EVICR(I)=0.0
        EVRCR(I)=0.0
        BICR(I)=0.0
        BRCR(I)=0.0
C
        EHEUR(I)=0.0
        EHIUR(I)=0.0
        EVEUR(I)=0.0
        EVIUR(I)=0.0
        BIUR(I)=0.0
C
   23   CONTINUE
C
        IMAGE=.FALSE.
C
```

```
C       TIME LOOP
C
   25   CONTINUE
C
C       INITIALIZE FIELD ARRAYS
C
        DO 26 I=1,1005
C
        EHEP(I)=0.0
        EHIP(I)=0.0
        EHRP(I)=0.0
        EVEP(I)=0.0
        EVIP(I)=0.0
        EVRP(I)=0.0
        BIP(I)=0.0
        BRP(I)=0.0
C
        EHEC(I)=0.0
        EHIC(I)=0.0
        EHRC(I)=0.0
        EVEC(I)=0.0
        EVIC(I)=0.0
        EVRC(I)=0.0
        BIC(I)=0.0
        BRC(I)=0.0
C
        EHEU(I)=0.0
        EHIU(I)=0.0
        EVEU(I)=0.0
        EVIU(I)=0.0
        BIU(I)=0.0
C
   26   CONTINUE
C
        K=1
        ISTART=TRETD/MINDT+1.0
        ISTOP=ISTART+ISTEP
        T=MINDT*FLOAT(ISTART-1)
        MAXAE=1.0
        PEVTCT=0.0
        TIME(1)=0.0
        DT(1)=MINDT
C
        DO 90 I=ISTART,ISTOP
        T=T+DT(K)
        TTEST=TIME(K)
        IF(TTEST.GT.TSTOP) GO TO 100
        IF (K.GE.1000) GO TO 100
```

```
C
C       INTEGRATION OVER THE CHANNEL
C
        Z=0.0
        DIFF=MINDT*FLOAT(ISTART)
        DIFFC=DIFF+TON
        A1=D*ZA
        A2=2.0*ZASQ-DSQ
        R3=RSQ*R
        CR4=C*RSQ*RSQ
        C2R3=CSQ*R3
        R5=R3*RSQ
        H14=1.0
C
        DO 50 J=1,NZ
        N=(T-DIFF)/MINDT+1.0
C
C       COMPUTE PULSE CURRENT, ITS DERIVATIVE AND ITS INTEGRAL
C
        P=EXP(-ABS(Z)/PDECAY)
        CURPZ=CURP(N)*P
        CURPDZ=CURPD(N)*P
        CURPIZ=CURPI(N)*P
C
C       COMPUTE CORONA CURRENT, ITS DERIVATIVE AND ITS INTEGRAL
C
        TRE=T-DIFFC
        ZMAX=TRE/H1
        IF (ZMAX.LE.Z) GO TO 35
        IF (ZMAX.GT.ZCHANL) ZMAX=ZCHANL
        H4=-ALPHA*TRE
        H5=-BETA*TRE
        H11=H2*ZMAX+H4
        H12=H3*ZMAX+H5
        H15=H2*Z+H4
        H16=H3*Z+H5
        H13=EXP(-ZMAX/LAMBDA)
        H6=(EXP(H11)-EXP(H15))/H2
        IF(H16.LE.-150.0) GO TO 30
        H7=(EXP(H12)-EXP(H15))/H3
        GO TO 32
   30   H7=EXP(H12)/H3
C
   32   CONTINUE
C
        CURCZ=CURC0*(H6-H7)
        CURCDZ=CURC0*(BETA*H7-ALPHA*H6)
        CURCIZ=(H8*(H13-H14))+(H9*H6)+(H10*H7)
```

```
C
      GO TO 36
C
   35 CURCZ=0.0
      CURCDZ=0.0
      CURCIZ=0.0
C
   36 CONTINUE
C
C     COMPUTE FIELD CONTRIBUTIONS
C
      EHEPZ=((3.0*A1)/R5)*CURPIZ
      EHIPZ=((3.0*A1)/CR4)*CURPZ
      EHRPZ=(A1/C2R3)*CURPDZ
      EVEPZ=(A2/R5)*CURPIZ
      EVIPZ=(A2/CR4)*CURPZ
      EVRPZ=-(DSQ/C2R3)*CURPDZ
      BIPZ=(D/R3)*CURPZ
      BRPZ=(D/(C*RSQ))*CURPDZ
C
      EHECZ=((3.0*A1)/R5)*CURCIZ
      EHICZ=((3.0*A1)/CR4)*CURCZ
      EHRCZ=(A1/C2R3)*CURCDZ
      EVECZ=(A2/R5)*CURCIZ
      EVICZ=(A2/CR4)*CURCZ
      EVRCZ=-(DSQ/C2R3)*CURCDZ
      BICZ=(D/R3)*CURCZ
      BRCZ=(D/(C*RSQ))*CURCDZ
C
      IF(Z.GE.1.0E-10) GO TO 40
C
      EHEPT=EHEPZ
      EHIPT=EHIPZ
      EHRPT=EHRPZ
      EVEPT=EVEPZ
      EVIPT=EVIPZ
      EVRPT=EVRPZ
      BIPT=BIPZ
      BRPT=BRPZ
C
      EHECT=EHECZ
      EHICT=EHICZ
      EHRCT=EHRCZ
      EVECT=EVECZ
      EVICT=EVICZ
      EVRCT=EVRCZ
      BICT=BICZ
      BRCT=BRCZ
```

```
C
      CURC(K)=CURCZ
      CURU(K)=CURU0
      CURTOT(K)=CURPZ+CURCZ+CURU0
C
   40 CONTINUE
C
   45 CONTINUE
C
C     ADD IN THE DIPOLE CONTRIBUTION TO THE FIELDS
C
      EHEP(K)=EHEP(K)+EHEPZ
      EHIP(K)=EHIP(K)+EHIPZ
      EHRP(K)=EHRP(K)+EHRPZ
      EVEP(K)=EVEP(K)+EVEPZ
      EVIP(K)=EVIP(K)+EVIPZ
      EVRP(K)=EVRP(K)+EVRPZ
      BIP(K)=BIP(K)+BIPZ
      BRP(K)=BRP(K)+BRPZ
C
      EHEC(K)=EHEC(K)+EHECZ
      EHIC(K)=EHIC(K)+EHICZ
      EHRC(K)=EHRC(K)+EHRCZ
      EVEC(K)=EVEC(K)+EVECZ
      EVIC(K)=EVIC(K)+EVICZ
      EVRC(K)=EVRC(K)+EVRCZ
      BIC(K)=BIC(K)+BICZ
      BRC(K)=BRC(K)+BRCZ
C
      Z=ZSTEP*FLOAT(J)
      IF(IMAGE) Z=-Z
      ZAZ=ZA-Z
      ZAZSQ=ZAZ*ZAZ
      RSQ=DSQ+ZAZSQ
      R=(RSQ)**0.5
      A1=D*ZAZ
      A2=2.0*ZAZSQ-DSQ
      R3=RSQ*R
      CR4=C*R*R3
      C2R3=CSQ*R3
      R5=R3*RSQ
      IF (IMAGE) Z=-Z
      DIFF=Z/V+R/C
      DIFFC=TCN+(R-Z)/C
      H14=EXP(-Z/LAMBDA)
C
      IF (T.LE.DIFF) GO TO 60
C
```

```
   50   CONTINUE
C
   60   CONTINUE
C
C
        EHEP(K)=ECONST*(2.0*EHEP(K)-EHEPT-EHEPZ)
        EHIP(K)=ECONST*(2.0*EHIP(K)-EHIPT-EHIPZ)
        EHRP(K)=ECONST*(2.0*EHRP(K)-EHRPT-EHRPZ)
        EVEP(K)=ECONST*(2.0*EVEP(K)-EVEPT-EVEPZ)
        EVIP(K)=ECONST*(2.0*EVIP(K)-EVIPT-EVIPZ)
        EVRP(K)=ECONST*(2.0*EVRP(K)-EVRPT-EVRPZ)
        BIP(K)=BCONST*(2.0*BIP(K)-BIPT-BIPZ)
        BRP(K)=BCONST*(2.0*BRP(K)-BRPT-BRPZ)
C
        EHEC(K)=ECONST*(2.0*EHEC(K)-EHECT-EHECZ)
        EHIC(K)=ECONST*(2.0*EHIC(K)-EHICT-EHICZ)
        EHRC(K)=ECONST*(2.0*EHRC(K)-EHRCT-EHRCZ)
        EVEC(K)=ECONST*(2.0*EVEC(K)-EVECT-EVECZ)
        EVIC(K)=ECONST*(2.0*EVIC(K)-EVICT-EVICZ)
        EVRC(K)=ECONST*(2.0*EVRC(K)-EVRCT-EVRCZ)
        BIC(K)=BCONST*(2.0*BIC(K)-BICT-BICZ)
        BRC(K)=BCONST*(2.0*BRC(K)-BRCT-BRCZ)
C
        EHEU(K)=0.5*HEHU*TTEST
        EVEU(K)=0.5*HEVU*TTEST
        EHIU(K)=0.5*HIHU
        EVIU(K)=0.5*HIVU
        BIU(K)=0.5*HIBU
C
        IF (IMAGE) GO TO 77
C
C       STORE CONTRIBUTIONS DUE TO THE REAL CHANNEL
C
        EHEPR(K)=EHEP(K)
        EHIPR(K)=EHIP(K)
        EHRPR(K)=EHRP(K)
        EVEPR(K)=EVEP(K)
        EVIPR(K)=EVIP(K)
        EVRPR(K)=EVRP(K)
        BIPR(K)=BIP(K)
        BRPR(K)=BRP(K)
C
        EHECR(K)=EHEC(K)
        EHICR(K)=EHIC(K)
        EHRCR(K)=EHRC(K)
        EVECR(K)=EVEC(K)
        EVICR(K)=EVIC(K)
        EVRCR(K)=EVRC(K)
```

```
      BICR(K)=BIC(K)
      BRCR(K)=BRC(K)
C
      EHEUR(K)=EHEU(K)
      EHIUR(K)=EHIU(K)
      EVEUR(K)=EVEU(K)
      EVIUR(K)=EVIU(K)
      BIUR(K)=BIU(K)
C
   70 CONTINUE
C
      EVTOT=EVEP(K)+EVIP(K)+EVRP(K)+EVEC(K)+EVIC(K)+EVRC(K)+
     1      EVEU(K)+EVIU(K)
      AESEV=ABS(EVTOT)
      IF(ABSEV.GT.MAXAE) MAXAE=ABSEV
      CHECK=ABS((EVTOT-PEVTOT)/MAXAE)
      TSTEP=TSTEP*1.1
      IF(CHECK.GT.0.05) TSTEP=TSTEP*0.5
      IF(TSTEP.LT.MINDT) TSTEP=MINDT
      IF(TSTEP.GT.MAXDT) TSTEP=MAXDT
      PEVTOT=EVTOT
      KK=K+1
      TIME(KK)=TIME(K)+TSTEP
      DT(KK)=TSTEP
C
   77 K=K+1
   90 CONTINUE
C
  100 CONTINUE
C
      IF(.NOT.IMAGE) KSTOP=K-1
      IMAGE=.NOT.IMAGE
      IF (IMAGE) TSTEP=MINDT
      IF (IMAGE) GO TO 25
C
C     ADD CONTRIBUTIONS DUE TO THE REAL AND IMAGE CHANNELS
C
      DO 110 K=1,KSTOP
C
      EHEP(K)=EHEP(K)+EHEPR(K)
      EHIP(K)=EHIP(K)+EHIPR(K)
      EHRP(K)=EHRP(K)+EHRPR(K)
      EVEP(K)=EVEP(K)+EVEPR(K)
      EVIP(K)=EVIP(K)+EVIPR(K)
      EVRP(K)=EVRP(K)+EVRPR(K)
      BIP(K)=BIP(K)+BIPR(K)
      BRP(K)=BRP(K)+BRPR(K)
C
```

```
      EHEC(K)=EHEC(K)+EHECR(K)
      EHIC(K)=EHIC(K)+EHICR(K)
      EHRC(K)=EHRC(K)+EHRCR(K)
      EVEC(K)=EVEC(K)+EVECR(K)
      EVIC(K)=EVIC(K)+EVICR(K)
      EVRC(K)=EVRC(K)+EVRCR(K)
      BIC(K)=BIC(K)+BICR(K)
      BRC(K)=BRC(K)+BRCR(K)
C
      EHEU(K)=EHEU(K)+EHEUR(K)
      EHIU(K)=EHIU(K)+EHIUR(K)
      EVEU(K)=EVEU(K)+EVEUR(K)
      EVIU(K)=EVIU(K)+EVIUR(K)
      BIU(K)=BIU(K)+BIUR(K)
C
  110 CONTINUE
C
      DO 120 K=1,KSTOP
C
      EHP(K)=EHEP(K)+EHIP(K)+EHRP(K)
      EVP(K)=EVEP(K)+EVIP(K)+EVRP(K)
      BP(K)=BIP(K)+BRP(K)
C
      EHC(K)=EHEC(K)+EHIC(K)+EHRC(K)
      EVC(K)=EVEC(K)+EVIC(K)+EVRC(K)
      BC(K)=BIC(K)+BRC(K)
C
      EHU(K)=EHEU(K)+EHIU(K)
      EVU(K)=EVEU(K)+EVIU(K)
      BU(K)=BIU(K)
C
      EH(K)=EHP(K)+EHC(K)+EHU(K)
      EV(K)=EVP(K)+EVC(K)+EVU(K)
      B(K)=BP(K)+BC(K)+BU(K)
C
  120 CONTINUE
C
C     SELECT LONG OR SHORT PRINTED OUTPUT
C
      GO TO (125,140),IOUTPT
  125 KSTA=1
      DO 130 J=1,300
      KSTP=KSTA+2
      IF(KSTP.GT.KSTOP) KSTP=KSTOP
      WRITE(6,500)
      WRITE(6,501)(TIME(K),EHEP(K),EHIP(K),EHRP(K),EHP(K),EHEC(K),
     1      EHIC(K),EHRC(K),EHC(K),EHEU(K),EHIU(K),EHU(K),EH(K),EVEP(K)
     2      ,EVIP(K),EVRP(K),EVP(K),EVEC(K),EVIC(K),EVRC(K),EVC(K),
```

```
     3      EVEU(K),EVIU(K),EVU(K),EV(K),BIP(K),BRP(K),BP(K),BIC(K),
     4      ERC(K),BC(K),BIU(K),BU(K),B(K),CURP(K),CURC(K),CURU(K),
     5      CURTOT(K),K=KSTA,KSTP)
       IF(KSTP.EQ.KSTOP) GO TO 135
       KSTA=KSTP+1
 130   CONTINUE
 135   CONTINUE
       GO TO 145
 140   WRITE(6,508)
       WRITE(6,509)(TIME(K),EH(K),EV(K),B(K),CURTOT(K),K=1,KSTOP)
 145   CONTINUE
C
C      SUPPRESS PLOT IF TLEN IS LE 0.0
C
       IF (TLEN.LE.0.0) GO TO 160
       CALL RTMPLT
 160   CONTINUE
C
       STOP
       END
       SUBROUTINE RTMPLT
C
C                          TIME DOMAIN PLOT
C      THIS SUBROUTINE PLOTS OUT THE RESULTS ON THE GOULD ELECTROSTATIC
C      PLOTTER.  FOUR PLOTS ARE GENERATED BY EACH CALL TO THIS ROUTINE.
C      THE HORIZONTAL AND THE VERTICAL COMPONENTS OF THE ELECTRIC FIELD,
C      THE MAGNETIC FIELD AND A CURRENT IS PLOTTED.
C      THE CURRENT PLOTTED CORRESPONDS TO THE CURRENT AT GROUND LEVEL
C
       DIMENSION EH(1005),EV(1005),B(1005),ISTEP(1005),TIME(1005)
       REAL ISTEP
       COMMON EH,EV,B,ISTEP,TIME,TLEN,NSTEP
C
       NSTEP1=NSTEP+1
       NSTEP2=NSTEP+2
       CALL PLOTS (-100.0,-20.0,2,1,1.0,1.0)
       CALL SCALE(TIME,TLEN,NSTEP,1)
       CALL SCALE(EH,5.0,NSTEP,1)
       CALL AXIS(0.0,0.0,'TIME IN SECONDS',-15,TLEN,0.0,TIME(NSTEP1),
      * TIME(NSTEP2))
       CALL AXIS(0.0,0.0,'HORIZONTAL ELECTRIC FIELD - IN V/M',34,5.0,90.,
      * EH(NSTEP1),EH(NSTEP2))
       CALL LINE (TIME,EH,NSTEP,1,0,0)
C
       CALL PLOT(0.0,6.0,-3)
       CALL SCALE(EV,5.0,NSTEP,1)
       CALL AXIS(0.0,0.0,'TIME IN SECONDS',-15,TLEN,0.0,TIME(NSTEP1),
      * TIME(NSTEP2))
```

```
      CALL AXIS(0.0,0.0,'VERTICAL ELECTRIC FIELD - IN V/M',32,5.0,90.0,
     * EV(NSTEP1),EV(NSTEP2))
      CALL LINE(TIME,EV,NSTEP,1,0,0)
C
      TT=TLEN+1.0
      CALL PLOT(TT,-6.0,-3)
      CALL SCALE(B,5.0,NSTEP,1)
      CALL AXIS(0.0,0.0,'TIME IN SECONDS',-15,TLEN,0.0,TIME(NSTEP1),
     * TIME(NSTEP2))
      CALL AXIS (0.0,0.0,'MAGNETIC FIELD - IN T',21,5.0,90.0,
     * B(NSTEP1),B(NSTEP2))
      CALL LINE(TIME,B,NSTEP,1,0,0)
C
      CALL PLOT(0.0,6.0,-3)
      CALL SCALE(ISTEP,5.0,NSTEP,1)
      CALL AXIS(0.0,0.0,'TIME IN SECONDS',-15,TLEN,0.0,TIME(NSTEP1),
     * TIME(NSTEP2))
      CALL AXIS(0.0,0.0,'CURRENT - IN AMPS',17,5.0,90.0,
     * ISTEP(NSTEP1),ISTEP(NSTEP2))
      CALL LINE(TIME,ISTEP,NSTEP,1,0,0)
C
      CALL PLOT(0.0,0.0,999)
C
      RETURN
      END
```

C.2 Parameters of Lossless Transmission Lines

The following is a FORTRAN listing of a computer program which can be used to determine the inductance and capacitance matrices for any overhead transmission line. The program allows lines with multiple phases, multiple conductors per phase (bundling) and multiple skywires.

```
C
C     PROGRAM TO COMPUTE THE INDUCTANCE AND CAPACITANCE
C     MATRICES FOR A LOSSLESS TRANSMISSION LINE HAVING
C           NPHASE - PHASES
C           NBUND  - NUMBER OF CONDUCTORS PER PHASE
C     AND   NSKY   - NUMBER OF SKY WIRES.
C     THE INPUT CONSISTS OF THE (X,Y) COORDINATES OF EACH
C     CONDUCTOR AND THE RADIUS OF EACH CONDUCTOR.
C     ALL INPUT IS IN THE SI SYSTEM OF UNITS.
C     CONDUCTOR INPUT ORDER IS ILLUSTRATED BELOW:
C
C                           7             8
C                           *             *
C
C                     * *           * *           * *
C                     1 4           2 5           3 6
C
C                  -- WRITTEN BY  MANECK J MASTER --
C                        -- OCTOBER 1980 --
C
      DIMENSION L(12,12),L12(9,9),L21(9,9),L22(12,12),
     1          A(9,9),B(9,9),B22(12,12),P(12,12),
     2          C(12,12),X(12),Y(12),R0(12)
      REAL LCONST,L,L12,L21,L22
C
      READ (5,500) NPHASE,NBUND,NSKY
      NTOT=NPHASE*NBUND+NSKY
      NREM=NTOT-NPHASE
      NPC=NPHASE*NBUND
      NS=NPC+1
      READ (5,501) (X(I),Y(I),R0(I),I=1,NTOT)
      IF(NSKY.LE.0) R0(NS)=0.0
C
      CVEL=3.0E+08
      CSQ=CVEL*CVEL
      LCONST=2.0E-07
C
      WRITE(6,209) R0(1),R0(NS)
      DO 7 I=1,NPHASE
    7 WRITE(6,206) I,(X(J),Y(J),J=I,NPC,NPHASE)
      IF(NSKY.GT.0.0) WRITE(6,208) (X(I),Y(I),I=NS,NSKY)
      WRITE(6,210) NPC,NSKY
C
      DO 10 I=1,NTOT
      J=I
      L(I,J)=LCONST*ALOG((2.0*Y(I))/R0(I))
```

```
 10   CONTINUE
C
      DO 20 I=2,NTOT
      JSTOP=I-1
      DO 20 J=1,JSTOP
      XDSQ=(X(I)-X(J))**2
      DIJM=((Y(I)+Y(J))**2+XDSQ)**0.5
      DIJ=((Y(I)-Y(J))**2+XDSQ)**0.5
      L(I,J)=LCONST*ALOG(DIJM/DIJ)
      L(J,I)=L(I,J)
 20   CONTINUE
C
      DO 22 I=1,NTOT
      DO 22 J=1,NTOT
 22   P(I,J)=CSQ*L(I,J)
C
      WRITE(6,201) NTOT
      DO 30 I=1,NTOT
 30   WRITE (6,200) (L(I,J),J=1,NTOT)
      WRITE(6,202) NTOT
      DO 32 I=1,NTOT
 32   WRITE(6,200) (P(I,J),J=1,NTOT)
C
      IF (NBUND.LE.1) GO TO 55
C
      DO 40 M=2,NBUND
      NPH=NPHASE*(NBUND-1)
      DO 40 K=1,NPHASE
      DO 40 I=1,NTOT
      J=K+NPH
 40   L(I,J)=L(I,J)-L(I,K)
C
      DO 50 M=2,NBUND
      NPH=NPHASE*(NBUND-1)
      DO 50 K=1,NPHASE
      DO 50 J=1,NTOT
      I=K+NPH
 50   L(I,J)=L(I,J)-L(K,J)
C
 55   CONTINUE
C
      IF (NREM.LE.0) GO TO 91
      DO 60 I=1,NPHASE
      DO 60 J=1,NREM
 60   L12(I,J)=L(I,J+NPHASE)
C
      DO 70 I=1,NREM
      DO 70 J=1,NPHASE
```

```
   70   L21(I,J)=L(I+NPHASE,J)
C
        DO 80 I=1,NREM
        DO 80 J=1,NREM
   80   L22(I,J)=L(I+NPHASE,J+NPHASE)
C
C       COMPUTE INVERSE OF L22
C
        CALL MINV(L22,B22,NREM)
C
        DO 82 I=1,NREM
        DO 82 J=1,NPHASE
   82   A(I,J)=0.0
        DO 83 I=1,NREM
        DO 83 J=1,NPHASE
        DO 83 K=1,NREM
   83   A(I,J)=A(I,J)+B22(I,K)*L21(K,J)
C
        DO 85 I=1,NPHASE
        DO 85 J=1,NPHASE
   85   B(I,J)=0.0
        DO 86 I=1,NPHASE
        DO 86 J=1,NPHASE
        DO 86 K=1,NREM
   86   B(I,J)=B(I,J)+L12(I,K)*A(K,J)
C
        DO 90 I=1,NPHASE
        DO 90 J=1,NPHASE
   90   L(I,J)=L(I,J)-B(I,J)
C
   91   CONTINUE
C
        WRITE(6,203) NPHASE
        DO 94 I=1,NPHASE
   94   WRITE(6,207) (L(I,J),J=1,NPHASE)
C
        DO 95 I=1,NPHASE
        DO 95 J=1,NPHASE
   95   P(I,J)=CSQ*L(I,J)
        WRITE(6,204) NPHASE
        DO 96 I=1,NPHASE
   96   WRITE(6,207) (P(I,J),J=1,NPHASE)
C
        CALL MINV(P,C,NPHASE)
        WRITE(6,205) NPHASE
        DO 97 I=1,NPHASE
   97   WRITE(6,207) (C(I,J),J=1,NPHASE)
C
```

```
  500  FORMAT (3I5)
  501  FORMAT (3F10.2)
C
  200  FORMAT (/,2X,1PE10.3,10E12.3)
  201  FORMAT('1',//,5X,'THE INDUCTANCE MATRIX FOR THE ',I2,
     1       ' CONDUCTOR SYSTEM IS  (IN HENRYS/METRE) ',/)
  202  FORMAT('1',//,5X,'THE POTENTIAL COEFFICIENT MATRIX ',
     1  'FOR THE ',I2,' CONDUCTOR SYSTEM IS ',/)
  203  FORMAT('1',//,5X,'THE INDUCTANCE MATRIX FOR THE ',I2,
     1  ' PHASE EQUIVALENT SYSTEM IS  (IN HENRYS/METRE) ',/)
  204  FORMAT(///,5X,'THE POTENTIAL COEFFICIENT MATRIX FOR ',
     1  'THE ',I2,' PHASE EQUIVALENT SYSTEM IS ',/)
  205  FORMAT(///,5X,'THE CAPACITANCE MATRIX FOR THE ',I2,
     1  ' PHASE EQUIVALENT SYSTEM IS  (IN FARADS/METRE) ',/)
  206  FORMAT(//,20X,'PHASE ',I2,' COORDINATES (X,Y) ARE',
     1       //,22X,1PE12.3,E12.3,5(/,22X,2E12.3))
  207  FORMAT(/,15X,1PE12.4,4E13.4)
  208  FORMAT(//,20X,'SKYWIRE COORDINATES (X,Y) ARE',//,22X,
     1       1PE12.3,4E12.3)
  209  FORMAT('1',//,20X,'ALL VALUES GIVEN BELOW ARE IN ',
     1  'METERS',///,20X,'THE WIRE RADII ARE',/,21X,
     2  'PHASE WIRE : ',F9.5,/,21X,'SKYWIRE : ',F9.5)
  210  FORMAT(///,20X,'THE TOTAL NUMBER OF PHASE  ',I3,
     1  ' IS = ',20X,'THE TOTAL NUMBER OF SKY WIRES IS = ',I3)
C
      STOP
      END
      SUBROUTINE MINV(G,GIN,NK)
C
C     INVERTS A GIVEN MATRIX BY GAUSS ELIMINATION WITH
C     PIVOTING
C
      DIMENSION A(12,12),LT(12)
      DIMENSION G(NK,NK),GIN(NK,NK)
      DO 10 I=1,NK
      DO 10 J=1,NK
   10  A(I,J)=G(I,J)
      DO 20 J=1,NK
   20 LT(J)=0
      R=0.0
      DO 110 M=1,NK
      DO 50 L=1,NK
      IF(LT(L)-1)30,50,30
   30 IF(ABS(A(L,L))-ABS(R))50,50,40
   40 R=A(L,L)
      K=L
   50 CONTINUE
      R=0.0
```

```
      LT(K)=1
      DO 90 I=1,NK
      IF(I-K)60,90,60
   60 DO 80 J=1,NK
      IF(J-K)70,80,70
   70 A(I,J)=A(I,J)-A(I,K)*A(K,J)/A(K,K)
   80 CONTINUE
   90 CONTINUE
      A(K,K)=-1/A(K,K)
      DO 110 I=1,NK
      IF(I-K)100,110,100
  100 A(I,K)=A(I,K)*A(K,K)
      A(K,I)=A(K,I)*A(K,K)
  110 CONTINUE
      DO 120 J=1,NK
      DO 120 K=1,NK
  120 GIN(J,K)=-A(J,K)
      RETURN
      END
```

C.3 Wavetilt Program

The following FORTRAN listing is for a program written to compute the horizontal electric field from the vertical electric field using the wavetilt formulation described in Chapter III. The user specifies a piecewise linear version of the vertical electric field, and the soil parameters σ and ε_r. The computation time step and the total time of interest are also specified. The vertical and horizontal fields are plotted on the Gould plotter as output. The vertical and horizontal electric fields as a function of time are written onto a disk file to be used in the coupling program listed in the next section.

```
C
C       PROGRAM TO COMPUTE HORT E FROM VERT E
C       EH(W)/EV(W) = 1 / (EPSR+(SIGMA/(J*W*EPS0))) = F(W)
C       EV(T) IS DECOMPOSED INTO PIECEWISE LINEAR RAMPS
C       RAMP RESPONSE OF F(W) IS CALCULATED AND
C       EH(T) IS THEN OBTAINED BY DIRECT TIME-DOMAIN PRODUCT
C
C               MANECK  J  MASTER  -  JUNE 1982
C
        COMMEN N,NSTOP,SLP(50),T(50),EV(50),TOUT(2100),
       *       EVOUT(2100),EHOUT(2100)
C
        READ(5,911) N
  911   FORMAT(I3)
        READ(5,900) (T(I),EV(I),I=1,N)
  900   FORMAT(2F6.0)
        DO 5 I=1,N
    5   T(I)=T(I)*1.0E-06
C
        TSTEP=0.5E-07
    .   TSTOP=50.0E-06
        NSTOP=TSTOP/TSTEP+0.5
        TTT=0.0
C
        N1=N-1
        DO 10 I=1,N1
   10   SLP(I)=(EV(I+1)-EV(I))/(T(I+1)-T(I))
        WRITE(6,510) (I,T(I),EV(I),SLP(I),I=1,N)
  510   FORMAT(1X,I5,3E15.5)
C
        DO 30 I=1,NSTOP
        B=0.0
           DO 20 J=1,N
           IF(TTT.LT.T(J)) GO TO 25
           CALL FUN(TTT,J,A)
           B=B+A
   20      CONTINUE
   25   CONTINUE
        TOUT(I)=TTT
        EHOUT(I)=B
        TTT=TTT+TSTEP
   30   CONTINUE
        CALL EQSP
  500   FORMAT(I5,3E15.6)
        WRITE(18,500)(I,TOUT(I),EVOUT(I),EHOUT(I),I=1,NSTOP)
        EVOUT(1)=-0.1
```

```
      EHOUT(1)=0.1
      CALL DOTPLT(TOUT,EVOUT,1000,0,'TIME',4,'EV',2)
      CALL DOTPLT(TOUT,EHOUT,1000,0,'TIME',4,'EH',2)
C
      STOP
      END
      SUBROUTINE FUN(TTT,J,A)
C
      COMMON N,NSTOP,SLP(50),T(50),EV(50),TOUT(2100),
     *       EVOUT(2100),EHOUT(2100)
      REAL MMBSI0,MMBSI1
C
      EPSR=16.0
      EPS0=8.854E-12
      SIGMA=1.0E-02
      Q9=SQRT(1.0/EPSR)
      Q1=SIGMA/(2.0*EPS0*EPSR)
      TT=TTT-T(J)
      Q2=Q1*TT
      Q3=MMBSI0(2,Q2,IER1)
      Q4=MMBSI1(2,Q2,IER2)
C
      A=SLP(J)*TT*(Q3+Q4)
      IF(J.GE.2) A=(SLP(J)-SLP(J-1))*TT*(Q3+Q4)
      IF(J.EQ.N) A=-(TT*SLP(N-1)+EV(N))*Q3-SLP(N-1)*TT*Q4
C
      A=(-A)*Q9
C
      RETURN
      END
      SUBROUTINE EQSP
      COMMON N,NSTOP,SLP(50),X(50),Y(50),A(2100),B(2100),
     *       EHOUT(2100)
C
      XMIN=0.5E-07
C
      A(1)=X(1)
      B(1)=Y(1)
      REM = 0.0
      N2 = 1
C
      DO 30 I = 2,N
      N1 = N2 + 1
      XINT = X(I) - X(I-1)
      N2=(XINT+REM)/XMIN
      N2 = N1 + N2 - 1
      SLOPEY = SLP(I-1)
      WRITE(6,500) I,N1,N2,X(I),Y(I),REM
```

```
  500 FORMAT(5X,3I10,1PE15.3,2E15.3)
C
      IF(N2.GT.1000) N2=1000
      DO 20 J = N1,N2
      ALAST = A(J-1) + XMIN
      A(J)=ALAST
      B(J) = Y(I-1) + ( ALAST - X(I-1) ) * SLOPEY
   20 CONTINUE
      REM=X(I)-ALAST
   30 CONTINUE
C
      RETURN
      END
```

C.4 Coupling Program

The following is a FORTRAN listing of the program used to determine the voltages and currents induced on overhead lines by nearby lightning. The inductance and capacitance parameters are specified as obtained from the program listed in Section C.2. The program allows parallel R-C termination at either end. The coordinates of the line, the location of the ground strike point, the time step, the number of segments into which the line is split, and the total time for which calculations are desired are all specified as input. The incident fields are read off the disk file generated by the program listed in Section C.3. The output presents the voltage plotted on the Gould plotter as a function of time for any point on the line.

```
C
C      PROGRAM TO COMPUTE TRANSMISSION LINE VOLTAGES
C      GIVEN THE HORZ AND VERT COMPONENTS OF E
C      EFFECT OF MEASUREMENT ACROSS CAPACITOR
C
       DIMENSION VOUT(2,2,400),TIMEV(402),TIMEC(402),VPT(402)
      *          ,V(2,400),CUR(2,400),C(2,2),L(2,2),CI(2,2),
      *          LI(2,2),G0(2,2),GL(2,2),Y0(2,2),YL(2,2),
      *          WK1(2),WK2(2),EHOLD(2,400),EVOLD(2,400),
      *          EHNEW(2,400),EVNEW(2,400),R(2,2),WK3(2),
      *          WK4(2),CTER0(2,2),CTERL(2,2)
       REAL L,LI
       COMMON TV,TC,DT,DZ,DFACT
       COMMON A1,A2,ZT0,D,DMIN,CVEL
       COMMON TINC(2100),EHINC(2100),EVINC(2100)
       COMMON EHINC2(2100),EVINC2(2100)
C
       C(1,1)=7.6799E-12
       C(2,2)=7.9399E-12
       C(1,2)=-2.1010E-12
       C(2,1)=C(1,2)
C
       L(1,1)=1.5597E-06
       L(2,2)=1.5086E-06
       L(1,2)=4.1272E-07
       L(2,1)=L(1,2)
C
       R(1,1)=1.0
       R(2,2)=1.0
       R(1,2)=0.0
       R(2,1)=0.0
C
       G0(1,1)=1.0/1.0E+06
       G0(2,2)=1.0/20.0
       G0(1,2)=1.0E-06
       G0(2,1)=1.0E-06
C
       GL(1,1)=1.0/1.0E+06
       GL(2,2)= 1.0/60.0
       GL(1,2)=1.0E-06
       GL(2,1)=1.0E-06
C
       CTER0(1,1)=1.145E-11
       CTER0(1,2)=0.0
       CTER0(2,1)=0.0
       CTER0(2,2)=0.0
```

```
C
      CTERL(1,1)=0.0
      CTERL(1,2)=0.0
      CTERL(2,1)=0.0
      CTERL(2,2)=0.0
C
      NTOT=2
      PII=ACOS(-1.0)
      D=10.0E+03
      ANG=84.0*(PII/180.0)
      ZT0=-150.0
      ZTL=-628.0
      ZLINE=ZT0-ZTL
      NZTOT=27
      TSTOP=50.0E-06
C
      CVEL=3.0E+08
      A1=D*COS(ANG)
      A2=D*SIN(ANG)
      ZFIRST=A1
      IF(A1.GE.ZT0) ZFIRST=ZT0
      IF(A1.LE.ZTL) ZFIRST=ZTL
      A3=A1-ZFIRST
      DMINSQ=A3**2+A2**2
      DMIN=SQRT(DMINSQ)
      TMIN=DMIN/CVEL
C
      NZT1=NZTOT-1
      NZT2=NZTOT-2
      DZ=ZLINE/NZT1
      DT=5.0E-08
      NTTOT=TSTOP/DT
      DTZ=DT/DZ
      HALFDT=DT/2.0
C
      WRITE(6,916) NTOT
      WRITE(6,915) NZTOT,NZT1,NZT2,ZLINE,DZ
      WRITE(6,916) NTTOT,TSTOP,DT,DTZ
  915 FORMAT(5X,3I10,1PE20.5,E20.5)
  916 FORMAT(5X,I10,1PE20.5,3E20.5)
      WRITE(6,940)((L(I,J),J=1,NTOT),I=1,NTOT)
      WRITE(6,940)((C(I,J),J=1,NTOT),I=1,NTOT)
      WRITE(6,940)((G0(I,J),J=1,NTOT),I=1,NTOT)
      WRITE(6,940)((GL(I,J),J=1,NTOT),I=1,NTOT)
  940 FORMAT(5X,1PE15.3,E15.3,/)
C
C     COMPUTE CONSTANTS
C
```

```
      DO 10 I=1,NTOT
      A=0.0
      B=0.0
      BA=0.0
      BB=0.0
      DO 5 J=1,NTOT
      L(I,J)=L(I,J)/DT
      C(I,J)=C(I,J)/DT
      Y0(I,J)=(-4.0/3.0)*DTZ*G0(I,J)
      YL(I,J)=(-4.0/3.0)*DTZ*GL(I,J)
      A=A+G0(I,J)
      B=B+GL(I,J)
      BA=BA+CTER0(1,J)
      BB=BB+CTERL(I,J)
      CTER0(I,J)=(-8.0/3.0)*(CTER0(I,J)/DZ)
      CTERL(I,J)=(-8.0/3.0)*(CTERL(I,J)/DZ)
    5 CONTINUE
      Y0(I,I)=(4.0/3.0)*DTZ*A
      YL(I,I)=(4.0/3.0)*DTZ*B
      CTER0(I,I)=(8.0/3.0)*(BA/DZ)
      CTERL(I,I)=(8.0/3.0)*(BB/DZ)
   10 CONTINUE
      WRITE(6,940)((Y0(I,J),J=1,NTOT),I=1,NTOT)
      WRITE(6,940)((YL(I,J),J=1,NTOT),I=1,NTOT)
      WRITE(6,940)((CTER0(I,J),J=1,NTOT),I=1,NTOT)
      WRITE(6,940)((CTERL(I,J),J=1,NTOT),I=1,NTOT)
C
      CALL MINV(L,LI,NTOT)
      CALL MINV(C,CI,NTOT)
C
C     DEFINE INDUCING FIELD
C
      READ (18,932)(IJ,TINC(I),EVINC(I),EHINC(I),I=1,1000)
  932 FORMAT(I5,3E15.6)
      DCOR1=1.0
      DO 13 I=1,1000
      EHINC(I)=EHINC(I)*DCOR1
   13 EVINC(I)=EVINC(I)*DCOR1
C
C     INITIALIZE VOLTAGES AND CURRENTS
C
      DO 20 I=1,NTOT
      DO 18 J=1,NZTOT
      V(I,J)=0.0
      CUR(I,J)=0.0
   18 CONTINUE
      TIMEV(I)=0.0
      TIMEC(I)=0.0
```

```
      VPT(I)=0.0
   20 CONTINUE
C
      DO 21 I=1,NTOT
      DO 21 J=1,NZTOT
      EHOLD(I,J)=0.0
      EVOLD(I,J)=0.0
   21 CONTINUE
C
C    BEGIN TIME LOOP
C
      KT=1
      DO 55 KKKK=1,NTTOT
      TV=FLOAT(KKKK-1)*DT
      TC=TV+HALFDT
C
C     COMPUTE FORCING FUNCTIONS
C
      DO 24 I=1,NTOT
      DO 22 J=1,NZT1
      EHNEW(I,J)=EHS(I,J)
   22 CONTINUE
      EVNEW(I,1)=EVS(I,1)
      EVNEW(I,NZTOT)=EVS(I,NZTOT)
   24 CONTINUE
C
C     COMPUTE CURRENTS AT ALL NODES
C
      DO 35 I=1,NTOT
      DO 35 J=1,NTOT
   35 G0(I,J)=L(I,J)+R(I,J)/2.0
      CALL MINV(G0,GL,NTOT)
C
      DO 50 J=1,NZT1
      DO 45 I=1,NTOT
      WK1(I)=0.0
      DO 40 KK=1,NTOT
   40 WK1(I)=WK1(I)+(L(I,KK)-R(I,KK)/2.0)*CUR(KK,J)
      WK1(I)=WK1(I)+(EHNEW(I,J)+EHOLD(I,J))/2.0
     *              -(V(I,J+1)-V(I,J))/DZ
   45 CONTINUE
C
      DO 48 I=1,NTOT
      WK2(I)=0.0
      DO 47 KK=1,NTOT
   47 WK2(I)=WK2(I)+GL(I,KK)*WK1(KK)
   48 CUR(I,J)=WK2(I)
   50 CONTINUE
```

```
C
C       COMPUTE VOLTAGES AT ALL INTERNAL NODES
C
        DO 70 J=2,NZT1
        DO 70 I=1,NTOT
        A=0.0
        DO 65 KK=1,NTOT
        A=A+CI(I,KK)*((CUR(KK,J-1)-CUR(KK,J))/DZ)
   65   CONTINUE
        V(I,J)=V(I,J)+A
   70   CONTINUE
C
C       COMPUTE VOLTAGES AT LEFT END - V(I,1)
C
        DO 100 I=1,NTOT
        DO 100 J=1,NTOT
        G0(I,J)=C(I,J)*DT+Y0(I,J)+CTER0(I,J)
  100   CONTINUE
        CALL MINV(G0,GL,NTOT)
C
        DO 200 I=1,NTOT
        WK1(I)=0.0
        WK3(I)=0.0
        WK4(I)=0.0
        DO 150 J=1,NTOT
        WK1(I)=WK1(I)+(DT*C(I,J)-Y0(I,J)+CTER0(I,J))*V(J,1)
        WK3(I)=WK3(I)+Y0(I,J)*(EVNEW(J,1)+EVOLD(J,1))
        WK4(I)=WK4(I)+CTER0(I,J)*(EVNEW(J,1)-EVOLD(J,1))
  150   CONTINUE
        WK1(I)=WK1(I)-(DTZ/3.0)*(9.0*CUR(I,1)-CUR(I,2))
       *                -WK3(I)-WK4(I)
  200   CONTINUE
C
        DO 300 I=1,NTOT
        WK2(I)=0.0
        DO 250 J=1,NTOT
        WK2(I)=WK2(I)+GL(I,J)*WK1(J)
  250   CONTINUE
        V(I,1)=WK2(I)
  300   CONTINUE
C
C       COMPUTE VOLTAGES AT RIGHT END - V(I,NZTOT)
C
        DO 400 I=1,NTOT
        DO 400 J=1,NTOT
        G0(I,J)=C(I,J)*DT+YL(I,J)+CTERL(I,J)
  400   CONTINUE
        CALL MINV(G0,GL,NTOT)
```

```
C
      DO 500 I=1,NTOT
      WK1(I)=0.0
      WK3(I)=0.0
      WK4(I)=0.0
      DO 450 J=1,NTOT
      WK1(I)=WK1(I)+(DT*C(I,J)-YL(I,J)+CTERL(I,J))*V(J,NZTOT)
      WK3(I)=WK3(I)+YL(I,J)*(EVNEW(J,NZTOT)+EVOLD(J,NZTOT))
      WK4(I)=WK4(I)+CTERL(I,J)*(EVNEW(J,NZTOT)-EVOLD(J,NZTOT))
  450 CONTINUE
      WK1(I)=WK1(I)+(DTZ/3.0)*(9.0*CUR(I,NZT1)-CUR(I,NZT2))
     *              -WK3(I)-WK4(I)
  500 CONTINUE
C
      DO 600 I=1,NTOT
      WK2(I)=0.0
      DO 550 J=1,NTOT
      WK2(I)=WK2(I)+GL(I,J)*WK1(J)
  550 CONTINUE
      V(I,NZTOT)=WK2(I)
  600 CONTINUE
C
C     SAVE OLD FORCING FUNCTIONS
C
      DO 615 I=1,NTOT
      DO 610 J=1,NZT1
      EHOLD(I,J)=EHNEW(I,J)
      EVOLD(I,J)=EVNEW(I,J)
  610 CONTINUE
      EVOLD(I,NZTOT)=EVNEW(I,NZTOT)
  615 CONTINUE
C
C     STORE VALUES FOR OUTPUT
C
      IF((KKKK/5)*5.NE.KKKK) GO TO 55
      DO 620 I=1,NTOT
      VOUT(I,1,KT)=V(I,1)+EVOLD(I,1)
      VOUT(I,2,KT)=V(I,NZTOT)+EVOLD(I,NZTOT)
  620 CONTINUE
      TIMEV(KT)=TV+DT
      TIMEC(KT)=TV+HALFDT
      VPT(KT)=VOUT(1,1,KT)
      WRITE(6,910) KT,TIMEV(KT),TIMEC(KT),V(1,1),V(2,1),
     *     V(1,NZTOT),V(2,NZTOT),VOUT(1,1,KT),VOUT(2,1,KT),
     *     VOUT(1,2,KT),VOUT(2,2,KT)
      KT=KT+1
C
   55 CONTINUE
```

```
  910 FORMAT(1X,I5,1PE12.3,9E12.3)
      KT=KT-1
      CALL DOTPLT(TIMEV,VPT,KT,0,'TIME',4,'V',1)
      DO 700 I=1,KT
  700 VPT(I)=VOUT(1,2,I)
      CALL DOTPLT(TIMEV,VPT,KT,0,'TIME',4,'V',1)
C
C     END TIME LOOP
C
      STOP
      END
      FUNCTION EHS(I,J)
C
C     FORCING FUNCTION USED IN CURRENT EQUATION -
C     DUE TO THE HORIZONTAL ELECTRIC FIELD
C
      COMMON TV,TC,DT,DZ,DFACT
      COMMON A1,A2,ZT0,D,DMIN,CVEL
      COMMON TINC(2100),EHINC(2100),EVINC(2100)
      COMMON EHINC2(2100),EVINC2(2100)
      EHS=0.0
      FLTJ=FLOAT(J)
      ZT=-DZ*(FLTJ-0.5)+ZT0
      A3=A1-ZT
      DNEWSQ=A3**2+A2**2
      DNEW=SQRT(DNEWSQ)
      TAR=TC-(DNEW-DMIN)/CVEL
      N=TAR/DT+1.1
      IF(N.LT.1) GO TO 10
      ATTN=D/DNEW
      DFACT=A3/DNEW
      EHS=EHINC(N)*DFACT*ATTN
   10 CONTINUE
      RETURN
      END
      FUNCTION EVS(I,J)
C
C     FORCING FUNCTION USED IN TERMINATIONS
C     DUE TO THE VERTICAL ELECTRIC FIELD
C
      COMMON TV,TC,DT,DZ,DFACT
      COMMON A1,A2,ZT0,D,DMIN,CVEL
      COMMON TINC(2100),EHINC(2100),EVINC(2100)
      COMMON EHINC2(2100),EVINC2(2100)
      H1=9.8
      H2=7.6
      EVS=0.0
      ZT=-DZ*FLOAT(J-1)+ZT0
```

```
      A3=A1-ZT
      DNEWSQ=A3**2+A2**2
      DNEW=SQRT(DNEWSQ)
      TAR1=TV-(DNEW-DMIN)/CVEL
      N1=TAR1/DT+1.1
      IF(N1.LT.1) GO TO 10
      ATTN=D/DNEW
      EVS=EVINC(N1)
      EVS=EVS*ATTN
      IF(I.EQ.1) EVS=EVS*(-H1)
      IF(I.EQ.2) EVS=EVS*(-H2)
   10 CONTINUE
      RETURN
      END
      SUBROUTINE MINV(G,GIN,NK)
C
C     INVERTS A GIVEN MATRIX BY GAUSS ELIMINATION WITH
C     PIVOTING
C
      DIMENSION A(12,12),LT(12)
      DIMENSION G(NK,NK),GIN(NK,NK)
      DO 10 I=1,NK
      DO 10 J=1,NK
   10 A(I,J)=G(I,J)
      DO 20 J=1,NK
   20 LT(J)=0
      R=0.0
      DO 110 M=1,NK
      DO 50 L=1,NK
      IF(LT(L)-1)30,50,30
   30 IF(ABS(A(L,L))-ABS(R))50,50,40
   40 R=A(L,L)
      K=L
   50 CONTINUE
      R=0.0
      LT(K)=1
      DO 90 I=1,NK
      IF(I-K)60,90,60
   60 DO 80 J=1,NK
      IF(J-K)70,80,70
   70 A(I,J)=A(I,J)-A(I,K)*A(K,J)/A(K,K)
   80 CONTINUE
   90 CONTINUE
      A(K,K)=-1/A(K,K)
      DO 110 I=1,NK
      IF(I-K)100,110,100
  100 A(I,K)=A(I,K)*A(K,K)
      A(K,I)=A(K,I)*A(K,K)
```

```
110 CONTINUE
    DO 120 J=1,NK
    DO 120 K=1,NK
120 GIN(J,K)=-A(J,K)
    RETURN
    END
```

APPENDIX D

DISTRIBUTION OF PEAK VOLTAGES

In this Appendix we present a distribution of the peak voltages induced on the test-line by first return strokes during a one hour and thirty minute period of run #79220TR57. The storm was primarily to the S-SW of the Mobile Lightning Laboratory (MLL) and in the end moved east. Due to the location of the storm, most of the induced line voltages were of positive polarity. Unfortunately, the TV network was not operating during this period and hence no flashes were located. However, from the records kept in the data book it was clear that during the last half hour the storm moved very close to the MLL. Hence, relatively large voltages were induced on the test-line at that time due to flashes which were much closer to the test-line than any presented in the body of this thesis. In Figure D.1 we present the distribution of the measured voltages. We note that there are induced voltages in excess of 250 kV. Voltages this large do not appear to be reasonable because the line was designed to spark-over at 250 kV. Thus, either the line spark-over gap was improperly set or there was an error in the voltage calibration so that the actual voltages were smaller than the measured values indicated.

Figure D.1. Distribution of first return stroke peak induced voltage on the test-line during run #79220TR57 for times between 184000 UT and 201000 UT.

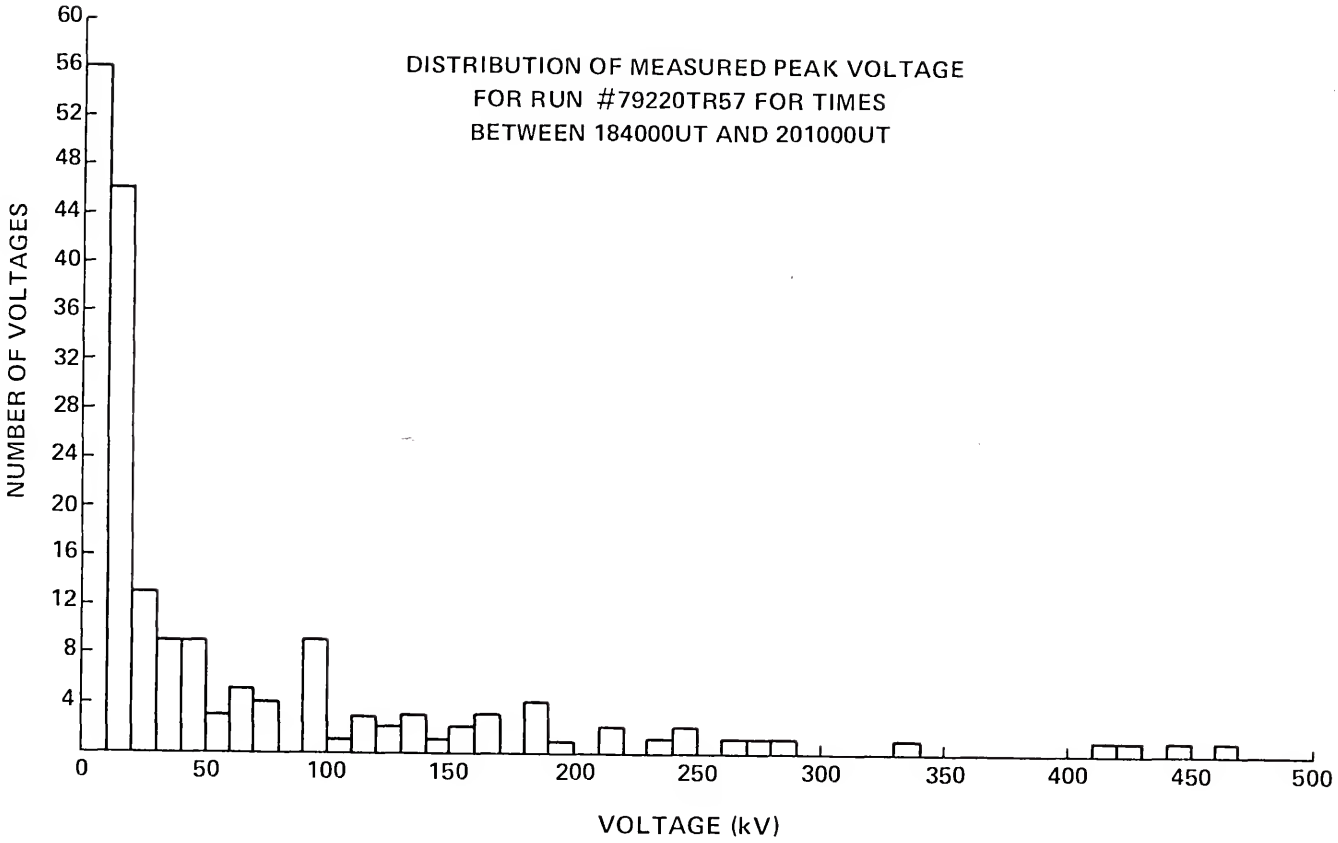
DISTRIBUTION OF MEASURED PEAK VOLTAGE
FOR RUN #79220TR57 FOR TIMES
BETWEEN 184000UT AND 201000UT
NUMBER OF VOLTAGES
60
56
52
48
44
40
36
32
28
24
20
16
12
8
4
0
50
100
150
200
250
300
350
400
450
500
VOLTAGE (kV)

REFERENCES

Abramowitz, M., and I. A. Stegun (Editors), Handbook of Mathematical Functions, Nat. Bur. of Stand., 1968.

Adendorff, G. V., Atmospheric phenomena and their relation to the production of over-voltages in overhead electric transmission lines, Trans. SAIEE, 2, 154-179, August 1911.

Agrawal, A. K., H. J. Price, and S. H. Gurbaxani, Transient response of multiconductor transmission lines excited by a non-uniform electromagnetic field, Trans. IEEE, EMC-22, 119-129, May 1980.

Anderson, R. B., and A. J. Eriksson, A summary of lightning parameters for engineering applications, Electra, 69, 65-102, 1980.

Beasley, W. H., M. A. Uman, and P. L. Rustan, Electric fields preceding cloud-to-ground lightning flashes, J. of Geophys. Res., 87, 4883-4902, 1982.

Berger, K., R. B. Anderson, and H. Kroninger, Parameters of lightning flashes, Electra, 41, 23-27, 1975.

Bewley, L. V., Travelling waves on transmission systems, Trans. AIEE, 50, 532-550, June 1931.

Brantley, R. D., J. A. Tiller, and M. A. Uman, Lightning properties in Florida thunderstorms from video tape records, J. of Geophys. Res., 80, 3402-3406, 1975.

Brook, M., M. Nakano, P. Krehbiel, and T. Takeuti, The electrical structure of the Hokuriku winter thunderstorms, J. of Geophys. Res., 87, 1207-1215, 1982.

Bruce, C. E. R., and R. H. Golde, The lightning discharge, J. of IEE, 88, 487-520, December 1941.

Carson, J. R., Wave propagation in overhead wires with ground return, Bell System Technical Journal, 5, 539-554, 1926.

Chalmers, J. A., Atmospheric Electricity, 2nd Edition, Pergamon Press, Ltd., Oxford, 1967.

Chowdhuri, P., Voltage surges induced on overhead lines by lightning strokes, D. Engg. Thesis, Rensselaer Polytech. Inst., New York, May 1966.

Chowdhuri, P., and E. T. B. Gross, Voltages induced on overhead multiconductor lines by lightning strokes, Proc. IEE, 116, 561-565, April 1969.

Clarence, N. D., and D. J. Malan, Preliminary discharge processes in lightning flashes to ground, Quart. J. of the Roy. Meteor. Soc., 83, 161-172, April 1957.

Cox, J. H., P. H. McAuley, and L. G. Huggins, Klydonograph surge investigations, Trans. AIEE, 46, 315-329, February 1927.

Cox, J. H., and E. Beck, Cathode ray oscillograph studies, Trans. AIEE, 49, 857-865, July 1930.

Dennis, A. S., and E. P. Pierce, The return stroke of the lightning flash to earth as a source of VLF atmospherics, Radio Science J. Res. Nat. Bur. Stand., 68D, 777-794, 1964.

Djebari, B., J. Hamelin, C. Leteinturier, and J. Fontaine, Comparison between experimental measurements of the electromagnetic field emitted by lightning and different theoretical models, Presented at Symposium on Electromagnetic Compatibility, Zurich, 1981.

Eriksson, A. J., and D. V. Meal, Lightning overvoltages in rural distribution line--preliminary results, Trans. SAIEE, 71, 158-163, 1980.

Eriksson, A. J., and D. V. Meal, Lightning performance and overvoltage surge studies on a rural distribution line, Proc. IEE, 129C, 59-69, 1982.

Eriksson, A. J., M. F. Stringfellow, and D. V. Meal, Lightning-induced overvoltages on overhead distribution lines, Trans. IEEE, PAS-101, 960-968, 1982.

Evans, W. H., and R. L. Walker, High speed photographs of lightning at close range, J. of Geophys. Res., 68, 4455-4461, 1963.

Fieux, R. P., C. H. Gary, B. P. Hutzler, A. R. Eybert-Berard, P. L. Hubert, A. C. Meesters, P. H. Perrond, J. G. Hamelin, and J. M. Person, Research on artificially triggered lightning in France, Trans. IEEE, PAS-97, 725-733, 1978.

Fisher, R. J., and M. A. Uman, Measured electric field risetimes for first and subsequent lightning return strokes, J. of Geophys. Res., 77, 399-406, 1972.

Fortescue, C. L., A. L. Asherton, and J. H. Cox, Theoretical and field investigations of lightning, Trans. AIEE, 48, 449-479, April 1929.

Golde, R. H., Lightning surges on overhead distribution lines caused by indirect and direct lightning strokes, Trans. AIEE, 73, 437-447, 1954.

Golde, R. H. (editor), Lightning--Volume 1 (Physics of Lightning), Academic Press, Inc., London, 1977a.

Golde, R. H. (editor), Lightning--Volume 2 (Lightning Protection), Academic Press, Inc., London, 1977b.

Griscom, S. B., The prestrike theory and other effects in the lightning stroke, Trans. AIEE, 77, 919-933, 1958.

Griscom, S. B., J. W. Skooglund, and A. R. Hileman, The influence of the prestrike on transmission-line lightning performance, Trans. AIEE, 77, 933-941, 1958.

Hamelin, J., B. Djebari, R. Barreau, and J. Fontaine, Electromagnetic field resulting from a lightning discharge, surges induced on overhead lines, mathematical model, Presented at the Symposium of Electromagnetic Compatibility, Rotterdam, May 1979.

Hill, R. D., Electromagnetic radiation from erratic paths of lightning strokes, J. of Geophys. Res., 74, 1922-1929, 1969.

Huzita, A., and T. Ogawa, Charge distribution in the average thunderstorm cloud, J. of the Meteor. Soc. of Japan, 54, 284-288, 1976.

Kitagawa, N., M. Brook, and E. J. Workman, Continuing currents in cloud-to-ground lightning discharges, J. of Geophys. Res., 67, 637-647, 1962.

Koga, H., T. Motomitsu, and M. Taguchi, Lightning surge waves induced in transmission lines, Review of the Electrical Communication Laboratory, 29, 797-810, 1981.

Krider, E. P., and G. J. Radda, Radiation field waveforms produced by lightning stepped leaders, J. of Geophys. Res., 80, 2653-2657, 1975.

Krider, E. P., C. D. Weidman, and R. C. Noggle, The electric fields produced by lightning stepped leaders, J. of Geophys. Res., 82, 951-959, 1977.

Latham, J., The electrification of thunderstorms, Quart. J. of Roy. Meteor. Soc., 107, 277-298, 1981.

Lax, P. D., Differential equations, difference equations, and matrix theory, Comm. on Pure and Appl. Math., 11, 175-194, 1958.

Leteinturier, C., B. Djebari, J. Hamelin, and J. Fontaine, Electromagnetic field emitted by lightning stroke, Presented at Symposium on Electromagnetic Compatibility, Wroclaw, 1980.

Lewis, W. W., and C. M. Foust, Lightning investigation on transmission lines--VII, Trans. AIEE, 49, 917-948, July 1930.

Lin, Y. T., Lightning return stroke models, Ph.D. dissertation, University of Florida, 1978.

Lin, Y. T., and M. A. Uman, Electric radiation fields of lightning return strokes in three isolated Florida thunderstorms, J. of Geophys. Res., 78, 7911-7915, 1973.

Lin, Y. T., M. A. Uman, J. A. Tiller, R. D. Brantley, W. H. Beasley, E. P. Krider, and C. D. Weidman, Characterization of lightning return stroke electric and magnetic fields from simultaneous two-station measurements, J. of Geophys. Res., 84, 6307-6314, 1979.

Lin, Y. T., M. A. Uman, and R. B. Standler, Lightning return stroke models, J. of Geophys. Res., 85, 1571-1583, 1980.

Little, P. F., Transmission line representation of a lightning return stroke, J. Phys. D, 11, 1893-1910, 1978.

Livingston, J. M., and E. P. Krider, Electric fields produced by Florida thunderstorms, J. of Geophys. Res., 83, 385-401, 1978.

Lundholm, R., Induced overvoltage surges on transmission lines and their bearing on the lightning performance on medium voltage networks, Trans. Chalmers Univ. of Tech., No. 188, Gothenburg, Sweden, 1957.

Malan, D. J., Physics of Lightning, The English Universities Press, Ltd., London, 1963.

Magono, C., Thunderstorms, Elsevier, New York, 1980.

Master, M. J., M. A. Uman, Y. T. Lin, and R. B. Standler, Calculations of lightning return stroke electric and magnetic fields above ground, J. of Geophys. Res., 86, 12,127 - 12,132, 1981.

McCann, G. D., The measurement of lightning currents in direct strokes, Trans. AIEE, 63, 1157-1164, 1944.

McDonald, T. B., M. A. Uman, J. A. Tiller, and W. H. Beasley, Lightning location and lower-ionospheric height determination from two-station magnetic field measurements, J. of Geophys. Res., 84, 1727-1734, 1979.

Norton, K. A., Propagation of radio waves over a plane earth, Nature, 135, 954-955, 1935.

Norton, K. A., Propagation of radio waves over the surface of the earth and in the upper atmosphere-Part I, Proc. IRE, 24, 1367-1387, 1936.

Norton, K. A., Propagation of radio waves over the surface of the earth and in the upper atmosphere-Part II, Proc. IRE, 25, 1203-1236, 1937.

Owa, G., Study of induced lightning surges and their frequency of occurrence, Elec. Engg. in Japan, 84, 44-55, December 1964.

Peek, F. W., Lightning, Trans. AIEE, 50, 1077-1089, September 1931.

Perala, R. A., Excitation functions for multiconductor transmission lines illuminated by non-uniform electromagnetic fields, Report AMRC-R-24, Mission Research Corporation, Alburquerque, New Mexico, June 1974.

Perry, F. R., The measurement of lightning voltages and currents in South Africa and Nigeria, 1935 to 1937, J. of IEE, 88, 69-86, 1941.

Perry, F. R., G. H. Webster, and P. W. Baguley, The measurement of lightning voltages and currents in Nigeria, 1939-1939, J. of IEE, 89, 185-203, 1942.

Pierce, E. T., Latitudinal variation of lightning parameters, J. of Appl. Meteor., 9, 194-195, 1970.

Prentice, S. A., and D. Mackerras, The ratio of cloud to cloud-to-ground lightning flashes in thunderstorms, J. of Appl. Meteor., 16, 545-550, 1977.

Price, G. H., and E. T. Pierce, The modeling of channel current in the lightning return stroke, Radio Science, 12, 381-388, 1977.

Putzer, E. J., Matrix formulation and solution of the driven transmission line equations, American Nucleonics Corp., Glendale, California, Report ANC TM30-49, January 1968.

Rendell, E. F., and H. D. Gaff, An anaylsis of the lightning faulting characteristics of the 132 kV lines of the Victoria Falls and Transvaal Power Company Ltd., Trans. SAIEE, 24, 258-276, November 1933.

Rusck, S., Induced lightning over-voltages on power transmission lines with special reference to the overvoltage protection of low-voltage networks, Trans. Roy. Inst. of Tech., No. 120, Stockholm, Sweden, 1958.

Rustan, P. L., M. A. Uman, D. G. Childers, W. H. Beasley, and C. L. Lennon, J. of Geophys. Res., 85, 4893-4903, 1980.

Schonland, B. F. J., The lightning discharge, Handbuch der Physik, 22, 576-628, Springer-Verlag, Berlin, 1956.

Schonland, B. F. J., D. J. Malan, and H. Collens, Progressive lightning-II, Proc. Roy. Soc. (London), A152, 595-625, 1935.

Serhan, G. I., M. A. Uman, D. G. Childers, and Y. T. Lin, The RF spectra of first and subsequent lightning return strokes in the 1 to 200 km range, Radio Science, 15, 1089-1094, 1980.

Simpson, C. G., and F. J. Scrase, The distribution of electricity in thunderclouds, Proc. Roy Soc. (London), A161, 309-352, 1937.

Singarajah, C., Surges induced on overhead transmission lines by indirect lightning strokes, with particular reference to Nigeria, Ph.D. Thesis, Univ. of London, September 1971.

Smith, A. A., A more convenient form of the equations for the response of a transmission line excited by non-uniform fields, Trans. IEEE, EMC-15, 151-152, August 1973.

Smith, A. A., Coupling of External Electromagnetic Fields to Transmission Lines, John Wiley and Sons, Inc., 1977.

Sommerfeld, A., Ann. der Phys., 28, 665, 1909.

Sommerfeld, A., Ann. der Phys., 81, 1135, 1926.

Stratton, J. A., Electromagnetic Theory, McGraw-Hill, New York, 1941.

Strawe, D. F., Non-linear modeling of lightning return strokes, Proc. FAA/FIT Workshop on Grounding and Lightning Technology, Report FAA-RD-79-6, 9-15, March 1979.

Sunde, E. D., Earth Conduction Effects in Transmission Systems, Dover, New York, 1968.

Szpor, S., A new theory of induced overvoltages, CIGRE, Report #308, Paris, 1948.

Takeuti, T., Studies on thunderstorm electricity, Proc. Res. Inst. Atmos., Nagoya University (Japan), 12A, 1-70, 1965.

Taylor, C. D., R. S. Satterwhite, and C. W. Harrison, The response of a terminated two-wire transmission line excited by a non-uniform electromagnetic field, Trans. IEEE, AP-13, 987-989, 1965.

Taylor, W. L., Radiation field characteristics of lightning discharges in the band 1 kc/s to 100 kc/s, J. Res. Nat. Bur. Stand., 67D, 539-550, 1963.

Thomson, E. M., Characteristics of Port Moresby ground flashes, J. of Geophys. Res., 85, 1027-1036, 1980a.

Thomson, E. M., The dependence of lightning return stroke characteristics on latitude, J. of Geophys. Res., 85, 1050-1056, 1980b.

Tiller, J. A., M. A. Uman, Y. T. Lin, R. D. Brantley, and E. P. Krider, Electric field statistics for close lightning return strokes near Gainesville, Florida, J. of Geophys. Res., 81, 4430-4434, 1976.

Uman, M. A., Lightning, McGraw-Hill Book Company, New York, 1969.

Uman, M. A., and D. K. McLain, Lightning return stroke current from magnetic and radiation field measurements, J. Geophys. Res., 75, 5143-5147, 1970.

Vance, E. F., Coupling to Shielded Cables, John Wiley, 1977.

Wagner, C. F., and G. D. McCann, Induced voltages on transmission lines, Trans. AIEE, 61, 916-930, 1942.

Wagner, K. W., Electromagnetische Ausgleishvorgange in Freileitungen und Kabeln, Par. 5, Leipzig, 1908.

Wait, J. R., Electromagnetic Waves in Stratified Media, Pergamon, New York, 1962.

Weidman, C. D., and E. P. Krider, The fine structure of lightning return stroke waveforms, J. of Geophys. Res., 83, 6239-6247, 1978.

Weidman, C. D., and E. P. Krider, Submicrosecond risetimes in lightning return-stroke fields, Geophys. Res. Lett., 7, 955-958, 1980.

Whitescarver, C. D., Transient electromagnetic field coupling with two-wire transmission lines, Ph.D. Dissertation, University of Florida, 1969.

Winn, W. P., C. B. Moore, and C. R. Holmes, Electric field structure in an active part of a small isolated thundercloud, J. of Geophys. Res., 86, 1187-1193, 1981.

Zenneck, J., Wireless Telegraphy, 1907. English translation by A. E. Seelig, McGraw Hill, 1915.

BIOGRAPHICAL SKETCH

Maneck Jal Master was born March 7, 1955, in Bombay, India. He was awarded the Degree of Bachelor of Technology in Electrical Engineering from the Indian Institute of Technology, Bombay, in May 1977, and the Degree of Master of Engineering from the University of Florida, Gainesville, in August, 1979. After completing his Master's degree, Maneck has been working towards his Ph.D. in the Electrical Engineering Department, and has been involved in a US-DOE-sponsored study to understand the effects of lightning on power distribution systems.

Maneck is a member of Phi Kappa Phi, Tau Beta Pi, and Eta Kappa Nu. He is also a student member of the Institute of Electrical and Electronics Engineers (IEEE), and the American Geophysical Union (AGU).

After graduation he will take up a temporary position with Bell Telephone Laboratories, Holmdel, New Jersey, as a Member of Technical Staff.

I certify that I have read this study and that in my opinion it conforms to acceptable standards of scholarly presentation and is fully adequate, in scope and quality, as a dissertation for the degree of Doctor of Philosophy.

Martin A. Uman, Chairman
Professor of Electrical Engineering

I certify that I have read this study and that in my opinion it conforms to acceptable standards of scholarly presentation and is fully adequate, in scope and quality, as a dissertation for the degree of Doctor of Philosophy.

Alan D. Sutherland
Professor of Electrical Engineering

I certify that I have read this study and that in my opinion it conforms to acceptable standards of scholarly presentation and is fully adequate, in scope and quality, as a dissertation for the degree of Doctor of Philosophy.

Robert L. Sullivan
Professor of Electrical Engineering

I certify that I have read this study and that in my opinion it conforms to acceptable standards of scholarly presentation and is fully adequate, in scope and quality, as a dissertation for the degree of Doctor of Philosophy.

Thomas E. Bullock
Professor of Electrical Engineering

I certify that I have read this study and that in my opinion it conforms to acceptable standards of scholarly presentation and is fully adequate, in scope and quality, as a dissertation for the degree of Doctor of Philosophy.

George R. Lebo
Associate Professor of Astronomy

This dissertation was submitted to the Graduate Faculty of the College of Engineering and to the Graduate Council, and was accepted as partial fulfillment of the requirements for the degree of Doctor of Philosophy.

August 1982

Dean, College of Engineering

Dean, Graduate School

UNIVERSITY OF FLORIDA
3 1262 08666 320 9